M. Zoutewelle

Structural and Dynamic Design Criteria for a Quad Trolley Ship-to-Shore Crane Concept

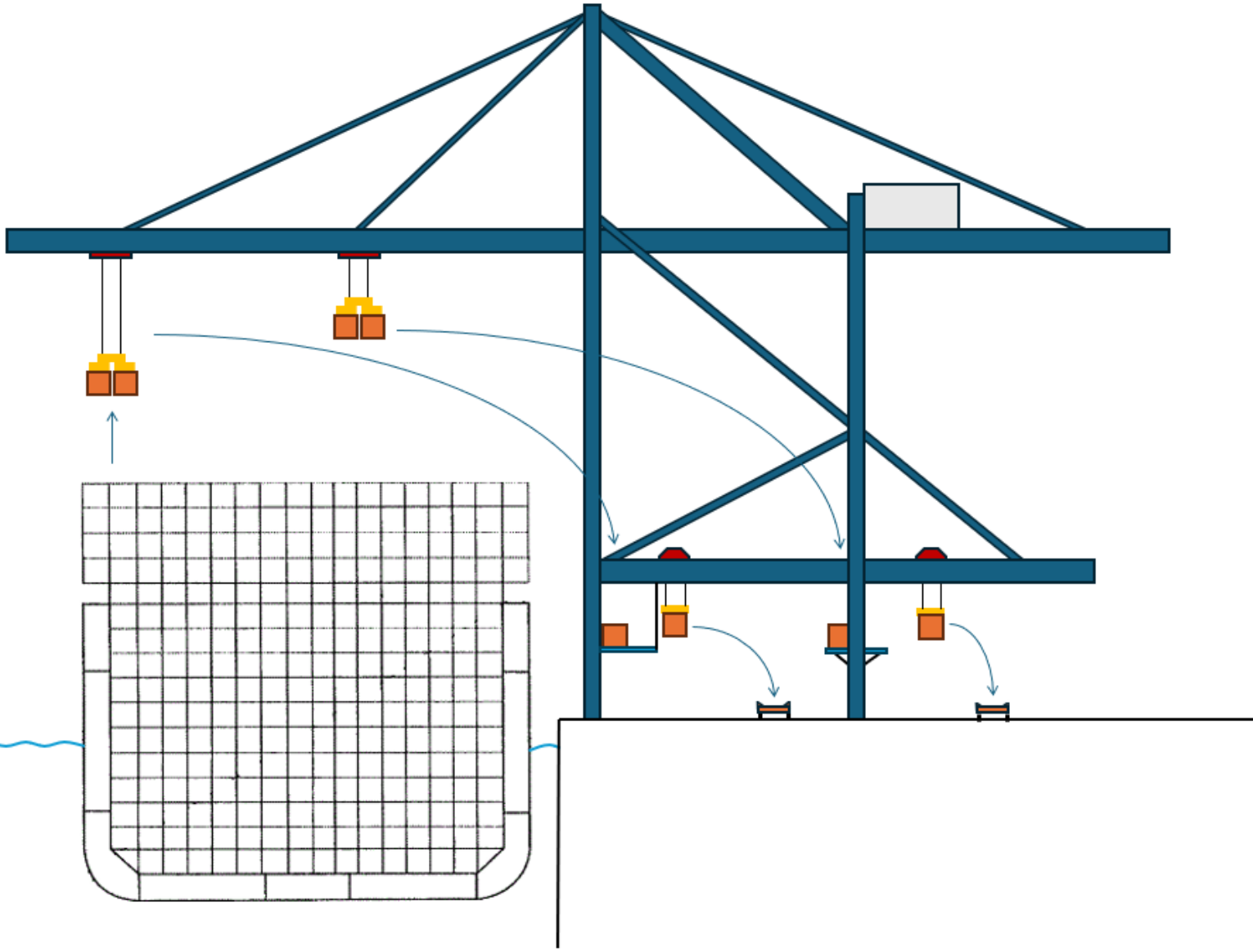

TU Delft

Huisman

Structural and Dynamic Design Criteria for a Quad Trolley Ship-to-Shore Crane Concept

By

M. Zoutewelle

Master Thesis

in partial fulfillment of the requirements for the degree of

Master of Science

in Mechanical Engineering

at the Department Maritime and Transport Technology of Faculty Mechanical, Maritime and Materials Engineering of Delft University of Technology
to be defended publicly on May 11, 2026 at 2:00 PM

Student number:	4456289	
MSc track:	Multi-Machine Engineering	
Report number:	2026.MME.9190	
Supervisors:	ir. W. van den Bos	Supervisor
Thesis committee:	Dr. J. Jovanova	TU Delft committee Chair, Faculty
	ir. R. Nouwens	Company Supervisor, Huisman
	ing. M. van Wingerden	Company Supervisor, Huisman
Date:	May 4, 2026	

An electronic version of this thesis is available at `http://repository.tudelft.nl/`.

It may only be reproduced literally and as a whole. For commercial purposes only with written authorization of Delft University of Technology. Requests for consult are only taken into consideration under the condition that the applicant denies all legal rights on liabilities concerning the contents of the advice.

TU Delft

Huisman

Preface

This thesis marks the completion of my Master's degree in Mechanical Engineering at the Delft University of Technology, within the Multi-Machine Engineering track. The research was carried out in collaboration with Huisman Equipment B.V. and was conducted almost entirely at their office in Schiedam.

I would like to thank my supervisor at TU Delft, ir. W. van den Bos, for his guidance and feedback throughout the project. I am also grateful to Dr. J. Jovanova for chairing the thesis committee.

At Huisman, I would like to thank my company supervisors ir. R. Nouwens and ing. M. van Wingerden for their continuous support, technical insight, and willingness to make time for my questions throughout the project. I would also like to thank ir. B. Holtzer for his involvement in the early stages of the project, particularly in defining its scope and direction. His input helped shape the foundation on which the rest of the work was built.

Finally, I would like to thank my family and friends for their continuous support and encouragement throughout my studies.

M. Zoutewelle
Delft, May 4, 2026

Abstract

The continued growth of global container shipping has made the productivity of ship-to-shore (STS) cranes a critical factor in port competitiveness. However, conventional single-trolley configurations are approaching the practical limits of cycle time. At the same time, the shift toward remote and automated operation has removed the operator-per-trolley constraint that previously limited the feasibility of multi-trolley systems. Together, these developments motivate the exploration of alternative crane configurations that increase handling capacity through parallel operation rather than further reductions in individual cycle time.

This thesis presents a structural and dynamic feasibility assessment of the Quad Trolley STS crane concept, in which two main trolleys and two secondary trolleys operate simultaneously on a single crane structure. The main trolleys are additionally equipped with a direct transverse drive that allows controlled transverse displacement of the load independently of the gantry. A beam-element finite element model is developed to assess structural strength, fatigue, stability, quay loading, and modal properties in accordance with EN 13001. The resulting structural properties are subsequently used as input for simplified dynamic models of the trolley–payload system, which are used to evaluate the transverse and trolley travel dynamic performance through reference case simulations and a full factorial parameter sensitivity study. A conventional single-trolley STS crane of identical outreach and capacity is analysed in parallel as a consistent reference case.

The results show that the concept is structurally feasible within the conventional 27 m buffer-to-buffer width constraint, with fatigue governing the final cross-sectional dimensions. The resulting structural mass of approximately 1161 mt represents an increase of only 53 mt (about 5%) compared to the conventional reference crane analysed using the same methodology. Stability is identified as a governing design consideration, with operational uplift of approximately 180 kN at the landside legs that can be resolved through ballast or operational positioning constraints, and storm uplift of approximately 2350 kN at the waterside legs requiring tie-downs. In the transverse direction, the direct trolley actuation concept provides a fundamental and substantial improvement in positioning accuracy over conventional gantry-based actuation, with the Quad Trolley configuration consistently achieving tracking errors within or close to the 50 mm accuracy threshold, while the conventional gantry-actuated crane exceeds it across all reference cases. In the trolley travel direction, performance is comparable to that of a conventional STS crane, as the second trolley introduces no meaningful dynamic interaction and structural stiffness has no meaningful effect on positioning accuracy. Wind loading is identified as the dominant disturbance in both directions. Together, the results confirm that the Quad Trolley STS crane concept is both structurally and dynamically viable as a high-performance container handling system.

Summary

The continued growth of global container shipping has made the productivity of ship-to-shore (STS) cranes a critical factor in port competitiveness. Conventional single-trolley configurations are approaching the practical limits of cycle times, and substantial further throughput gains within this architecture are increasingly marginal. At the same time, the shift toward remote and automated operation has removed the operator-per-trolley constraint that previously made multi-trolley concepts impractical from an operational and economic perspective. Together, these developments motivate the exploration of crane configurations that increase handling capacity through parallel operation rather than through further increases in individual motion speeds.

This thesis investigates the structural and dynamic feasibility of the Quad Trolley STS crane concept, a novel configuration in which two main trolleys and two secondary trolleys operate simultaneously on a single crane structure. The two main trolleys transport containers between the vessel and two intermediate twistlock stations, while the two secondary trolleys transfer containers between the twistlock stations and the quayside transport equipment. The main trolleys are additionally equipped with a direct transverse drive that allows controlled transverse displacement of the load independently of the gantry, eliminating the need to move the entire crane for small transverse adjustments. The concept is studied within the conventional 27 m buffer-to-buffer width constraint, which allows adjacent cranes to service alternating bays of a vessel and forms an important constraint on the structural layout.

The research is structured around a sequential workflow that links a structural analysis to a dynamic analysis. A global beam-element finite element model of the crane is developed in ANSYS and used to verify the structure against the strength, fatigue, and stability requirements of EN 13001, to evaluate the resulting quay loading, and to extract the global stiffness and modal properties of the crane. These structural properties are subsequently used as input for simplified dynamic models in the transverse and trolley travel directions, combined with a linear quadratic control framework, to evaluate controllability and disturbance rejection performance. A full factorial parameter sensitivity study is carried out to assess the influence of payload mass, hoisting length, trolley position, and disturbances on dynamic performance. A conventional single-trolley STS crane of identical outreach and capacity is analysed in parallel using the same workflow, providing a consistent reference for comparison.

The structural assessment shows that the Quad Trolley concept is feasible within the considered design constraints. After iterative optimisation of the cross-sectional dimensions, the structure satisfies both strength and fatigue requirements in accordance with EN 13001, with fatigue governing the final cross-sectional dimensions rather than peak strength. The resulting structural mass is approximately 1161 mt, an increase of only 53 mt (about 5%) compared to the conventional reference crane analysed using the same methodology, despite the considerably higher loading associated with the multi-trolley configuration. This limited increase reflects the partial compensation of higher per-cycle stress ranges by a lower number of cycles. In the Quad Trolley configuration, each of the two main trolleys perform 2×10^6 cycles, whereas in the conventional configuration a single main trolley performs the full 4×10^6 cycles, resulting in comparable total container throughput. Stability is identified as a governing design consideration: operational

uplift of approximately 180 kN at the landside legs can be resolved through ballast or an operational positioning constraint on the main trolleys, while storm conditions require tie-downs at the waterside legs to resist an uplift force of approximately 2350 kN. Quay loading remains within the range reported for existing STS crane infrastructure, confirming compatibility with modern port facilities subject to site-specific verification.

The dynamic assessment shows that the Quad Trolley concept is dynamically feasible under the control framework applied. In the transverse direction, the direct trolley actuation enables rapid and responsive control, with tracking errors remaining within or close to the 50 mm accuracy threshold across all but the most severe operating conditions. The conventional STS crane, by contrast, exceeds this threshold across all reference cases, as the indirect gantry-based actuation introduces structural compliance and lag in the force transmission path. This represents a fundamental performance advantage of the Quad Trolley concept that is inherent to the actuation concept and cannot be replicated through control improvements alone. In the trolley travel direction, the addition of a second main trolley introduces no meaningful dynamic interaction, and the relatively low structural stiffness and natural frequency of the baseline design have no meaningful effect on positioning accuracy. Across both motion scenarios, wind loading is identified as the dominant disturbance affecting positioning accuracy and actuator demand.

Together, these findings indicate that the structural design criteria established by EN 13001 are both necessary and sufficient for dynamic feasibility, and that no additional stiffness requirements need to be imposed beyond those already implied by structural code compliance. The Quad Trolley STS crane concept can therefore be realised as a structurally sound and code-compliant design within the conventional 27 m width constraint, although global stability remains a critical design consideration. The concept offers a substantial improvement in transverse positioning performance and comparable trolley travel performance relative to the conventional reference. It represents a structurally sound and dynamically viable direction for high-performance container handling, with the potential to significantly increase throughput through multi-trolley operation.

Samenvatting

De voortdurende groei van het wereldwijde containertransport heeft de productiviteit van ship-to-shore (STS) kranen tot een bepalende factor gemaakt voor de concurrentiepositie van havens. Conventionele STS kranen met één trolley naderen echter de praktische limieten van cyclustijd, waardoor verdere substantiële verbeteringen in overslagcapaciteit binnen deze configuratie beperkt zijn. Tegelijkertijd heeft de opkomst van remote en geautomatiseerde bediening de traditionele koppeling tussen operator en trolley doorbroken, waardoor configuraties met meerdere gelijktijdig opererende trolleys operationeel en economisch haalbaar zijn geworden. Deze ontwikkelingen vormen de aanleiding voor het onderzoeken van kraanconcepten die hun capaciteit vergroten door parallelle operatie in plaats van door verdere verkorting van individuele cyclustijden.

In dit onderzoek wordt de structurele en dynamische haalbaarheid onderzocht van het Quad Trolley STS kraanconcept. Dit concept omvat twee hoofdtrolleys en twee secundaire trolleys die gelijktijdig opereren op één kraanstructuur. De hoofdtrolleys verzorgen het transport tussen schip en twee tussenliggende twistlockstations, terwijl de secundaire trolleys het transport tussen deze stations en het kadegebonden transportsysteem uitvoeren. Daarnaast zijn de hoofdtrolleys uitgerust met een directe dwarse aandrijving, waarmee de last gecontroleerd in dwarse richting kan worden verplaatst zonder het verplaatsen van de volledige kraan. Het concept wordt geëvalueerd binnen de conventionele buffer-tot-buffer breedtebeperking van 27 m, die bepalend is voor de inzetbaarheid van meerdere kranen langs één schip.

De gehanteerde methodologie bestaat uit een sequentiële koppeling tussen structurele en dynamische analyse. Een globaal eindige-elementenmodel op basis van balk-elementen wordt opgesteld in ANSYS en gebruikt voor verificatie van sterkte, vermoeiing en stabiliteit volgens EN 13001. Daarnaast wordt het model gebruikt om kadebelastingen te bepalen en globale stijfheids- en modale eigenschappen te verkrijgen. Deze structurele eigenschappen vormen vervolgens de input voor vereenvoudigde dynamische modellen van het trolley–lastsysteem in zowel dwarse richting als katrijrichting. Met behulp van een lineair-kwadratische regelaar wordt de dynamische prestatie geëvalueerd op basis van positioneringsnauwkeurigheid en verstoringsonderdrukking. Door middel van een volledige factoriele parameterstudie wordt de invloed van systeemparameters, zoals lastmassa, hijshoogte, trolleypositie en verstoringen, systematisch geanalyseerd. Ter referentie wordt een conventionele STS kraan met identieke geometrie en capaciteit volgens dezelfde methodologie onderzocht.

De structurele analyse toont aan dat het Quad Trolley concept realiseerbaar is binnen de gestelde ontwerpbeperkingen. Na iteratieve optimalisatie van de doorsneden voldoet de structuur aan zowel sterkte- als vermoeiingseisen volgens EN 13001, waarbij vermoeiing maatgevend is voor de uiteindelijke dimensionering. De structurele massa bedraagt circa 1161 mt, wat slechts 53 mt (ongeveer 5%) hoger is dan die van de conventionele referentiekraan, ondanks de hogere belastingen als gevolg van de multi-trolley configuratie. Deze beperkte toename wordt verklaard door de verdeling van vermoeiingscycli over meerdere trolleys: in de Quad Trolley configuratie voert elk van de twee hoofdtrolleys circa 2×10^6 cycli uit, terwijl in de conventionele configuratie één trolley de volledige 4×10^6 cycli uitvoert, voor een gelijke totale overslagcapaciteit. Stabiliteit blijkt een kritisch ontwerpaspect: operationele uplift aan de landzijde kan worden opgelost met

aanvullende ballast of operationele beperkingen, terwijl voor stormcondities verankering aan de waterzijde noodzakelijk is. De kadebelasting blijft binnen de bandbreedte van bestaande STS kraaninfrastructuur, wat de praktische toepasbaarheid ondersteunt.

De dynamische analyse laat zien dat het Quad Trolley concept ook vanuit regeltechnisch perspectief haalbaar is. In de dwarse richting biedt de directe dwars-aandrijving een duidelijk prestatievoordeel, doordat correcties direct op het ophangpunt van de last worden aangebracht. Hierdoor blijven positioneringsfouten in de meeste gevallen binnen de gestelde nauwkeurigheidsgrens, terwijl een conventionele kraan met gantry-aandrijving deze grens in alle onderzochte gevallen overschrijdt. Dit verschil is inherent aan het aandrijfprincipe en kan niet worden opgeheven door aanpassingen in de regeling. In de katrijrichting blijkt dat de aanwezigheid van een tweede hoofdtrolley geen significante invloed heeft op de dynamische prestaties, en dat structurele flexibiliteit en eigenfrequentie geen bepalende rol spelen voor de positioneringsnauwkeurigheid. In beide richtingen wordt windbelasting geïdentificeerd als de dominante verstoringsbron.

De resultaten tonen aan dat de ontwerpcriteria uit EN 13001 niet alleen noodzakelijk zijn voor structurele veiligheid, maar ook voldoende blijken om dynamische haalbaarheid te waarborgen. Het Quad Trolley STS kraanconcept kan daarmee worden gerealiseerd als een structureel en dynamisch haalbare configuratie binnen de conventionele breedtebeperking van 27 m, mits stabiliteit expliciet wordt meegenomen in het ontwerp. Het concept biedt een significante verbetering in dwarse positioneringsprestaties en behoudt vergelijkbare prestaties in de katrijrichting, terwijl het tegelijkertijd het potentieel heeft om de overslagcapaciteit substantieel te verhogen door parallelle operatie.

AI Statement

For this report for the course ME-MME MSc Thesis - ME54035, I have used Generative AI to:

- Create (part of) the code in Matlab for solving the problem
- Obtain inspiration for the overall structure of the report
- Improve the grammar, style, layout, and/or spelling of the text

In all cases I have reviewed and corrected the work and remain fully responsible for the content of the report.

List of Symbols

Symbol	Description
$f_{Rd,\sigma}$	Limit design stress for normal stress
$f_{Rd,\tau}$	Limit design stress for shear stress
f_y	Yield strength of the material
γ_{Rm}	Material resistance factor
γ_m	Partial material factor
γ_{sm}	Material factor for structural detail category
γ_p	Partial safety factor for loads
N	Number of load cycles
D	Fatigue damage
x_b	Structural displacement
x_t	Trolley displacement
x_D	Drive-side displacement
x_s	Suspension point position
x_L	Horizontal position of the load
z_L	Vertical position of the load
$\dot{x}$	First time derivative of displacement
$\ddot{x}$	Second time derivative of displacement
θ	Load sway angle
$\dot{\theta}$	Angular velocity of the load sway
$\ddot{\theta}$	Angular acceleration of the load sway
m	Payload mass (parameter in the parametric study)
m_c	Equivalent structural mass
m_t	Trolley mass
m_L	Load mass (used in the dynamic model)
k_c	Equivalent structural stiffness
c_c	Equivalent structural damping
k	Equivalent stiffness (DOE parameter)
f_n	Natural frequency
g	Gravitational acceleration
L	Hoisting length / pendulum length
F_{dist}	Disturbance force from the second trolley
$F_{\text{wind},b}$	Wind force acting on the crane structure
$F_{\text{wind},l}$	Wind force acting on the suspended load
$u(t)$	Control input
$u_{\max}$	Maximum actuator acceleration
u_{RMS}	Root-mean-square actuator acceleration
$e_{\max}$	Maximum tracking error
e_{MAE}	Mean absolute tracking error
s_F	Disturbance force scale factor
U_{mean}	Mean wind speed

List of Abbreviations

Abbreviation	Description
STS	Ship-to-Shore
FEM	Finite Element Method
FEA	Finite Element Analysis
SWL	Safe Working Load
AGV	Automated Guided Vehicle
DOE	Design of Experiments
LQR	Linear Quadratic Regulator
LQI	Linear Quadratic Integral
RMS	Root Mean Square
MAE	Mean Absolute Error
EN	European Standard
ISO	International Organization for Standardization
ULCV	Ultra-Large Container Vessel

List of Figures

1 Typical STS crane and its main components, *adapted from* [1] 3
2 Illustration of three main girder and boom structural designs 4
3 Example of an STS crane with multiple forestays and backstays [2] 5
4 Stinis split-headblock for tandem lifting operations [3] 6
5 Bromma STR40/45 Twin-Lift and its corresponding lift combinations [4] . 6
6 Bromma Tandem Quattro and its corresponding lift combinations [4] . . . 6
7 Traditional cabin location on an STS crane [5] 7
8 The position of the crane operator in his cabin [6] 7
9 Example of an eight wheeled bogie set with four drive motors [7] 8
10 Buffer mounted on the end of the rail track [8] 8
11 Buffer mounted on the trolley of an overhead crane [9] 8
12 First Paceco STS crane, 1959 [10] 9
13 Size evolution of STS cranes [11] 9
14 STS crane dimensions [1] 10
15 STS crane movements, *adapted from* [12] 11
16 Illustration of trim, list and skew axes, and hydraulic mechanism, *adapted from* [13] 12
17 Schematic overview of the Quad Trolley STS Crane concept 16
18 Schematic overview of the Quad Trolley STS Crane geometry 19
19 Schematic overview of the integrated simulation and analysis workflow for the Quad Trolley STS crane concept 25
20 FEM model, showing beam elements and mesh sizing 28
21 Depiction of constraints used in FEM model 31
22 Selected main trolley positions used for structural analysis 32
23 Selected secondary trolley positions used for structural analysis 33
24 Excerpt of drag coefficient (C_d) values automatically generated by SDC Verifier in accordance with EN 13001. 34
25 Storm wind pressures as a function of height 35
26 Load Combinations as specified in EN13001-2 [14] 36
27 Cumulative distribution of fatigue cycles along the outreach region based on the operational positions of the main trolleys. 38
28 Cumulative distribution of fatigue cycles along the boom for both outreach and backreach operations, based on the operational positions of the main trolleys. 39
29 Simplified fatigue cycle for the secondary trolleys, assuming full (100%) occurrence of the defined operational movement. 40
30 Selected notch classes for different structural details in accordance with EN 13001. 45
31 Load combinations and partial safety factors for the proof of crane stability according to EN 13001-2 [14] 47
32 Example of the generated disturbance signal, showing a smooth, band-limited force with dominant frequency content around the structural natural frequency. 52
33 Generated wind speed profile used in simulations. 54

34 Simplified dynamic model of the Quad Trolley STS crane in the transverse direction. . . . 55
35 Transverse compliant-drive model with fixed trolley (in transverse) and suspended load. . . . 58
36 Dynamic model of the trolley travel direction with flexible boom and suspended load. . . . 61
37 Utilisation factors for Load Combination A3 (operational), showing the maximum value per element over all operational load cases. . . . 78
38 Utilisation factors for Load Combination B3 (operational with wind), showing the maximum value per element over all load cases. . . . 78
39 Utilisation factors for Load Combination C2 (storm, boom up), showing the maximum value per element over all storm load cases. . . . 79
40 Fatigue utilisation factors per element, based on the applied load spectrum and cycle distribution. . . . 80
41 Deformation of the structure under Load Combination A3 (operational). . 81
42 Deformation of the structure under Load Combination B3 (operational with wind). . . . 81
43 Deformation of the structure under Load Combination C2 (storm, boom up). 82
44 Utilisation factors for Load Combination A3 (operational), showing the maximum value per element over all operational load cases for the conventional STS crane. . . . 84
45 Utilisation factors for Load Combination B3 (operational with wind), showing the maximum value per element over all load cases for the conventional STS crane. . . . 85
46 Utilisation factors for Load Combination C2 (storm, boom up), showing the maximum value per element over all storm load cases for the conventional STS crane. . . . 86
47 Fatigue utilisation factors per element, based on the applied load spectrum and cycle distribution for the conventional STS crane. . . . 87
48 Operational stability critical load case 88
49 Operational positioning constraint on the main trolleys. (A) Minimum spacing of 10 m, with the rear trolley at position P6. (B) Increased spacing requirement under critical stability conditions, with the rear trolley shifted to position P10. . . . 89
50 Example of storm tie-downs connecting the crane structure to the quay. . . 90
51 Boom positions under storm conditions: (A) 80°, (B) 60°, and (C) 45°. . . 91
52 Primary vibration mode shapes of the Quad Trolley STS crane: (a) boom sway, (b) frame torsion, and (c) portal sway. . . . 93
53 Positioning accuracy (mean ± standard deviation over 20 stochastic realizations) for all six reference cases. . . . 96
54 Actuator demand (mean ± standard deviation over 20 stochastic realizations) for all six reference cases. . . . 97
55 Time-domain tracking error for the worst case reference case (RC3: maximum outreach position, high severity), showing that the 50 mm accuracy threshold is exceeded only occasionally, while the error remains within the threshold for the majority of the motion. . . . 97
56 Positioning accuracy (mean ± standard deviation over 20 stochastic realizations) for all six reference cases, conventional gantry drive. . . . 99

57 Actuator demand (mean ± standard deviation over 20 stochastic realizations) for all six reference cases, conventional gantry drive. 99
58 Positioning accuracy comparison (mean ± standard deviation over 20 stochastic realizations) between the Quad Trolley and conventional STS crane for all six reference cases. 100
59 Actuator comparison (mean ± standard deviation over 20 stochastic realizations) between the Quad Trolley and conventional STS crane for all six reference cases. 101
60 Main effects of system parameters on positioning accuracy for the Quad Trolley transverse direction. 103
61 Main effects of system parameters on actuator demand for the Quad Trolley transverse direction. 104
62 Positioning accuracy (mean ± standard deviation over 20 stochastic realizations) for all three reference cases, trolley travel direction. 105
63 Actuator demand (mean ± standard deviation over 20 stochastic realizations) for all three reference cases, trolley travel direction. 106
64 Time-domain tracking error for the nominal reference case in the trolley travel direction (RC2: medium severity), showing the tracking error relative to the 30 mm accuracy threshold. 106
65 Time-domain tracking error for the worst case reference case in the trolley travel direction (RC3: high severity), showing the tracking error relative to the 30 mm accuracy threshold. 106
66 Main effects of system parameters on positioning accuracy for the trolley travel direction. 108
67 Main effects of system parameters on actuator demand for the trolley travel direction. 108
68 Effect of structural stiffness on trolley travel performance with fixed modal mass. Stiffness is varied from half to twice the baseline design value of $k = 16.670$ MN/m, with the corresponding natural frequency range shown in the top subplot. 110
69 Effect of structural stiffness on trolley travel performance with fixed natural frequency ($f_n = 0.542$ Hz). Modal mass increases proportionally with stiffness as shown in the top subplot. 111
70 Effect of natural frequency on trolley travel performance with fixed stiffness ($k = 16.670$ MN/m). Modal mass decreases with increasing natural frequency as shown in the top subplot. 112
A.1 Schematic overview of the Quad Trolley STS crane concept, showing the two main trolleys, two secondary trolleys, and intermediate twistlock stations. 128
A.2 Overview of the sequential coupled modelling approach linking the FE model to the simplified dynamic models. 128
A.3 Utilisation factors for Load Combination B3 (operational with wind), showing the maximum value per element over all load cases. Peak utilisation of approximately 0.94 occurs at the main girder support. 129
A.4 Fatigue utilisation factors per element, based on the applied load spectrum and 2×10^6 load cycles per main trolley. Utilisation approaches unity across a large portion of the structure, confirming that fatigue governs the final structural design. 129
A.5 Primary global vibration modes obtained from the FE model. 130

A.6 Maximum transverse tracking error for all reference cases, comparing the Quad Trolley concept with conventional gantry-based actuation. 130
A.7 Main effects of system parameters on maximum transverse tracking error. Wind speed dominates, while trolley position (represented by equivalent stiffness k) and inter-trolley disturbance (s_F) both show notable secondary effects. 131
A.8 Main effects of system parameters on maximum trolley travel tracking error. Wind speed dominates, while the inter-trolley disturbance (s_F) has a negligible effect, confirming that the second trolley does not compromise trolley travel performance. 131
A.9 Effect of structural stiffness on maximum tracking error $e_{\max}$ with fixed modal mass. The natural frequency increases with stiffness as shown in the top panel. The response remains essentially constant across the full range from half to twice the baseline design value of $k = 16.670$ MN/m. Results for all four KPIs show the same trend. 132
A.10 Effect of structural stiffness on maximum tracking error $e_{\max}$ with fixed natural frequency ($f_n = 0.542$ Hz). All other KPIs show the same response. 132
A.11 Effect of natural frequency on maximum tracking error $e_{\max}$ with fixed stiffness ($k = 16.670$ MN/m). The natural frequency is swept from 0.4 to 1.0 Hz, covering the full range from below the ISO 22986 minimum to above the industry specification minimum. All four KPIs remain completely flat throughout. 132
12 Bogie reaction forces for the governing operational stability load case. Node 81: waterside left, Node 815: waterside right, Node 822: landside left, Node 461: landside right. 215
13 Bogie reaction forces for the stability storm load case (boom at 80°). Node 1527: waterside left, Node 1534: waterside right, Node 1520: landside left, Node 1513: landside right. 216
14 Bogie reaction forces for the stability storm load case (boom at 60°). Node 520: waterside left, Node 527: waterside right, Node 111: landside left, Node 539: landside right. 216
15 Bogie reaction forces for the stability storm load case (boom at 45°). Node 1499: waterside left, Node 1506: waterside right, Node 1492: landside left, Node 1485: landside right. 217
16 Bogie reaction forces for the governing operational corner load case. Node 81: waterside left, Node 815: waterside right, Node 822: landside left, Node 461: landside right. 217
17 Bogie reaction forces for the governing corner loading storm load case (boom at 80°). Node 1527: waterside left, Node 1534: waterside right, Node 1520: landside left, Node 1513: landside right. 218

List of Tables

1 Typical Specifications for a Panamax Crane [1] 9
2 Typical Specifications for a Post Panamax Crane [1] 10
3 Typical Specifications for a Super Post Panamax Crane [1] 10
4 Overview of lifting configurations and associated masses per trolley 21
5 Reference speeds and accelerations for crane motions 22
6 Material properties of structural steel S355. 29
7 Access and auxiliary mass contributions. 30
8 Fatigue load cases and corresponding number of cycles 41
9 Distribution of lifting configurations for the main trolleys. 41
10 Container mass distribution used for fatigue load definition. 42
11 Fatigue strength specific resistance factor γ_{mf} according to EN 13001 . . . 44
12 LQI weighting parameters used for the different crane models. 68
13 Parameters and levels used in the three-level DOE 73
14 Natural frequency of the suspended load as a function of hoisting length. . 75
15 Boom tip displacements at maximum outreach for the governing load combinations. 82
16 Mass breakdown of the Quad Trolley STS crane. 83
17 Mass breakdown of the conventional and Quad Trolley STS crane configurations. 87
18 Maximum line loads for the Quad Trolley and conventional STS crane compared to reference values from existing STS crane infrastructure. 91
19 Natural frequencies of the three primary vibration modes of the Quad Trolley STS crane, corresponding to the trolley positions between maximum outreach and maximum backreach. 92
20 Comparison of natural frequencies of the Quad Trolley STS crane with values reported in the literature and industry specifications. 93
21 Definition of reference cases for dynamic response evaluation. The cases represent low, medium, and high control difficulty at two characteristic structural locations. 96
22 Maximum relative sheave block displacement with respect to the boom across 20 realizations for each transverse reference case. 98
23 Definition of reference cases for the trolley travel direction, representing low, medium, and high control difficulty at a fixed structural configuration. 105
A.1 Key operational parameters of the Quad Trolley STS crane concept. 128
A.2 Mass comparison between the Quad Trolley and conventional STS crane. . 129
A.3 Natural frequencies of the primary vibration modes compared to literature and industry specification limits. 130

Contents

Preface i

Abstract ii

Summary iii

Samenvatting v

AI Statement vii

List of Symbols viii

List of Abbreviations ix

List of Figures x

List of Tables xiv

1 Introduction 1
1.1 Thesis Structure . . . 2

2 Ship-to-shore Cranes 3
2.1 Main Components . . . 3
2.1.1 Gantry Structure . . . 3
2.1.2 Main Girder and Boom . . . 4
2.1.3 Stays . . . 4
2.1.4 Trolley . . . 5
2.1.5 Headblock and Spreader . . . 5
2.1.6 Cabin . . . 6
2.1.7 Machine house . . . 7
2.1.8 Bogie sets . . . 7
2.1.9 Buffers . . . 8
2.2 Evolution of Design . . . 8
2.3 Sizes . . . 9
2.4 Movements . . . 11
2.5 Productivity . . . 12
2.6 Automation . . . 13
2.7 Conventional STS Crane as Reference Configuration and Its Limitations . 13

3 Concept Overview 15
3.1 General Concept Description . . . 15
3.2 Operational Workflow . . . 17
3.3 Geometric Configuration . . . 18
3.4 Moving Masses and Payload Characteristics . . . 19
3.5 Operational Speeds and Accelerations . . . 21
3.6 Comparison with Conventional STS Cranes . . . 22

4 Methodology **24**
4.1 Overview of the Research Approach . . . 24
4.2 Modelling Strategy . . . 24
4.3 Integrated Simulation and Analysis Workflow . . . 25

5 Finite Element Model **27**
5.1 Model Description . . . 27
5.1.1 Model Type . . . 27
5.1.2 Geometry Idealisation . . . 28
5.1.3 Material Properties . . . 28
5.2 Mass Modelling . . . 29
5.2.1 Non-Structural Mass Estimation . . . 29
5.3 Boundary Conditions and Supports . . . 31
5.4 Load Modelling . . . 31
5.4.1 Load Combinations . . . 35
5.5 Structural Verification . . . 36
5.5.1 Strength Verification . . . 36
5.5.2 Fatigue Verification . . . 37
5.5.3 Verification Approach . . . 45
5.6 Stability Assessment . . . 46
5.7 Quay Loading . . . 47
5.8 Modal Analysis . . . 48

6 Dynamic Model **49**
6.1 Modelling Approach and Assumptions . . . 49
6.1.1 Modelling Approach . . . 49
6.1.2 Structural Representation . . . 50
6.1.3 Load Modelling . . . 51
6.1.4 Disturbance Modelling . . . 51
6.1.5 Model Scope and Limitations . . . 54
6.2 Quad Trolley STS Crane – Transverse Dynamic Model . . . 54
6.2.1 Kinematics . . . 55
6.2.2 Equations of Motion . . . 55
6.2.3 Linearised Model . . . 56
6.2.4 State-Space Representation . . . 56
6.3 Conventional STS Crane – Transverse Dynamic Model . . . 57
6.3.1 Kinematics . . . 58
6.3.2 Equations of Motion . . . 59
6.3.3 Linearised Model . . . 59
6.3.4 State-Space Representation . . . 59
6.4 Trolley Travel Direction Dynamic Model . . . 61
6.4.1 Kinematics . . . 61
6.4.2 Equations of Motion . . . 62
6.4.3 Linearised Model . . . 62
6.4.4 State-Space Representation . . . 62
6.5 Control Design . . . 64
6.5.1 Control Objective . . . 64
6.5.2 Linear Quadratic Regulator . . . 64
6.5.3 Integral Action . . . 65

6.5.4 Application to the Crane Models . . . 66
6.5.5 Weighting Strategy . . . 66
6.5.6 Comparison Between Configurations . . . 68
6.5.7 Motivation for LQR/LQI Control . . . 69
6.6 Simulation Setup and Performance Metrics . . . 69
6.6.1 Simulation Setup . . . 69
6.6.2 Reference Cases . . . 70
6.6.3 Performance Metrics . . . 70
6.7 Parameter Sensitivity Analysis . . . 72
6.7.1 DOE Structure . . . 72
6.7.2 Parameter Definition . . . 73
6.7.3 Performance Evaluation . . . 74
6.7.4 Analysis Method . . . 74
6.7.5 Hoisting Length Sweep . . . 75
6.7.6 Targeted Stiffness and Natural Frequency Sweep . . . 75

7 Results **77**
7.1 Structural Results . . . 77
7.1.1 Structural Verification (EN13001) . . . 77
7.1.2 Deflection Behaviour . . . 80
7.1.3 Structural Mass Overview . . . 82
7.1.4 Comparison with Conventional STS Crane . . . 83
7.1.5 Stability Assessment . . . 88
7.1.6 Quay Loading . . . 91
7.1.7 Modal Analysis . . . 92
7.1.8 Summary of Structural Performance . . . 94
7.2 Dynamic Results . . . 94
7.2.1 Transverse Motion . . . 95
7.2.2 Transverse Parameter Sensitivity . . . 101
7.2.3 Trolley Travel . . . 104
7.2.4 Trolley Travel Parameter Sensitivity . . . 106
7.2.5 Influence of Structural Stiffness on Trolley Travel Performance . . . 109
7.2.6 Summary of Dynamic Performance . . . 113

8 Conclusion **115**

9 Recommendations and Future Work **118**
9.1 Trolley System Design . . . 118
9.2 Structural Model Refinement . . . 119
9.3 Wind Loading Assessment . . . 119
9.4 Stability Provisions . . . 119
9.5 Dynamic Model Extension . . . 119
9.6 Control Development . . . 120
9.7 Throughput and Economic Assessment . . . 120

A Scientific Paper **126**

B Load definitions **134**
B.1 Main Trolley Hoist load . . . 134

B.2 Main Trolley acceleration load . . . 134
B.3 Main trolley transverse acceleration load . . . 135
B.4 Secondary trolley hoist load . . . 136
B.5 Secondary trolley acceleration load . . . 136
B.6 Gantry acceleration load . . . 137
B.7 Hoisting force on boom (main trolleys) . . . 137
B.8 Trolley buffer force . . . 138
B.9 Secondary trolley buffer force . . . 138
B.10 Gantry buffer acceleration . . . 139

C Transverse model derivation **140**

D Conventional Transverse Dynamic Model derivation **145**

E Trolley travel model derivation **150**

F Structural Cross sections **156**

G FEM - Bogie Reaction Forces **215**

1 Introduction

As global maritime trade continues to grow, the efficiency and reliability of container terminal operations have become critical factors in port competitiveness. One of the key components in the maritime logistics chain is the ship-to-shore (STS) crane, which serves as the primary interface for transferring containers between container vessels and the quayside. Due to their central role in terminal operations, the performance of STS cranes has a direct impact on vessel turnaround times and overall terminal throughput. As container volumes and vessel sizes continue to increase, there is increasing pressure to further improve the productivity and efficiency of these cranes.

Recent advances in automation and remote operation are reshaping the design possibilities of STS cranes. In particular, the combination of automation and remote control has reduced the operational constraints associated with traditional crane operation, where each crane typically required a dedicated operator in a cabin mounted on the trolley. With remote operation, a single operator can supervise multiple crane functions or systems, enabling more complex operational configurations that were previously impractical from a labour and operational cost perspective. One such opportunity is the introduction of multi-trolley crane concepts that enable parallel container handling.

This research is conducted in collaboration with Huisman, a leading company in the design and manufacturing of heavy construction equipment for the offshore, energy, and maritime sectors. As part of their strategic ambition to expand into the port logistics market, Huisman is exploring innovative STS crane concepts capable of delivering substantially higher handling performance while remaining structurally and economically viable. One of the concepts under consideration is a Quad Trolley STS crane, which integrates two coordinated main trolleys operating along a common rail on the boom and main girder of the crane, together with two secondary trolleys operating in the lower part of the crane structure. By distributing container handling tasks across multiple trolleys, the concept enables parallel operation and therefore offers the potential for significantly increased container throughput while retaining a largely conventional STS crane architecture.

However, introducing multiple trolleys fundamentally alters the structural and dynamic characteristics of the crane. The presence of several moving masses operating simultaneously leads to higher structural loads, increased deformations, and more complex dynamic interactions between the crane structure, the trolleys, and the suspended loads. Ensuring that such a concept remains structurally feasible, dynamically stable, and controllable under realistic operational conditions, therefore, becomes a key engineering challenge.

The aim of this research is to investigate the structural and dynamic feasibility of the Quad Trolley STS crane concept and to determine the design criteria required to enable its feasible and controllable operation. This includes evaluating the structural behaviour of the crane under operational and environmental loading, assessing its dynamic performance during operation, and analysing the interaction between structural flexibility, disturbances, control performance, and inter-trolley dynamics.

This directly leads to the central research question:

What structural and dynamic design criteria are required to enable feasible and controllable operation of the Quad Trolley Ship-to-Shore crane concept?

This research question is supported by the following sub-questions:

- To what extent can the Quad Trolley STS crane concept be realised with an acceptable structural mass, given the increased loading and functional complexity?
- Is the concept feasible within the conventional 27 m width constraint, or should a larger 39 m width constraint be explored?
- To what extent is the Quad Trolley STS crane concept dynamically feasible under representative control?
- To what extent is supplemental mechanical damping necessary for maintaining dynamic feasibility of the Quad Trolley STS crane concept?
- What design trade-offs can be identified between structural flexibility and system controllability in the Quad Trolley STS crane concept?
- What degree of structural optimisation is possible without compromising the dynamic feasibility of the Quad Trolley STS crane concept?

1.1 Thesis Structure

The remainder of this thesis is organised as follows. Chapter 2 describes the conventional STS crane, its main components and operating principles, and identifies the limitations that motivate the Quad Trolley concept. Chapter 3 introduces the concept itself, covering its geometry, operational workflow, moving masses, and main design characteristics, and compares it against the conventional reference configuration. Chapter 4 presents the methodology and the integrated workflow that links the structural and dynamic analyses.

Chapter 5 describes the finite element model used for the structural assessment, including the modelling approach, load cases, and verification framework. Chapter 6 describes the dynamic models and the control framework used to evaluate controllability, together with the simulation setup and parameter sensitivity study. Chapter 7 reports the structural and dynamic results, including a direct comparison with the conventional reference crane.

Chapter 8 presents the conclusions, answering the research question and its sub-questions. Chapter 9 provides recommendations and directions for future work.

2 Ship-to-shore Cranes

Ship-to-shore (STS) cranes are large gantry cranes used in container terminals to transfer containers between ships and the quay. As the primary interface between maritime and landside logistics operations, their performance strongly influences container terminal productivity and vessel turnaround times.

This chapter introduces the conventional STS crane configuration, which serves as the reference case for the concept study presented in this thesis. The main structural components, dimensions, and operational principles of STS cranes are described to establish a clear understanding of how these systems are typically designed and operated.

By defining this baseline configuration, a structured comparison can be made with the Quad Trolley crane concept introduced in the following chapter. The focus is therefore not only on describing existing STS cranes, but also on identifying the key functions and design choices that may be altered or redistributed in an alternative crane concept.

2.1 Main Components

Although STS cranes differ in size and configuration, their fundamental design and operating principles are largely identical. Figure 1 illustrates a traditional STS crane and its main components. Together, these components define the conventional functional architecture of an STS crane, which forms the basis for comparison with alternative configurations.

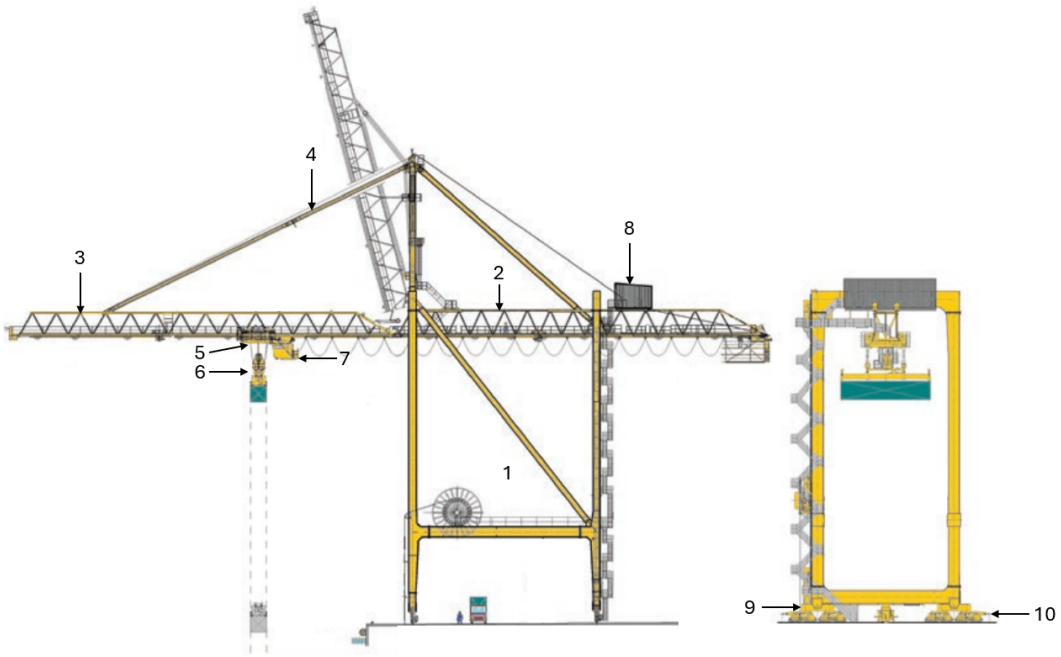

Ref.	Component
1	Gantry structure
2	Main girder
3	Boom
4	Forestay
5	Trolley
6	Headblock and Spreader
7	Cabin
8	Machine house
9	Bogie set
10	Buffer

Figure 1: Typical STS crane and its main components, *adapted from* [1]

2.1.1 Gantry Structure

The gantry structure forms the primary load-bearing framework of the STS crane, supporting all major components. It typically consists of vertical legs connected by horizontal

and diagonal members, forming a portal frame. The gantry must withstand dynamic loads from crane operations, wind loading, and self-weight, and its design strongly influences global stiffness, stability, fatigue performance, and load distribution.

2.1.2 Main Girder and Boom

The main girder and boom form the horizontal structure that carries the trolley. The main girder spans the landside structure and backreach, while the boom extends over the vessel and can be raised when not in operation. The boom length determines the crane's outreach and, together with the overall height, defines the maximum vessel size that can be serviced.

Three main structural configurations are commonly used:

Monobox: A single enclosed box section offering high bending and torsional stiffness. However, the monobox is relatively heavy and material-intensive, which can adversely affect the crane's global dynamics and energy consumption.

Double box: Two parallel box girders providing high bending capacity and load-carrying capability. Torsional stiffness is lower than that of a monobox, but the configuration offers practical advantages such as accessible space between girders for rope routing.

Lattice: An open truss structure composed of interconnected members. Lattice girders are lightweight, structurally efficient, and exhibit reduced wind loading, but their geometric complexity increases fabrication effort and maintenance requirements.



(a) Monobox [15]



(b) Double Box [16]

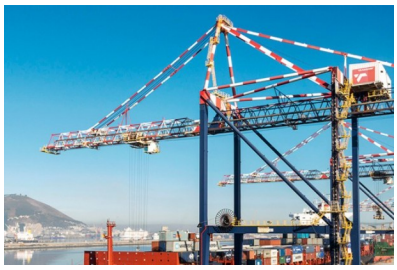

(c) Lattice [17]

Figure 2: Illustration of three main girder and boom structural designs

2.1.3 Stays

Stays are tension members that support and stabilise the boom and main girder by transferring part of the vertical loads into the gantry structure. This load redistribution reduces bending moments in the boom, enabling long cantilevered outreaches without excessive structural mass, thereby improving the overall crane's structural efficiency.



Figure 3: Example of an STS crane with multiple forestays and backstays [2]

2.1.4 Trolley

The trolley is a wheeled carriage running on rails along the boom and main girder, responsible for horizontal transport of the spreader and container between quay and ship. It must support both the hoisting system and the travel mechanism. Based on the location of drive and hoisting equipment, three main trolley configurations can be distinguished [7]:

Machine Trolley: Both the hoisting and trolley drive mechanisms are mounted on the trolley. This configuration enables precise, independent positioning and benefits from short hoist ropes, reducing rope elasticity and improving dynamic response. The main disadvantage is the relatively high trolley mass due to the onboard machinery.

Full-rope Trolley: The trolley carries no drive or hoisting machinery and is moved by wire ropes connected to winches in the machinery house. Hoisting is also performed via long ropes. This results in a lightweight trolley and centralised maintenance but requires a complex rope system and careful rope management.

Semi-rope Trolley: The trolley drive is mounted on the trolley, while hoisting is performed from the machinery house. Because trolley drive equipment is considerably lighter than hoisting machinery, the trolley can be self-propelled with limited mass increase, forming a compromise between machine and full-rope trolley designs.

In modern STS cranes, the full-rope trolley is by far the most common configuration, with semi-rope trolleys appearing only occasionally [18]. Machine trolleys exist primarily as a conceptual configuration and are not used in current STS crane practice.

2.1.5 Headblock and Spreader

The headblock is an intermediate structure suspended from the trolley that connects the hoist ropes to the spreader. It houses the hoist sheaves and provides the mechanical and electrical interface between trolley and spreader. Headblocks also enable rapid spreader exchange and can support advanced lifting configurations. For example, tandem headblocks supplied by manufacturers such as Stinis and RAM allow two spreaders to be operated simultaneously, enabling tandem container handling [19, 3].

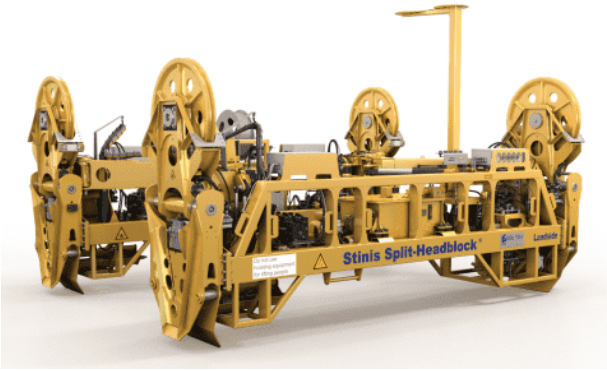

Figure 4: Stinis split-headblock for tandem lifting operations [3]

The spreader is the lifting attachment that engages with the corner castings of containers. While containerization was intended to standardise cargo handling, multiple container lengths, primarily 20 ft, 40 ft, and 45 ft, are now in use, requiring adaptable spreader designs. As a result, modern STS cranes almost exclusively use telescopic spreaders, which can accommodate different container sizes and often support twin-lift operations, such as lifting two 20ft containers simultaneously [20]. In this context, twin lifting refers to the handling of two 20 ft containers using a single spreader, while tandem lifting refers to the simultaneous handling of multiple containers using two spreaders connected to a tandem headblock.

Modern spreaders are equipped with automatic twistlocks and increasingly incorporate sensing and control systems to improve safety and positioning accuracy. These include twistlock detection, load monitoring, and vision- or laser-based alignment systems [21, 22, 23, 24].

Both headblocks and spreaders are typically supplied by specialised manufacturers rather than crane OEMs, with companies such as Bromma, Stinis, and RAM offering solutions ranging from simple telescopic spreaders to advanced tandem lifting systems.

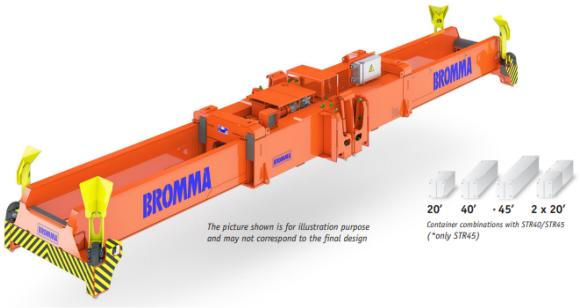

Figure 5: Bromma STR40/45 Twin-Lift and its corresponding lift combinations [4]

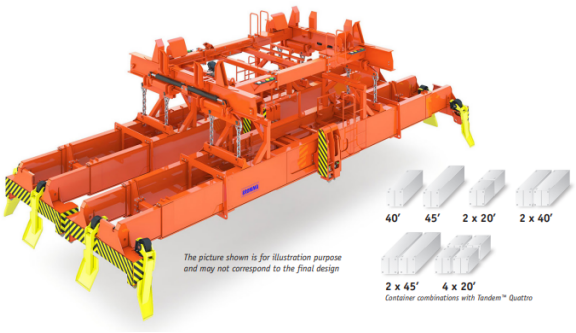

Figure 6: Bromma Tandem Quattro and its corresponding lift combinations [4]

2.1.6 Cabin

The cabin is the workstation from which the crane operator controls all crane movements. Traditionally, the cabin is mounted on the trolley to provide direct visual contact with the spreader and container. While this configuration offers good visibility, it requires

prolonged downward viewing, resulting in a non-ergonomic working posture that can cause operator discomfort during extended operations.

Advances in sensor technology, high-resolution cameras, and automation have enabled remote-controlled and semi-automated crane operation. In these systems, the operator is relocated to a remote control room and monitors crane operation via real-time video and digital interfaces. This improves ergonomics and safety, reduces operator fatigue, and allows a single operator to supervise multiple cranes if required [25].



Figure 7: Traditional cabin location on an STS crane [5]



Figure 8: The position of the crane operator in his cabin [6]

2.1.7 Machine house

The machine house is typically located at the rear upper section of the gantry and contains the main electromechanical drive systems. Depending on the trolley configuration, it may house the hoisting machinery, trolley drives, and the boom hoist system, as well as electrical and control equipment. Its rearward position provides space for large machinery and contributes to counterbalancing the cantilevered boom.

2.1.8 Bogie sets

Bogie sets are wheel assemblies located at each corner of the crane base that allow the crane to travel along quay rails. Driven by electric motors, they enable repositioning of the crane along the vessel. Each bogie set comprises multiple wheels to distribute the crane's weight and operational loads, with the number of wheels determined by the total crane mass, dynamic loads, and the load-bearing capacity of the quay and rail system.



Figure 9: Example of an eight wheeled bogie set with four drive motors [7]

2.1.9 Buffers

Buffers are safety devices designed to limit impact forces during unintended collisions or overruns. On STS cranes, they are typically installed on the bogie sets or at the ends of the crane runway, as well as at the ends of the trolley travel along the boom and main girder. Buffers absorb kinetic energy and reduce structural damage in the event of overtravel or crane-to-crane contact.



Figure 10: Buffer mounted on the end of the rail track [8]



Figure 11: Buffer mounted on the trolley of an overhead crane [9]

2.2 Evolution of Design

The development of STS cranes has closely followed the growth of containerised shipping and the increasing size of container vessels. Since the introduction of the first container crane by Paceco in 1959 [10], the fundamental configuration of the STS crane has remained largely unchanged. However, its scale, performance, and level of automation have evolved significantly.

Early STS cranes were designed for smaller vessels and lower handling rates. They were manually operated, structurally conservative, and primarily optimised for mechanical robustness [26]. As global trade volumes increased and vessel sizes progressed from Panamax to Post Panamax and Super Post Panamax, cranes had to accommodate longer outreach,

higher lifting capacities, and increased handling speeds, while maintaining positioning accuracy and safety.



Figure 12: First Paceco STS crane, 1959 [10]

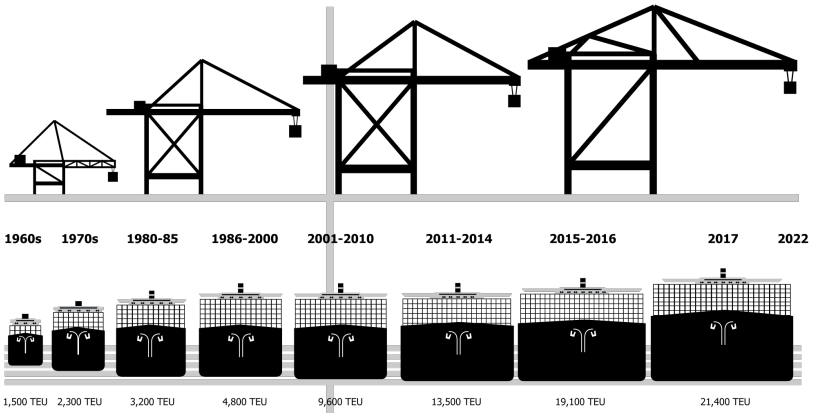

Figure 13: Size evolution of STS cranes [11]

Over time, design emphasis has shifted from purely increasing structural strength to improving performance, energy efficiency, and automation. Modern STS cranes incorporate advanced drive systems, optimised lightweight structures, and sophisticated control architectures. Semi-automation, remote operation, and integrated safety systems have become standard, supported by feedback control and high-precision positioning technologies [27].

Today's STS cranes are the result of this progression: large, structurally optimised, and increasingly automated systems designed to handle the largest container vessels in operation.

2.3 Sizes

There are a few vital dimensions that govern the design of an STS crane, these are given in Figure 14. STS cranes come in a range of sizes, each tailored to accommodate specific vessel classes. These cranes are typically categorised into three main classes based on their outreach and lifting capabilities:

1. **Panamax:**
   Designed to handle ships that fit through the original Panama Canal locks, these cranes typically have an outreach of around 30 to 40 meters and can service vessels up to 13 container rows wide.

Table 1: Typical Specifications for a Panamax Crane [1]

Outreach	**No. of Containers across deck**	**Lift height**	**Safe Working Load**	**Hoisting Speed**	**Trolley Speed**	**Gantry Travel Speed**	**Wheel Load**
30 - 40 m	up to 13	24 - 30 m	40 - 50 t (single), 65 t (twin)	50 - 125 m/min	150 - 180 m/min	45 m/min	30 - 45 t/m*
* Wheel loads based on 8 wheels per corner							

2. **Post Panamax:**
   Post Panamax cranes were developed for vessels exceeding the original Panama Canal width, prior to the 2016 canal expansion. With outreaches of roughly 40 to 45 meters, they typically handle ships with 16 to 18 container rows across

Table 2: Typical Specifications for a Post Panamax Crane [1]

Outreach	No. of Containers across deck	Lift height	Safe Working Load	Hoisting Speed	Trolley Speed	Gantry Travel Speed	Wheel Load
40 - 45 m	up to 18	30 - 35 m	40 - 50 t (single), 65 t (twin)	60 - 150 m/min	180 - 210 m/min	45 m/min	40 - 55 t/m*
* Wheel loads based on 8 wheels per corner							

3. **Super Post Panamax:**
   Super Post Panamax cranes represent the largest STS crane class. Initially designed for Neo-Panamax vessels following the Panama Canal expansion, their capabilities have since been extended to service ultra-large container vessels (ULCVs). These cranes feature outreaches ranging from approximately 46 to more than 70 meters, enabling handling of vessels with up to 24 container rows across.

Table 3: Typical Specifications for a Super Post Panamax Crane [1]

Outreach	No. of Containers across deck	Lift height	Safe Working Load	Hoisting Speed	Trolley Speed	Gantry Travel Speed	Wheel Load
46 - 73+ m	up to 24+	30 - 54+ m	70t (twin), 120 t (tandem)	90 - 180 m/min	210 - 240 m/min	45 m/min	60 - 80 t/m*
* Wheel loads based on 8 wheels per corner							

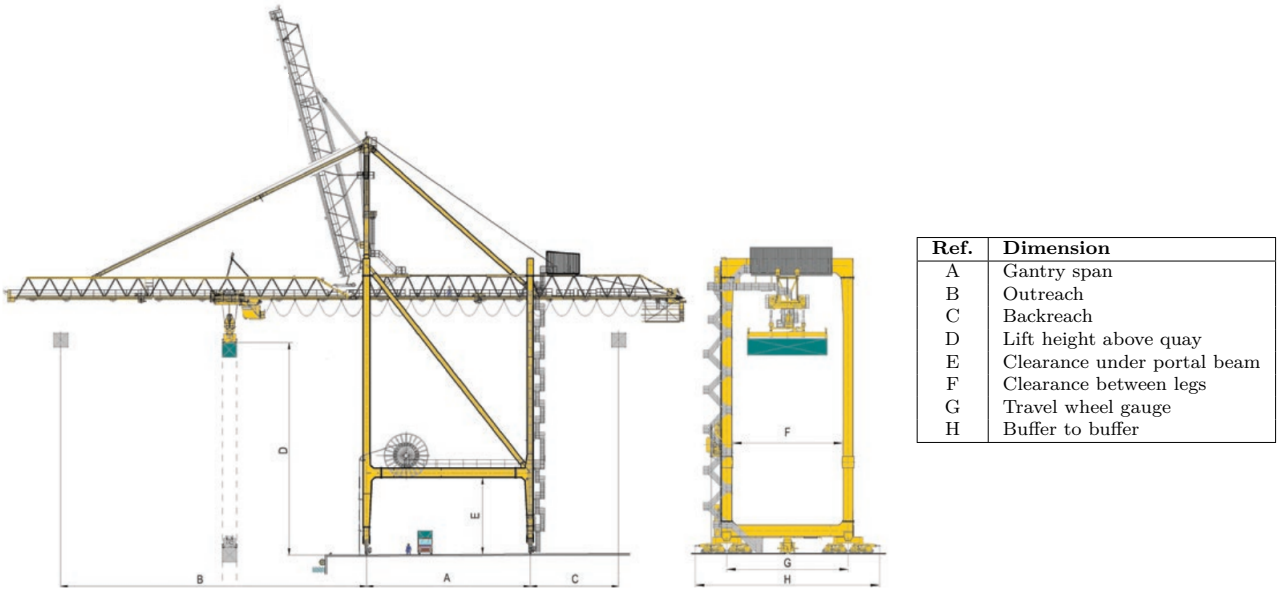

Ref.	Dimension
A	Gantry span
B	Outreach
C	Backreach
D	Lift height above quay
E	Clearance under portal beam
F	Clearance between legs
G	Travel wheel gauge
H	Buffer to buffer

Figure 14: STS crane dimensions [1]

The dimensions in Tables 1–3 describe the geometry and operational characteristics required to service different vessel classes, and are primarily determined by vessel size and

handling requirements. In addition, the overall buffer-to-buffer width of the crane (dimension H in Figure 14) is an important operational dimension that is governed by the spacing of cranes along the quay. A smaller buffer-to-buffer width allows adjacent cranes to be positioned closer together, increasing the number of cranes that can simultaneously service a single vessel and contributing to overall berth productivity. For modern STS cranes, a maximum buffer-to-buffer width of 27 m is adopted, allowing two adjacent cranes to operate on alternating bays of a vessel: one crane services a given bay while the second services the bay two positions further along, with the bay in between left empty to provide clearance between the two cranes. This width therefore defines the lateral envelope within which the entire crane structure must be accommodated, and forms a key constraint on the structural layout of an STS crane.

2.4 Movements

The operation of an STS crane consists of three primary motions: trolley travel, hoisting, and gantry travel. Together, these movements enable accurate container handling during loading and unloading operations. These motions are illustrated in Figure 15.

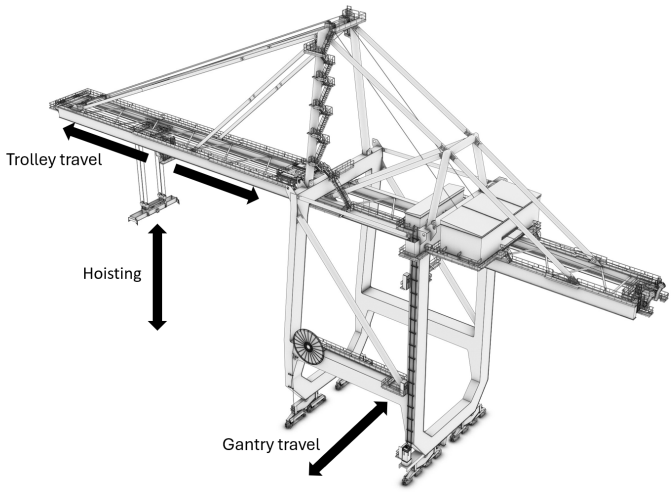

Figure 15: STS crane movements, *adapted from* [12]

Trolley travel: Trolley travel is the horizontal motion of the trolley along the main girder and boom, transporting the spreader and container between the quay and the vessel. Typical trolley speeds range from 150 to 240 m/min, depending on crane size [1, 28, 29]. Accurate trolley positioning is essential for precise container placement.

Hoisting: Hoisting refers to the vertical lifting and lowering of the spreader and container using wire ropes driven by winches. Containers are lifted from the vessel and placed on the quay, or vice versa. Typical hoisting speeds are approximately 60–90 m/min under load and up to 120–180 m/min when unloaded [1, 28, 29]. Hoisting performance strongly influences cycle time and operational safety.

Gantry travel: Gantry travel is the longitudinal movement of the entire crane along quay rails, allowing repositioning between vessel bays. During container handling cycles, gantry travel is generally inactive, making trolley and hoisting motions the dominant contributors to cycle time. Typical gantry speeds are 30–45 m/min [1, 28, 29].

Trim, list, and skew control: In addition to the main crane motions, modern STS cranes incorporate trim, list, and skew control to correct spreader orientation disturbances caused by wind or uneven load distribution (Figure 16). The headblock and spreader are suspended by multiple hoist ropes routed over sheaves connected to hydraulic or electric actuators. By locally adjusting rope lengths, the orientation of the spreader is controlled, enabling precise correction of trim, list, and skew angles [13].

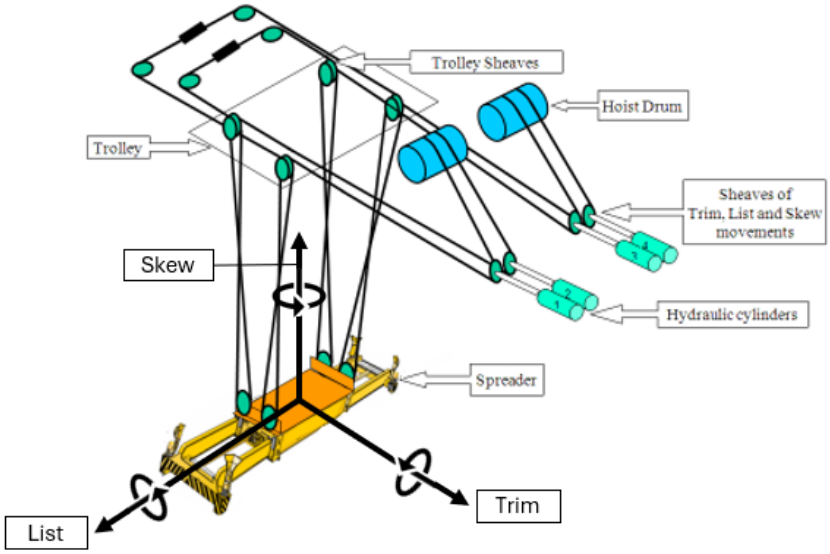

Figure 16: Illustration of trim, list and skew axes, and hydraulic mechanism, *adapted from* [13]

2.5 Productivity

STS crane productivity is a key contributor to overall container terminal productivity and performance [30]. It is commonly expressed in moves per hour, where one move corresponds to the transfer of containers between a vessel and a transport vehicle on the quay. When twin-lift or tandem spreaders are employed, a single move may involve multiple containers, effectively increasing handling capacity. Modern STS cranes typically achieve approximately 30 to 50 moves per hour [31].

High STS crane productivity directly reduces vessel turnaround time and increases terminal throughput, which are critical factors in minimising port congestion and maintaining tight shipping schedules. Consequently, ongoing efforts to improve both crane- and terminal-level productivity continue to drive advancements in STS crane design, operational strategies, and system integration.

Within a single-trolley architecture, productivity gains have traditionally been pursued by increasing trolley travel and hoisting speeds, lifting capacity, and the number of containers handled per move through twin-lift and tandem spreaders. However, with trolley speeds already approaching 240 m/min and cycle times near their practical minimum, further productivity gains along these axes are increasingly marginal [30]. This has motivated interest in alternative concepts, such as parallelising the handling process across multiple trolleys rather than further increasing the speed or capacity of a single one.

2.6 Automation

Automation of STS cranes has become a major trend in the modernization of container terminals, driven by the goals of improving efficiency, safety, and operational consistency while reducing labour demands and costs. Although fully autonomous STS crane operation has not yet been realised in commercial practice, substantial progress has been made toward higher levels of automation.

Most modern STS cranes are equipped with semi-automated functions such as continuous load sway and skew control, which stabilize the load during operation. More advanced automation features include collision avoidance, ship profiling, optimised motion paths, and automated container landing [32]. These systems support the operator by reducing workload and improving repeatability and safety.

A significant development has been the transition from crane-mounted operator cabins to remote operation from centralised control rooms. Using high-resolution video feeds and real-time sensor data, operators can control cranes from ergonomically optimised and safer environments. In combination with automation, remote operation enables a single operator to supervise multiple cranes, increasing terminal-level efficiency and reducing labour costs [25].

Despite these advances, automation adoption varies widely across terminals. As of 2025, only about 8.3% of container terminals worldwide have implemented automation technologies of any type [33]. Nevertheless, market studies indicate that approximately 59% of newly installed STS cranes are now delivered with semi-automated control systems [34]. Fully autonomous operation remains challenging due to the need for human intervention in non-standard situations, such as misaligned containers or adverse weather conditions, as well as the high investment and system-integration requirements associated with automation.

Beyond its direct benefits in efficiency and labour reduction, the shift toward remote and automated operation also acts as a key enabler for alternative crane configurations. In conventional manually operated systems, each trolley requires a dedicated operator, which makes configurations involving multiple trolleys impractical from an operational and economic perspective. With remote and automated operation, a single operator can supervise multiple trolleys simultaneously, removing this constraint and opening the design space for multi-trolley crane concepts such as the one investigated in this thesis.

2.7 Conventional STS Crane as Reference Configuration and Its Limitations

The conventional STS crane can be characterised as a portal-based system in which container handling is performed by a trolley travelling along a horizontal boom and main girder, combined with a hoisting system suspended from the trolley. Although STS cranes have evolved significantly in scale, performance, and level of automation, this fundamental configuration has remained largely unchanged. Design developments have primarily focused on increasing outreach, lifting capacity, and operational speed. The preceding sections, however, reveal that this trajectory of incremental improvement now confronts a set of interlocking limitations:

Throughput ceiling: As discussed in Section 2.5, single-trolley productivity is approaching its practical limits, and substantial further throughput gains require alternative concepts, such as the parallelisation of handling operations across multiple trolleys.

Structural mass growth: Accommodating greater outreach and higher payloads requires heavier structural members, which in turn increase the crane's self-weight and the resulting wheel and quay loads. Each increment in outreach or lifting height therefore carries a structural penalty.

Dynamic sensitivity: Longer and more flexible booms, combined with higher operating speeds, produce larger structural deformations that couple with pendulum sway in the suspended load. This coupling limits achievable positioning accuracy and places greater demands on the control system.

Manual control limitation: In manually operated systems, each trolley requires a dedicated operator, which has historically made multi-trolley configurations economically impractical. The ongoing shift toward automated and remotely supervised operation removes this constraint and makes such configurations viable.

These limitations collectively define the design space in which the Quad Trolley STS crane concept operates. The concept does not attempt to push further along the same axis of individual speed and capacity, but instead restructures the handling workflow to achieve parallelism within a largely conventional structural envelope. The design criteria required to make this restructuring structurally and dynamically viable form the central subject of this thesis. In the following chapter, the Quad Trolley STS crane concept is introduced, and its geometry, mass distribution, and operational workflow are described in the context of the limitations identified above.

3 Concept Overview

As established in Chapter 2, conventional single-trolley STS crane configurations are approaching their practical throughput limits, while the shift toward remote and automated operation has removed the operator-per-trolley constraint that previously made multi-trolley configurations impractical. Together, these developments motivate the exploration of crane concepts that increase handling capacity through parallel operation rather than through further increases in individual motion speeds or lifting capacities.

Building on this, the Quad Trolley STS crane concept investigated in this thesis introduces multiple coordinated trolleys on a largely conventional STS crane structure to enable parallel container handling. With two main trolleys operating in parallel between the vessel and intermediate transfer points, the concept offers the potential for substantially higher handling productivity than a conventional single-trolley STS crane, while limiting structural mass growth.

The purpose of this chapter is to introduce the Quad Trolley STS crane concept and to establish a clear understanding of its geometry, mass distribution, and operational principles. This conceptual overview provides the necessary context for the structural and dynamic analyses presented in subsequent chapters. The emphasis is placed on system-level behaviour and design intent, rather than on detailed mechanical or control system implementation.

3.1 General Concept Description

The Quad Trolley STS crane concept combines two coordinated main trolleys operating on a common rail along the boom and main girder of the crane, together with two secondary trolleys positioned in the lower part of the crane structure. Two twistlock stations are incorporated into the crane layout: one located between the waterside legs and one between the landside legs. These stations function as intermediate transfer points within the container handling process. A schematic overview of the concept is shown in Figure 17.

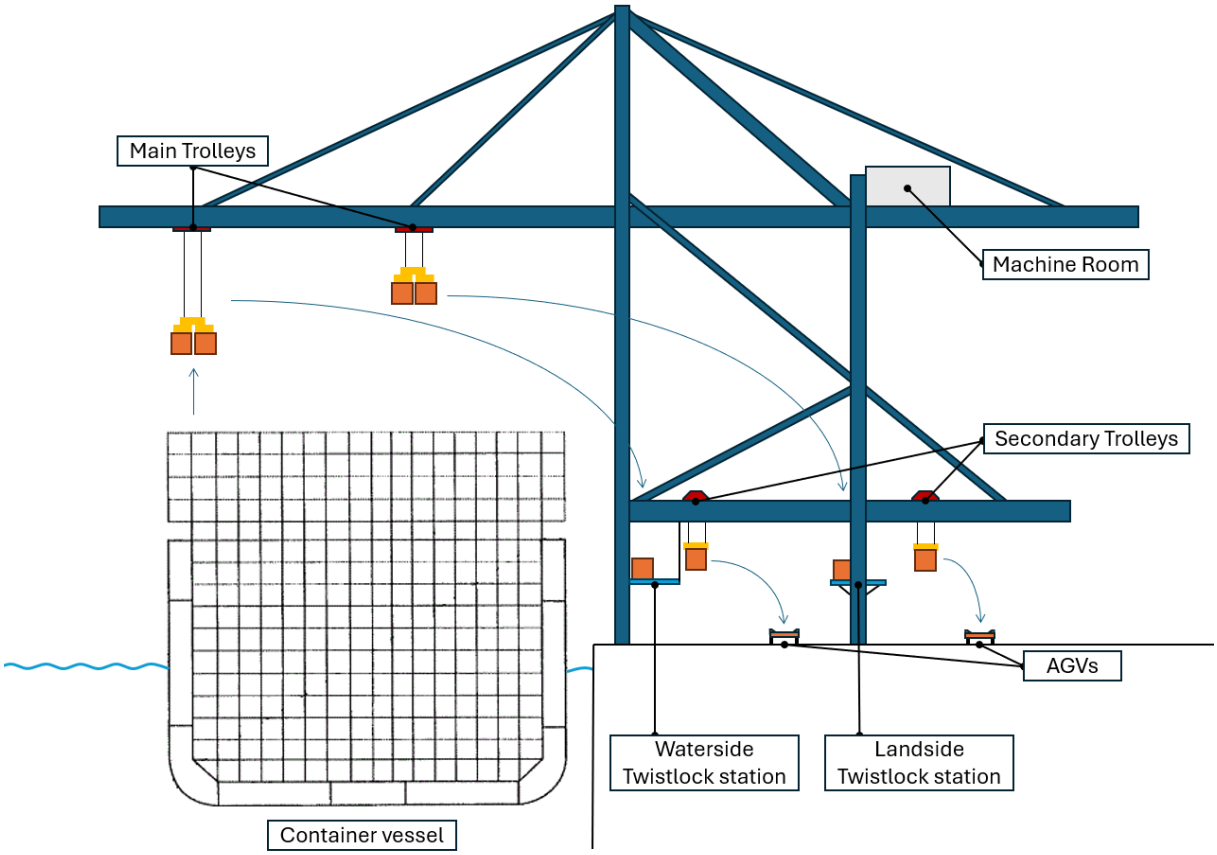

Figure 17: Schematic overview of the Quad Trolley STS Crane concept
Note: Relative dimensions are not to scale

The two main trolleys are responsible for container transport between the vessel and the twistlock stations. They are capable of tandem operation, enabling the simultaneous handling of two 40 ft containers, twin handling of two 20 ft containers, and single-container handling. Simultaneous lifting of four 20 ft containers is also possible, provided that the total lifted mass does not exceed 82 mt. This limit reflects the low practical occurrence of higher combined loads and avoids unnecessary structural mass and over-dimensioning of the crane for rarely occurring load cases. The main trolleys are self-propelled, while the hoisting function is provided by a centralised winching system located in the machine room, which also contributes to the counterbalancing of the crane. This configuration represents a trade-off between reducing the moving mass of the trolley system and reducing reeving complexity. To accommodate the required rope routing and enable transverse trolley motion, a double-girder boom configuration is adopted, providing sufficient space between the girders for the reeving system and trolley mechanisms.

The secondary trolleys provide comparable operational flexibility on the landside by supporting both single and twin container handling, but are not intended for tandem lifting. In contrast to the primary trolleys operating above the vessel, the secondary trolleys travel over a shorter distance and primarily interface with the quayside transport equipment. Restricting the lifting capability of the secondary trolleys to single lifts and twin-lift operations for 20 ft containers simplifies the transfer of containers to the landside transport system and avoids the logistical constraints associated with tandem operations. Quayside transport equipment, such as automated guided vehicles (AGVs), typically carry either one 40 ft container or two 20 ft containers [35], meaning that twin-lift operations remain

compatible with a single transport vehicle, whereas tandem lifts require multiple vehicles and additional coordination. Since the landside transfer distance is comparatively short, these simplified lifting configurations are sufficient to maintain efficient container flow between the crane and the terminal transport system. Like the main trolleys, the secondary trolleys are self-propelled. In contrast to the main trolleys, however, the hoisting winches are mounted directly on the trolley.

By enabling parallel operation of multiple trolleys, the Quad Trolley concept aims to increase container handling capacity while retaining a largely conventional STS crane architecture. By effectively integrating two parallel handling systems within a single crane structure, the concept has the potential to significantly improve productivity, potentially approaching twice the throughput of conventional STS cranes, while remaining structurally and economically viable.

A distinguishing feature of the concept is the inclusion of transverse drives on the main trolleys. In addition to their primary motion along the boom (trolley travel), each trolley is equipped with a secondary drive system that allows controlled transverse displacement in the direction of traditional gantry travel. This transverse capability enables independent trolley operation and eliminates the need to move the entire crane when small transverse adjustments are required.

3.2 Operational Workflow

The operational workflow of the Quad Trolley STS crane is organised around two twistlock stations: one located between the waterside legs and one between the landside legs. These stations function as intermediate transfer points within the container handling process and act as buffers between vessel-side and landside operations.

During container discharge, the two main trolleys transport containers between the vessel and their assigned twistlock stations. The front main trolley is assigned to the waterside twistlock station, while the rear main trolley is assigned to the landside twistlock station. The two main trolleys operate largely synchronously, typically moving together between the vessel and the twistlock stations in order to avoid delays caused by one trolley waiting for the other. At these stations, containers are temporarily placed and twistlock handling operations are performed.

From the twistlock stations, the secondary trolleys transport containers to the quayside transport equipment. One secondary trolley is assigned to the waterside twistlock station and transfers containers from this station to transport vehicles located between the crane legs. The other secondary trolley is assigned to the landside twistlock station and transfers containers from this station to transport vehicles positioned at the backreach of the crane.

This configuration allows vessel-side and landside transport operations to be performed largely independently. By functioning as intermediate buffers, the twistlock stations decouple the operational cycles of the main trolleys and the secondary trolleys. As a result, the main trolleys can operate primarily between the vessel and the twistlock stations without being directly constrained by the availability or positioning of quayside transport vehicles.

At the same time, the secondary trolleys independently transfer containers between the twistlock stations and the transport vehicles. Because both trolley systems operate on

separate segments of the handling process, container movements between the vessel, twistlock stations, and transport vehicles can occur in parallel. This parallelisation of container handling operations increases the overall throughput potential of the crane.

The Quad Trolley STS crane concept is assumed to operate within a highly automated control framework. Routine handling operations, including trolley coordination, hoisting, and positioning, are executed automatically, with a remote operator intervening only when the automated system is unable to complete a task reliably or when non-standard conditions arise. This framework allows a single operator to oversee multiple trolleys simultaneously, meaning that the increased number of trolleys does not lead to a proportional increase in operator requirements.

3.3 Geometric Configuration

The Quad Trolley STS crane concept is based on a largely conventional STS crane geometry, consisting of a portal frame with two waterside legs, two landside legs, a main girder, and a luffing boom. The global arrangement follows established design practice in order to remain compatible with existing terminal layouts, quay infrastructure, and vessel interfaces.

Compared to conventional single-trolley STS cranes, the overall geometry of the Quad Trolley STS crane concept remains largely similar. The main distinction lies in the increased functional width of the boom and the main trolley system, driven by the inclusion of transverse trolley travel capability. This transverse drive is integrated into the trolley and requires additional clearance between the boom girders to accommodate transverse motion. Consequently, the spacing between the girders is increased from approximately 6 m in conventional designs to 10 m in the proposed configuration, providing approximately ± 2 m of transverse travel relative to the nominal trolley position.

The primary geometric parameters governing the crane configuration include the outreach, backreach, lifting height above rail and crane gauge. These dimensions directly determine the vessel classes that can be serviced and define the compatibility with the quay infrastructure. In this concept, the geometric dimensions are selected such that the crane can service the largest container vessels currently in operation, while maintaining compatibility with traditional container terminal infrastructure.

The most important geometric dimensions are illustrated in Figure 18.

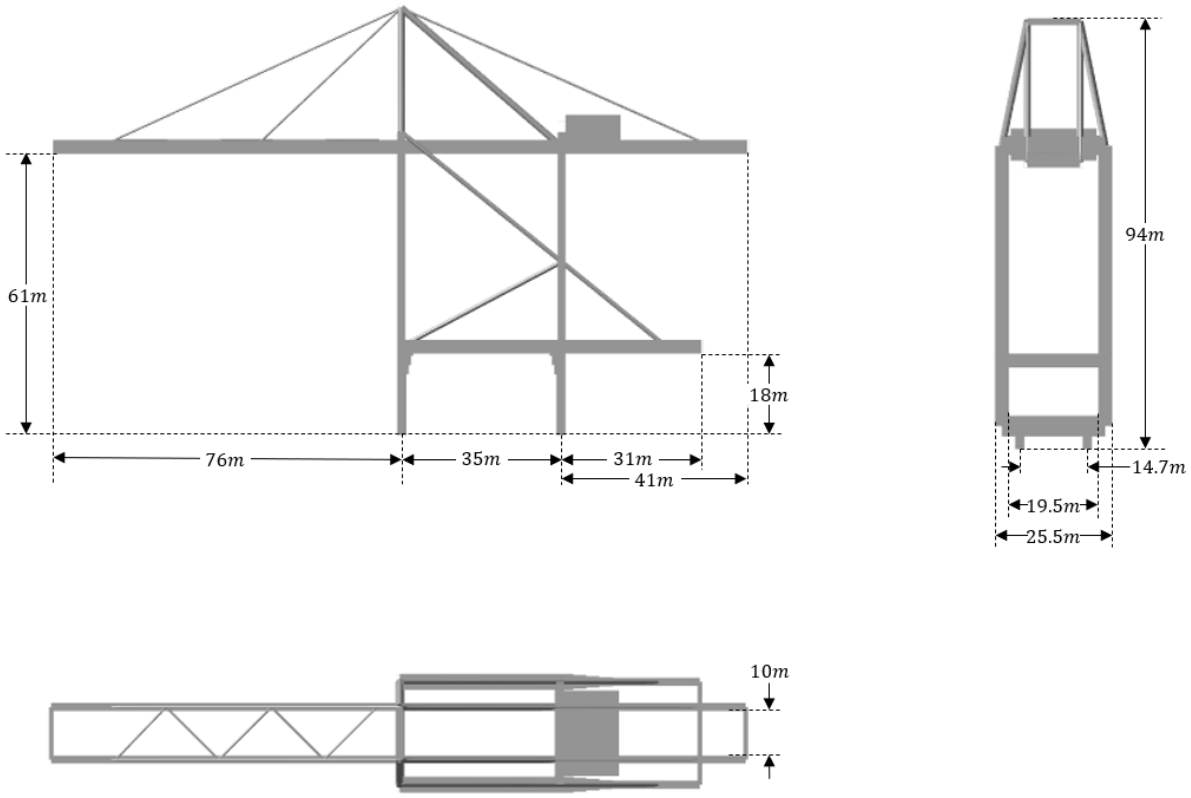

Figure 18: Schematic overview of the Quad Trolley STS Crane geometry

In addition to these conventional parameters, the buffer-to-buffer width of the crane is constrained by operational considerations. As discussed in Section 2.3, a maximum buffer-to-buffer width of 27 m is adopted to enable two adjacent cranes to service alternating bays of a vessel. The same constraint is adopted for the Quad Trolley concept, which therefore must accommodate its increased functional complexity within the same transverse envelope as a conventional STS crane. This dimension is not illustrated in Figure 18, as the bogies and buffer system are not included in the schematic representation.

3.4 Moving Masses and Payload Characteristics

The moving masses of the Quad Trolley STS crane consist of two main trolleys, two secondary trolleys, and their respective hoisting assemblies. These subsystems differ considerably in mass and configuration, reflecting their distinct roles within the overall handling workflow. An overview of the relevant masses and lifting configurations is provided in this section.

Main Trolleys

Each of the main trolleys has a total mass of 30 mt. The trolleys are self-propelled, with drive motors mounted directly on the trolley for independent and precise positioning along the boom rails. Two considerations motivate this choice. First, each main trolley is connected to the central winch room in the machine house by four hoist ropes, resulting in a total of eight hoist ropes already running along the boom structure. Adding trolley drive ropes on top of this would further increase the complexity and congestion of the rope

routing system considerably, and is therefore avoided. Second, self-propelled trolleys offer inherently better positioning accuracy and faster actuation compared to rope-driven systems, as the absence of long drive ropes eliminates the elasticity of the rope transmission, which would otherwise introduce lag into the drive system.

Hoisting is handled centrally from the machine room rather than from the trolley itself, which is a deliberate design decision driven by two considerations. Since hoisting machinery is considerably heavier than trolley drive equipment, relocating it to the machine room results in a significant mass saving of the trolleys, which not only limits the inertia loads introduced into the boom structure during trolley travel, but also benefits the overall stability of the crane by keeping the mass of the main trolleys, mainly operating on the cantilevered boom, as low as possible. Furthermore, positioning the heavy hoisting machinery in the machine room at the landside of the crane allows it to act as a counterweight, improving the overall load distribution across the structure.

Each main trolley additionally incorporates a transverse drive system, which enables the controlled transverse displacement introduced in Section 3.1 and accommodated by the boom geometry described in Section 3.3. The drive actuators are mounted statically on the trolley structure and travel with the trolley along the boom during normal trolley travel. During transverse actuation, these actuators move the sheave block, together with its supporting frame, transversely relative to the trolley frame. The sheave block has a mass of 5 mt, which represents the effective moving mass in the transverse direction, the remainder of the 30 mt trolley mass remains stationary relative to the boom. This distinction is important for the dynamic analysis presented in subsequent chapters, as the inertial load introduced into the boom structure during transverse actuation corresponds solely to this 5 mt rather than the full trolley mass.

Secondary Trolleys

Each secondary trolley has a structural mass of 100 mt, considerably higher than that of the main trolleys. Two factors drive this difference. Unlike the main trolleys, the secondary trolleys carry both their drive motors and their full hoisting winch system on board, with the hoisting machinery alone accounting for the majority of the mass difference. While centralising the hoisting of the secondary trolleys in a dedicated machine room would be feasible in principle, it would considerably complicate the rope routing. Such an arrangement would require hoist ropes to run horizontally from the machine room towards the secondary trolleys, passing through the same zone in which the vertical hoist ropes of the main trolleys descend with their loads. Routing around this conflict would necessitate additional sheaves and supporting structures, adding mechanical complexity, weight, and maintenance burden to the system. Mounting the hoisting system directly on the secondary trolleys avoids this complexity entirely and preserves the independence of both trolley systems. Furthermore, since the secondary trolleys operate within the portal frame rather than on the cantilevered boom, their higher mass does not introduce the overturning moment concerns that would arise for equivalent mass positioned on the long cantilevered boom.

Payload and Hoisting Configurations

The payload characteristics of the crane are governed by the lifting configurations supported by each trolley type, and are determined by the hoisting assembly suspended from each trolley.

Each main trolley is equipped with a split headblock of 10 mt [36], enabling both single-spreader and tandem lifting configurations. In single-spreader configuration, a single twin-lift telescopic spreader of 15 mt [37] is attached to the headblock, giving a total suspended assembly mass of 25 mt per main trolley, excluding payload. In tandem configuration, two spreaders are attached to the headblock, each with a mass of 15 mt, bringing the total suspended assembly mass to 40 mt per trolley, excluding payload.

Each secondary trolley is equipped with a generic headblock of 5 mt [38] and a single twin-lift telescopic spreader of 15 mt, giving a total suspended assembly mass of 20 mt per trolley, excluding payload. As discussed in Section 3.1, the secondary trolleys are not intended for tandem lifting, consistent with their role in transferring containers between the twistlock stations and quayside transport equipment.

For the main trolleys, a maximum Safe Working Load (SWL) of 82 mt applies in tandem configuration, where two spreaders simultaneously handle containers. In tandem configuration, each spreader can operate in twin-lift mode, meaning that up to four 20 ft containers could theoretically be lifted simultaneously. However, the 82 mt limit is deliberately set below the theoretical maximum combined mass of four fully loaded 20 ft containers, reflecting the low practical occurrence of such a load case and avoiding unnecessary over-dimensioning of the structure for a rarely occurring combination. The 82 mt SWL is sufficient to accommodate two fully loaded 40 ft or 45 ft containers in tandem mode. In single-spreader configuration, the SWL is 70 mt, accommodating either a single 40 ft container or two 20 ft containers in twin-lift operation. The secondary trolleys operate exclusively in single-spreader configuration, with the same SWL of 70 mt.

The total suspended masses for each configuration are summarised in Table 4.

Table 4: Overview of lifting configurations and associated masses per trolley

Trolley	**Configuration**	**Headblock** [mt]	**Spreaders** [mt]	**Max. Payload** [mt]	**Total Suspended** [mt]
Main	Tandem lift	10	30	82	122
Main	Single / Twin lift	10	15	70	95
Secondary	Single / Twin lift	5	15	70	90

3.5 Operational Speeds and Accelerations

The Quad Trolley STS crane concept does not primarily aim to increase individual motion speeds beyond those of contemporary high-performance STS cranes. Instead, productivity gains are achieved through the parallelisation of container handling operations across multiple trolleys. The selected operating speeds and accelerations are therefore based on established industry practice and are treated as fixed input parameters throughout the study, ensuring that the analysis focuses on the influence of structural and dynamic characteristics rather than operational assumptions.

For the main trolleys, a travel speed of 240 m/min is adopted, consistent with the upper range of modern high-performance STS cranes [1, 28, 29]. The corresponding trolley travel acceleration is set at 1.2 m/s^2, based on a rail wheel friction coefficient of 0.12–0.15 [39, 40], which defines the maximum achievable acceleration before wheel slip occurs. The transverse drive system on the main trolleys is assigned an acceleration of 2.0 m/s^2. Unlike trolley travel along the boom, which is limited by wheel–rail traction, the transverse motion is directly actuated and is therefore not governed by traction constraints but by actuator capacity and structural limitations. The selected value of 2.0 m/s^2 is adopted as a design assumption for this study, reflecting the relatively low actuated mass (primarily the sheave block) and the direct nature of the actuation mechanism, and has been confirmed as achievable in principle through discussions with Huisman engineering [41]. A detailed actuator sizing is outside the scope of this thesis.

The secondary trolleys operate at a lower travel speed of 180 m/min, reflecting their shorter travel distances and operational role within the handling workflow. A travel acceleration of 0.8 m/s^2 is adopted, somewhat lower than that of the main trolleys given the considerably higher mass of the secondary trolley system.

Hoisting is assigned a speed of 90 m/min under full load conditions and up to 180 m/min when unloaded, with an acceleration of 0.5 m/s^2, providing efficient vertical transport without introducing excessive loading into the structure. Gantry travel is assigned a speed of 45 m/min with an acceleration of 0.25 m/s^2, consistent with typical industry practice [1, 28, 29]. All reference values are summarised in Table 5.

Table 5: Reference speeds and accelerations for crane motions

Motion	**Value**
Trolley travel speed	240 m/min
Trolley travel acceleration	1.2 m/s^2
Trolley transverse acceleration	2.0 m/s^2
Secondary trolley travel speed	180 m/min
Secondary trolley travel acceleration	0.8 m/s^2
Gantry travel speed	45 m/min
Gantry acceleration	0.25 m/s^2
Hoisting speed (full load)	90 m/min
Hoisting speed (empty)	180 m/min
Hoisting acceleration	0.5 m/s^2

3.6 Comparison with Conventional STS Cranes

In many respects, the Quad Trolley STS crane retains the defining characteristics of conventional STS cranes. The overall structural form, load-bearing mechanisms, and interaction with vessels and terminal infrastructure remain largely unchanged. This continuity supports feasibility and integration into existing port environments, and balances increased operational capability and productivity with controlled structural complexity and cost-effective development.

The most significant departure from conventional practice is the introduction of multiple coordinated trolleys operating in parallel. Rather than a single trolley performing sequential container handling cycles, the Quad Trolley configuration distributes handling

tasks across four trolleys, enabling parallel operation and substantially increasing potential throughput without increasing individual motion speeds or lifting capacities.

This parallel operation alters the structural loading conditions of the crane. Multiple simultaneously moving masses introduce more complex load distributions, and concurrent trolley operations can result in increased local and global structural demands. Accommodating these loads within the conventional 27 m width constraint places additional requirements on quay loading and global stability, and forms one of the central feasibility questions addressed in this study.

From a dynamic perspective, the interaction between multiple moving subsystems adds complexity that is not present in conventional cranes. The dynamic response of the structure is no longer governed by a single trolley–payload system, but by several coupled motions that may influence each other through the flexible structure, potentially affecting positioning accuracy and disturbance rejection performance.

The transverse drive on the main trolleys represents the most novel mechanical feature of the concept. By enabling controlled transverse displacement of each trolley independently, small transverse positioning corrections can be made without moving the entire crane, reducing the associated inertia loads and energy demand considerably. In addition, the direct nature of the actuation, in which the control force is applied locally at the trolley rather than through the full crane structure, has the potential to improve transverse positioning performance compared to conventional gantry-based actuation. Since this feature has no direct equivalent in conventional STS cranes, and no prior literature on its structural and dynamic implications could be identified, a dedicated evaluation is required.

The structural and dynamic implications of these differences form the basis of the analyses presented in the following chapters, starting with the methodology outlined in Chapter 4.

4 Methodology

This chapter outlines the methodology used to evaluate the structural and dynamic feasibility and performance of the Quad Trolley STS crane concept under representative operating conditions. The aim is to provide a clear and systematic framework for analysing the behaviour of the crane and for assessing its performance in comparison with a conventional STS crane. The chapter first describes the overall research approach, then explains the modelling strategy adopted, and finally presents the integrated simulation and analysis workflow that links the structural and dynamic analyses.

4.1 Overview of the Research Approach

The methodology consists of four main components that together link the structural behaviour of the crane to its dynamic performance. First, a literature review is conducted to establish the theoretical background on conventional STS crane design, structural and dynamic behaviour, and control and damping strategies, while also providing a reference framework for the Quad Trolley concept. Second, a global finite element (FE) model is constructed to assess the global structural response of the crane. Third, a dynamic model is formulated to represent the motion of the trolley–payload system and to evaluate its behaviour under different operating scenarios. Finally, an integrated simulation and analysis workflow is applied, in which the structural properties obtained from the FE model are used within the dynamic model to assess performance and identify limiting factors. The reasoning behind this two-model decomposition is described in Section 4.2, and the workflow itself is detailed in Section 4.3.

4.2 Modelling Strategy

The crane is analysed using two complementary models rather than a single fully coupled model. A fully coupled model of the complete structure and its dynamic behaviour would require substantial computational effort, and would limit the ability to perform systematic design studies in which structural and operational parameters are varied to explore their influence on system performance. Separating the structural and dynamic analyses avoids these limitations and allows each to be modelled at a level of detail appropriate to its role.

Within this approach, the FE model is used to capture the global structural characteristics of the crane, including stiffness, mass distribution, and modal behaviour, as well as to verify the structure against the relevant design standards. The dynamic model, in turn, represents the essential motion of the trolley–payload system and is formulated at a lower level of detail, retaining only those structural properties that are relevant for the dynamic response. This decomposition preserves the dominant physical effects in each domain while avoiding unnecessary modelling complexity.

The two models are coupled in a sequential manner. Structural properties obtained from the FE model, in particular global stiffness and modal characteristics, are used as input for the dynamic model. This sequential coupling provides a direct link between the structural design and the dynamic behaviour of the system, allowing the influence of structural properties on dynamic performance to be evaluated in a controlled and transparent manner.

The resulting strategy preserves a clear relationship between structural design parameters and the dynamic response of the system, while keeping the analysis straightforward and computationally manageable. It provides a suitable framework for assessing the structural and dynamic performance of the Quad Trolley STS crane concept and for comparing it with the conventional STS crane configuration used as a reference case.

4.3 Integrated Simulation and Analysis Workflow

The structural and dynamic models are combined in a sequential and iterative workflow that assesses the structural feasibility and dynamic performance of the Quad Trolley STS crane concept under representative operating conditions, identifies the parameters that govern its behaviour, and enables a direct comparison with a conventional single-trolley STS crane used as a reference case. The same workflow is applied to both configurations, ensuring that any observed differences can be attributed to the crane concept itself rather than to differences in modelling or evaluation methodology. The overall workflow is illustrated schematically in Figure 19.

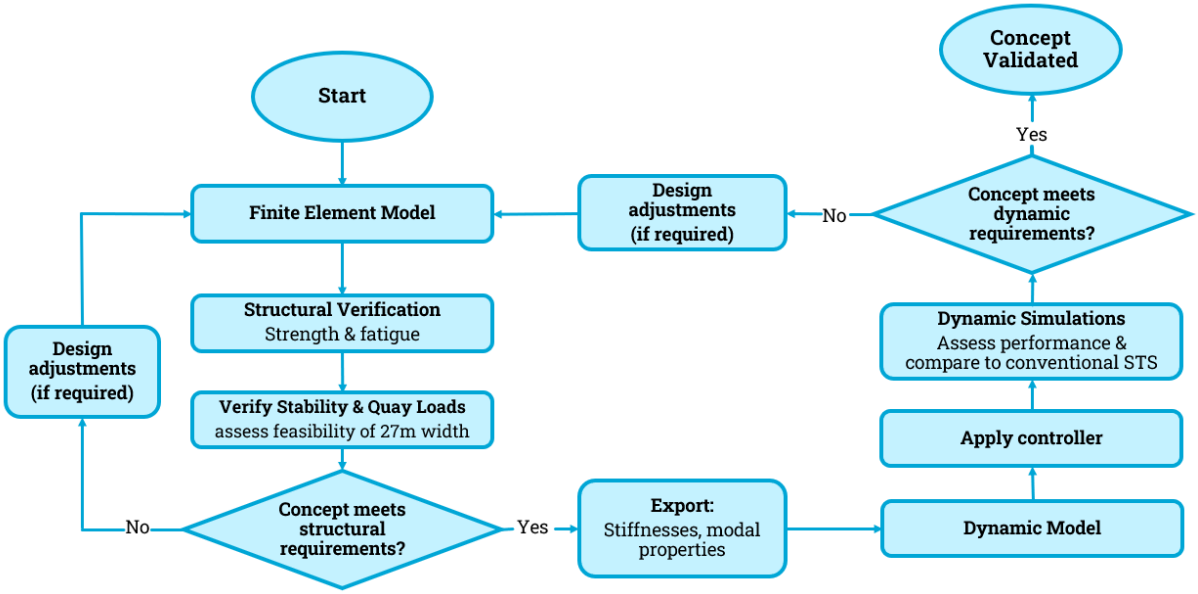

Figure 19: Schematic overview of the integrated simulation and analysis workflow for the Quad Trolley STS crane concept

The workflow starts with the development of the finite element (FE) model, which represents the global structural behaviour of the crane and forms the basis for the structural assessment. The FE model is used to verify the structure against the relevant design standards, including checks on strength, fatigue, and stability. The verification process yields the minimum plate thicknesses required for a safe and code-compliant structure, together with a representative structural weight that is used in the comparison with the conventional configuration. In addition, the FE model is used to evaluate operational aspects such as quay loading and global stability, which are essential for determining the feasibility of the considered crane configuration and for assessing whether the conventional 27 m buffer-to-buffer width constraint can be maintained.

Following structural verification, the structural properties that govern the dynamic response of the system are extracted from the FE model. These include the global stiffness characteristics and modal properties of the crane, which are used as input for the dynamic model. In this way, the structural design and the operational behaviour of the crane are directly linked, allowing the influence of structural flexibility on the dynamic response to be evaluated within a consistent framework.

The dynamic model is then used to simulate the behaviour of the trolley–payload system under various operating scenarios. A suitable control strategy is applied to evaluate the ability of the system to achieve accurate positioning and to suppress load sway in the presence of disturbances. Performance is assessed primarily on the basis of positioning accuracy of the load, expressed as the tracking error, while the required actuator effort is evaluated as a constraint to ensure that the obtained performance remains achievable within realistic system limits. Equivalent simulations are performed for the conventional STS crane configuration using the same modelling assumptions and evaluation criteria, providing a consistent basis for comparison.

Based on the simulation results, the dynamic performance of the crane is evaluated against predefined performance requirements and compared with that of the conventional STS crane configuration. If the system meets the performance criteria, the corresponding structural configuration is considered feasible. If the performance is insufficient, the results are used to identify the governing limitations, such as insufficient structural stiffness or unfavourable dynamic characteristics, and the workflow allows for iterative refinement of the design. Structural parameters can be adjusted in the FE model, for example by modifying stiffness distributions or introducing additional structural elements, after which the updated structural properties are reintroduced into the dynamic model and the performance evaluation is repeated. This iterative loop ensures that the final structural configuration not only satisfies the structural design requirements, but also delivers the dynamic performance required for feasible and controllable operation of the crane, while allowing its performance to be assessed in relation to a conventional reference.

5 Finite Element Model

The finite element model is developed to evaluate the global structural behaviour of the Quad Trolley STS crane, capturing the overall mass distribution, stiffness characteristics, and modal properties of the structure. The focus is placed on global behaviour rather than local stress concentrations or detailed joint modelling, which is sufficient for the purposes of this study.

Within the scope of this research, the model serves four main roles. First, it forms the basis for structural verification in accordance with EN 13001, including checks on strength, fatigue, and stability. Second, it is used to assess the global stability of the crane under operational and storm load cases. Third, quay loading is evaluated by determining the reaction forces at the crane supports. Finally, the model provides the global mass, stiffness, and modal properties of the structure, which are subsequently used as input for the dynamic model developed in MATLAB.

As such, the finite element model establishes a direct link between structural design choices and their influence on dynamic performance, forming the basis for both the structural assessment and the dynamic controllability analysis presented in the following chapter.

5.1 Model Description

5.1.1 Model Type

The crane structure is modelled using a beam-element finite element model developed in ANSYS. Beam elements are selected to efficiently represent the large-scale structural behaviour while capturing the dominant global response of the system, allowing for accurate representation of the primary load-bearing components while maintaining a manageable model size and computational effort. Given the focus of this study on global structural behaviour and dynamic characteristics, this level of detail is sufficient without resorting to full detailed modelling of individual structural components.

Element sizes are defined such that the beam element length does not exceed 2 m, ensuring adequate resolution of the structural geometry and global deformation behaviour.

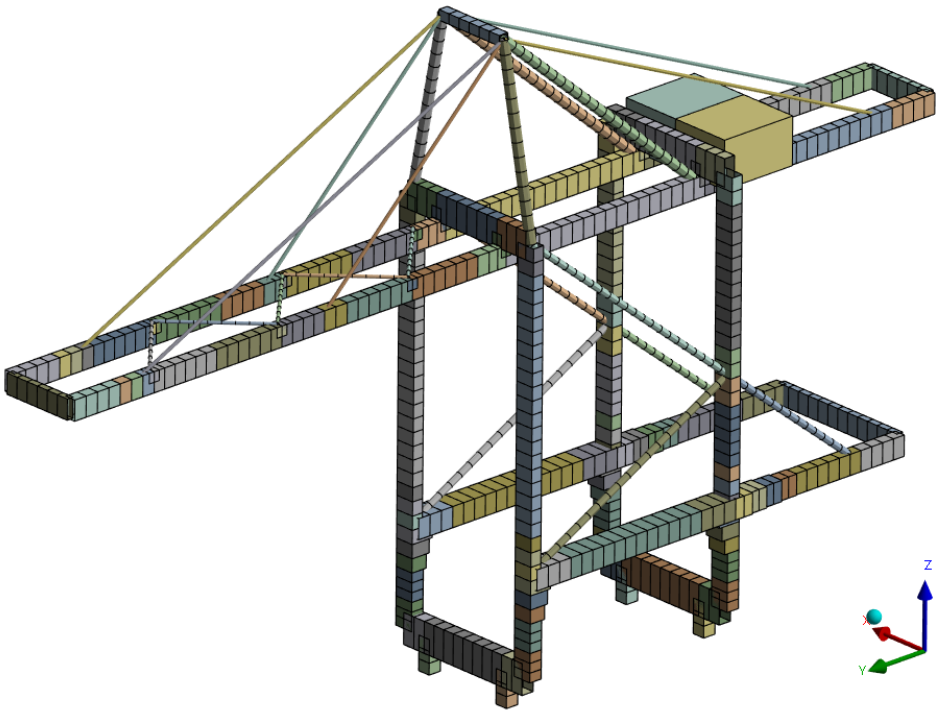

Figure 20: FEM model, showing beam elements and mesh sizing

5.1.2 Geometry Idealisation

The primary structural components of the crane are modelled as elements defined along their centrelines. This idealisation reduces the three-dimensional structure to a line model while preserving the global geometry and load paths of the crane structure.

As a result, the model captures global structural behaviour, including overall stiffness, mass distribution, and dominant vibration modes, while local effects such as joint flexibility, stress concentrations, and plate-level behaviour are not explicitly represented.

Non-structural components are similarly not modelled explicitly, but are accounted for through equivalent loads and mass contributions, as will be described in Section 5.2.

This modelling approach ensures that the global stiffness and mass distribution remain representative of the actual crane structure, while avoiding unnecessary model complexity.

5.1.3 Material Properties

All structural components are modelled using structural steel grade S355 with linear elastic material behaviour. The material properties used in the model are summarised in Table 6.

Table 6: Material properties of structural steel S355.

Property	**Symbol**	**Value**
Young's modulus	E	210 GPa
Poisson's ratio	ν	0.3
Density	ρ	7850 kg/m^3
Yield strength	f_y	355 MPa
Ultimate tensile strength	f_u	510 MPa

5.2 Mass Modelling

5.2.1 Non-Structural Mass Estimation

To account for structural details not explicitly modelled in the beam element representation, such as stiffeners, section plates, and joint reinforcements, a mass correction factor of 1.25 is applied to the structural steel density. These details contribute significantly to the total mass of the crane but are not directly represented in the simplified geometry. This correction ensures that the total mass and its distribution remain representative of a realistic crane configuration.

Certain components with a significant and well-defined mass and location are modelled explicitly in the finite element model. In particular, the machine house is included using its actual geometry and a dedicated material density, resulting in a total mass of approximately 230 mt. The bogies are similarly represented using beam elements with a representative height corresponding to their physical geometry, with a dedicated material density assigned such that each bogie has a total mass of approximately 78 mt. The mass values for both components are based on reference data from existing Huisman crane designs, scaled to match the dimensions and capacity of the present concept.

In addition to these components, a number of other non-structural mass contributions are accounted for separately, as described below.

Rail Systems:
The rail systems for both the main and secondary trolleys are explicitly accounted for due to their significant contribution to the overall mass and their influence on the mass distribution of the crane.

The wheel loads are first estimated to determine the required rail section. The wheel load is approximated as the total load on the trolley divided by the number of wheels:

$$F_{\text{wheel}} = \frac{m_{\text{trolley}} + m_{\text{load, full}}}{n_{\text{wheels}}} \tag{1}$$

For the main trolleys, this results in:

$$F_{\text{wheel}} = \frac{30 + 122}{4} = 38 \text{ mt per wheel} \tag{2}$$

For the secondary trolleys, the corresponding wheel load is:

$$F_{\text{wheel}} = \frac{100 + 90}{4} = 47.5 \text{ mt per wheel} \tag{3}$$

Based on these loads, an A100 rail section is selected for both systems, with a mass of 74.3 kg/m [42, 43].

For the main trolley rails, the rail is supported by a T-profile mounted on the boom girder, with the rail seated on top of the T-profile. A T-profile of 500×500 mm is adopted, with a flange thickness of 30 mm and a web thickness of 20 mm. This results in an approximate mass of 196.25 kg/m for the supporting structure. Including the rail, the total mass is approximately 270 kg/m.

Over an estimated total boom and girder length of 150 m and two rails, this results in a total mass of approximately 81 mt.

For the secondary trolley rails, which are located on top of the cross girder, a simpler support configuration is used. The rails are supported by a plate of 500×30 mm, resulting in a mass of approximately 117.75 kg/m for the supporting structure. Including the rail, the total mass is approximately 192 kg/m.

Over a total length of 65 m and two rails, this results in a total mass of 25 mt.

Both rail systems are applied in the finite element model as equivalent distributed loads along the corresponding structural members, ensuring their contribution to the mass distribution is accurately represented.

Access and Auxiliary Components:
A range of access structures and auxiliary components are included based on reference data from existing Huisman STS crane designs of comparable size. These include platforms, walkways, conductor bars, drag chains, staircases, cable reels, sheaves, and twistlock stations. Rather than modelling these elements explicitly, their mass is applied as equivalent static loads at representative locations, introduced as either point loads or distributed loads depending on the physical distribution of each component. The mass contributions of these components are summarised in Table 7.

Table 7: Access and auxiliary mass contributions.

Component	**Total Mass [mt]**
Twistlock station (waterside)	50
Twistlock station (landside)	50
Main girder – access, conductor bars, drag chain	30
Boom – access, conductor bars, drag chain	22
Boom – boom hoist sheaves	6
Landside leg – staircase and elevator	14
A-frame – access and boom hoist sheaves	26
Lower frame – access and cable reel	26
Total	**224**

5.3 Boundary Conditions and Supports

The boundary conditions of the finite element model are defined to represent the support of the crane on the quay through its bogie system. The crane is supported on rails at both the landside and waterside, which provide vertical load transfer and lateral guidance to the structure.

At each support location, vertical translations are constrained to represent the load-bearing function of the rails and quay structure. Horizontal translations in the trolley travel direction are constrained to reflect the lateral guidance provided by the rail system. In the gantry travel direction, only one side of the crane is constrained in the horizontal direction, while the opposite side remains free. This approach prevents rigid body motion while avoiding over-constraint, allowing the structure to deform realistically under load. The applied boundary conditions are illustrated in Figure 21.

All rotational degrees of freedom at the supports are left unconstrained, enabling the structure to develop natural bending behaviour and avoiding artificial stiffening that could otherwise lead to an overestimation of global stiffness and natural frequencies.

The compliance of the quay structure and rail system is not modelled explicitly. Instead, the supports are assumed to be rigid in the constrained translational directions, which is considered appropriate given the focus of the model on global structural behaviour.

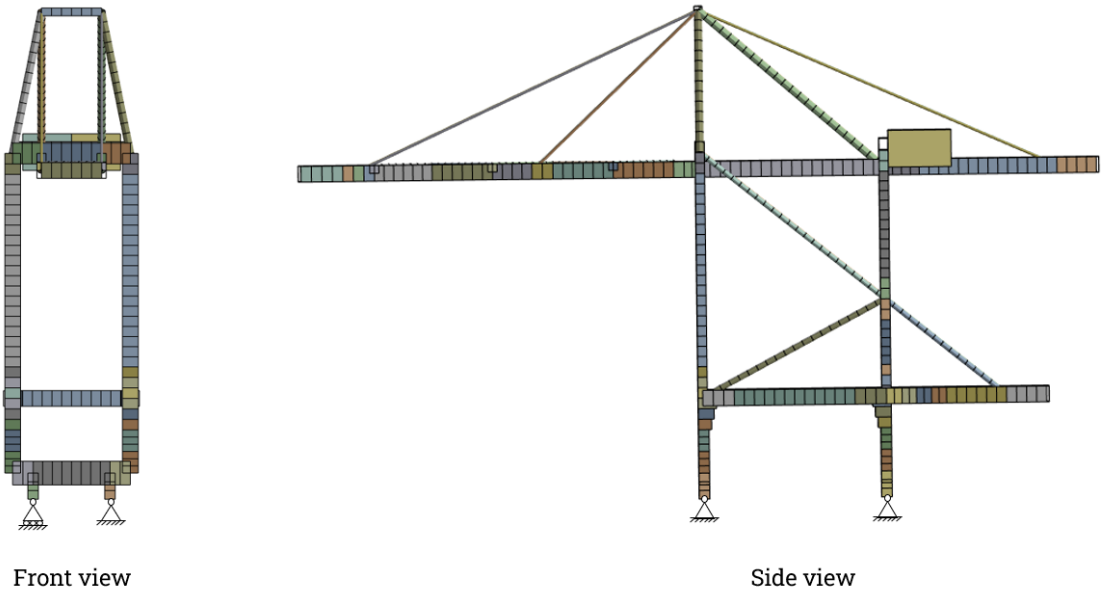

Figure 21: Depiction of constraints used in FEM model

5.4 Load Modelling

The loading of the crane is defined in accordance with EN 13001-2 [14] and EN 15011 [44]. EN 13001 provides the general framework for crane structural verification, including load combinations, safety factors, and stability checks, while EN 15011 provides the specific load modelling and dynamic factors applicable to bridge and gantry cranes.

The primary loads considered are gravitational loads, payload loads, wind loads, and inertial loads resulting from crane and trolley accelerations.

Gravitational loads of the structural components are modelled through a body acceleration applied to the structure in ANSYS. Additional non-structural masses that are not explicitly modelled are represented by equivalent forces applied to the structure, as described in Section 5.2.

An initial set of main trolley positions covering the full operational range of the crane is considered. This includes positions along the entire boom, from backreach to outreach, in order to capture all possible loading configurations.

From this initial set, a reduced number of positions is selected based on their relevance for governing structural response. Not all trolley locations result in critical loading conditions, as many positions lead to similar structural behaviour or lower load effects.

The selected positions are chosen to represent critical loading conditions for specific structural components. For example, trolley positions near full outreach govern the loading in the front forestays, boom tip and waterside portal, while intermediate positions govern the loading of the corresponding boom sections. The remaining positions are similarly selected to capture the governing load conditions for other structural members.

The main trolleys are assumed to operate at a minimum spacing of 10 m. Given the beam element discretisation with a maximum element length of 2 m, this corresponds to a spacing of five element positions. This discretisation is used to define the relative positions of the two main trolleys in the considered load cases.

By selecting a representative subset of trolley positions that incorporates this spacing constraint, the number of load cases is reduced while ensuring that all governing structural effects are captured. The final set of positions used in the analysis is illustrated in Figure 22.

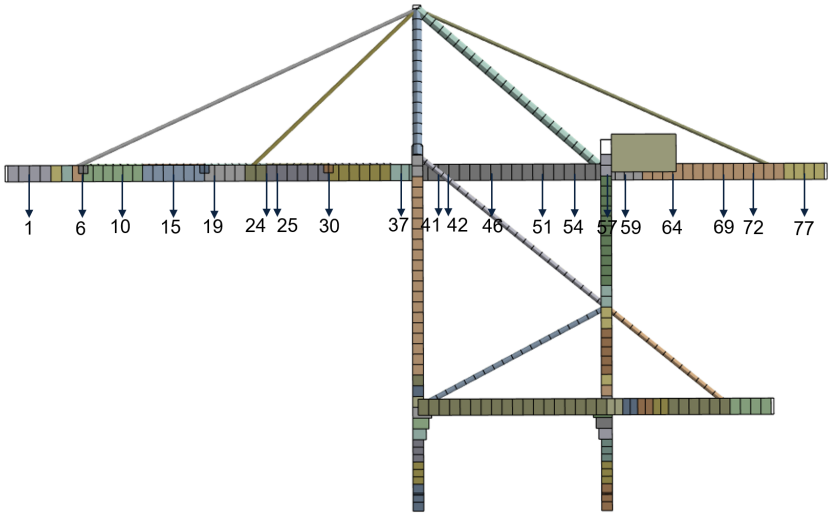

Figure 22: Selected main trolley positions used for structural analysis

A similar approach is applied to the secondary trolleys, which operate along the cross girder between the crane legs. An initial set of positions covering the full operational range is considered, from which a reduced subset is selected based on governing structural effects.

The final set of secondary trolley positions used in the analysis is illustrated in Figure 23.

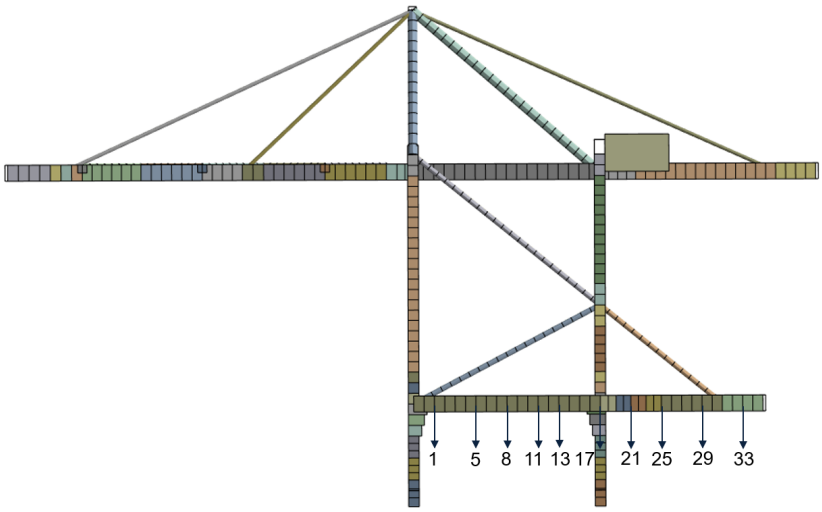

Figure 23: Selected secondary trolley positions used for structural analysis

In addition, inertial loads resulting from trolley accelerations are included in the analysis. These inertial forces arise from longitudinal trolley travel for both the main and secondary trolleys, as well as from transverse accelerations of the main trolleys.

The inertial loads are applied at all considered trolley positions described above. For each position, both positive and negative acceleration directions are evaluated.

Gantry travel acceleration is modelled as a body acceleration applied to the entire crane structure, with additional inertial loads applied at the trolley locations to account for the mass of the trolleys themselves. Since the trolleys are unloaded during gantry travel, the inertial loads at the trolley locations are reduced compared to operational load cases involving trolley transverse motion.

Wind loads are applied in accordance with EN 13001 using the wind load implementation available in SDC Verifier. The drag coefficients are determined automatically by the software based on the cross-sectional properties of the structural components, in accordance with the classifications provided in the standard, as illustrated in Figure 24.

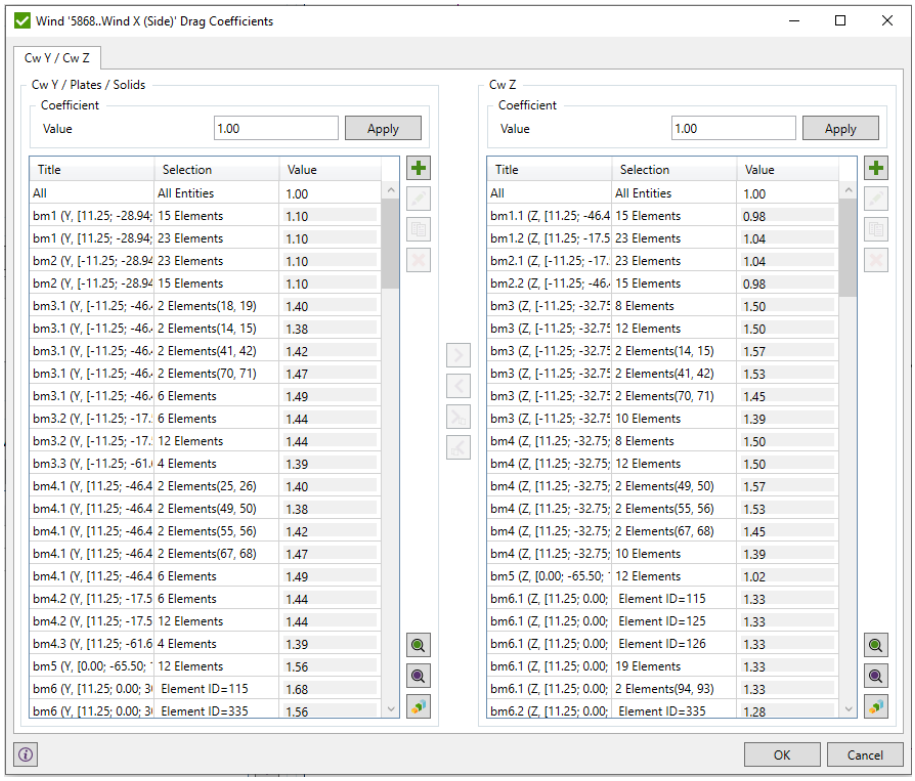

Figure 24: Excerpt of drag coefficient (C_d) values automatically generated by SDC Verifier in accordance with EN 13001.

A mean wind pressure of 250 Pa is adopted, corresponding to a 3-second mean gust velocity of 20 m/s [14]. The resulting wind loads are applied based on the defined geometry, projected areas, and corresponding drag coefficients.

In addition, an out-of-service storm load case is considered, based on EN 13001. The equivalent static wind pressure is calculated as:

$$q(z) = 0.5\,\rho\,v(z)^2 \tag{4}$$

where $\rho = 1.25$ kg/m^3 is the air density. The wind velocity at height z is given by:

$$v(z) = f_{\text{rec}} \left(\frac{z}{10}^{0.14} + 0.4 \right) v_{\text{ref}} \tag{5}$$

For this study, a recurrence factor corresponding to $R = 25$ years is adopted, resulting in $f_{\text{rec}} = 0.9463$, and a reference wind velocity of $v_{\text{ref}} = 28$ m/s is used, corresponding to region C as described by EN13001 [14].

The resulting height-dependent wind velocity is used to determine the corresponding wind pressure distribution over the crane structure, which is subsequently applied as an out-of-service storm load case with the boom up. The corresponding storm pressure as a function of height is depicted in Figure 25.

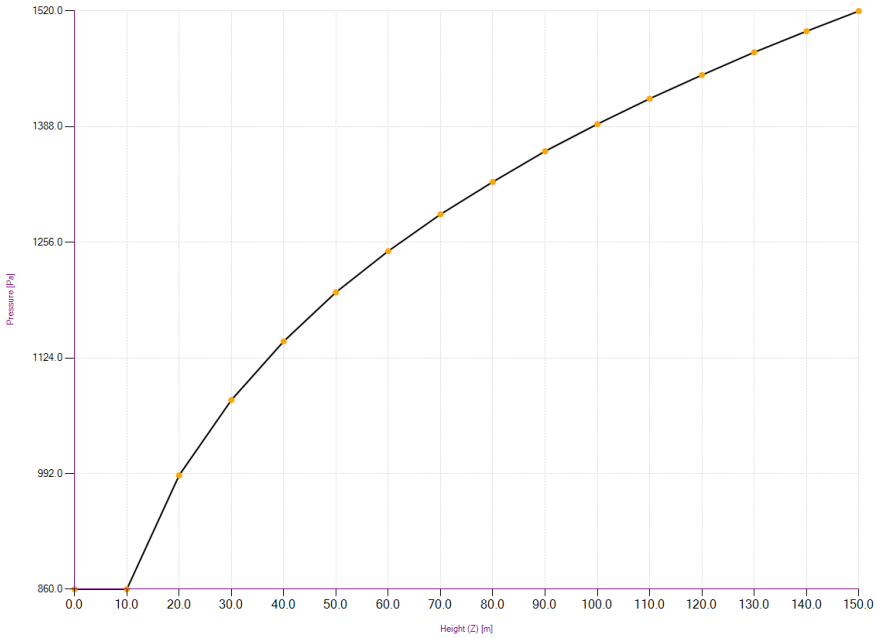

Figure 25: Storm wind pressures as a function of height

For the present study, the resulting wind and storm loads are reduced by 20% to account for shielding effects between structural components, which are not adequately captured in the standard calculation. Research has shown, through wind tunnel testing and computational fluid dynamics on STS cranes, that shielded structural members experience substantially lower aerodynamic loads than those obtained from standard calculations, as mutual shielding between elements in both the longitudinal and lateral directions is not sufficiently accounted for in current standards [45]. The applied reduction provides a representative yet conservative estimate of the effective wind loading.

A complete overview of the applied loads and their magnitudes is provided in Appendix B.

5.4.1 Load Combinations

The load combinations used for structural verification are defined in accordance with EN 13001-2 [14]. The standard specifies a range of load combinations that account for different operational and environmental conditions, including regular operation, wind loading, and exceptional events.

For the present study, three load combinations are considered. Load combination A3 represents the most critical operational scenario in the absence of wind, capturing the effects of payload, inertial loads from crane and trolley motions, and the associated dynamic factors. This load combination is used for both strength and fatigue verification. Load combination B3 extends this by including in-service wind loading and is used for strength verification only. In addition, load combination C2 represents out-of-service storm conditions with the boom in the raised position and is used for both strength verification and the storm stability assessment.

The applied partial safety factors and dynamic factors are taken from EN 13001-2 [14] and EN 15011 [44] for the selected load combinations. An overview of the load combinations and corresponding factors is shown in Figure 26.

Categories of loads	Loads f_i		Ref.	Load combinations A					Load combinations B						Load combinations C												
				Factor γ_p	A1	A2	A3	A4	Factor γ_p	B1	B2	B3	B4	B5	Factor γ_p	C1	C2	C3	C4	C5	C6	C7	C8	C9	C10	C11	C12
Regular	Gravitation acceleration and impact actions	Mass of the crane	4.2.2.1	a	ϕ_1	ϕ_1	1	–	a	ϕ_1	ϕ_1	1	–	–	a	ϕ_1	1	ϕ_1	1	1	1	1	1	1	1	1	1
		Mass of the hoist load	4.2.2.2 4.2.2.3	1,34	ϕ_2	ϕ_3	1	–	1,22	ϕ_2	ϕ_3	1	–	–	1,1	ϕ_{2C}	η_W	–	1	1	1	ϕ_L	ϕ_9	1	1	–	–
		Travelling on uneven surface	4.2.2.4	1,22	–	–	–	ϕ_4	1,16	–	–	–	ϕ_4	ϕ_4	–	–	–	–	–	–	–	–	–	–	–	–	–
		Vessel inclinations and accelerations[c]	4.2.2.7	1,34	1	1	1	1	1,22	1	1	1	1	1	1,16	1	–	–	1	1	1	1	1	1	1	1	–
	Acceleration actions from drives	Hoisting movements excluded	4.2.2.5	1,34	ϕ_5	ϕ_5	–	ϕ_5	1,22	ϕ_5	ϕ_5	–	ϕ_5	–	1,1	–	–	ϕ_5	–	–	–	–	–	–	–	–	–
		All movements			–	–	ϕ_5	–		–	–	ϕ_5	–	–		–	–	–	–	–	–	–	–	–	–	–	–
	Displacements		4.2.2.6	b	1	1	1	1	b	1	1	1	1	1	b	1	1	1	1	1	1	1	1	1	1	1	1
	Relative vessel motions		4.2.2.7.4	1,34	1	1	–	–	1,22	1	1	–	–	–	1,16	1	–	–	–	1	1	1	1	1	1	–	–
Occasional	Environmental effects	In-service wind loads	4.2.3.1	–	–	–	–	–	1,22	1	1	1	1	1	1,16	–	–	1	–	–	–	–	–	–	–	1	–
		Snow and ice loads	4.2.3.2	–	–	–	–	–	1,22	1	1	1	1	1	1,1	–	1	–	–	–	–	–	–	–	–	–	1
		Temperature variations	4.2.3.3	–	–	–	–	–	1,16	1	1	1	1	1	1,05	–	1	–	–	–	–	–	–	–	–	–	1
	Skewing		4.2.3.4	–	–	–	–	–	1,16	–	–	–	–	1	–	–	–	–	–	–	–	–	–	–	–	–	–
Exceptional	Out-of-service wind loads		4.2.4.2	–	–	–	–	–	–	–	–	–	–	–	1,1	–	1	–	–	–	–	–	–	–	–	–	1
	Test loads		4.2.4.3	–	–	–	–	–	–	–	–	–	–	–	1,1	–	–	ϕ_6	–	–	–	–	–	–	–	–	–
	Buffer forces		4.2.4.4	–	–	–	–	–	–	–	–	–	–	–	1,1	–	–	–	ϕ_7	–	–	–	–	–	–	–	–
	Tilting forces		4.2.4.5	–	–	–	–	–	–	–	–	–	–	–	1,1	–	–	–	–	1	–	–	–	–	–	–	1
	Drive forces due to E-stop		4.2.4.7	–	–	–	–	–	–	–	–	–	–	–	1,1	–	–	–	–	–	ϕ_5	–	–	–	–	–	–

Figure 26: Load Combinations as specified in EN13001-2 [14]

All combinations of main and secondary trolley positions are considered. For each case, all combinations of inertial loads, including both positive and negative acceleration directions, are evaluated to capture the most unfavourable loading conditions.

For the storm load case, load combination C2 is considered. In this condition, the trolleys are assumed to be stationary and unloaded, and the boom is in the raised position.

5.5 Structural Verification

5.5.1 Strength Verification

Strength verification is carried out using the limit state method in accordance with EN 13001-3-1, as implemented in SDC Verifier. The stresses resulting from the defined load combinations are evaluated and compared to the allowable limits specified by the standard.

The limit design stress is defined based on the material yield strength and the relevant resistance factors. For normal stresses, the limit design stress is given by:

$$f_{\mathrm{Rd},\sigma} = \frac{f_y}{\gamma_{\mathrm{Rm}}} \tag{6}$$

For shear stresses, the corresponding limit is:

$$f_{\mathrm{Rd},\tau} = \frac{f_y}{\sqrt{3}\,\gamma_{\mathrm{Rm}}} \tag{7}$$

where f_y is the yield strength of the material and γ_{Rm} is the material resistance factor, defined in accordance with EN 13001 as:

$$\gamma_{\mathrm{Rm}} = \gamma_m \cdot \gamma_{sm} \tag{8}$$

with $\gamma_m = 1.1$ and $\gamma_{sm} = 0.95$ for rolled structural steel such as plates and profiles.

Both operational and storm load cases are considered, incorporating the appropriate dynamic and safety factors. The strength verification is performed using load combinations A3, B3, and C2 (boom up), as defined in the previous section.

5.5.2 Fatigue Verification

Fatigue verification is performed to assess the structural integrity of the crane under repeated cyclic loading over its design life. Due to the high number of load cycles associated with container handling operations, fatigue is expected to be a governing design criterion for several structural components.

A total of 2×10^6 load cycles is considered, representing the expected operational usage of the crane over its design life. One cycle is defined as the synchronous movement of the two main trolleys across the boom, which is considered representative for the dominant fatigue loading mechanism.

This choice is also consistent with conventional single-trolley STS cranes, which are typically designed for approximately 4×10^6 cycles [18]. Since the present concept employs two main trolleys operating in parallel, each cycle corresponds to two container handling events. As a result, 2×10^6 cycles for the dual main trolley system correspond to an equivalent number of container handling cycles as 4×10^6 cycles in a single-trolley configuration.

The fatigue assessment is based exclusively on load combinations corresponding to normal operational conditions (Load Combinations A) in accordance with EN 13001, as fatigue damage is primarily accumulated during regular operation. Extreme or occasional load cases are therefore not considered relevant for fatigue verification. Partial safety factors for loads are set to $\gamma_p = 1$, with relevant dynamic factors included as prescribed by EN 13001.

The fatigue load spectrum is defined based on the expected operational distribution of the main trolleys along the boom. To capture this distribution, the boom is discretised into representative trolley positions, as shown in Figure 22, with each position assigned a probability of occurrence over the design life of the crane.

For outreach operations, container positions along the vessel are assumed to be equally probable, resulting in a uniform distribution of trolley positions over the outreach region. The load distribution is defined in discrete groups, each representing 25% of the total number of cycles. For example, 25% of the cycles originate from positions 1 and 6, 10 and 15, 19 and 24, and 25 and 30, corresponding to the positions of the two main trolleys at their minimum spacing of 10 m.

During operation, the front trolley transports containers from these outreach positions to the waterside twistlock station located at position 41, while the rear trolley transports containers further to the landside twistlock station at position 57. Due to this sequential movement along the boom, cycles originating from positions further along the outreach pass through all intermediate positions before reaching the respective twistlock stations.

As a result, the number of load cycles at each position is cumulative, with positions closer to the twistlock stations experiencing the combined contribution of all upstream cycles, as illustrated in Figure 27.

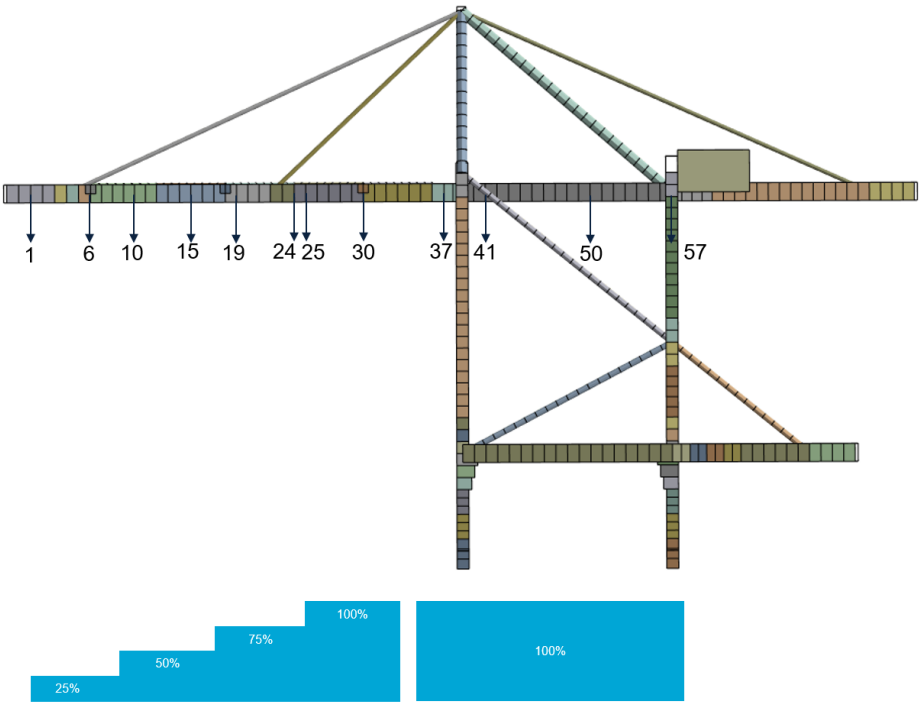

Figure 27: Cumulative distribution of fatigue cycles along the outreach region based on the operational positions of the main trolleys.

Approximately 95% of the total number of cycles follow this outreach-based distribution, including the repeated loading at the twistlock stations. The remaining 5% of the cycles (approximately 1×10^5 cycles) correspond to backreach operations. These cycles are modelled using a similar cumulative distribution approach, but also applied to the landside region of the crane, reflecting the operational movement of the trolleys during outreach to backreach handling, illustrated in Figure 28.

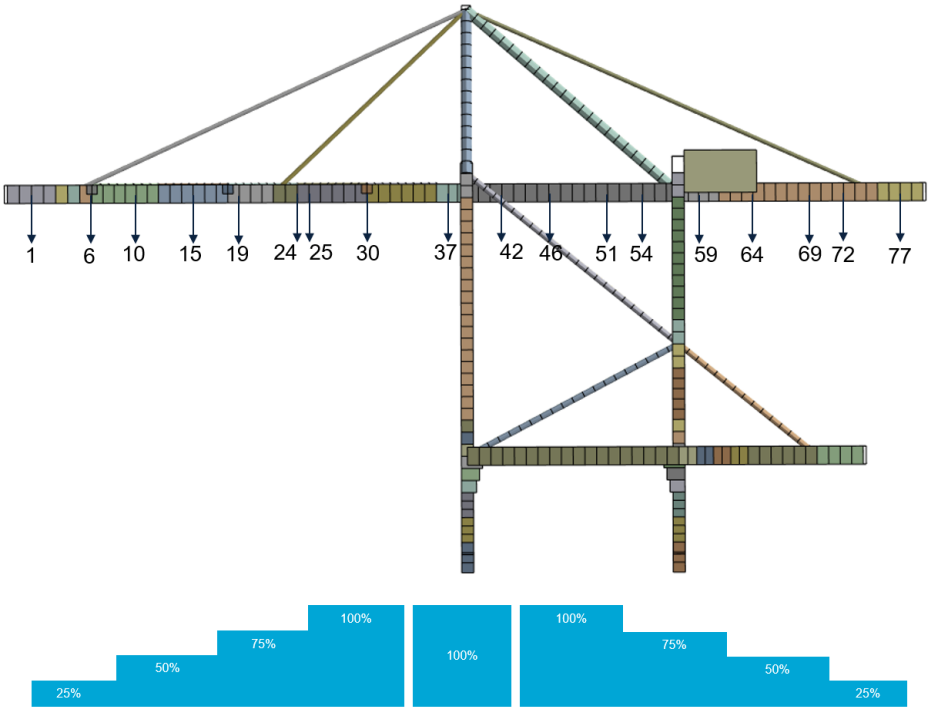

Figure 28: Cumulative distribution of fatigue cycles along the boom for both outreach and backreach operations, based on the operational positions of the main trolleys.

The adopted fatigue load distribution is a simplified representation of crane operation. In reality, container positions, trolley spacing, and handling sequences may vary, for example due to different vessel sizes. However, the present approach captures the main loading behaviour and cumulative effects along the boom, and is therefore considered sufficiently accurate for this study.

For the secondary trolleys, a simplified operational pattern is assumed. During each cycle, the trolley is assumed to move from its corresponding twistlock station to a position slightly beyond the midpoint of its travel path, illustrated in Figure 29. This simplification is considered acceptable, as the secondary trolleys are expected to have a smaller influence on the overall structural fatigue behaviour.

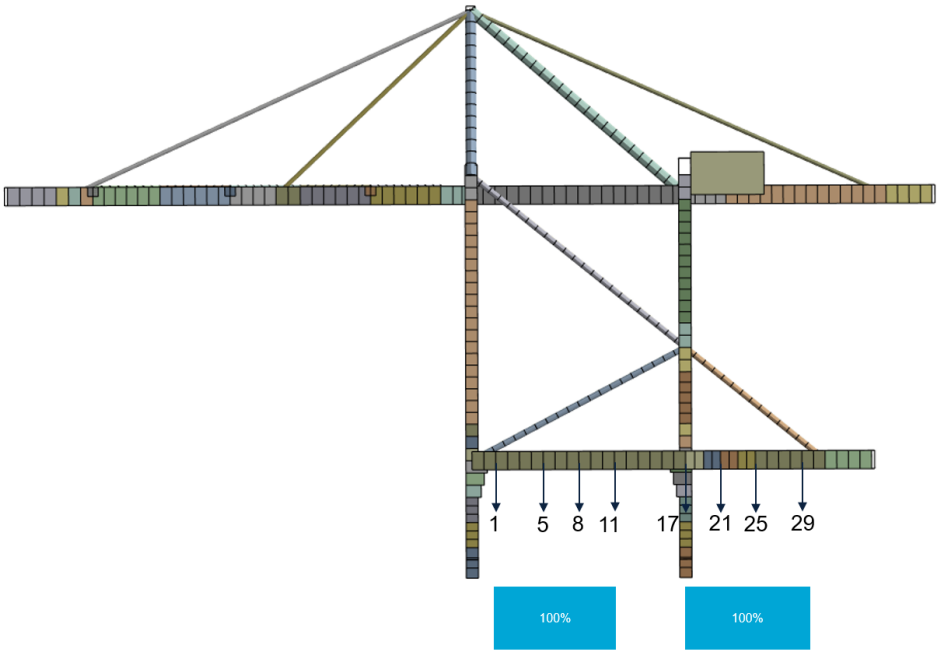

Figure 29: Simplified fatigue cycle for the secondary trolleys, assuming full (100%) occurrence of the defined operational movement.

In addition, the effect of tandem operations is considered for the secondary trolleys. It is assumed that 40% of the total cycles correspond to 40 ft tandem lifts performed by the main trolleys. Since the secondary trolleys do not perform tandem lifts, these operations are handled as two separate single lifts. As a result, the secondary trolleys experience an additional 800,000 load cycles.

The resulting fatigue load cases and the corresponding number of cycles are summarised in Table 8.

Table 8: Fatigue load cases and corresponding number of cycles

Fatigue Load Case	**Cycles**
Position 1 and 6 to 41 and 57	475 000
Position 10 and 15 to 41 and 57	475 000
Position 19 and 24 to 41 and 57	475 000
Position 25 and 30 to 41 and 57	475 000
Position 1 and 6 to 72 and 77	6 250
Position 1 and 6 to 64 and 69	6 250
Position 1 and 6 to 54 and 59	6 250
Position 1 and 6 to 46 and 51	6 250
Position 10 and 15 to 72 and 77	6 250
Position 10 and 15 to 64 and 69	6 250
Position 10 and 15 to 54 and 59	6 250
Position 10 and 15 to 46 and 51	6 250
Position 19 and 24 to 72 and 77	6 250
Position 19 and 24 to 64 and 69	6 250
Position 19 and 24 to 54 and 59	6 250
Position 19 and 24 to 46 and 51	6 250
Position 25 and 30 to 72 and 77	6 250
Position 25 and 30 to 64 and 69	6 250
Position 25 and 30 to 54 and 59	6 250
Position 25 and 30 to 46 and 51	6 250
Secondary trolley extra cycles	800 000

While the number and distribution of load cycles are now defined, the magnitude of the fatigue loading must also be specified. This is done using an equivalent load approach based on the distribution of container masses and lifting configurations.

For the main trolleys, it is assumed that 35% of the operations correspond to single lifts, while the remaining 65% correspond to tandem or twin-lift operations. These values reflect typical terminal operation. The assumed distribution of lifting configurations is summarised in Table 9.

Table 9: Distribution of lifting configurations for the main trolleys.

Definition	**% of lifts**
40’ Tandem	40%
20’ Single	5%
40’ Single	28%
45’ Single	2%
2x20’ Twin Single	25%

The container mass distribution is used to define representative load levels. The adopted distribution, shown in Table 10, represents the assumed probability of occurrence of different container masses.

Table 10: Container mass distribution used for fatigue load definition.

Mass [mt]	**Occurrence [%]**	**Mass [mt]**	**Occurrence [%]**
1	0	21	3.0
2	0.1	22	2.9
3	5.7	23	5.3
4	2.2	24	4.5
5	10.6	25	3.5
6	2.2	26	2.8
7	2.2	27	3.7
8	2.6	28	3.9
9	2.9	29	4.0
10	3.1	30	4.8
11	3.0	31	2.2
12	2.9	32	0.4
13	2.9	33	0.3
14	2.7	34	0.2
15	2.6	35	0.1
16	2.2	36	0
17	2.1	37	0
18	2.5	38	0
19	3.0	39	0
20	2.9	40	0

By combining the container mass distribution with the lifting configuration distribution, a representative fatigue load spectrum is obtained. This is expressed in terms of an equivalent fatigue load, defined as a constant-amplitude load that results in the same fatigue damage as the variable load spectrum. The formulation is based on Miner's rule, in which damage is proportional to the load raised to the power m, corresponding to the slope of the S–N curve. In this study, a value of $m = 3$ is adopted, corresponding to the S–N curve slope for welded steel details as specified in EN 13001-3-1 [46].

Based on this framework, the equivalent fatigue load for the main trolleys is formulated as:

$$M_{\text{eq,main}} = \left(\alpha_{\text{single}} \sum_i p_i (M_i + 25)^m + \alpha_{\text{double}} \sum_i \sum_j p_i p_j (M_i + M_j + 40)^m \right)^{1/m} \tag{9}$$

In this expression, the first term represents single-lift operations, where a container of mass M_i is lifted together with a combined lifting gear mass of 25 mt. The second term represents tandem or twin-lift operations, where two containers of masses M_i and M_j are lifted simultaneously together with a combined lifting gear mass of 40 mt. The factors $\alpha_{\text{single}} = 0.35$ and $\alpha_{\text{double}} = 0.65$ represent the fraction of single and double lifts, respectively. The probabilities p_i and p_j correspond to the occurrence of the container masses given in Table 10.

The double summation accounts for all possible combinations of two container masses during tandem or twin-lift operations. Raising the load to the power m reflects the nonlinear relationship between load magnitude and fatigue damage. Taking the $1/m$ power of the total expression results in a single equivalent load that produces the same accumulated damage.

This results in an equivalent fatigue load for the main trolleys of:

$$M_{\text{eq,main}} = 67.9 \text{ mt} \tag{10}$$

For the secondary trolleys, a different lifting configuration distribution is adopted. Approximately 75% of the cycles correspond to single-lift operations, while 25% correspond to twin-lift operations. The combined lifting gear mass is taken as 20 mt for all configurations. The equivalent fatigue load is given by:

$$M_{\text{eq,sec}} = \left(\alpha_{\text{single}} \sum_i p_i (M_i + 20)^m + \alpha_{\text{double}} \sum_i \sum_j p_i p_j (M_i + M_j + 20)^m \right)^{1/m} \tag{11}$$

with $\alpha_{\text{single}} = 0.75$ and $\alpha_{\text{double}} = 0.25$. This results in:

$$M_{\text{eq,sec}} = 44.8 \text{ mt} \tag{12}$$

The equivalent fatigue loads defined above are used to represent the magnitude of the applied loads in the fatigue load cases. Combined with the previously defined cycle distribution, these loads are translated into stress ranges in the structural model, forming the basis for the fatigue assessment.

The fatigue assessment is carried out in accordance with EN 13001-3-1 [46], as implemented in SDC Verifier. The software provides two approaches: the direct use of stress history method and a simplified method. In this study, the direct use of stress history method is adopted, as it allows the full stress range distribution over the design life to be taken into account.

The stress history parameter s_m is determined based on the stress spectrum and is defined as:

$$s_m = \nu \cdot k_m \tag{13}$$

with

$$k_m = \sum_i \left(\frac{\Delta\sigma_i}{\Delta\hat{\sigma}} \right)^m \frac{n_i}{N_t} \tag{14}$$

and

$$\nu = \frac{N_t}{N_{\text{ref}}} \tag{15}$$

where ν is the relative total number of occurrences of stress ranges, k_m is the stress spectrum factor dependent on m, $\Delta\sigma_i$ is the stress range for load case i, $\Delta\hat{\sigma}$ is the maximum stress range, n_i is the number of occurrences of stress range i, N_t is the total number of stress cycles during the design life, N_{ref} is the reference number of cycles, and m is the slope constant of the S–N curve.

The fatigue resistance is defined using the fatigue strength specific resistance factor γ_{mf}. This factor depends on the accessibility of the detail for inspection and the consequences of failure. The values defined in EN 13001 are summarised in Table 11.

Table 11: Fatigue strength specific resistance factor γ_{mf} according to EN 13001

Accessibility for inspection	**Fail-safe detail**	**Non fail-safe detail**	
		Without hazard for persons	With hazard for persons
Detail accessible without disassembly	1.00	1.05	1.15
Detail accessible by disassembly	1.05	1.10	1.20
Non-accessible detail	N/A	1.15	1.25

In this study, a value of $\gamma_{\text{mf}} = 1.15$ is adopted. The considered structural details are accessible without disassembly, but failure of these details may pose a hazard to persons. This is considered appropriate, as the crane operates above vessels and quay areas where personnel may be present, and personnel may also be present on the twistlock stations during operation.

The limit design stress range for fatigue is defined as:

$$\Delta\sigma_{\text{Rd}} = \frac{\Delta\sigma_c}{\gamma_{\text{mf}}\, s_m^{1/m}} \tag{16}$$

where $\Delta\sigma_c$ is the characteristic fatigue strength and s_m is the stress history parameter.

The fatigue verification is carried out by comparing the applied stress ranges to the corresponding design resistance. For combined normal and shear stresses, the following interaction criterion is used:

$$\left(\frac{\Delta\sigma_{\text{Sd}}}{\Delta\sigma_{\text{Rd}}}\right)^2 + \left(\frac{\Delta\tau_{\text{Sd}}}{\Delta\tau_{\text{Rd}}}\right)^2 \leq 1 \tag{17}$$

This interaction criterion accounts for the combined influence of cyclic normal and shear stresses, particularly in regions where both bending and shear contribute to fatigue loading.

The fatigue strength of structural details is determined based on notch classes in accordance with EN 13001.

A notch class defines the characteristic fatigue strength $\Delta\sigma_c$ of a structural detail at a reference number of 2×10^6 cycles. It represents the cyclic stress range associated with the fatigue resistance of the detail under constant amplitude loading. The value is defined based on a probability of survival of 97.7%, corresponding to a mean value minus two standard deviations, as illustrated in Figure 30.

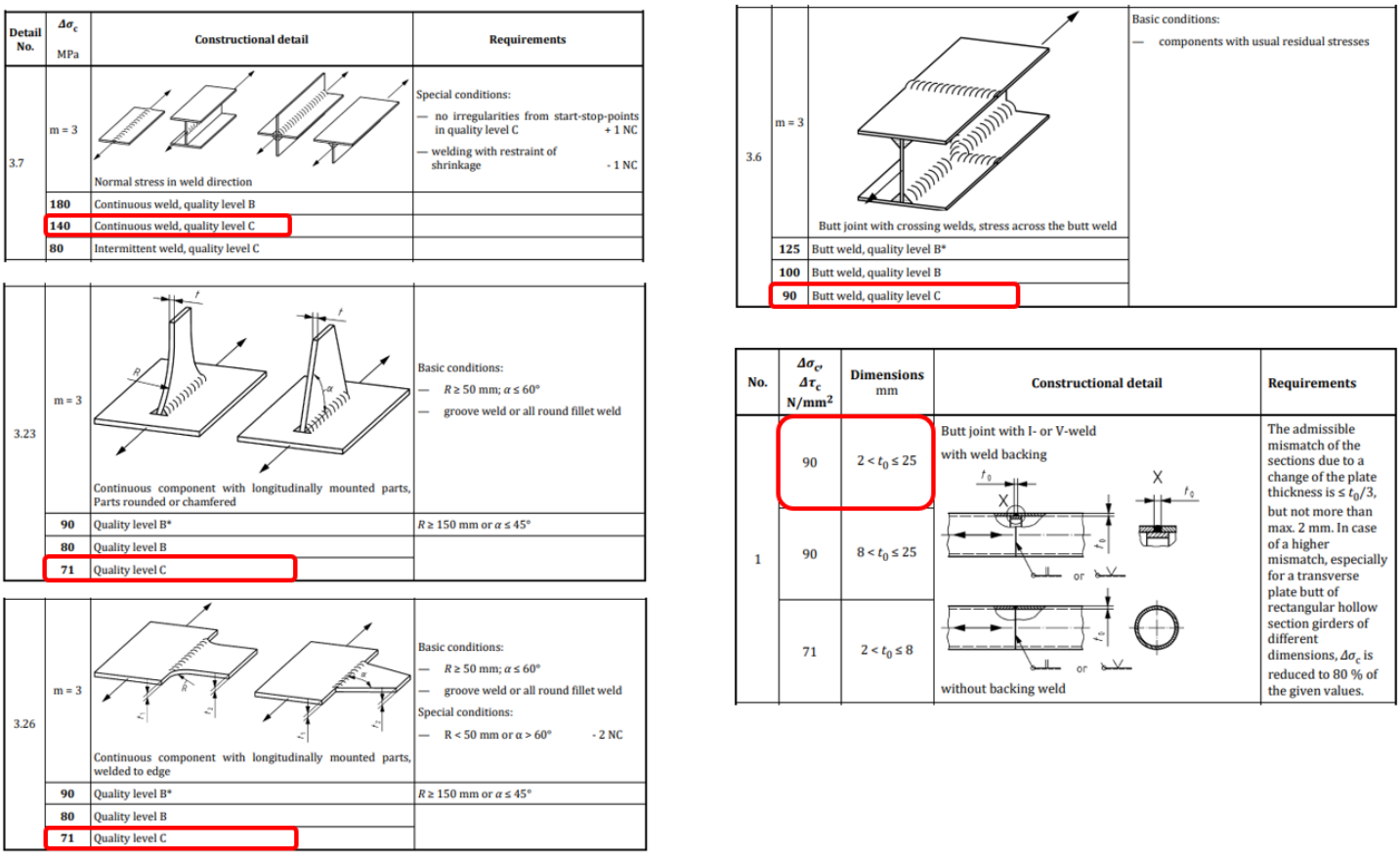

Figure 30: Selected notch classes for different structural details in accordance with EN 13001.

For continuous welded beams between joints, a notch class of $\Delta\sigma_c = 140$ MPa is adopted.

At structural joints, a lower notch class of $\Delta\sigma_c = 71$ MPa is used to account for increased stress concentrations.

For butt welds at sections, a notch class of $\Delta\sigma_c = 90$ MPa is applied. A similar value is used for stay connections.

5.5.3 Verification Approach

The structural verification is carried out using SDC Verifier, which evaluates both static strength and fatigue performance of all structural members in accordance with EN 13001. For each load case and structural detail, the software computes utilisation factors based on the relevant limit state formulations, taking into account material properties, resistance factors, and fatigue parameters. A utilisation factor below unity indicates that the structural requirement is satisfied, while a value exceeding unity indicates that the corresponding limit state is not fulfilled.

SDC Verifier enables visualisation of utilisation factors across the entire structure, where the governing utilisation over all associated load cases can be plotted in a single figure for each load combination. This allows for rapid identification of critical regions and components that require strengthening, supporting targeted and efficient structural modifications.

The design process is initiated using a minimum plate thickness of 10 mm for all structural components. From this baseline, the structure is iteratively adjusted based on the utilisation results. Structural members are locally modified by increasing cross-sections or plate thicknesses in regions where utilisation exceeds unity, and this process is repeated until all elements satisfy both strength and fatigue requirements throughout the structure. This approach ensures that material is only added where required, while the minimum plate thickness prevents unrealistically thin structural elements and ensures that the resulting design remains representative of practical industrial crane structures.

The outcome of this procedure is a baseline design that is neither over-dimensioned nor under-designed, but represents an efficient and code-compliant structural configuration, which is subsequently used as input for the dynamic analysis.

5.6 Stability Assessment

The stability of the crane is evaluated again in accordance with EN 13001. A crane supported on multiple supports is considered stable when the stabilising moment exceeds the overturning moment about any potential tipping line.

A tipping line is defined as the line passing through two adjacent effective support points of the crane. Stability must be verified for all possible tipping lines, taking into account the applied loads and corresponding safety factors.

The proof of crane stability is based on the balance of moments about the tipping line. The crane is considered stable when:

$$M_{\text{stab}} \geq M_{\text{overturn}} \tag{18}$$

where M_{stab} is the stabilising moment generated by favourable loads, and M_{overturn} is the overturning moment resulting from unfavourable loads.

In accordance with EN 13001, uplift of individual supports is permitted, provided that the crane does not overturn and the remaining supports maintain a statically determinate system. However, in the context of this study, uplift is not considered acceptable. Loss of contact between the crane supports and the rails may lead to impact loading when contact is re-established, resulting in potential damage to wheels, rails, and structural components. Therefore, stability is defined here as the absence of uplift at all supports under the considered load cases. This results in a more conservative stability criterion than the minimum requirement defined in the standard.

The stability assessment is performed using a dedicated set of load combinations, partial safety factors, and dynamic factors, as prescribed in EN 13001-2 for the proof of crane stability [14]. These combinations are specifically intended to evaluate overturning behaviour and support reactions under operational and environmental loading. An overview of the applied load combinations and corresponding factors is shown in Figure 31.

Categories of loads	Loads f_i		Load comb. A			Load comb. B		Load combinations C										
			Factor γ_p	A1	A2	Factor γ_p	B1	Factor γ_p	C2	C3	C4	C6	C7	C8	C9	C10	C11	C12
Regular	Unfavourable dead weight effects	Weight determined by calculation	1,16	1	1	1,1	1	1,05	1	1	1	1	1	1	1	1	1	1
		Weight determined by weighing[b]	1,1	1	1	1,05	1	1,0										
	Favourable dead weight effects		1,0	1	1	1,0	1	1,0	1	1	1	1	1	1	1	1	1	1
	Mass of the hoist load		1,22	1	ϕ_3	1,16	1	1,1	–	–	1[a]	1	ϕ_{ML}	ϕ_9	1	1	–	–
	Vessel inclinations and accelerations		1,22	1	1	1,16	1	1,1	–	–	1	1	1	1	1	1	1	–
	Acceleration actions from drives, all movements taken into account		1,22	1	1	1,16	1	1,1	–	1	–	–	–	–	–	–	–	–
	Displacements		1,1	1	1	1,05	1	1,0	1	1	1	1	1	1	1	1	1	1
	Relative vessel motions		1,22	1	1	1,16	1	1,1	–	–	1	1	1	1	1	1	–	–
Occasional	Environmental actions	In-service wind loads	–	–	–	1,16	1	1,1	–	1	–	–	–	–	–	–	1	—
		Snow and ice loads	–	–	–	1,16	1	–	–	–	–	–	–	–	–	–	–	1
Exceptional	Out-of-service wind loads		–	–	–	–	–	1,1	1	–	–	–	–	–	–	–	–	1
	Test loads		–	–	–	–	–	1,1	–	1	–	–	–	–	–	–	–	–
	Buffer forces		–	–	–	–	–	1,1	–	–	1	–	–	–	–	–	–	–
	Drive forces due to E-stop		–	–	–	–	–	1,1	–	–	–	1	–	–	–	–	–	–
	Forces due to failure of mechanism		–	–	–	–	–	1,1	–	–	–	–	–	–	1	–	–	–
	Excitation of the crane support		–	–	–	–	–	1,1	–	–	–	–	–	–	–	1	–	1
	Loads while the crane is in stowage position on a vessel		–	–	–	–	–	1,1	–	–	–	–	–	–	–	–	–	1
Descriptions of load combinations (A1, A2, B1, C2 to C12) are in accordance with Tables 13 and 14.																		

Figure 31: Load combinations and partial safety factors for the proof of crane stability according to EN 13001-2 [14]

For the stability verification, the governing load cases are identified, and the corresponding dynamic amplification factors and partial safety factors for stability are applied. All dynamic amplification factors are taken equal to 1. Relevant unfavourable masses are multiplied by a partial safety factor of 1.1 for load combination B (operational with wind), while a factor of 1.05 is applied for load combination C (storm).

The stability of the crane is evaluated based on the support reactions obtained from the finite element model. For each load combination, the reaction forces at all support points are determined. A loss of stability is indicated by the occurrence of uplift, corresponding to zero or negative reaction forces at one or more supports.

The results of the stability assessment are used to verify that the crane remains stable under all relevant load combinations. The governing load cases are identified based on the minimum support reactions, providing direct insight into the most critical conditions for crane stability.

5.7 Quay Loading

The loading of the quay is evaluated based on the support reactions obtained from the finite element model. These reactions represent the forces transferred from the crane structure to the rail and quay system. The assessment is performed for both operational and storm load cases.

In contrast to the structural verification, quay loading is evaluated without the use of partial safety factors. The loads are considered at their characteristic values, while dynamic factors are retained. This provides a more realistic representation of the loads acting on the quay during crane operation.

The governing load cases are first identified based on the factored load combinations. For these load cases, the partial safety factors are subsequently removed, while the dynamic amplification factors are retained. The vertical reaction forces at all support points are then extracted, which correspond to point loads at the bogies. To obtain the line loads acting on the quay, these forces are distributed over the bogie length. The resulting line loads form the basis for assessing the loading on the quay structure.

The resulting line loads are compared with typical values reported in literature to assess the feasibility of the crane concept. This provides a reference for evaluating whether the induced loads are within the range of existing or newly designed quay infrastructure.

5.8 Modal Analysis

A modal analysis is performed to determine the natural frequencies and corresponding mode shapes of the crane structure. These properties provide insight into the dynamic behaviour of the system and form a key input for the dynamic model developed in MATLAB.

The analysis is carried out using the finite element model described in the previous sections. All structural and non-structural mass contributions are included, with non-structural components represented as point masses or distributed masses depending on their physical distribution, and the trolleys modelled as point masses at their corresponding locations along the structure.

Since the trolley positions affect the mass distribution along the boom, the modal properties of the structure depend on the trolley location. The modal analysis is therefore performed for multiple trolley positions, allowing the variation in natural frequency and mode shapes to be evaluated. This variation is particularly relevant for the transverse direction, where the dominant structural modes are sensitive to the trolley position along the boom.

The resulting natural frequencies are used as input for the simplified dynamic model, where the structural behaviour is represented by an equivalent single-degree-of-freedom system. In this way, the finite element results are directly linked to the dynamic simulations, ensuring consistency between the structural and dynamic models.

6 Dynamic Model

This chapter presents the dynamic modelling framework used to evaluate the dynamic behaviour and performance of the Quad Trolley STS crane concept. The structural behaviour of the crane is represented using an equivalent mass–spring–damper system derived from the finite element model, while the suspended load is modelled as a pendulum. This simplified, control-oriented formulation retains the dominant physical interactions between the crane structure, the trolley system, and the suspended load, while allowing efficient simulation across a large number of operating scenarios.

Three modelling cases are considered. First, the Quad Trolley STS crane is modelled in the transverse direction, in which the trolley is actuated directly by the onboard transverse drive. Second, a conventional STS crane is modelled in the transverse direction, in which the transverse motion is achieved indirectly through the gantry drive, providing a reference for comparison. Third, the trolley travel direction is analysed separately, as it represents a different dynamic system with distinct structural characteristics. The same control strategy is applied to all three cases, and a parameter sensitivity analysis is performed for the Quad Trolley transverse and trolley travel directions to evaluate the influence of key parameters on system performance.

6.1 Modelling Approach and Assumptions

This section describes the modelling approach used to represent the dynamic behaviour of the crane system. The objective is not to capture all structural details, but to develop a model that accurately represents the dominant dynamic effects relevant for performance evaluation and comparison between different crane configurations.

6.1.1 Modelling Approach

The dynamic behaviour of the crane is represented using a simplified dynamic model that captures the interaction between the structure, the trolley, and the suspended load. The structural flexibility is modelled using an equivalent mass–spring–damper representation, which reflects the dominant vibration mode of the crane in the considered direction of motion. This allows the global structural response to be included without explicitly modelling the full structural geometry.

The trolley is modelled as a translating mass, and the suspended load is modelled as a pendulum attached to the trolley, capturing the essential sway dynamics that arise during crane operation. The actuation point differs between the modelling cases: in the Quad Trolley transverse and trolley travel models, the drive force is applied directly at the trolley, while in the conventional transverse model, the drive force is applied at the base of the crane through the gantry drive. In all cases, the result is a coupled dynamic system in which trolley motion, structural deformation, and load sway influence each other.

The models are formulated in state-space form, allowing for efficient simulation and straightforward implementation of control strategies. This also enables a consistent evaluation of system performance across the different modelling cases considered in this chapter.

6.1.2 Structural Representation

The structural behaviour of the crane is represented by a single equivalent degree of freedom corresponding to the dominant vibration mode in the direction of interest. This mode represents the global deformation of the structure in the considered direction and is assumed to govern the dynamic response during operation.

The properties of this equivalent system are derived from the finite element model presented in the previous chapter. The natural frequency of the dominant mode is obtained from modal analysis, while the corresponding structural stiffness is extracted from the finite element model.

The equivalent structural stiffness is obtained from the finite element model using a simple load–displacement method. A load is applied at the reference point, corresponding to the selected trolley location, in the direction of interest, and the resulting displacement is calculated. Assuming linear elastic behaviour, the stiffness is then determined from the relation $F = Ku$, where F is the applied load and u the corresponding displacement. This approach ensures that the stiffness represents the structural stiffness of the crane at the chosen trolley location in the considered direction.

The modal mass of the equivalent system is then determined using the relationship between natural frequency, stiffness, and mass:

$$f_n = \frac{1}{2\pi}\sqrt{\frac{k}{m}} \tag{19}$$

Rearranging this expression yields:

$$m = \frac{k}{(2\pi f_n)^2} \tag{20}$$

This approach ensures that both the stiffness and dynamic response of the structure are consistently represented in the simplified model, while maintaining a direct link to the finite element results.

Structural damping is modelled as equivalent viscous damping. A constant damping ratio of $\zeta = 1\%$ is assumed for the structural mode, which is considered representative for large welded steel structures [47]. The corresponding damping coefficient is defined as:

$$c = 2\zeta\sqrt{km} \tag{21}$$

where ζ is the damping ratio, k the equivalent stiffness, and m the modal mass of the structure. This formulation ensures that the damping is consistent with the natural frequency and dynamic properties of the equivalent structural system.

The rotational damping of the load sway is neglected, i.e. $c_\theta = 0$, as the controller actively suppresses sway motion, resulting in small angular velocities and a negligible contribution of the damping term to the overall dynamics.

6.1.3 Load Modelling

The suspended load is modelled as a point mass attached to the trolley via a massless rigid link, forming a pendulum system. This representation captures the dominant sway behaviour of the load, which is governed primarily by the hoisting length.

The corresponding natural frequency of the load is given by:

$$f_l = \frac{1}{2\pi}\sqrt{\frac{g}{L}} \tag{22}$$

where f_l is the natural frequency of the load, g is the gravitational acceleration, and L is the hoisting length. This relation shows that an increase in hoisting length results in a lower natural frequency and therefore a slower sway motion.

Both the hoisting length and the hoisted mass are treated as parameters in the model and are varied during the parameter sensitivity analysis to reflect different operational conditions.

6.1.4 Disturbance Modelling

External disturbances are included in the model to represent the main sources of excitation affecting crane performance during operation, in addition to the trolley motion itself. Two types of disturbances are considered: interaction forces from the second main trolley and wind loading acting on both the structure and the suspended load.

Second Trolley Disturbance:
In the Quad Trolley configuration, the interaction between the two main trolleys is represented by modelling the second trolley as an external force acting on the structure. The magnitude of this disturbance is based on the combined inertial contributions of the trolley and the suspended load, and is defined as:

$$F_{\text{max}} = F_{\text{trolley}} + F_{\text{load}} \tag{23}$$

with

$$F_{\text{trolley,max}} = M_T a_{\text{max}} \tag{24}$$

and

$$F_{\text{load,max}} = m_l a_{L,\text{max}} + m_l g \theta_{\text{max}} \tag{25}$$

where M_T is the trolley mass, m_l is the payload mass, a_{max} is the maximum trolley acceleration, $a_{L,\text{max}}$ is the maximum load acceleration, and θ_{max} is the maximum sway angle. The effective trolley mass differs between the two directions: in the transverse direction, only the sheave block mass of 5 mt is actuated, while in the trolley travel direction, the full trolley mass of 30 mt applies, as described in Section 3.4.

To represent realistic operational behaviour, the disturbance signal is generated as a stochastic, band-limited force. A filtered white noise process is used to create a smooth, time-varying signal.

The frequency of the disturbance signal is linked to the natural frequency of the structure. The boom primarily vibrates and deflects at this frequency, and the trolleys respond to counteract this motion. The disturbance signal therefore reflects this behaviour and is dominated by frequencies around the structural natural frequency.

Additional filtering is applied to remove high-frequency components and low-frequency drift, resulting in a smooth and physically realistic disturbance signal. An example of the disturbance signal is shown in Figure 32.

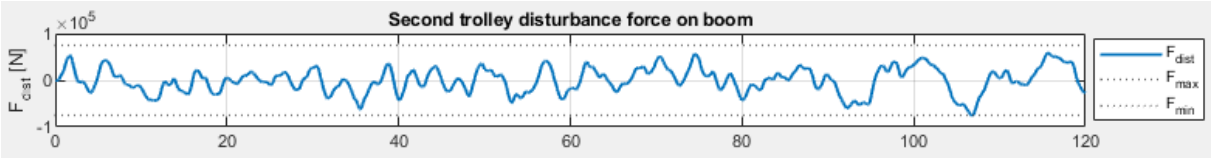

Figure 32: Example of the generated disturbance signal, showing a smooth, band-limited force with dominant frequency content around the structural natural frequency.

To ensure a consistent comparison between configurations and parameter combinations, the random disturbance signals are generated using a fixed set of random seeds. For each simulation case, multiple runs with different seeds are performed to capture the variability introduced by the stochastic disturbance, while the same set of seeds is used across all configurations and parameter combinations to ensure that any observed differences in performance are attributable to the system characteristics rather than to differences in the disturbance realisation.

Wind Disturbance:
Wind loading is modelled as a time-varying stochastic force acting on both the structure and the suspended load.

The aerodynamic forces are computed using a quadratic drag model:

$$F = \frac{1}{2}\rho C_d A U^2 \tag{26}$$

where ρ is the air density, C_d is the drag coefficient, A is the projected area, and U is the wind speed. In the model, the product $C_d A$ is treated as a single parameter representing the combined aerodynamic properties of the structure or load.

For the crane structure, an equivalent $C_d A$ value is determined by calibrating the wind force to the static deflection obtained from the finite element model. The target force corresponding to the FEM deflection is defined as:

$$F_{\text{target}} = k\,\delta_{\text{FEM}} \tag{27}$$

where k is the equivalent structural stiffness and δ_{FEM} is the structural deflection obtained from the finite element model at the same location and degree of freedom. Equating this force to the aerodynamic drag force at a chosen calibration wind speed U_{cal} gives:

$$F_{\text{target}} = \frac{1}{2}\rho(C_dA)_b U_{\text{cal}}^2 \tag{28}$$

from which the equivalent C_dA value for the structure follows as:

$$(C_dA)_b = \frac{2F_{\text{target}}}{\rho U_{\text{cal}}^2} \tag{29}$$

This ensures that the simplified dynamic model reproduces the same static wind-induced boom deflection as the finite element model.

For the suspended load, the C_dA value is estimated from the projected areas of the container, spreader, and headblock. A drag coefficient of $C_d = 2.1$ is assumed [48]:

$$(C_dA)_l = 2.1\left(A_{\text{headblock}} + A_{\text{spreader(s),tot}} + A_{\text{container(s),tot}}\right) \tag{30}$$

The resulting wind forces acting on the structure and suspended load are then given by:

$$F_{\text{wind},b} = \frac{1}{2}\rho(C_dA)_b U^2 \tag{31}$$

$$F_{\text{wind},l} = \frac{1}{2}\rho(C_dA)_l U^2 \tag{32}$$

The wind speed signal $U(t)$ is generated using a stochastic model with two components: a slowly varying gust component and a smaller, faster turbulence component. This allows the wind profile to capture both gradual changes and short-term fluctuations.

The stochastic wind components are generated from Gaussian white noise processes and subsequently filtered to obtain band-limited signals with realistic temporal correlation. This approach is consistent with common turbulence modelling assumptions, where wind fluctuations are often represented as Gaussian stochastic processes due to the superposition of many independent atmospheric effects [49].

Both components are generated by filtering random noise using first-order filters. The gust component has a low characteristic frequency, resulting in slow variations over time, while the turbulence component has a higher frequency and introduces smaller, faster fluctuations.

The two components are scaled and added to a mean wind speed:

$$U(t) = U_{\text{mean}} + 6.0\,U_{\text{gust}}(t) + 1.2\,U_{\text{micro}}(t) \tag{33}$$

The scaling factors are selected through iterative tuning to produce a wind profile in which the low-frequency gust component dominates the overall variation, while the high-frequency component introduces smaller fluctuations representative of atmospheric turbulence.

To ensure realistic wind conditions, the wind speed is limited to a maximum value of $1.5\,U_{\text{mean}}$ by scaling the fluctuations around the mean, avoiding artificial clipping of the signal. Negative wind speeds are prevented by enforcing $U(t) \geq 0$.

This results in a realistic wind profile that captures both gradual variations and short-term fluctuations, as shown in Figure 33.

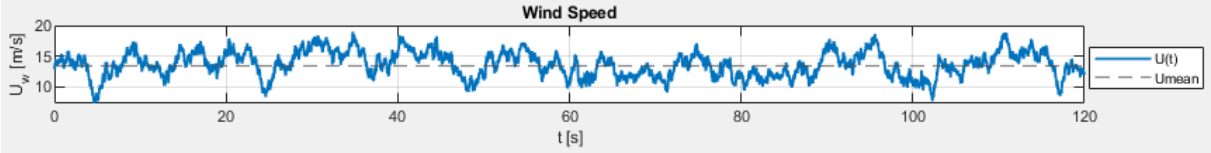

Figure 33: Generated wind speed profile used in simulations.

6.1.5 Model Scope and Limitations

The structural behaviour is represented by a single equivalent mode corresponding to the dominant global deformation of the crane in the considered direction. Higher-order modes, such as local boom bending and torsional deformation, are not included. This simplification is consistent with the modelling objective of capturing the dominant global dynamics governing the interaction between the structure, trolley, and suspended load.

The suspended load is modelled as a pendulum under the assumption of small sway angles. This allows linearisation of the equations of motion using $\sin(\theta) \approx \theta$ and $\cos(\theta) \approx 1$, thereby neglecting the nonlinear behaviour of the pendulum at larger sway angles. This assumption is considered valid for normal crane operation, where sway angles remain small.

The model is formulated as a linear time-invariant system, meaning that parameters such as hoisting length, payload mass, and trolley position are held constant during each simulation. In practice, these parameters vary continuously during a container handling cycle. The influence of these parameters on dynamic performance is instead assessed through the parameter sensitivity study described in Section 6.7.

Despite these simplifications, the model captures the primary dynamic interactions between the structure, trolley, and load, and provides a consistent basis for evaluating system performance and comparing different crane configurations.

6.2 Quad Trolley STS Crane – Transverse Dynamic Model

This section presents the dynamic model used to describe the transverse motion of the Quad Trolley STS crane. The model represents one of the main trolleys equipped with a direct transverse drive, together with the dominant transverse deformation of the crane structure and the sway motion of the suspended load.

The system is illustrated in Figure 34. The crane structure is represented by a single equivalent degree of freedom with displacement x_b, stiffness k_c, damping c_c, and equivalent modal mass m_c. The trolley's sheave block, with mass m_t, moves transversely relative to the boom and is actively driven by the transverse drive. As a result, its motion is directly controlled and included explicitly in the system dynamics. The suspended load, with mass m_L, is modelled as a pendulum of length L with sway angle θ.

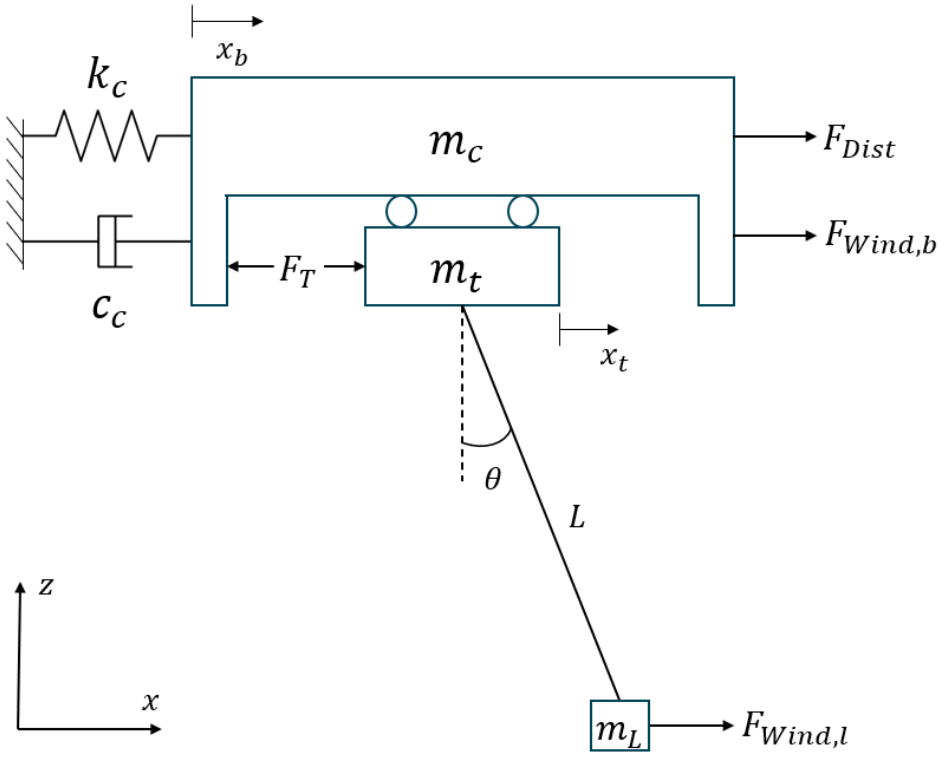

Figure 34: Simplified dynamic model of the Quad Trolley STS crane in the transverse direction.

External forces acting on the system include the disturbance force from the second trolley, F_{dist}, and wind forces acting on the structure and the load, denoted by $F_{\text{wind},b}$ and $F_{\text{wind},l}$, respectively.

The generalised coordinates are chosen as the structural displacement x_b and the load sway angle θ, while the transverse sheave block displacement x_t is treated as the controlled degree of freedom. A full derivation of the model using Lagrange's equations is provided in Appendix C.

6.2.1 Kinematics

The absolute horizontal position of the trolley suspension point is given by

$$x_s = x_b + x_t \tag{34}$$

and the position of the load becomes

$$x_L = x_b + x_t + L\sin\theta \tag{35}$$
$$z_L = L - L\cos\theta \tag{36}$$

6.2.2 Equations of Motion

Applying Lagrange's equations to the system yields the following nonlinear equations of motion:

$$(m_c + m_t + m_L)\ddot{x}_b + (m_t + m_L)\ddot{x}_t + m_L L\left(-\sin\theta\,\dot{\theta}^2 + \cos\theta\,\ddot{\theta}\right) + c_c\dot{x}_b + k_c x_b = F_{\text{dist}} + F_{\text{wind},b} + F_{\text{wind},l} \tag{37}$$

$$m_L L^2\ddot{\theta} + m_L g L\sin\theta + m_L L\cos\theta(\ddot{x}_b + \ddot{x}_t) = F_{\text{wind},l} L\cos\theta \tag{38}$$

These equations describe the coupled dynamics between structural deformation, trolley motion, and load sway.

6.2.3 Linearised Model

For normal crane operation, the sway angles are assumed to remain small. The model is therefore linearised using the approximations $\sin\theta \approx \theta$ and $\cos\theta \approx 1$, while neglecting higher-order nonlinear terms.

This results in the following linearised equations:

$$(m_c + m_t + m_L)\ddot{x}_b + (m_t + m_L)\ddot{x}_t + m_L L\ddot{\theta} + c_c\dot{x}_b + k_c x_b = F_{\text{dist}} + F_{\text{wind},b} + F_{\text{wind},l} \tag{39}$$

$$m_L L^2\ddot{\theta} + m_L g L\theta + m_L L(\ddot{x}_b + \ddot{x}_t) = F_{\text{wind},l} L \tag{40}$$

6.2.4 State-Space Representation

The linearised system is rewritten in first-order state-space form as

$$\dot{\mathbf{x}} = A\mathbf{x} + B_u u + B_d \mathbf{d} \tag{41}$$

with the state vector

$$\mathbf{x} = \begin{bmatrix} x_b \\ \dot{x}_b \\ \theta \\ \dot{\theta} \\ x_t \\ \dot{x}_t \end{bmatrix} \tag{42}$$

the control input

$$u = \ddot{x}_t \tag{43}$$

and the disturbance vector

$$\mathbf{d} = \begin{bmatrix} F_{\text{dist}} \\ F_{\text{wind},b} \\ F_{\text{wind},l} \end{bmatrix} \tag{44}$$

The system matrices can be written as

$$A = \begin{bmatrix} 0 & 1 & 0 & 0 & 0 & 0 \\ -\dfrac{k_c}{m_c + m_t} & -\dfrac{c_c}{m_c + m_t} & \dfrac{g\, m_L}{m_c + m_t} & 0 & 0 & 0 \\ 0 & 0 & 0 & 1 & 0 & 0 \\ \dfrac{k_c}{L(m_c + m_t)} & \dfrac{c_c}{L(m_c + m_t)} & -\dfrac{g}{L}\left(1 + \dfrac{m_L}{m_c + m_t}\right) & 0 & 0 & 0 \\ 0 & 0 & 0 & 0 & 0 & 1 \\ 0 & 0 & 0 & 0 & 0 & 0 \end{bmatrix} \tag{45}$$

$$B_u = \begin{bmatrix} 0 \\ -\dfrac{m_t}{m_c + m_t} \\ 0 \\ -\dfrac{m_c}{L(m_c + m_t)} \\ 0 \\ 1 \end{bmatrix} \tag{46}$$

$$B_d = \begin{bmatrix} 0 & 0 & 0 \\ \dfrac{1}{m_c + m_t} & \dfrac{1}{m_c + m_t} & \dfrac{1}{m_c + m_t} \\ 0 & 0 & 0 \\ -\dfrac{1}{L(m_c + m_t)} & -\dfrac{1}{L(m_c + m_t)} & \left(\dfrac{1}{m_L L} - \dfrac{1}{L(m_c + m_t)}\right) \\ 0 & 0 & 0 \\ 0 & 0 & 0 \end{bmatrix} \tag{47}$$

The absolute horizontal load position is written in output form as

$$x_{\text{load}} = C_{\text{load}}\mathbf{x} \tag{48}$$

with

$$C_{\text{load}} = \begin{bmatrix} 1 & 0 & L & 0 & 1 & 0 \end{bmatrix} \tag{49}$$

6.3 Conventional STS Crane – Transverse Dynamic Model

This section presents the dynamic model used to describe the transverse motion of a conventional STS crane. In contrast to the Quad Trolley configuration, the trolley is fixed relative to the boom in the transverse direction and does not have an independent transverse drive. Transverse positioning is instead achieved by moving the entire crane along the quay using the gantry drive system.

The system is illustrated in Figure 35. The crane structure is represented by an equivalent mass m_c located at the boom–trolley–suspension point coordinate x_t, while the structural flexibility between the gantry drive and the suspension point is represented by an equivalent spring–damper element with stiffness k_c and damping c_c. The suspended load, with mass m_L, is modelled as a pendulum of length L with sway angle θ.

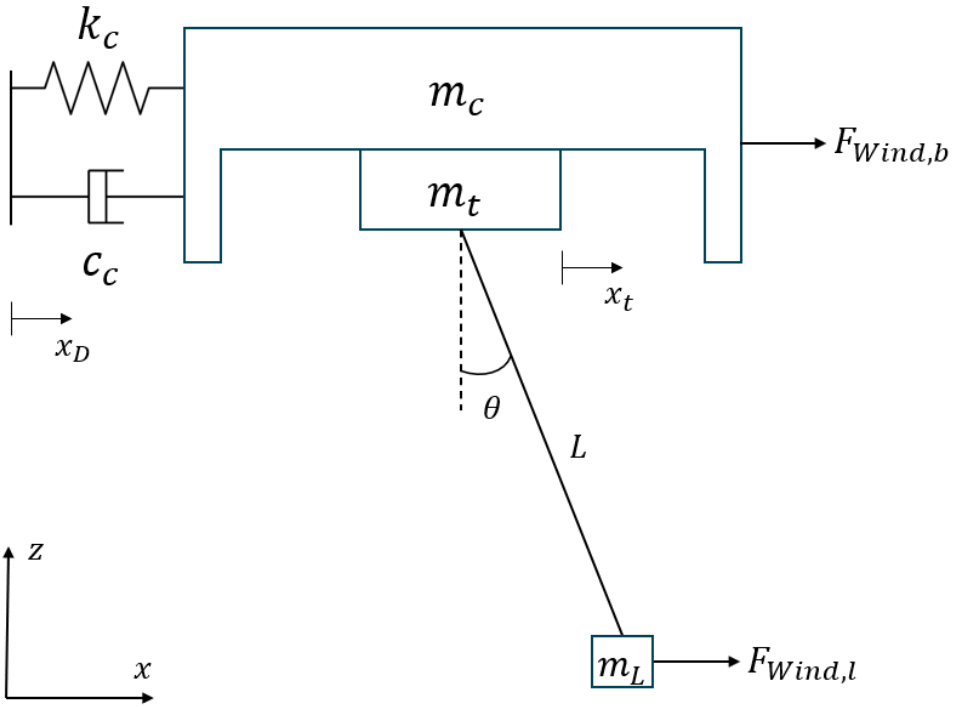

Figure 35: Transverse compliant-drive model with fixed trolley (in transverse) and suspended load.

The gantry drive imposes a commanded transverse motion on the drive-side coordinate $x_D(t)$, which is transmitted to the boom–trolley–suspension point coordinate $x_t(t)$ through the compliant element. This explicitly captures the structural flexibility between the actuation point and the suspension point.

In this work, the gantry actuation is modelled at the motion-control level. The drive acceleration $\ddot{x}_D$ is the control input, from which the drive displacement $x_D(t)$ follows. The analysis therefore focuses on how this motion is transmitted through the compliant structure and how it affects structural response and load sway. Since this model represents a conventional single-trolley crane, no inter-trolley disturbance force is included.

The generalised coordinates are chosen as the structural displacement x_t and the load sway angle θ, while the drive-side displacement x_D is treated as the controlled degree of freedom. A full derivation of the model using Lagrange's equations is provided in Appendix D. This model serves as a reference case for comparison with the Quad Trolley transverse configuration.

6.3.1 Kinematics

The absolute horizontal position of the suspension point is given by

$$x_s = x_t \tag{50}$$

and the position of the load becomes

$$x_L = x_t + L\sin\theta \tag{51}$$
$$z_L = L - L\cos\theta \tag{52}$$

6.3.2 Equations of Motion

Applying Lagrange's equations to the system yields the following nonlinear equations of motion:

$$(m_c+m_L)\ddot{x}_t+m_L L\cos\theta\,\ddot{\theta}-m_L L\sin\theta\,\dot{\theta}^2 = c_c(\dot{x}_D-\dot{x}_t)+k_c(x_D-x_t)+F_{\text{wind},b}+F_{\text{wind},l} \tag{53}$$

$$m_L L^2\ddot{\theta} + m_L gL\sin\theta + m_L L\cos\theta\,\ddot{x}_t = F_{\text{wind},l}L\cos\theta \tag{54}$$

The drive-side motion is generated through

$$\ddot{x}_D = u(t) \tag{55}$$

These equations describe the coupled dynamics between gantry drive motion, structural compliance, and load sway.

6.3.3 Linearised Model

For normal crane operation, the sway angles are assumed to remain small. The model is therefore linearised using the approximations $\sin\theta \approx \theta$ and $\cos\theta \approx 1$, while neglecting higher-order nonlinear terms.

This results in the following linearised equations:

$$(m_c + m_L)\ddot{x}_t + m_L L\ddot{\theta} = c_c(\dot{x}_D - \dot{x}_t) + k_c(x_D - x_t) + F_{\text{wind},b} + F_{\text{wind},l} \tag{56}$$
$$m_L L^2\ddot{\theta} + m_L gL\,\theta + m_L L\ddot{x}_t = F_{\text{wind},l}L \tag{57}$$
$$\ddot{x}_D = u \tag{58}$$

6.3.4 State-Space Representation

The linearised system is rewritten in first-order state-space form as

$$\dot{\mathbf{x}} = A\mathbf{x} + B_u u + B_d\mathbf{d} \tag{59}$$

with the state vector

$$\mathbf{x} = \begin{bmatrix} x_D \\ \dot{x}_D \\ x_t \\ \dot{x}_t \\ \theta \\ \dot{\theta} \end{bmatrix} \tag{60}$$

the control input

$$u = \ddot{x}_D \tag{61}$$

and the disturbance vector

$$\mathbf{d} = \begin{bmatrix} F_{\text{wind},b} \\ F_{\text{wind},l} \end{bmatrix} \tag{62}$$

The system matrices are given by

$$A = \begin{bmatrix} 0 & 1 & 0 & 0 & 0 & 0 \\ 0 & 0 & 0 & 0 & 0 & 0 \\ 0 & 0 & 0 & 1 & 0 & 0 \\ \dfrac{k_c}{m_c} & \dfrac{c_c}{m_c} & -\dfrac{k_c}{m_c} & -\dfrac{c_c}{m_c} & \dfrac{gm_L}{m_c} & 0 \\ 0 & 0 & 0 & 0 & 0 & 1 \\ -\dfrac{k_c}{Lm_c} & -\dfrac{c_c}{Lm_c} & \dfrac{k_c}{Lm_c} & \dfrac{c_c}{Lm_c} & -\dfrac{g}{L}\left(1+\dfrac{m_L}{m_c}\right) & 0 \end{bmatrix} \tag{63}$$

$$B_u = \begin{bmatrix} 0 \\ 1 \\ 0 \\ 0 \\ 0 \\ 0 \end{bmatrix} \tag{64}$$

$$B_d = \begin{bmatrix} 0 & 0 \\ 0 & 0 \\ 0 & 0 \\ \dfrac{1}{m_c} & \dfrac{1}{m_c} \\ 0 & 0 \\ 0 & \left(\dfrac{1}{m_L L} - \dfrac{1}{Lm_c}\right) \end{bmatrix} \tag{65}$$

The absolute horizontal load position is written in output form as

$$x_{\text{load}} = C_{\text{load}}\mathbf{x} \tag{66}$$

with

$$C_{\text{load}} = \begin{bmatrix} 0 & 0 & 1 & 0 & L & 0 \end{bmatrix} \tag{67}$$

6.4 Trolley Travel Direction Dynamic Model

This section presents the dynamic model used to describe the motion of the trolley along the boom. The model represents the trolley travel direction, including the dominant structural deformation of the crane and the sway motion of the suspended load.

The system is illustrated in Figure 36. The crane structure is represented by a single equivalent degree of freedom with displacement x_b, stiffness k_c, damping c_c, and equivalent modal mass m_c. The trolley, with mass m_t, moves along the boom and is directly actuated in trolley travel direction. The suspended load, with mass m_L, is modelled as a pendulum of length L with sway angle θ.

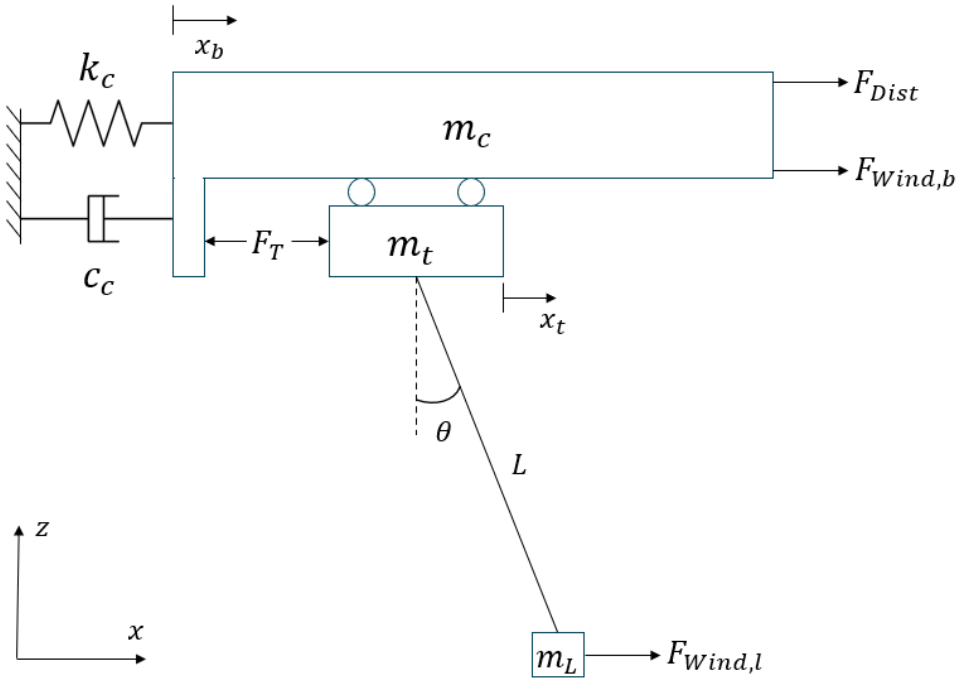

Figure 36: Dynamic model of the trolley travel direction with flexible boom and suspended load.

External forces acting on the system include the disturbance force from the second main trolley F_{dist}, and wind forces acting on the structure and the suspended load, denoted by $F_{\text{wind},b}$ and $F_{\text{wind},l}$, respectively.

The generalised coordinates are chosen as the structural displacement x_b and the load sway angle θ, while the trolley displacement x_t is treated as the controlled degree of freedom. A full derivation of the model using Lagrange's equations is provided in Appendix E.

6.4.1 Kinematics

The absolute horizontal position of the trolley suspension point is given by

$$x_s = x_b + x_t \tag{68}$$

and the position of the load becomes

$$x_L = x_b + x_t + L\sin\theta \tag{69}$$
$$z_L = L - L\cos\theta \tag{70}$$

6.4.2 Equations of Motion

Applying Lagrange's equations to the system yields the following nonlinear equations of motion:

$$\begin{aligned}(m_c + m_t + m_L)\ddot{x}_b + (m_t + m_L)\ddot{x}_t + m_L L\left(-\sin\theta\,\dot{\theta}^2 + \cos\theta\,\ddot{\theta}\right) + c_c\dot{x}_b + k_c x_b \\ = F_{\text{dist}} + F_{\text{wind},b} + F_{\text{wind},l}\end{aligned} \tag{71}$$

$$m_L L^2\ddot{\theta} + m_L g L\sin\theta + m_L L\cos\theta(\ddot{x}_b + \ddot{x}_t) = F_{\text{wind},l} L\cos\theta \tag{72}$$

These equations describe the coupled dynamics between structural deformation, trolley motion, and load sway in the trolley travel direction.

6.4.3 Linearised Model

For normal crane operation, the sway angles are assumed to remain small. The model is therefore linearised using the approximations $\sin\theta \approx \theta$ and $\cos\theta \approx 1$, while neglecting higher-order nonlinear terms.

This results in the following linearised equations:

$$\begin{aligned}(m_c + m_t + m_L)\ddot{x}_b + (m_t + m_L)\ddot{x}_t + m_L L\ddot{\theta} + c_c\dot{x}_b + k_c x_b \\ = F_{\text{dist}} + F_{\text{wind},b} + F_{\text{wind},l}\end{aligned} \tag{73}$$

$$m_L L^2\ddot{\theta} + m_L g L\theta + m_L L(\ddot{x}_b + \ddot{x}_t) = F_{\text{wind},l} L \tag{74}$$

6.4.4 State-Space Representation

The linearised system is rewritten in first-order state-space form as

$$\dot{\mathbf{x}} = A\mathbf{x} + B_u u + B_d \mathbf{d} \tag{75}$$

with the state vector

$$\mathbf{x} = \begin{bmatrix} x_b \\ \dot{x}_b \\ \theta \\ \dot{\theta} \\ x_t \\ \dot{x}_t \end{bmatrix} \tag{76}$$

the control input

$$u = \ddot{x}_t \tag{77}$$

and the disturbance vector

$$\mathbf{d} = \begin{bmatrix} F_{\text{dist}} \\ F_{\text{wind},b} \\ F_{\text{wind},l} \end{bmatrix} \tag{78}$$

The system matrices can be written as

$$A = \begin{bmatrix} 0 & 1 & 0 & 0 & 0 & 0 \\ -\dfrac{k_c}{m_c + m_t} & -\dfrac{c_c}{m_c + m_t} & \dfrac{g\, m_L}{m_c + m_t} & 0 & 0 & 0 \\ 0 & 0 & 0 & 1 & 0 & 0 \\ \dfrac{k_c}{L(m_c + m_t)} & \dfrac{c_c}{L(m_c + m_t)} & -\dfrac{g}{L}\left(1 + \dfrac{m_L}{m_c + m_t}\right) & 0 & 0 & 0 \\ 0 & 0 & 0 & 0 & 0 & 1 \\ 0 & 0 & 0 & 0 & 0 & 0 \end{bmatrix} \tag{79}$$

$$B_u = \begin{bmatrix} 0 \\ -\dfrac{m_t}{m_c + m_t} \\ 0 \\ -\dfrac{m_c}{L(m_c + m_t)} \\ 0 \\ 1 \end{bmatrix} \tag{80}$$

$$B_d = \begin{bmatrix} 0 & 0 & 0 \\ \dfrac{1}{m_c + m_t} & \dfrac{1}{m_c + m_t} & \dfrac{1}{m_c + m_t} \\ 0 & 0 & 0 \\ -\dfrac{1}{L(m_c + m_t)} & -\dfrac{1}{L(m_c + m_t)} & \left(\dfrac{1}{m_L L} - \dfrac{1}{L(m_c + m_t)}\right) \\ 0 & 0 & 0 \\ 0 & 0 & 0 \end{bmatrix} \tag{81}$$

The absolute horizontal load position is written in output form as

$$x_{\text{load}} = C_{\text{load}}\mathbf{x} \tag{82}$$

with

$$C_{\text{load}} = \begin{bmatrix} 1 & 0 & L & 0 & 1 & 0 \end{bmatrix} \tag{83}$$

6.5 Control Design

To evaluate the dynamic performance of the crane concepts, a state-feedback control strategy is implemented for all considered dynamic models. The primary control objective is to achieve accurate positioning of the suspended load while limiting actuator effort in the presence of disturbances.

6.5.1 Control Objective

For all configurations, the controlled variable is chosen as the absolute horizontal position of the suspended load. For the Quad Trolley transverse model and the trolley travel model, this is given by

$$x_{\text{load}} = x_b + x_t + L\theta \tag{84}$$

using the small-angle approximation. For the conventional STS transverse model, since the trolley is fixed to the boom in transverse direction, the corresponding load position is

$$x_{\text{load}} = x_t + L\theta \tag{85}$$

The control objective is to make x_{load} follow a reference position x_{ref} as accurately as possible, while maintaining acceptable actuator demands.

6.5.2 Linear Quadratic Regulator

The controller is based on the Linear Quadratic Regulator (LQR) method. LQR is an optimal state-feedback control method for linear systems, in which the control input is chosen such that a quadratic performance index is minimised. Starting from the state-space system

$$\dot{\mathbf{x}} = A\mathbf{x} + B\mathbf{u} \tag{86}$$

the LQR problem determines the control law

$$\mathbf{u} = -K\mathbf{x} \tag{87}$$

that minimises the cost function

$$J = \int_0^\infty \left(\mathbf{x}^T Q\mathbf{x} + \mathbf{u}^T R\mathbf{u}\right) dt \tag{88}$$

where Q is the state weighting matrix and R is the control weighting matrix. In this study, the weighting matrix Q is formulated such that the load position is the primary regulated quantity, while R penalises the use of control effort. In this way, the controller determines an optimal balance between positioning performance and actuator demand.

The optimal feedback gain matrix K is obtained from

$$K = R^{-1}B^T P \tag{89}$$

where P is the positive semi-definite solution of the continuous-time algebraic Riccati equation

$$A^T P + PA - PBR^{-1}B^T P + Q = 0 \tag{90}$$

The Riccati equation follows from the minimisation of the quadratic cost function and determines the optimal trade-off between state regulation and control effort.

In this study, the feedback gain matrix K is recomputed for each simulation case based on the corresponding system matrices. Since the dynamic models differ between configurations and parameter variations, this ensures that the controller is optimally tuned for each individual system. As a result, the closed-loop performance reflects the inherent dynamic behaviour of the system rather than a fixed controller design. This approach is consistent with the objective of this study, where the controller is used as a comparative tool to evaluate system performance under optimal state-feedback control, rather than to assess a specific controller implementation.

6.5.3 Integral Action

A standard LQR controller minimises state deviations, but does not in general guarantee zero steady-state tracking error in the presence of constant disturbances or non-zero reference positions. To eliminate this steady-state error, integral action is added. The controller used in this study is therefore an LQR controller with integral action, also referred to as LQI.

An additional integral state ξ is introduced as

$$\dot{\xi} = x_{\text{load}} - x_{\text{ref}} \tag{91}$$

This state represents the accumulated tracking error over time. By including this integral state in the control design, the controller not only reacts to the instantaneous state of the system, but also to persistent tracking deviations.

The resulting control law becomes

$$u = -K_x \mathbf{x} - K_i \xi \tag{92}$$

where K_x is the feedback gain on the physical states and K_i is the integral gain. These gains are obtained by applying the LQR procedure to the augmented system.

6.5.4 Application to the Crane Models

Although the same LQI control framework is used for all dynamic models, the system formulation differs depending on the actuation mechanism.

For the Quad Trolley transverse model and the trolley travel model, the trolley is actuated. In these cases, the trolley motion is included explicitly in the state vector:

$$\mathbf{x} = \begin{bmatrix} x_b & \dot{x}_b & \theta & \dot{\theta} & x_t & \dot{x}_t \end{bmatrix}^T \tag{93}$$

and the control input is the trolley acceleration

$$u = \ddot{x}_t \tag{94}$$

For the conventional STS transverse model, the actuation is applied through the gantry drive. The state vector is therefore written as

$$\mathbf{x} = \begin{bmatrix} x_D & \dot{x}_D & x_t & \dot{x}_t & \theta & \dot{\theta} \end{bmatrix}^T \tag{95}$$

with control input

$$u = \ddot{x}_D \tag{96}$$

As a result, the conventional STS crane is actuated indirectly through the structural compliance between the gantry drive and the suspension point, whereas the Quad Trolley and trolley travel cases are actuated directly at trolley level.

The remaining inputs are treated as external disturbances. For the Quad Trolley transverse and trolley travel models, these include the disturbance force from the second trolley and wind forces acting on the structure and load, collected in

$$\mathbf{d} = \begin{bmatrix} F_{\text{dist}} & F_{\text{wind},b} & F_{\text{wind},l} \end{bmatrix}^\top \tag{97}$$

For the conventional STS transverse model, since there is no second trolley, only wind forces are considered, such that

$$\mathbf{d} = \begin{bmatrix} F_{\text{wind},b} & F_{\text{wind},l} \end{bmatrix}^\top \tag{98}$$

6.5.5 Weighting Strategy

The same control philosophy is applied to all models. The load position is selected as the regulated output and is assigned a high weighting in the cost function in order to prioritise positioning accuracy. In the LQI formulation, this is implemented by defining the state weighting matrix based on the load position output, such that deviations in x_{load} are directly penalised.

For the Quad Trolley transverse model and the trolley travel model, the load position is given by

$$x_{\text{load}} = x_b + x_t + L\theta, \tag{99}$$

which represents a combination of structural displacement, trolley motion, and load sway. The corresponding weighting is applied through the output matrix C_{load}, such that

$$Q_x = C_{\text{load}}^T \, q_{\text{load}} \, C_{\text{load}}, \tag{100}$$

resulting in the quadratic cost term

$$\mathbf{x}^T Q_x \mathbf{x} = q_{\text{load}} \, x_{\text{load}}^2. \tag{101}$$

This formulation implies that the controller directly penalises deviations in the absolute load position, rather than individual state variables. Since x_{load} is a linear combination of the states, the relative contribution of each state follows directly from its physical role in this expression. Structural displacement and trolley motion enter linearly, while load sway is scaled by the rope length L. Furthermore, the quadratic form inherently introduces cross-terms between the states, meaning that coupled motions contributing to load position error are penalised simultaneously.

For the conventional STS transverse model, the load position is defined differently due to the absence of an independently actuated trolley in the transverse direction. In this case, the load position is given by

$$x_{\text{load}} = x_t + L\theta, \tag{102}$$

where x_t represents the suspension point position, which already includes the effect of structural compliance between the gantry drive and the boom. The same output-based weighting approach is applied using the corresponding C_{load} matrix.

In addition to the load position weighting, the integral state is strongly weighted to eliminate steady-state tracking error in the presence of persistent disturbances. The integral weight q_i determines how aggressively accumulated tracking errors are driven to zero. A higher value of q_i results in faster elimination of steady-state offsets, but may lead to more aggressive control action.

The control input is penalised through the matrix R, which limits the magnitude of the commanded accelerations. This ensures that the resulting control inputs remain physically realistic and comparable between configurations.

The weighting matrices are therefore structured such that the absolute load position is the primary performance variable. Other states are not directly penalised but are influenced through the coupling in the system dynamics.

In practical terms, this means that the controller is tuned to:

- minimise load position error,
- reject persistent disturbances,
- and limit actuator effort.

The specific weighting values used in the LQI design are summarised in Table 12. The same weighting on load position and integral error is used for all models to ensure a consistent performance objective, while the control weighting R is adjusted to reflect differences in actuation mechanisms and effective moving mass.

Table 12: LQI weighting parameters used for the different crane models.

Parameter	**Quad Trolley STS Transverse**	**Conventional STS Transverse**	**Trolley Travel**
Load position weight q_{load}	1.0×10^6	1.0×10^6	1.0×10^6
Integral weight q_i	1.0×10^7	1.0×10^7	1.0×10^7
Control weight R	2.0×10^4	2.0×10^9	2.0×10^5

This ensures that differences in closed-loop performance are primarily attributed to the system dynamics and actuation characteristics, rather than to variations in controller tuning.

6.5.6 Comparison Between Configurations

The controllers used for the different configurations are therefore based on the same control principle, namely LQI control with load position tracking as the main objective. However, the resulting controller behaviour is not identical, because the system dynamics and actuation mechanisms differ.

For the Quad Trolley transverse model:

- the load is actuated directly through the transverse trolley drive,
- the effective actuated mass is relatively small,
- the controller can react quickly to disturbances and load motion,
- and the system can operate with a relatively high maximum acceleration of 2.0 m/s^2.

For the conventional STS transverse model:

- the load is actuated indirectly through gantry drive motion,
- the effective moving mass is significantly larger,
- structural flexibility between the drive and the load introduces additional lag,
- and the maximum acceleration is much lower, at 0.25 m/s^2.

For the trolley travel model:

- the control structure is similar to that of the Quad Trolley transverse model,
- but the structural stiffness and natural frequency are significantly higher,
- resulting in weaker coupling between structural motion and load response,
- while the maximum acceleration is 1.2 m/s^2.

Thus, the controllers are based on the same optimal control framework, but their closed-loop performance differs because of the physical differences between the systems. This ensures a consistent basis for comparing the dynamic performance of the different crane configurations.

6.5.7 Motivation for LQR/LQI Control

The LQR/LQI control approach is selected as a systematic and consistent method to design a stabilizing controller for the dynamic models considered in this study. The crane systems are linear, multi-degree-of-freedom systems with coupled dynamics between structural motion, trolley motion, and load motion. LQR provides a direct way to account for these interactions within a single state-feedback framework.

An important advantage of LQR is that it allows explicit weighting of performance objectives through the cost function. By assigning a high weight to the load position, the controller is tuned for positioning accuracy, while the control input weighting ensures that actuator demands remain realistic.

Furthermore, the addition of integral action ensures zero steady-state tracking error in the presence of constant disturbances, such as wind loading. This is essential for evaluating crane performance under realistic operating conditions.

In addition, LQR/LQI is relatively straightforward to implement and tune, making it well suited for use as a comparative tool. The objective of this study is not to develop an advanced control strategy, but to evaluate and compare the dynamic behaviour and performance of different crane configurations. A simple and consistent control framework therefore ensures that differences in performance can be attributed primarily to the system dynamics and actuation characteristics, rather than to variations in controller design.

6.6 Simulation Setup and Performance Metrics

The dynamic models and control framework presented in the preceding sections form the basis for the simulation studies. The simulations are used to evaluate the closed-loop positioning performance of the different crane configurations in the presence of external disturbances.

6.6.1 Simulation Setup

All simulations are performed in the time domain using the linear state-space models combined with the LQI controller described in Section 6.5. For each simulation case, the system matrices are constructed using the corresponding model parameters, after which the feedback gains are computed for that specific configuration. In this way, each case is evaluated using a controller that is optimally tuned for the underlying linear model.

A simulation duration of 120 s is used for all cases, with a fixed time step of 0.01 s. This duration is sufficient to capture both the transient response during motion and the subsequent settling behaviour after the reference position is reached.

The commanded motion is introduced through a smooth reference trajectory for the absolute horizontal load position. Rather than applying a step input, the reference is ramped in time to represent a more realistic crane motion and to avoid unrealistically large initial accelerations.

The role of the reference trajectory depends on the configuration considered. In the transverse cases, the reference mainly defines a fixed target position, typically $x_{\text{ref}} = 0$. In this direction, the required displacements are small and can be executed at low speeds, meaning that the commanded motion itself is not critical for performance. Instead, the dynamic behaviour is dominated by disturbance rejection, such as wind loading or interaction with the second trolley, and the analysis focuses on the ability of the system to maintain a stable position around the target.

For the trolley travel case, the situation is different. Here, the reference represents a significant commanded displacement along the boom, and the motion itself becomes an important source of excitation, especially for the load. As a result, both tracking performance and disturbance rejection play a role in the overall dynamic response.

External disturbances are applied simultaneously with the reference motion. For the Quad Trolley transverse model and the trolley travel model, these consist of the second trolley disturbance force and wind loads acting on both the structure and the suspended load. For the conventional STS transverse model, since there is no second trolley, only wind disturbances are applied. The disturbance signals are generated using the procedures described in Section 6.1.4.

For all cases, the simulations start from zero initial conditions. This means that the structure, trolley, and load are initially at rest and located at the initial reference position. As a result, no initial motion or sway is present, and the subsequent response is governed by the commanded motion, the applied disturbances, and the closed-loop behaviour of the system.

6.6.2 Reference Cases

Before performing the full parameter sensitivity analysis, each configuration is first evaluated for a limited set of reference cases. These cases provide an initial assessment of the closed-loop dynamic behaviour under representative operating conditions and support comparison between the different crane configurations.

The reference cases are constructed from the parameter ranges defined in Section 6.7.2. For the transverse direction, three levels of control difficulty are defined by combining favourable, nominal, and unfavourable values of payload mass, hoisting length, disturbance magnitude, and wind speed. These severity levels are evaluated at two characteristic locations along the boom, corresponding to the maximum outreach position and a stiffer position closer to the portal frame, above the waterside twistlock station. For the trolley travel direction, only the three severity levels are considered, as the structural properties do not vary significantly with trolley position in this direction.

Together, these cases form a structured subset of the full parameter space, allowing the influence of operating severity, structural flexibility, and actuation concept on system performance to be assessed. The detailed definition of the reference cases and the corresponding results are presented in Section 7.2.

6.6.3 Performance Metrics

To compare the dynamic performance of the different configurations, a set of primary performance indicators is evaluated from the simulations. The most important perfor-

mance variable is the absolute horizontal load position x_{load}, since this directly reflects the positioning performance of the crane.

The tracking error is defined as $e(t) = x_{\text{load}}(t) - x_{\text{ref}}(t)$, and is used to quantify the deviation between the actual and desired load position. The error is evaluated over the time interval after the reference position has been reached, such that the results reflect positioning accuracy and disturbance rejection rather than the initial transient motion. The positioning performance is quantified using the maximum absolute tracking error,

$$e_{\max} = \max |e(t)|, \tag{103}$$

and the mean absolute tracking error,

$$e_{\text{MAE}} = \frac{1}{T} \int_0^T |e(t)| \, dt. \tag{104}$$

These quantities form the primary performance indicators for positioning accuracy. For interpretation of the results, the achieved tracking errors are compared with the required positioning accuracy of 50 mm in the transverse direction and 30 mm in the trolley travel direction. These values correspond to the most demanding operational case of container placement, where the container is landed directly onto another container and the twistlocks must engage with the corner castings without the possibility of guided contact or controlled collision [50].

The required control effort is assessed through the commanded actuator acceleration. For the Quad Trolley transverse model and the trolley travel model, this corresponds to the trolley acceleration $\ddot{x}_t$, while for the conventional STS transverse model it corresponds to the gantry acceleration $\ddot{x}_D$. This actuator acceleration is denoted as the control input $u(t)$. The actuator demand is quantified using the maximum absolute value,

$$u_{\max} = \max |u(t)|, \tag{105}$$

and the RMS value,

$$u_{\text{RMS}} = \sqrt{\frac{1}{T} \int_0^T u(t)^2 \, dt}, \tag{106}$$

which captures the overall control activity over time. Together, these quantities serve as primary indicators of actuator demand and control effort.

The actuator accelerations are also compared against the maximum allowable values for each configuration, as defined in Section 6.5.6, to ensure that the required control inputs remain physically feasible.

In addition to these primary performance indicators, several response quantities are evaluated to support the interpretation of the results and to verify the feasibility of the system from a design perspective. These include the structural displacement and load sway, which provide insight into the dynamic behaviour of the system and the interaction between the structure, actuation, and suspended load.

In addition, several quantities directly related to the mechanical design are considered. For the Quad Trolley transverse configuration, the maximum trolley displacement relative to the boom is evaluated, as this determines the required spacing between the boom girders and therefore has a direct impact on the structural layout.

Furthermore, the actuator velocities are assessed for all configurations. For the transverse direction, the trolley velocity is limited by practical constraints on drive systems and allowable operating speeds. Similarly, in the trolley travel direction, the trolley velocity must remain within feasible limits given the required accelerations and travel distances. For the conventional STS transverse configuration, the gantry velocity is evaluated in the same way, as excessive speeds would be impractical from both a mechanical and operational perspective.

These quantities are not used as primary performance measures, but serve as additional checks to ensure that the simulated behaviour remains physically realistic and compatible with practical design constraints.

Together, these metrics provide a consistent basis for evaluating the dynamic behaviour of the crane, while ensuring that both performance and practical design constraints are taken into account.

6.7 Parameter Sensitivity Analysis

To evaluate the influence of system parameters on the dynamic behaviour of the crane, a Design of Experiments (DOE) approach is adopted. The dynamic model involves a number of operational, environmental, and structural parameters whose individual and combined influence on system performance is not directly evident from the model formulation. In practice, parameters such as hoisting length, payload mass, and trolley position vary continuously during crane operation, resulting in a time-varying system. Since the dynamic model is formulated as a time-invariant system, a systematic parameter sensitivity analysis is performed to assess how variations in these parameters affect positioning performance and actuator demand across the operational envelope.

The same simulation framework and performance metrics are used for all parameter combinations. For each combination, the dynamic model is updated according to the selected parameters and the controller is recomputed accordingly, representing an idealised scenario in which the control system is always optimally tuned to the current configuration. This isolates the influence of the physical system parameters from the controller design, ensuring that differences in performance between cases can be attributed to the system characteristics rather than to suboptimal control tuning.

6.7.1 DOE Structure

A three-level full factorial design is adopted. Compared to a two-level design, a three-level DOE enables the identification of nonlinear effects and curvature in the parameter–response relationships. This is particularly relevant for the present system, where parameters such as hoisting length, wind loading, effective structural stiffness, and natural frequency are expected to influence the response in a nonlinear manner.

The number of parameters considered depends on the configuration. For the Quad Trolley transverse model, six parameters are varied: payload mass m, hoisting length L, disturbance force scale s_F, mean wind speed U_{mean}, equivalent structural stiffness k, and natural frequency f_n. This results in a total number of design points of

$$N = 3^6 = 729. \tag{107}$$

In this direction, the effective structural stiffness and natural frequency depend on the trolley location along the boom. These quantities are therefore included as independent parameters in the DOE.

For the trolley travel configuration, a reduced parameter set is considered, consisting of payload mass m, hoisting length L, disturbance force scale s_F, and mean wind speed U_{mean}. In this direction, the effective stiffness and natural frequency remain approximately constant and are therefore not treated as independent parameters. This leads to a total number of design points of

$$N = 3^4 = 81. \tag{108}$$

Given the relatively low computational cost of the simplified dynamic model, the use of a full factorial design is feasible, allowing all possible combinations of the selected parameter levels to be evaluated.

6.7.2 Parameter Definition

The parameter levels used in the DOE are summarised in Table 13. The selected parameters represent key operational, environmental, and structural characteristics that are expected to influence the dynamic response of the system.

Table 13: Parameters and levels used in the three-level DOE

Parameter	**Low**	**Nominal**	**High**	**Applicable to**
Payload mass m [t]	46	80	122	All
Hoisting length L [m]	10	30	50	All
Disturbance force scale s_F [-]	0.1	0.5	1.0	All
Mean wind speed U_{mean} [m/s]	3	8	13.3	All
Equivalent stiffness k [kN/m]	533	1870	3200	Transverse only
Natural frequency f_n [Hz]	0.243	0.288	0.333	Transverse only

The physical meaning of each parameter is summarised below:

- **Payload mass** m: The mass of the load suspended from the ropes. This includes the container payload as well as the headblock and spreader system. The lower bound of 46 t corresponds to the handling of two empty containers, while the upper bound of 122 t represents the maximum payload condition. This parameter directly influences the inertia of the system and the resulting load dynamics.
- **Hoisting length** L: The length of the hoisting cable, which determines the pendulum length of the suspended load. The range is selected from a minimum of 10 m to a maximum of 50 m, which approximately corresponds to the maximum free hoisting length outside the cell guides. Increasing L leads to lower sway frequencies and slower load dynamics, resulting in more persistent sway under disturbances.
- **Disturbance force scale** s_F: A scaling factor applied to a fixed, band-limited disturbance force signal representing the force induced by the second trolley, as described in Section 6.1.4. This allows the disturbance intensity to be varied while keeping the time variation of the signal consistent across simulations.

- **Mean wind speed** U_{mean}: The average wind speed used in the turbulence model (see Section 6.1.4). Higher wind speeds result in increased aerodynamic loading on both the crane structure and the suspended load.
- **Equivalent stiffness** k (transverse only): The effective structural stiffness at the trolley location in the transverse direction. This parameter effectively corresponds to the trolley position along the boom, with lower stiffness values corresponding to positions closer to the boom tip. The lower bound of 533 kN/m represents the trolley at maximum outreach, while the upper bound of 3200 kN/m corresponds to a position between the waterside legs.
- **Natural frequency** f_n (transverse only): The dominant structural natural frequency in the transverse direction. The first two modes are both in the transverse direction and have similar frequencies, which vary with the trolley positions along the boom. The lower bound of 0.243 Hz corresponds to the lowest value of the first mode, occurring when both trolleys are at their frontmost position, while the upper bound of 0.333 Hz corresponds to the highest value of the second mode. The parameter is varied to capture the change in structural dynamics associated with different trolley positions and to assess its influence on control performance.

For the transverse direction, all parameters listed in Table 13 are varied. For the trolley travel configuration, only the parameters marked as applicable to all configurations are varied, while the structural stiffness and natural frequency are kept constant at representative values for this direction.

6.7.3 Performance Evaluation

The performance of each simulation is evaluated using the indicators defined in Section 6.6.3. The analysis focuses on positioning accuracy, quantified by $e_{\max}$ and e_{MAE}, and actuator effort, quantified by $u_{\max}$ and u_{RMS}.

All metrics are evaluated over the time interval after the reference position has been reached, such that the results reflect disturbance rejection and steady positioning behaviour.

6.7.4 Analysis Method

The influence of individual parameters is evaluated using main effects. In a factorial Design of Experiments, the main effect of a parameter represents its average influence on a selected performance metric, independent of the specific values of the remaining parameters.

Let $y(m, L, s_F, U_{\text{mean}}, k, f_n)$ denote a generic performance metric evaluated for a given combination of parameters. The main effect of a parameter at a given level is obtained by averaging the response over all combinations of the remaining parameters. For example, the main effect of the hoisting length at level L_i is defined as

$$\bar{y}(L_i) = \frac{1}{N} \sum_{m} \sum_{s_F} \sum_{U_{\text{mean}}} \sum_{k} \sum_{f_n} y(m, L_i, s_F, U_{\text{mean}}, k, f_n), \tag{109}$$

where the summations extend over all levels of the remaining parameters, and N denotes the total number of evaluated combinations.

This averaging process isolates the effect of the selected parameter by removing the influence of the others. As a result, the main effect represents the expected change in the performance metric when the parameter is varied across its levels, without assuming fixed values for the remaining parameters.

Since each design point is evaluated multiple times using different disturbance realizations, the resulting variability is represented using error bars. The main effects therefore represent the average performance at each parameter level, while the variability due to disturbances is shown separately.

This approach enables the identification of dominant parameters and overall trends in system behaviour, providing clear insight into how variations in operational, environmental, and structural parameters affect positioning performance and actuator effort.

6.7.5 Hoisting Length Sweep

The parameter sensitivity analysis evaluates the influence of hoisting length using three discrete levels. While this is sufficient to capture general trends, it does not fully represent the continuous variation of the load dynamics with hoisting length.

The suspended load is modelled as a pendulum, for which the natural frequency is given by

$$f_l = \frac{1}{2\pi}\sqrt{\frac{g}{L}} \tag{110}$$

This relation shows that the load natural frequency varies significantly with hoisting length. Over the considered operational range of $L = 6$–50 m, the corresponding natural frequency decreases from approximately 0.20 Hz to 0.07 Hz. As a result, different values of L may lead to varying levels of dynamic interaction between the load motion and the structural response.

To capture this behaviour in more detail, a dedicated parameter sweep is performed over a finer range of hoisting length values. This sweep is carried out for both the transverse and trolley travel directions, while all other parameters are kept fixed at their nominal values.

Table 14 lists the corresponding load natural frequencies over the considered hoisting length range.

Table 14: Natural frequency of the suspended load as a function of hoisting length.

L **[m]**	6	10	15	20	25	30	35	40	45	50
f_l **[Hz]**	0.204	0.158	0.129	0.111	0.100	0.091	0.084	0.079	0.074	0.070

6.7.6 Targeted Stiffness and Natural Frequency Sweep

In addition to the general parameter sensitivity analysis and the hoisting length sweep, a dedicated sweep is performed to assess the influence of structural stiffness and natural frequency on system performance under conditions where the required positioning accuracy is not achieved. This analysis is not part of the systematic Design of Experiments, but is

introduced as a targeted investigation to evaluate whether modifications to the structural properties can improve dynamic performance.

The objective of this analysis is to determine whether the observed performance limitations can be attributed to insufficient structural stiffness or low natural frequency, and to assess whether increasing these properties would result in acceptable positioning accuracy.

The equivalent structural representation used in the dynamic model is defined by the relation between stiffness, modal mass, and natural frequency:

$$f_n = \frac{1}{2\pi}\sqrt{\frac{k}{m}} \tag{111}$$

This relation shows that stiffness, modal mass, and natural frequency are inherently coupled. To isolate the individual influence of these quantities, three complementary parameter sweeps are defined:

- A stiffness sweep with fixed modal mass, in which the stiffness is varied while the modal mass is kept constant. In this case, variations in stiffness directly result in changes in natural frequency.
- A stiffness sweep with fixed natural frequency, in which stiffness and modal mass are varied simultaneously such that the natural frequency remains constant. This allows the effect of stiffness to be assessed independently of changes in dynamic response frequency.
- A natural frequency sweep with fixed stiffness, in which the modal mass is varied to adjust the natural frequency while keeping the stiffness constant. This isolates the influence of natural frequency on system behaviour.

The baseline structural properties are taken from the structural analysis. In the stiffness sweeps, the stiffness is varied over a range from half to twice the baseline value. In the natural frequency sweep, the natural frequency is varied over a wide range covering both lower and higher values than the baseline design.

The sweeps are performed across all combinations of payload mass, hoisting length, disturbance force scale, and mean wind speed defined in the Design of Experiments, while varying only the structural properties under consideration.

7 Results

This section presents the results of both the structural and dynamic analyses of the Quad Trolley STS crane concept. First, the structural behaviour obtained from the finite element model is evaluated, including strength, fatigue, stability, quay loading, and modal properties. Subsequently, the dynamic response of the different crane configurations is analysed using the simplified dynamic models and the parameter sensitivity study. The results are interpreted with respect to positioning performance, actuator demand, and overall system feasibility and performance.

7.1 Structural Results

7.1.1 Structural Verification (EN13001)

The structural performance of the Quad Trolley STS crane is evaluated using the finite element model and methodology described in Chapter 5. The verification covers both strength and fatigue limit states for all load cases and combinations.

The final structure is obtained through iterative adjustment of the cross-sectional dimensions and plate thicknesses, ensuring that utilisation factors remain below unity for both strength and fatigue across all load combinations.

Strength Verification:
The strength verification shows that all structural components satisfy the required criteria under all considered load combinations. The utilisation levels for the different load combinations are presented in Figures 37, 38 and 39. These plots show, for each element, the maximum utilisation factor obtained over all load cases within the corresponding load combination group.

Load Combinations A3: Operational: Under normal operational loading, the utilisation levels remain relatively low, with a local maximum of approximately 0.88, as shown in Figure 37. The highest utilisation is localised around the main girder support, where the main girder connects to the rear portal frame.

The boom itself exhibits relatively uniform and moderate utilisation along its length, while the portal frame also remains lightly loaded.

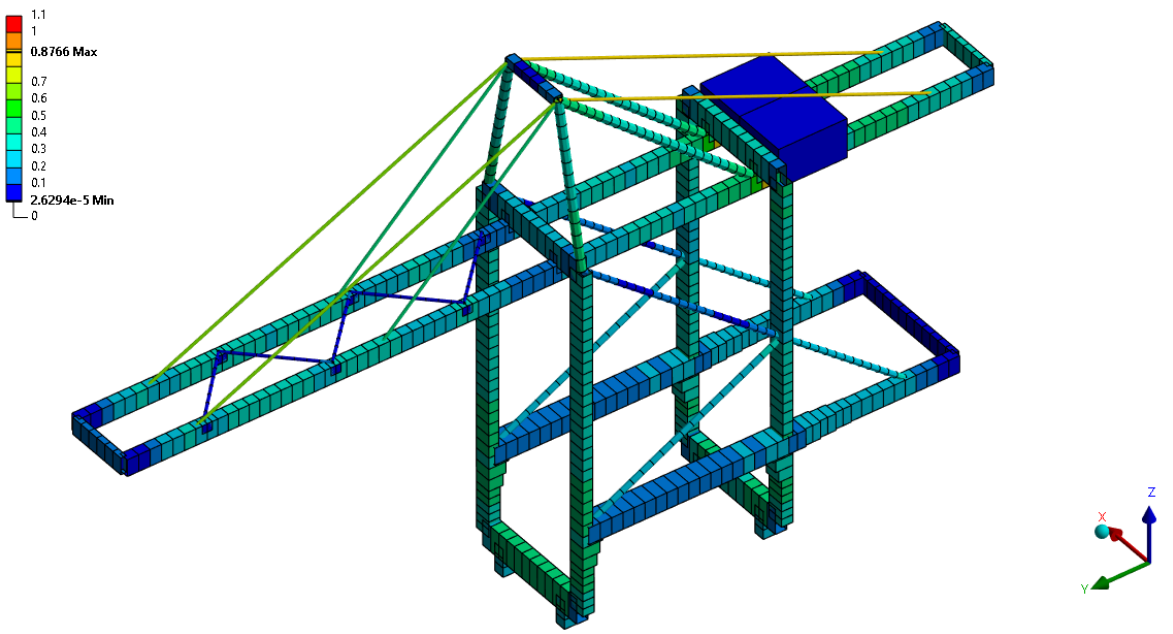

Figure 37: Utilisation factors for Load Combination A3 (operational), showing the maximum value per element over all operational load cases.

Load Combinations B3: Operational with Wind: Including wind loading increases the localised maximum utilisation to approximately 0.94, as shown in Figure 38.

Compared to the operational case without wind, the distribution of utilisation remains largely similar, but with consistently higher values throughout the structure.

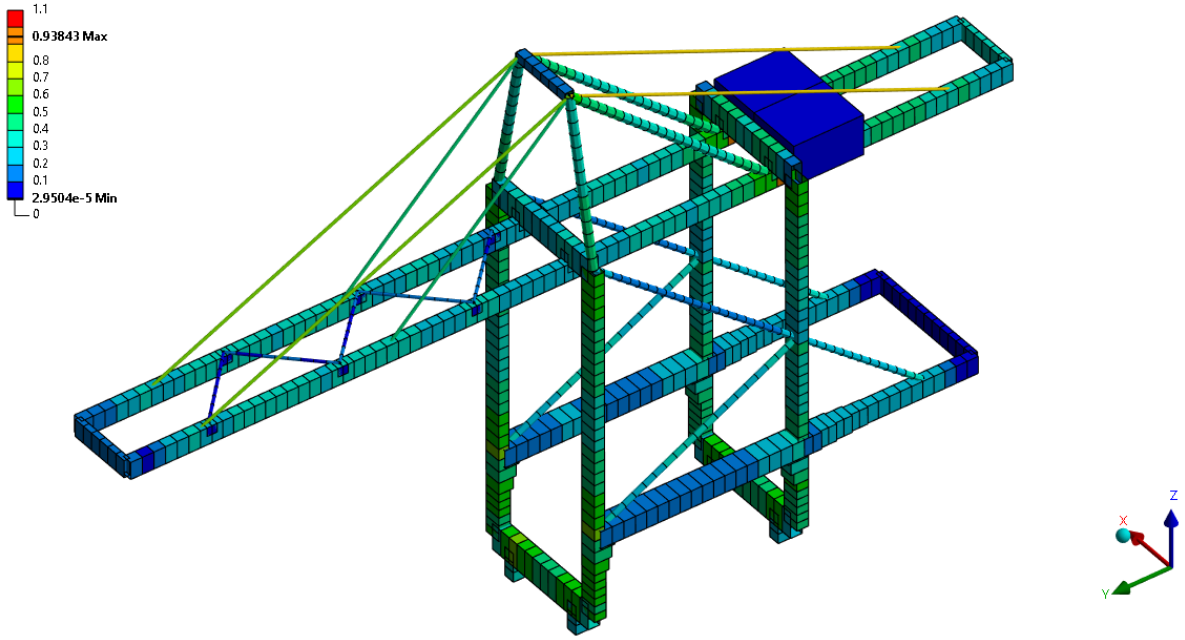

Figure 38: Utilisation factors for Load Combination B3 (operational with wind), showing the maximum value per element over all load cases.

Load Case C2: Storm (Boom Up): In the storm load case, with the boom in the raised position, the maximum utilisation is approximately 0.91, as shown in Figure 39. In contrast to the operational cases, the boom itself shows relatively low utilisation, while the highest stresses occur in the portal legs and lower structural frame, indicating that the structural response is dominated by global overturning effects due to wind loading. Despite this change in behaviour, all utilisation factors remain below unity.

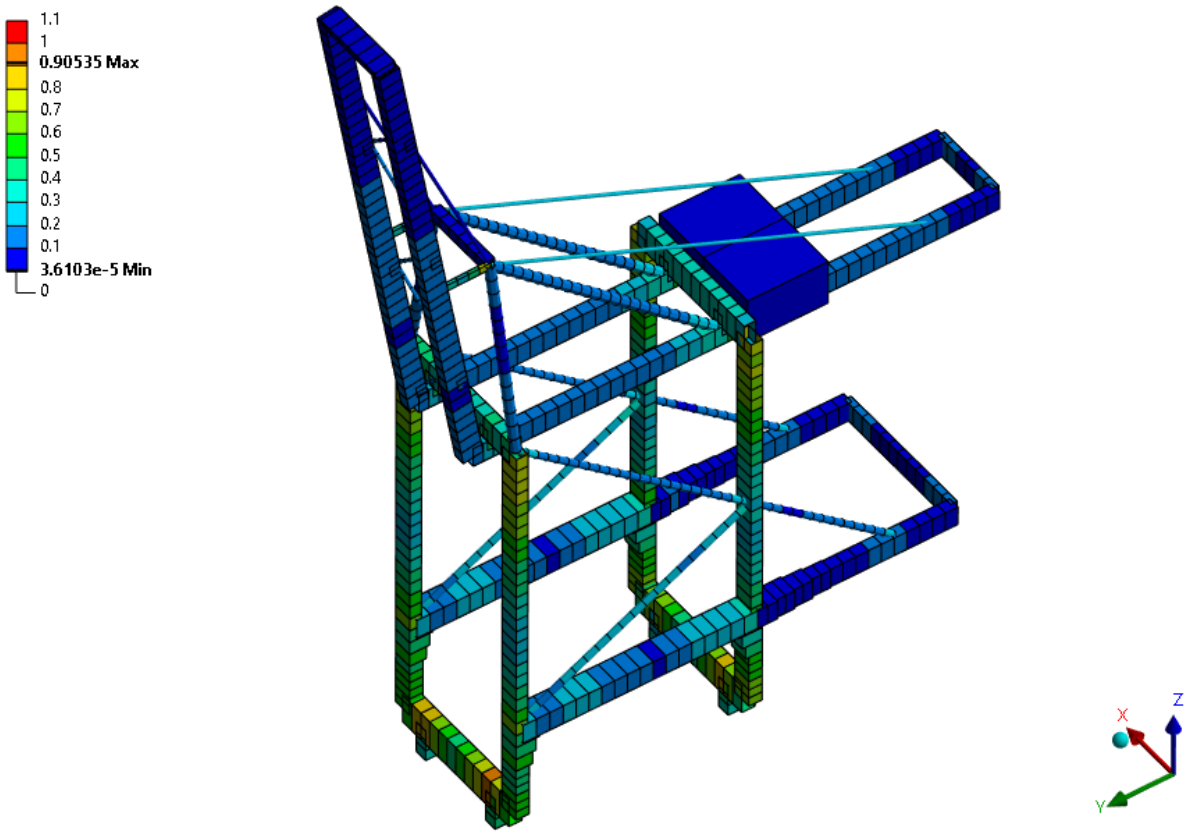

Figure 39: Utilisation factors for Load Combination C2 (storm, boom up), showing the maximum value per element over all storm load cases.

Fatigue Verification:
The fatigue verification is performed according to the methodology described in Section 5.5.2, based on an equivalent load approach and 2×10^6 load cycles per main trolley. The resulting fatigue utilisation is presented in Figure 40, showing, for each element, the utilisation based on the applied load spectrum and corresponding cycle distribution.

The fatigue verification shows that the structure is governed by fatigue rather than by peak strength. The cross-sectional dimensions were therefore iteratively adjusted until the fatigue utilisation remained just below unity. As a result, the fatigue utilisation is higher and more uniformly distributed across the structure compared to the strength results, with many members approaching unity.

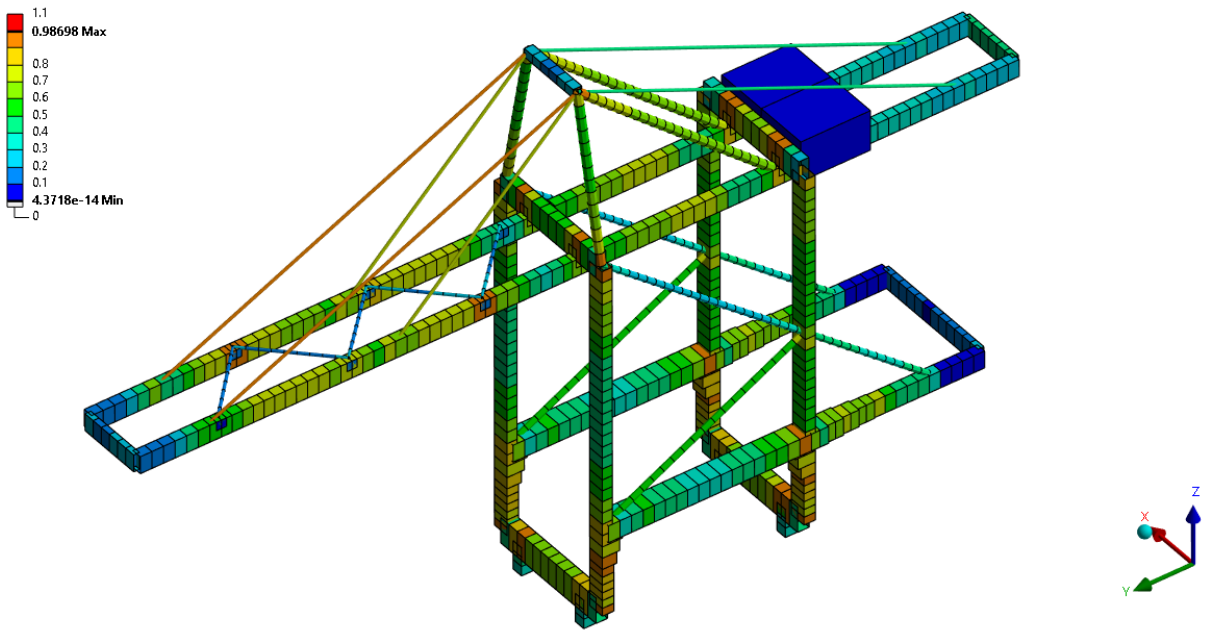

Figure 40: Fatigue utilisation factors per element, based on the applied load spectrum and cycle distribution.

Summary

The structural verification shows that the final design satisfies both strength and fatigue requirements for all considered load combinations. For strength, the highest utilisation occurs for operational loading with wind, while the storm condition leads to a different load distribution dominated by the portal frame and lower structure.

In contrast, fatigue governs the cross-sectional design. Since the structure was iteratively optimised to satisfy the fatigue criterion, the resulting fatigue utilisation is higher and more uniformly distributed across the structure, with many members approaching unity. This reflects that the final cross-sectional dimensions are primarily determined by fatigue rather than by strength.

7.1.2 Deflection Behaviour

The global deformation behaviour of the structure is evaluated for the governing load combinations A3 (operational), B3 (operational with wind), and C2 (storm). Each load combination represents the envelope of all corresponding load cases, with the reported deformation corresponding to the maximum total displacement magnitude (U_{sum}) per element over all load cases within that envelope. The resulting deformation plots are shown in Figures 41, 42, and 43. For all load combinations, the largest displacements occur at the boom tip, which is used as the reference location for comparison.

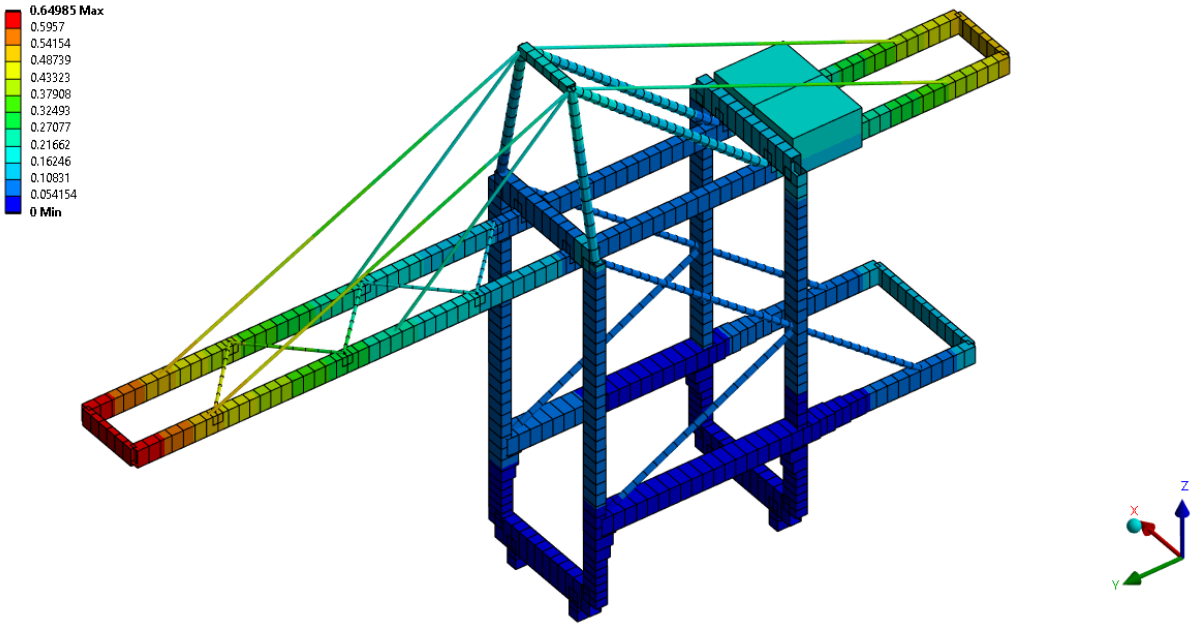

Figure 41: Deformation of the structure under Load Combination A3 (operational).

Figure 41 shows the deformation under operational loading without wind. The deformation is primarily concentrated in the boom, while the lower structure exhibits smaller absolute displacements.

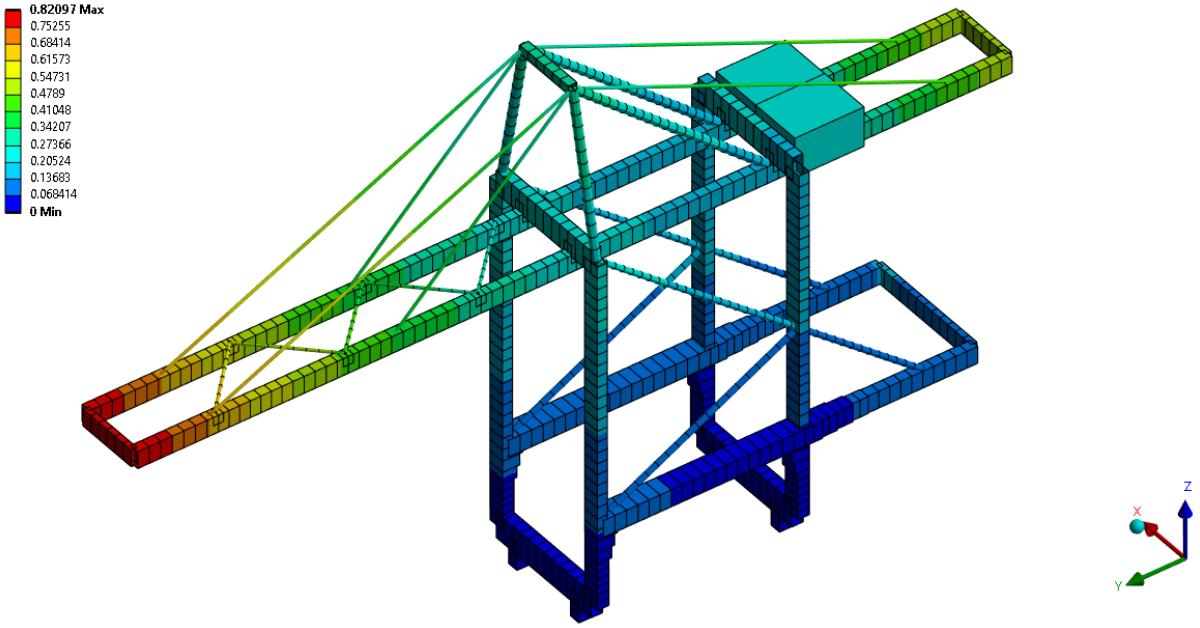

Figure 42: Deformation of the structure under Load Combination B3 (operational with wind).

Figure 42 shows the deformation under operational loading with wind. The deformation pattern of the boom remains similar to the A3 case, while additional deformation is observed in the upper structure due to the applied wind loading, resulting in increased overall displacement levels.

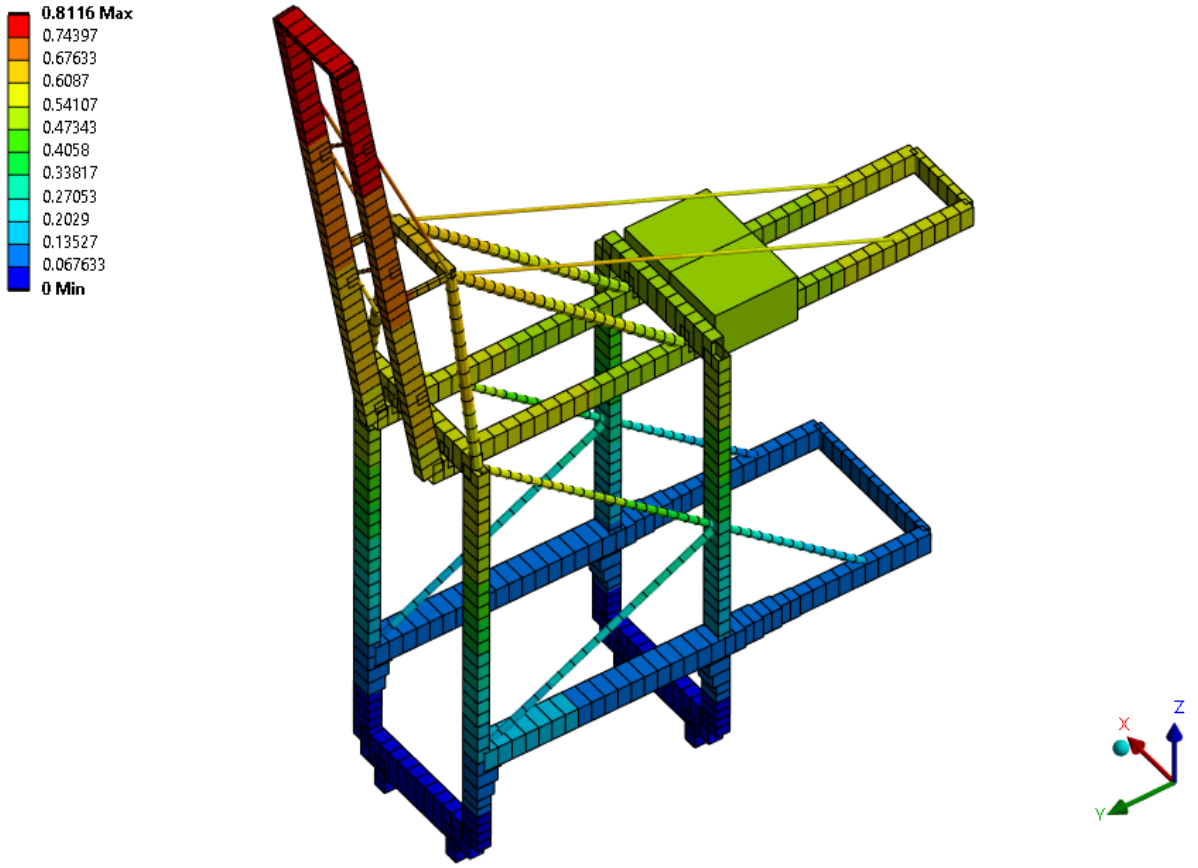

Figure 43: Deformation of the structure under Load Combination C2 (storm, boom up).

Figure 43 shows the deformation under storm conditions with the boom in the raised position. The deformation pattern differs from the operational cases, with a larger contribution from the portal frame and lower structure.

To quantify the deformation at the most outward structural location, the extreme displacement components at the boom tip are summarised in Table 15. The reported values correspond to the global displacements in the transverse (x), longitudinal (y), and vertical (z) directions, representing the maximum absolute response in each direction.

Table 15: Boom tip displacements at maximum outreach for the governing load combinations.

Load Combination	u_x **[m]**	u_y **[m]**	u_z **[m]**
A3 (Operational)	0.26	0.09	-0.59
B3 (Operational + Wind)	0.55	0.11	-0.60
C2 (Storm, Boom Up)	0.81	0.21	-0.07

7.1.3 Structural Mass Overview

Following the structural verification, the total structural mass of the Quad Trolley STS crane is evaluated based on the final, code-compliant design. This mass assessment forms

a critical input for subsequent analyses, including stability and quay loading evaluations, where the mass is converted into gravitational loads.

The steel structural mass of the crane is approximately 1161 mt, representing the total mass of the primary steel structure. This value includes the mass factor of 1.25 applied to the beam elements, as described in Section 5.2. The detailed cross-sectional dimensions and plate thicknesses of all structural members, as obtained from the iterative design process, are provided in Appendix F.

A complete mass breakdown of the crane is given in Table 16, based on the mass modelling approach described in Section 5.2.

Table 16: Mass breakdown of the Quad Trolley STS crane.

Component	**Mass**
Structural Mass (incl. factor 1.25)	1161 mt
Machine Room	230 mt
Bogies (12 m, ×4)	78 mt × 4
Twistlock station WS	50 mt
Twistlock station LS	50 mt
Access, conductor bars, sheaves, wire ropes, cable reel	149 mt
Main trolley rails and support	81 mt
Secondary trolley rails and support	25 mt
Total Weight (excluding trolleys)	**2058 mt**
Main trolley (×2)	30 mt × 2
Secondary trolley (×2)	100 mt × 2
Catenary trolley (×3)	5 mt × 3
Total Weight (including trolleys)	**2333 mt**

The total mass of the crane, including all equipment and trolleys, is approximately 2333 mt. The primary steel structure accounts for roughly 50% of the total mass, indicating that non-structural components contribute significantly to the overall system mass.

A substantial portion of the remaining mass is associated with mechanical systems, such as the machine room, trolley systems, and bogies, as well as auxiliary components. These components are essential for crane operation but do not directly contribute to the primary load-carrying capacity of the structure.

7.1.4 Comparison with Conventional STS Crane

To assess the influence of the Quad Trolley configuration on the structural design, a comparison is made with a conventional STS crane. The conventional crane is analysed using the same finite element model, modelling approach, and verification methodology as described in Chapter 5. For the strength verification, the same load cases and combinations are considered, but with only one main trolley and one secondary trolley operating at any given time. For the fatigue verification, the same equivalent load is applied, but now corresponds to a single main trolley performing 4×10^6 cycles rather than two trolleys each

performing 2×10^6 cycles, with the cycle distribution along the boom defined consistently with the Quad Trolley case.

This setup ensures that the comparison isolates the effect of the trolley configuration while maintaining consistency in the applied modelling assumptions, load definitions, and verification procedures. The only fundamental difference lies in the number of simultaneously operating trolleys, allowing the direct influence of the multi-trolley configuration on the structural response and design to be assessed.

Strength Verification:
The strength verification shows that all structural components satisfy the required criteria under all considered load combinations. Compared to the Quad Trolley configuration, the utilisation levels are lower, reflecting the reduced peak loading associated with single-trolley operation.

Load Combination A3: Operational

Under operational loading, the utilisation levels remain moderate, with peak values around 0.57. The overall distribution is similar to the Quad Trolley case, but with reduced magnitude due to the absence of simultaneous trolley loading.

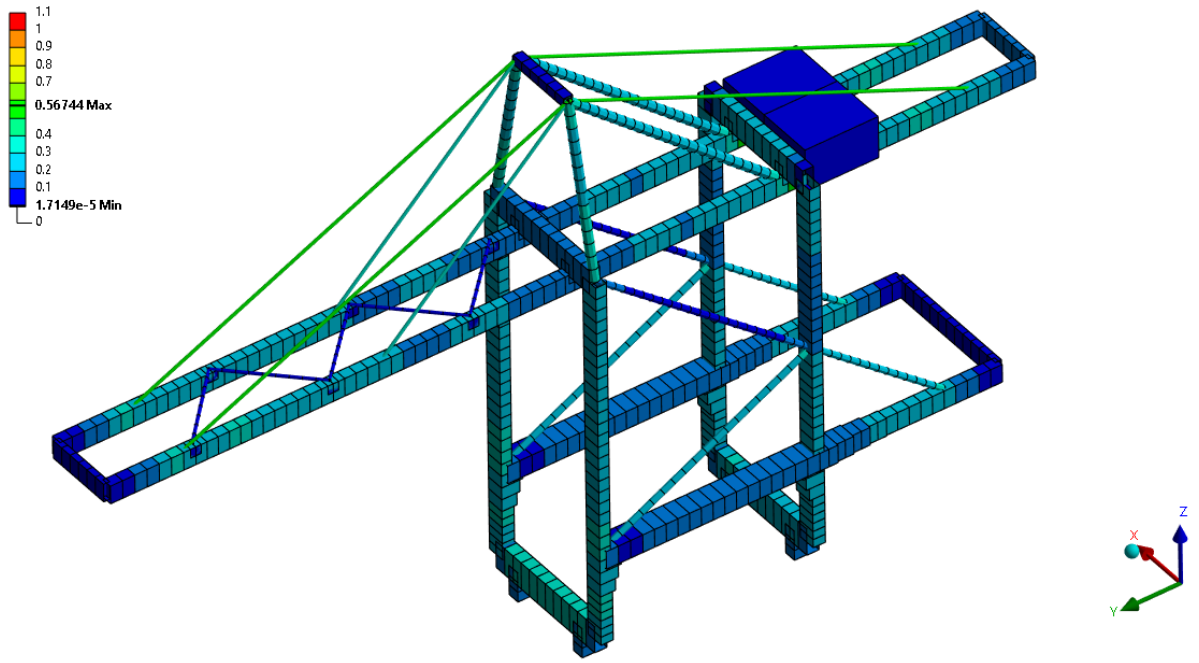

Figure 44: Utilisation factors for Load Combination A3 (operational), showing the maximum value per element over all operational load cases for the conventional STS crane.

Load Combination B3: Operational with Wind

Including wind loading increases the utilisation levels, but the overall distribution remains similar to the operational case. Compared to the Quad Trolley configuration, the utilisation levels are again consistently lower due to the reduced applied loading.

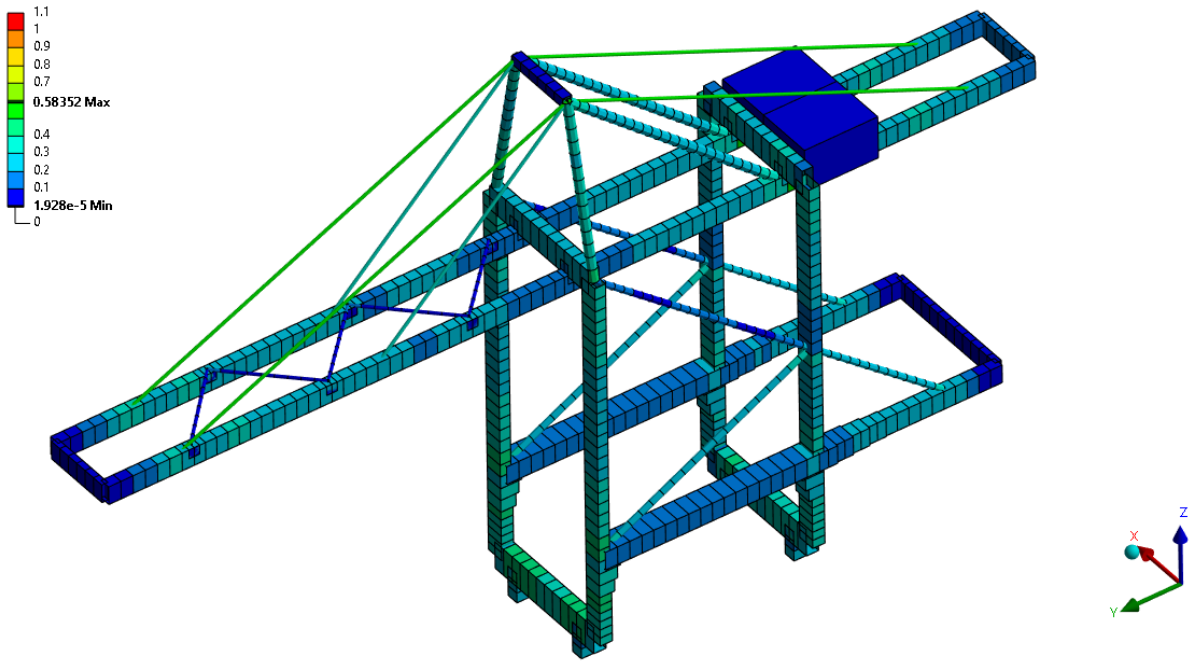

Figure 45: Utilisation factors for Load Combination B3 (operational with wind), showing the maximum value per element over all load cases for the conventional STS crane.

Load Combination C2: Storm (Boom Up)

In the storm configuration, the structural response is again dominated by global wind loading, with the highest utilisation occurring in the portal legs and lower structure. This behaviour is consistent with the Quad Trolley configuration.

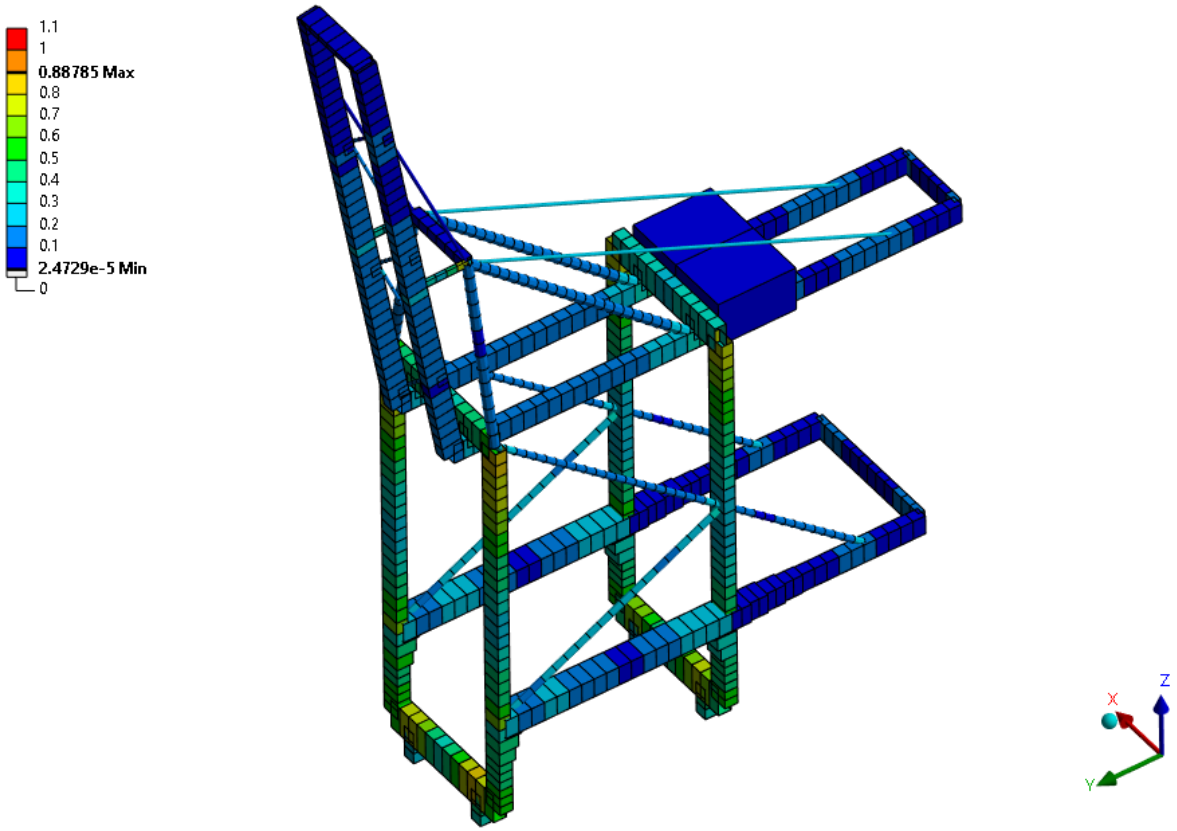

Figure 46: Utilisation factors for Load Combination C2 (storm, boom up), showing the maximum value per element over all storm load cases for the conventional STS crane.

Fatigue Verification:
The fatigue verification is performed according to the methodology described in Section 5.5.2, based on the same fatigue equivalent load and an equivalent of 4×10^6 container handling cycles. In the conventional configuration, this corresponds to a single main trolley performing 4×10^6 cycles, whereas in the Quad Trolley configuration, two main trolleys each perform 2×10^6 cycles.

The distribution of load cycles along the outreach is defined consistently with the Quad Trolley case, but now corresponds to a single trolley moving from the outreach region to one landside twistlock station.

The fatigue verification shows that fatigue again governs the structural design. The structural dimensions were therefore iteratively adjusted until the fatigue utilisation remained just below unity. As a result, the fatigue utilisation approaches unity across a large part of the structure.

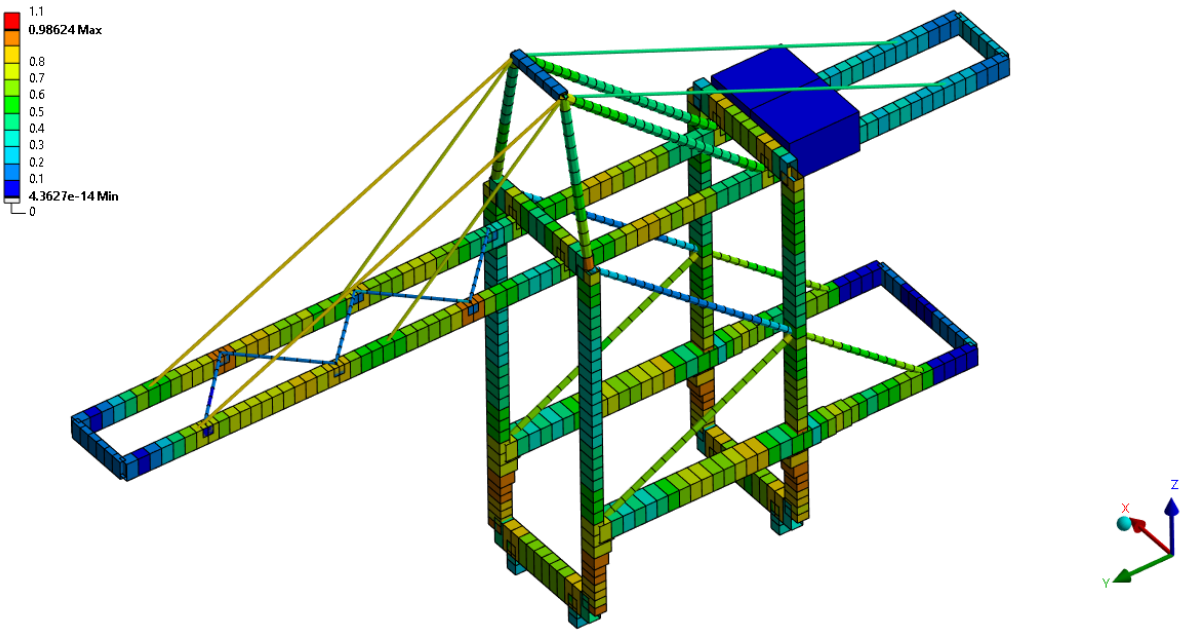

Figure 47: Fatigue utilisation factors per element, based on the applied load spectrum and cycle distribution for the conventional STS crane.

Mass Overview and Comparison:
The total structural mass of both configurations is evaluated based on the final, code-compliant designs. For the conventional STS crane, the structural mass is approximately 1108 mt, compared to 1161 mt for the Quad Trolley configuration.

A complete mass breakdown of both configurations is given in Table 17, based on the mass modelling approach described in Section 5.2.

Table 17: Mass breakdown of the conventional and Quad Trolley STS crane configurations.

Component	**Conventional STS**	**Quad Trolley STS**
Structural Mass (incl. factor 1.25)	1108 mt	1161 mt
Machine Room	150 mt	230 mt
Bogies (12 m, ×4)	78 mt × 4	78 mt × 4
Twistlock station WS	–	50 mt
Twistlock station LS	50 mt	50 mt
Access, conductor bars, sheaves, wire ropes, cable reel	149 mt	149 mt
Main trolley rails and support	81 mt	81 mt
Secondary trolley rails and support	25 mt	25 mt
Total Weight (excluding trolleys)	**1881 mt**	**2058 mt**
Main trolley	30 mt	30 mt × 2
Secondary trolley	100 mt	100 mt × 2
Catenary trolley	5 mt × 2	5 mt × 3
Total Weight (including trolleys)	**2021 mt**	**2333 mt**

The total mass of the conventional STS crane is approximately 2021 mt, compared to 2333 mt for the Quad Trolley configuration. The increase in total mass is mainly attributed to the additional trolley systems, the presence of a second twistlock station, and increased machine room requirements.

The structural mass shows a relatively limited increase. This is explained by the difference in fatigue loading between the two configurations: the Quad Trolley configuration is characterised by approximately 2×10^6 cycles with simultaneous loading of two trolleys, whereas the conventional configuration experiences approximately 4×10^6 cycles with single-trolley loading.

As a result, the increase in fatigue demand is governed by a combination of higher stress ranges and a reduced number of cycles, leading to a moderate overall increase rather than a proportional scaling.

7.1.5 Stability Assessment

In addition to strength and fatigue, the global stability of the crane is evaluated for both operational and storm conditions. As described in Section 5.6, the adopted stability criterion requires that no uplift occurs at any support location, meaning that all vertical reaction forces at the bogie supports must remain non-negative under all considered load cases. The assessment is based on the static vertical reaction forces obtained directly from the finite element model.

Operational Stability:

Under operational loading, the governing load cases include fully loaded main trolleys at maximum outreach, empty secondary trolleys at their frontmost position above their respective twistlock stations, longitudinal acceleration forces from all trolleys in the forward direction, transverse acceleration forces from the main trolleys, as well as wind loading from the side, as illustrated in Figure 48.

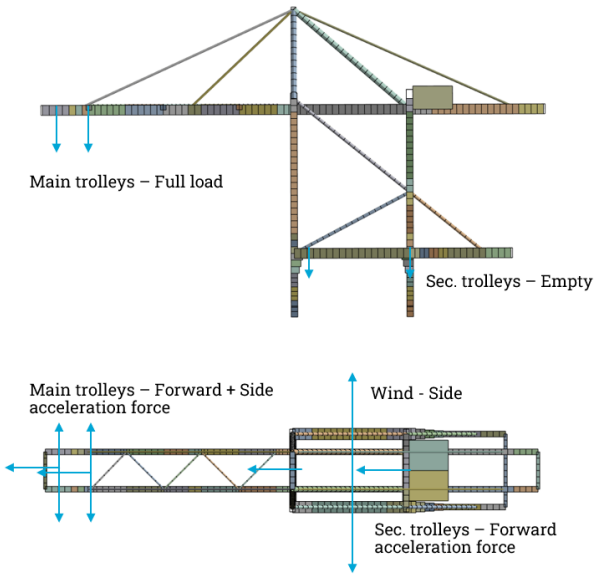

Figure 48: Operational stability critical load case

The bogie reaction forces obtained from the finite element model show that uplift occurs at the landside legs under these conditions, with a maximum uplift force of approximately 180 kN. This uplift is localised to a single landside leg at a time, with the governing leg determined by the direction of wind and transverse acceleration loading. Detailed bogie reaction forces for the governing load cases are provided in Appendix G. It should be noted that the restoring moment provided by the opposite leg is significantly greater than the uplift force, meaning that the crane would not overturn in practice. However, since the adopted

stability criterion requires zero uplift at all support locations, the baseline structural configuration does not satisfy this criterion under operational loading.

Two approaches can be considered to resolve this. The first is the addition of approximately 20 mt of ballast per leg in the lower landside legs, which increases the restoring moment sufficiently to eliminate all uplift. The second is the introduction of an operational positioning constraint on the main trolleys. Without any constraint, the minimum spacing between the two main trolleys is 10 m. To satisfy the stability criterion, this minimum spacing must be increased to 18 m when the front trolley is at maximum outreach at position P1 (72 m), meaning the rear trolley must be at position P10 rather than position P6, as shown in Figure 49. When the front trolley moves to position P2 (70 m), the required minimum spacing reduces to 14 m, corresponding to the rear trolley being at position P9 or further towards the landside. Once the front trolley reaches position P3 or beyond, the standard minimum spacing of 10 m is sufficient to maintain stability, and no additional constraint is required. As can be seen in Figure 49, this constraint affects only a small portion of the operational range, meaning that full stability can be achieved with minimal loss of operational flexibility. In either case, the uplift can therefore be resolved without fundamental changes to the structural concept.

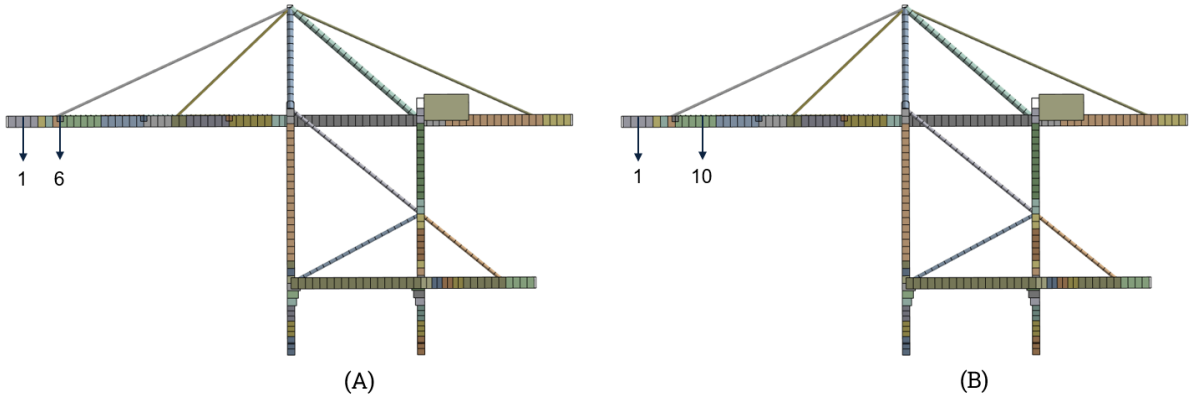

Figure 49: Operational positioning constraint on the main trolleys. (A) Minimum spacing of 10 m, with the rear trolley at position P6. (B) Increased spacing requirement under critical stability conditions, with the rear trolley shifted to position P10.

Storm Stability:
Under storm loading, with the boom in the boom rest position at 80°, storm loading from the sides of the crane governs the stability response. The bogie reaction forces obtained from the finite element model show that significant uplift occurs at the waterside legs, with a maximum uplift force of approximately 2350 kN. Detailed bogie reaction forces for the governing storm load cases are provided in Appendix G. As with the operational case, this uplift is localised to a single waterside leg at a time, with the governing leg determined by the direction of the storm wind. Unlike the operational case, the uplift forces under storm loading exceed the restoring moment provided by the opposite leg, meaning that the crane would overturn without additional measures.

Given the magnitude of the uplift forces involved, ballast alone is not a viable solution in this case. Instead, the application of tie-downs at each waterside leg of the crane is required to ensure stability during storm events. Tie-downs are mechanical anchoring

devices that anchor the crane's structure to the quay structure, resisting uplift forces and thereby preventing the crane from overturning, as illustrated in Figure 50. This is a well-established practice for large STS cranes, where storm tie-downs are used to ensure structural survival under extreme wind loading. Both the tie-down system and the anchoring structure must be designed to withstand the maximum uplift force of approximately 2350 kN.



Figure 50: Example of storm tie-downs connecting the crane structure to the quay.

If the foundation capacity is insufficient to accommodate these forces, lowering the boom from its boom rest position to a reduced angle can provide a more favourable weight distribution and significantly reduce the uplift demand, as illustrated in Figure 51. At a boom angle of 60°, the maximum uplift force reduces to approximately 1980 kN, and at 45° it further reduces to approximately 1680 kN, representing a reduction of approximately 17% and 29% respectively compared to the boom rest position. The corresponding bogie reaction forces are provided in Appendix G. The appropriate storm position would therefore depend on the capacity of the quay foundation and tie-down system.

However, when considering a reduced storm boom position, sufficient clearance for vessels berthed alongside the crane must be taken into account. Regardless of the selected storm position, the boom must always be raised high enough to allow a vessel to pass underneath, ensuring that a vessel breaking loose from its moorings during a storm cannot collide with the crane.

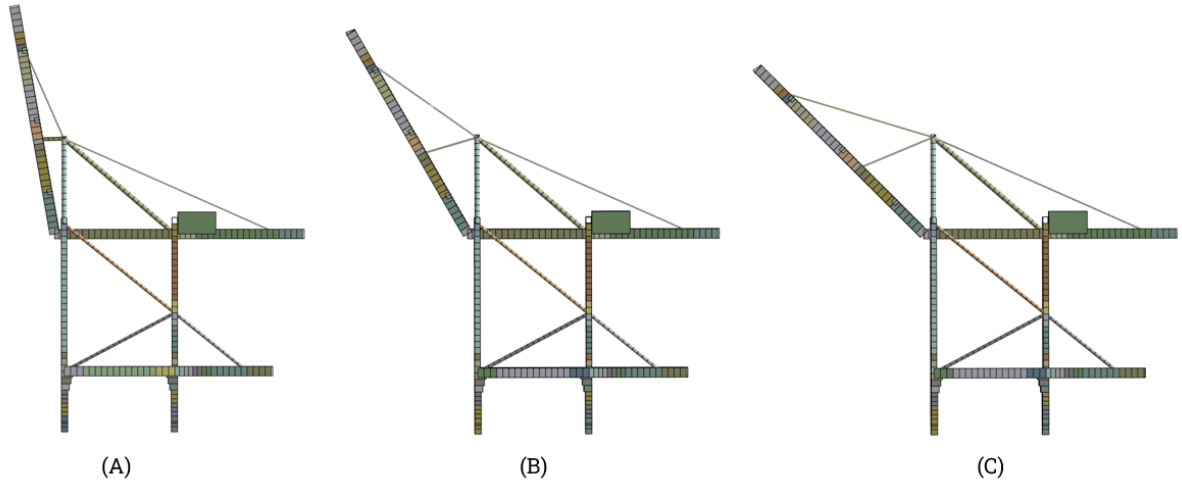

Figure 51: Boom positions under storm conditions: (A) 80°, (B) 60°, and (C) 45°.

7.1.6 Quay Loading

The quay loading is evaluated by deriving line loads from the bogie reaction forces obtained from the finite element model. The governing operational and storm load cases are considered, and the resulting reaction forces are distributed over the 12 m bogie length at each support location. The underlying bogie reaction forces are provided in Appendix G.

The resulting line loads for both the Quad Trolley and conventional STS crane, as obtained from the finite element model, are summarised in Table 18, together with reference values reported for existing STS crane infrastructure.

Table 18: Maximum line loads for the Quad Trolley and conventional STS crane compared to reference values from existing STS crane infrastructure.

Source	**Max. Line Load WS [kN/m]**	**Max. Line Load LS [kN/m]**
Quad Trolley STS – Operational	1010	1030
Quad Trolley STS – Storm	1060	980
Conventional STS – Operational	775	775
Conventional STS – Storm	930	970
Tech. Spec. 1 [39]	785	785
Tech. Spec. 2 [51]	1000	750
Tech. Spec. 3 [52]	1400	1400
Internal data [53]	900–1150	900–1150

The results show that under operational conditions, the conventional STS crane produces considerably lower line loads, with a maximum of approximately 775 kN/m compared to 1010–1030 kN/m for the Quad Trolley configuration, reflecting the significantly higher trolley-induced loading of the latter. Under storm conditions, however, the difference between the two configurations is much smaller, with maximum line loads of approximately

930–970 kN/m for the conventional crane and 980–1060 kN/m for the Quad Trolley crane. This is expected, as under storm conditions the trolleys are stationary and the structural response is governed by wind loading and the self-weight of the crane. Since both configurations share the same structural geometry and wind-exposed area, the somewhat higher storm line loads of the Quad Trolley configuration are primarily attributable to its greater total mass.

Comparing these results against the reference values reported for existing STS crane infrastructure, the line loads fall within the reported range, although at the upper end. This indicates that the concept does not impose exceptional demands on the quay structure and would generally be compatible with quay infrastructure designed for large STS cranes, subject to site-specific verification.

7.1.7 Modal Analysis

The natural frequencies of the crane structure vary with the position of the trolleys, as the moving trolley masses influence the overall mass distribution and therefore the dynamic properties of the structure. This effect is most pronounced in the transverse direction, where the trolley position has a significant influence on the mass distribution along the boom. For mode 1, the lowest frequency occurs when the trolleys are at maximum outreach, while the highest frequency occurs when the trolleys are positioned between the landside legs. For mode 2, the lowest frequency occurs when the trolleys are at maximum backreach, while the highest frequency occurs when the trolleys are at maximum outreach. The third vibration mode shows negligible variation with trolley positions and is therefore reported as a single value.

The resulting natural frequencies for the three primary vibration modes are summarised in Table 19, together with the corresponding mode shapes illustrated in Figures 52a, 52b, and 52c.

Table 19: Natural frequencies of the three primary vibration modes of the Quad Trolley STS crane, corresponding to the trolley positions between maximum outreach and maximum backreach.

Mode	**Description**	**Frequency [Hz]**
Mode 1	Boom Sway	0.243 – 0.273
Mode 2	Frame Torsion	0.306 – 0.333
Mode 3	Portal Sway	0.542

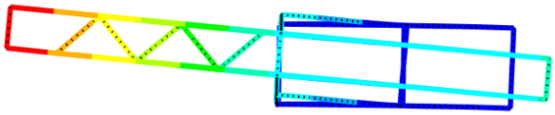

(a) Mode 1: Boom sway.

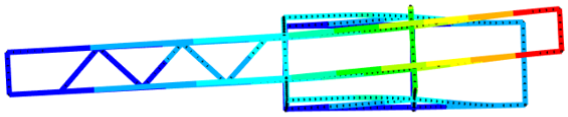

(b) Mode 2: Frame torsion.

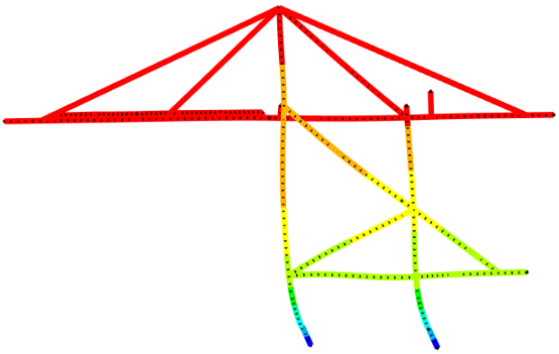

(c) Mode 3: Portal sway.

Figure 52: Primary vibration mode shapes of the Quad Trolley STS crane: (a) boom sway, (b) frame torsion, and (c) portal sway.

The natural frequencies of the Quad Trolley STS crane are compared against values reported in the literature for comparable STS cranes, as summarised in Table 20.

Table 20: Comparison of natural frequencies of the Quad Trolley STS crane with values reported in the literature and industry specifications.

Source	**Outreach [m]**	**Boom Sway [Hz]**	**Frame Torsion [Hz]**	**Portal Sway [Hz]**
Quad Trolley STS	72	0.243 – 0.273	0.306 – 0.333	0.542
Meisuh et al. (2022) [54]	63	0.25	0.33	0.60
Tran et al. (2018) [55]	63	0.26	0.47	0.74
Huang et al. (2021) [56]	55	0.26	0.42	–
Solazzi et al. (2024) [57]	36	0.60	0.83	–
Industry Spec.	71	$\geq$0.25	$\geq$0.25	$\geq$0.70
Industry Spec.	52	$\geq$0.30	$\geq$0.30	$\geq$0.68
ISO 22986 [58]	–	–	–	$\geq$0.50

The obtained natural frequencies are consistent with values reported in the literature for large STS cranes of comparable size, confirming that the dynamic properties of the model are representative. The transverse modes, comprising boom sway and frame torsion, fall mostly within the range reported in the literature and are largely above the minimum frequency requirement of $\geq$0.25 Hz, though the boom sway frequency approaches this limit at certain trolley positions. The portal sway frequency of 0.542 Hz satisfies the minimum of $\geq$0.50 Hz prescribed by ISO 22986 [58] for gantry cranes in process duty, but

falls below the minimum of ≥0.70 Hz found in industry specifications for conventional STS cranes. The implications of this for the dynamic performance are investigated in Section 7.2.

7.1.8 Summary of Structural Performance

The structural assessment demonstrates that the Quad Trolley STS crane concept is structurally feasible within the considered design constraints. Both strength and fatigue requirements are satisfied after iterative optimisation of the cross-sectional dimensions, with fatigue governing the final cross-sectional dimensions rather than peak strength. The resulting structural mass shows only a limited increase compared to a conventional STS crane, indicating that the additional loading introduced by the multi-trolley configuration does not disproportionately increase the structural demand.

Stability is identified as a governing design consideration. Under operational conditions, the occurring uplift at the landside legs can be resolved through either the addition of ballast or the introduction of an operational positioning constraint on the main trolleys, both of which require only minor modifications to the baseline concept. Under storm conditions, tie-downs are required to prevent overturning, with the option to lower the boom angle providing an additional means of reducing uplift forces if the foundation capacity is limited. While stability requires careful attention, the results confirm that the conventional 27 m width constraint is feasible for the Quad Trolley configuration, provided that the appropriate stability measures are implemented. Quay loading remains within the range reported for existing STS crane infrastructure, further confirming that the concept is compatible with modern port facilities, subject to site-specific verification.

The natural frequencies of the crane are consistent with values reported in the literature for large STS cranes of comparable size. The transverse modes satisfy the minimum frequency requirements, though the boom sway frequency approaches the lower limit at certain trolley positions. The portal sway frequency of 0.542 Hz satisfies the minimum requirement of ISO 22986, but falls below the minimum of ≥0.70 Hz found in industry specifications for conventional STS cranes. The implications of this for dynamic performance are investigated in the dynamic analysis presented in Section 7.2.

Together, these findings confirm that the Quad Trolley concept can be realised as a structurally sound and code-compliant design within the conventional 27 m width constraint, providing a consistent and representative basis for the dynamic analysis presented in the following sections.

7.2 Dynamic Results

This section presents the results of the dynamic analysis of the Quad Trolley STS crane concept. Two motion scenarios are evaluated: transverse trolley motion, in which the main trolleys move the sheave block transversely across the boom using their onboard transverse drive mechanism, and trolley travel along the boom, in which the trolleys travel between the outreach and landside positions during container handling. For each scenario, the dynamic response is first evaluated for a set of reference parameter combinations representing typical operating conditions, after which a parameter sensitivity study is performed to identify the most critical factors affecting positioning accuracy and actuator demand. The transverse results are compared against a conventional STS crane to assess

the performance advantage offered by the direct trolley transverse drive, which represents the most fundamental dynamic difference between the two concepts. The section closes with an integrated discussion of the influence of actuation concept, structural flexibility, and dominant disturbances on overall dynamic feasibility.

7.2.1 Transverse Motion

The transverse motion scenario evaluates the dynamic behaviour of the main trolleys as they move the sheave block transversely across the boom using the onboard transverse mechanism. This motion is unique to the Quad Trolley concept; in a conventional STS crane, transverse repositioning requires moving the entire crane using the gantry drive. The dynamic model and performance indicators used for this scenario are described in Sections 6.2 and 6.6.3 respectively.

Quad Trolley Transverse – Reference Cases:
The dynamic response of the Quad Trolley STS configuration in the transverse direction is evaluated for a set of reference parameter combinations representing typical operating conditions. These reference cases are selected from the parameter ranges defined in Chapter 6 and serve as a representative subset of the full parameter space, providing an intuitive basis for interpreting the results of the parameter sensitivity analysis and the comparison with the conventional STS crane.

The reference cases are defined along two primary dimensions. The first is control difficulty, for which three levels are considered: low, medium, and high severity. These levels are constructed by simultaneously varying the payload mass, hoisting length, disturbance magnitude, and wind speed. Low-severity cases correspond to favourable operating conditions, characterised by high payload mass, short hoisting length, and low disturbance levels. High-severity cases represent challenging conditions, with low payload mass, long hoisting length, and high disturbance levels. This definition reflects the controllability of the system rather than the structural loading, as lower payload mass and longer hoisting length increase the sensitivity of the system to disturbances and therefore result in more demanding control conditions.

The second dimension is trolley position along the boom. The reference cases are evaluated at two characteristic boom positions: the maximum outreach position and the position directly above the waterside twistlock station. These positions correspond to significantly different effective structural stiffness values, with $k = 533$ kN/m at maximum outreach and $k = 3200$ kN/m above the twistlock station. The outreach position represents the most flexible configuration of the structure, where the boom deflects most under transverse loading and structural compliance therefore has the strongest influence on the dynamic response. The position above the twistlock station, which is located inside the waterside portal frame, represents a considerably stiffer configuration in which the influence of structural flexibility is reduced. The natural frequencies associated with each position are obtained from the modal analysis described in Section 7.1.7, and reflect the variation in dynamic properties with trolley position along the boom.

The combination of three severity levels and two trolley positions results in six reference cases, as summarised in Table 21. Together, these cases provide a structured overview of system behaviour, allowing the influence of both operating conditions and trolley position on positioning performance and actuator demand to be clearly identified.

Table 21: Definition of reference cases for dynamic response evaluation. The cases represent low, medium, and high control difficulty at two characteristic structural locations.

Case	**Location**	**Severity**	k [kN/m]	f_n [Hz]	m [t]	L [m]	s_F [-]	U_{mean} [m/s]
RC1	Outreach	Low	533	0.243	122	10	0.1	3.0
RC2	Outreach	Medium	533	0.243	80	30	0.5	8.0
RC3	Outreach	High	533	0.243	46	50	1.0	13.3
RC4	Twistlock station	Low	3200	0.270	122	10	0.1	3.0
RC5	Twistlock station	Medium	3200	0.270	80	30	0.5	8.0
RC6	Twistlock station	High	3200	0.270	46	50	1.0	13.3

The positioning accuracy and actuator demand results for all six reference cases are presented in Figures 53 and 54. The results show that direct actuation of the trolley transverse mechanism enables rapid and responsive control across all considered cases. For the low and medium severity cases, the tracking error remains within the 50 mm accuracy threshold throughout the motion. Only under high-severity conditions do occasional peaks in tracking error exceed this threshold. This is illustrated in Figure 55, which shows the time-domain tracking error for the worst reference case (RC3), confirming that even under the most demanding conditions the error remains within the threshold for the majority of the motion. As expected, tracking errors and actuator demand increase with severity level. Cases evaluated above the waterside twistlock station consistently produce lower tracking errors and lower actuator demand compared to the outreach cases at the same severity level, reflecting the higher effective stiffness at this position and its beneficial effect on dynamic performance.

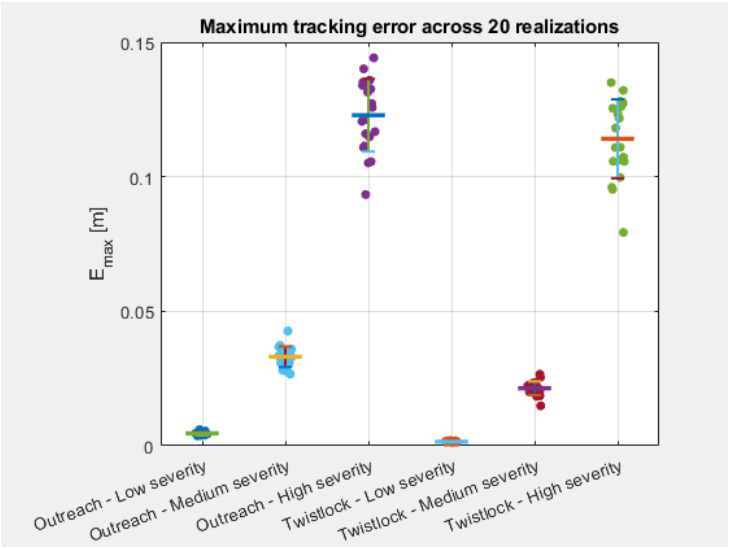

(a) Maximum tracking error.

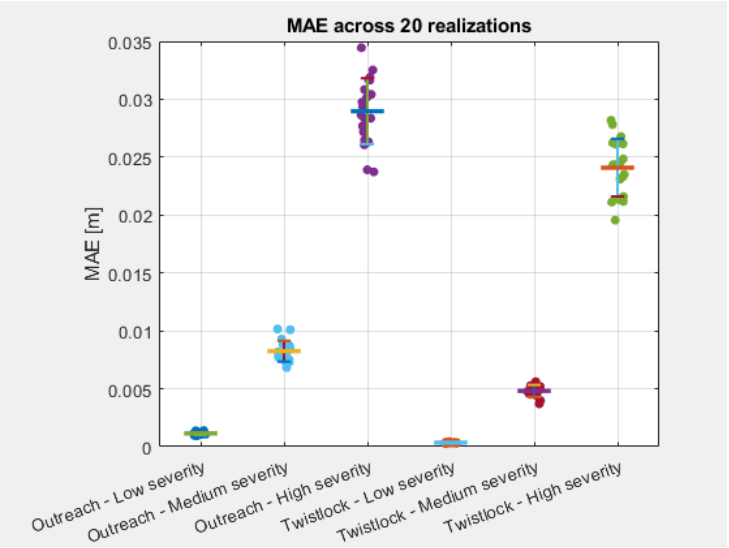

(b) Mean absolute error.

Figure 53: Positioning accuracy (mean ± standard deviation over 20 stochastic realizations) for all six reference cases.

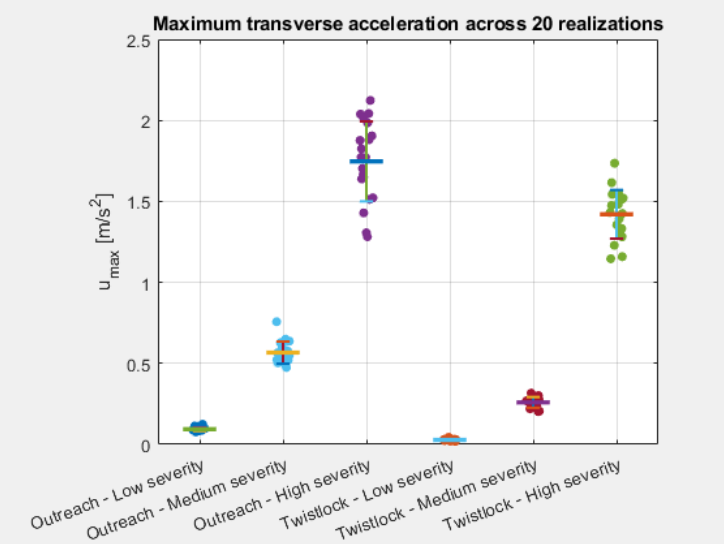

(a) Maximum trolley transverse acceleration.

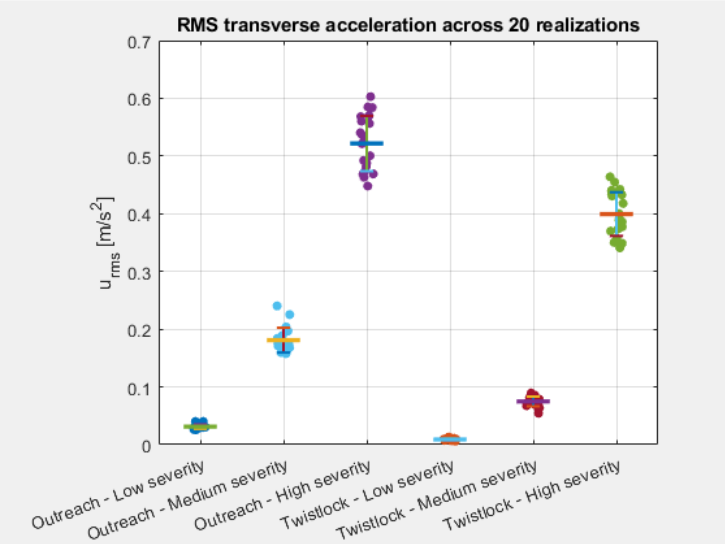

(b) RMS trolley transverse acceleration.

Figure 54: Actuator demand (mean ± standard deviation over 20 stochastic realizations) for all six reference cases.

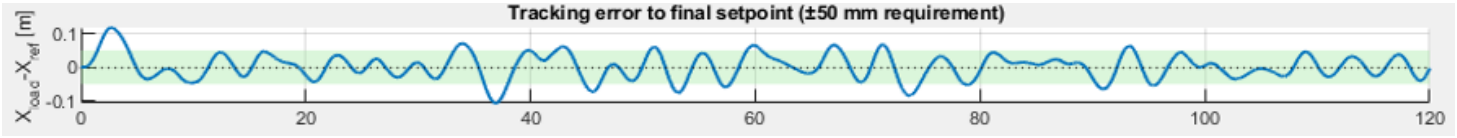

Figure 55: Time-domain tracking error for the worst case reference case (RC3: maximum outreach position, high severity), showing that the 50 mm accuracy threshold is exceeded only occasionally, while the error remains within the threshold for the majority of the motion.

Relative Transverse Trolley-sheave block Displacement:
In addition to positioning accuracy and actuator demand, the relative displacement of the sheave block with respect to the boom is evaluated to assess the feasibility of the transverse actuation concept from a geometric design perspective. This quantity represents the required motion of the sheave block relative to the supporting structure, and therefore indicates whether the demanded positioning remains within a physically achievable range. It further defines the required transverse travel stroke and thus has a direct implication for the spacing between the boom girders.

Table 22: Maximum relative sheave block displacement with respect to the boom across 20 realizations for each transverse reference case.

Case	Reference case	$\mathbf{x}_{\mathrm{t,rel,max}}$ [m]
RC1	Outreach – Low severity	0.064
RC2	Outreach – Medium severity	0.467
RC3	Outreach – High severity	1.95
RC4	Twistlock station – Low severity	0.017
RC5	Twistlock station – Medium severity	0.211
RC6	Twistlock station – High severity	1.53

The results show a strong increase in relative trolley displacement with increasing severity level, consistent with the trends observed in tracking error and actuator demand. At the outreach position, the maximum relative displacement increases from approximately 0.06 m under low-severity conditions to nearly 2.0 m in the high-severity case. At the twistlock station, the corresponding values are consistently lower, ranging from approximately 0.02 m to 1.5 m, reflecting the higher effective structural stiffness at this location.

For low- and medium-severity cases, the relative displacements remain limited, indicating that the required sheave block motion is modest and can be readily accommodated within a practical design. Under high-severity conditions, however, the relative displacement increases substantially, reaching values on the order of 1.5–2.0 m. These displacements govern the required transverse travel stroke on the trolley and, consequently, the spacing between the boom girders, but they remain within a geometrically feasible range.

Conventional STS Transverse – Reference Cases:
The transverse response of the conventional STS crane is evaluated for the same six reference cases using the compliant-drive model described in Section 6.3. In this model, the gantry drive actuates the base of the crane at the bogie level, from which the motion is transmitted through the flexible crane structure to the suspension point of the load. Unlike the Quad Trolley configuration, where the transverse drive is mounted directly on the trolley, the gantry drive must accelerate the entire crane structure to achieve transverse motion. This indirect force transmission path introduces structural compliance between the drive input and the suspension point, which limits the controller's ability to reject disturbances and maintain accurate positioning.

The positioning accuracy and actuator demand results for all six reference cases are presented in Figures 56 and 57. In contrast to the Quad Trolley configuration, the tracking error exceeds the 50 mm accuracy threshold across all reference cases, including the low-severity cases, reflecting the fundamental limitation of indirect gantry-based actuation. As with the Quad Trolley configuration, tracking errors increase with severity level, and cases evaluated above the waterside twistlock station produce lower tracking errors compared to the outreach cases at the same severity level, consistent with the higher effective stiffness at this position.

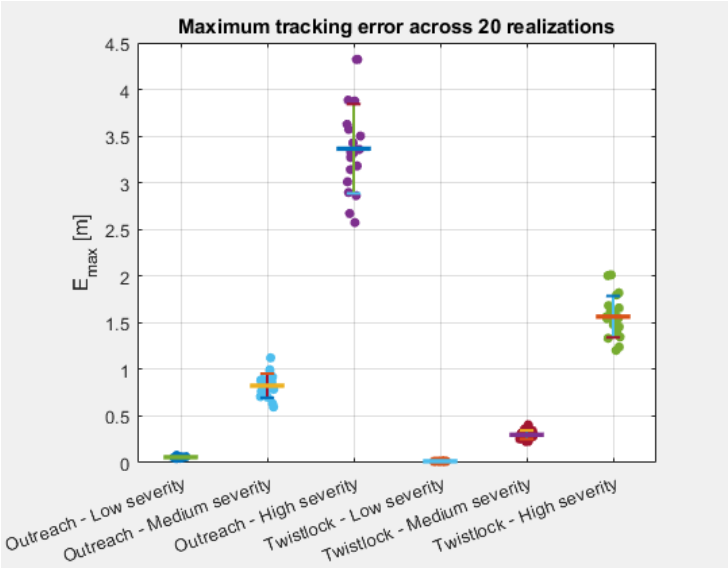

(a) Maximum tracking error.

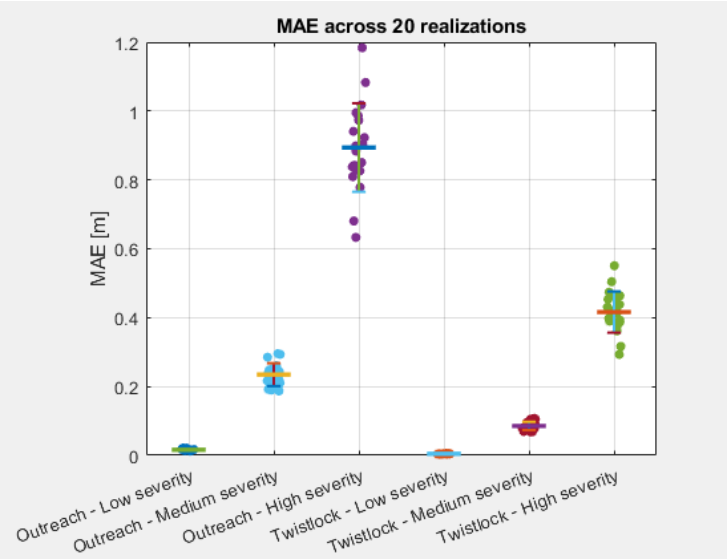

(b) Mean absolute error.

Figure 56: Positioning accuracy (mean ± standard deviation over 20 stochastic realizations) for all six reference cases, conventional gantry drive.

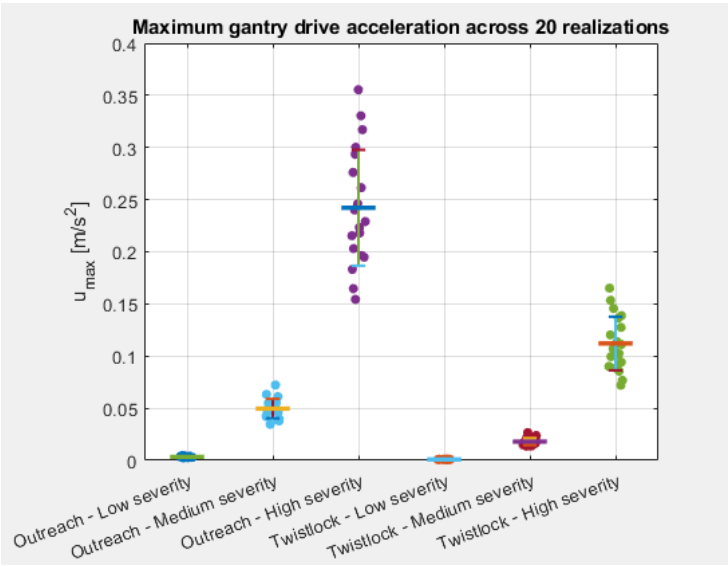

(a) Maximum gantry drive acceleration.

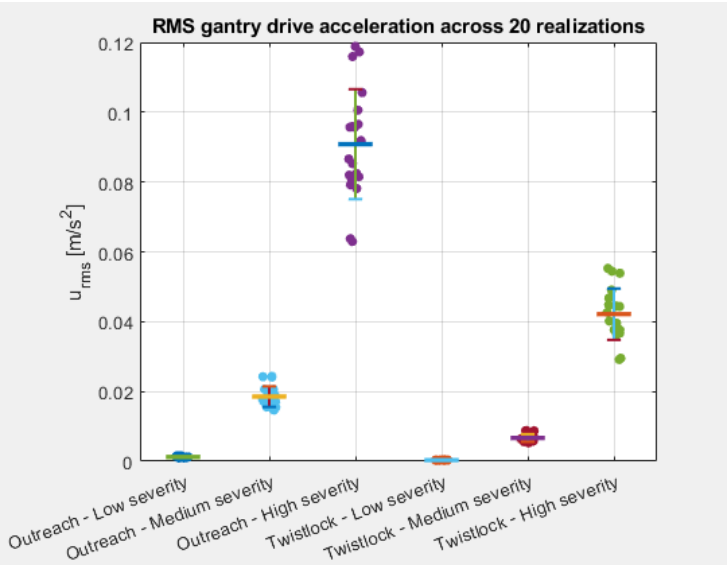

(b) RMS gantry drive acceleration.

Figure 57: Actuator demand (mean ± standard deviation over 20 stochastic realizations) for all six reference cases, conventional gantry drive.

Comparison Between Configurations:
A direct comparison between the Quad Trolley and conventional STS configurations across all reference cases is presented in Figures 58 and 59. Note that different vertical axis scales are used for the two configurations due to the large difference in magnitude. The results consistently demonstrate a substantial difference in positioning accuracy between the two configurations. The Quad Trolley configuration achieves tracking errors within or close to the 50 mm accuracy threshold across all reference cases, while the conventional STS crane exceeds this threshold across all cases, including the low-severity cases.

The fundamental cause of this difference lies in the actuation concept. In the Quad Trolley configuration, the transverse drive is mounted directly on the trolley, enabling corrective movements to be applied at the suspension point itself. This allows the controller to respond rapidly and precisely to disturbances, resulting in small tracking errors even under demanding conditions. In the conventional STS crane, the gantry drive actuates the base of the crane at the bogie level, from which the motion must be transmitted through the flexible crane structure to the suspension point. This indirect force transmission path introduces structural flexibility and lag between the drive input and the resulting motion at the suspension point. Furthermore, because the gantry drive must accelerate the entire crane structure, its maximum achievable acceleration is significantly lower than that of the direct trolley transverse drive, resulting in slower actuation and a reduced ability to make the corrective movements needed to reject disturbances. Together, the indirect actuation path and the lower maximum acceleration fundamentally limit the achievable positioning accuracy of the conventional configuration.

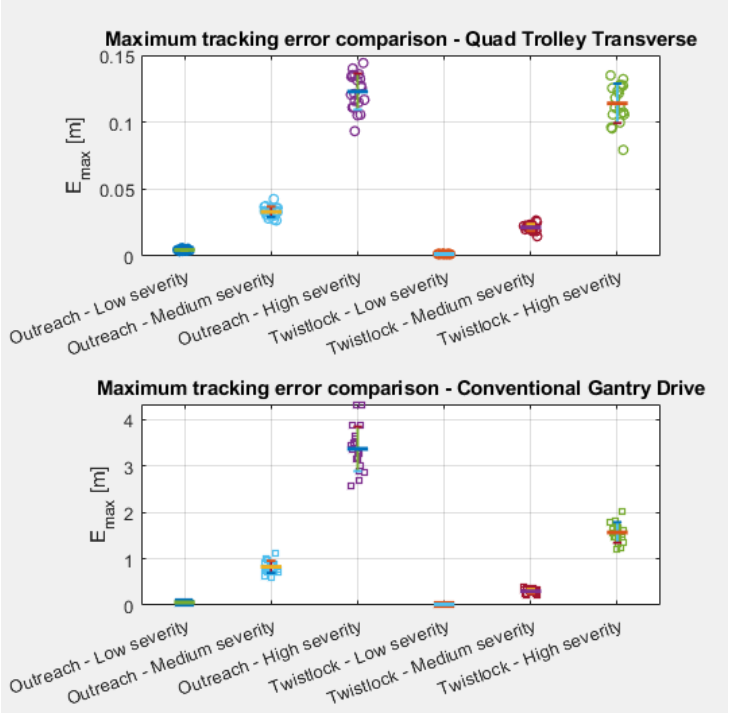

(a) Maximum tracking error.

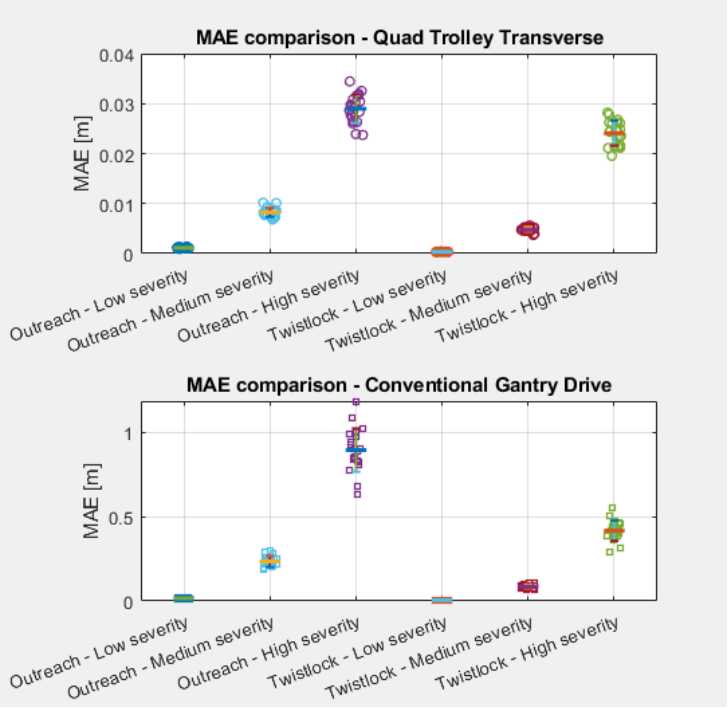

(b) Mean absolute error.

Figure 58: Positioning accuracy comparison (mean ± standard deviation over 20 stochastic realizations) between the Quad Trolley and conventional STS crane for all six reference cases.

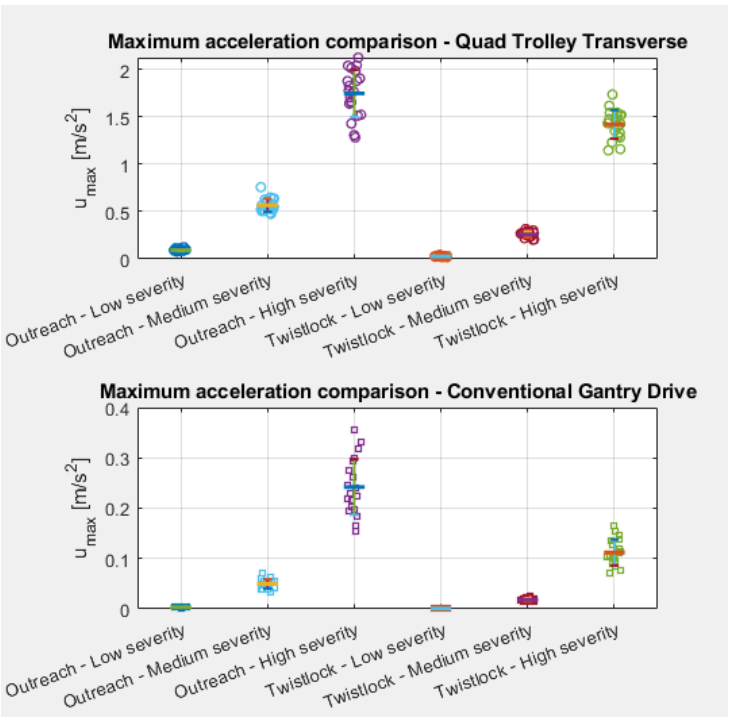

(a) Maximum actuator acceleration.

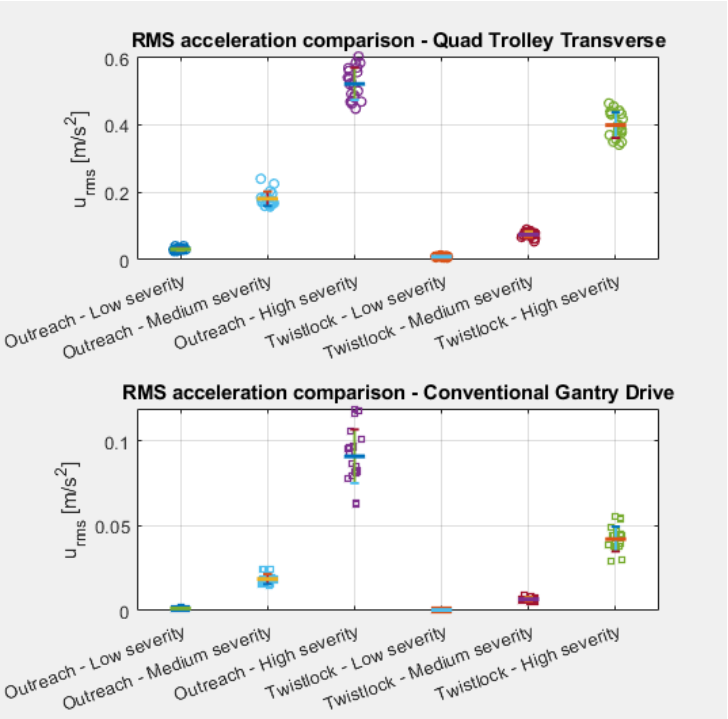

(b) RMS actuator acceleration.

Figure 59: Actuator comparison (mean ± standard deviation over 20 stochastic realizations) between the Quad Trolley and conventional STS crane for all six reference cases.

7.2.2 Transverse Parameter Sensitivity

The influence of system parameters on the transverse dynamic performance of the Quad Trolley STS crane is evaluated using a full factorial Design of Experiments with three levels per parameter, as described in Section 6.7.1. Six parameters are varied: payload mass m, hoisting length L, disturbance force scale s_F, mean wind speed U_{mean}, equivalent structural stiffness k, and natural frequency f_n, resulting in a total of $3^6 = 729$ design points. The parameter levels are defined in Table 13. As described in Section 6.7.2, the equivalent structural stiffness and natural frequency are not independent design variables but represent the variation in structural properties with trolley position along the boom, with lower values corresponding to positions closer to the boom tip and higher values corresponding to positions closer to the portal frame. The results are evaluated in terms of the four performance indicators defined in Section 6.6.3: maximum tracking error $e_{\max}$, mean absolute error e_{MAE}, maximum acceleration $u_{\max}$, and RMS acceleration u_{RMS}.

The main effects on positioning accuracy are presented in Figure 60, and the main effects on actuator demand are presented in Figure 61. The results reveal a clear hierarchy in parameter influence. Wind speed is by far the dominant factor affecting positioning accuracy, with $e_{\max}$ and e_{MAE} both increasing strongly and nonlinearly with U_{mean}. This reflects the direct excitation of both the crane structure and the suspended load by wind loading, which represents the primary disturbance source in the transverse direction. Payload mass and hoisting length also have a notable influence on tracking error, with lower payload mass and longer hoisting length both resulting in higher tracking errors. This is consistent with the reference case results, as lighter payloads and longer hoisting lengths increase the sensitivity of the system to external disturbances.

The disturbance force scale s_F, representing the dynamic interaction between the two main trolleys, shows a comparable influence on tracking error to that of payload mass and hoisting length. This indicates that the inter-trolley disturbance has a non-negligible effect on transverse positioning accuracy, consistent with the physical expectation that the disturbance force from the second trolley directly excites the flexible boom structure in the transverse direction.

The equivalent structural stiffness and natural frequency, which together reflect the influence of trolley position along the boom, both show a modest but consistent effect on tracking error. Trolley positions closer to the portal frame, corresponding to higher stiffness and higher natural frequency, result in lower tracking errors. This is consistent with the reference case results, where the position above the waterside twistlock station consistently outperformed the outreach position. The stiffness effect exhibits slight nonlinear behaviour, with diminishing returns at higher stiffness levels, suggesting that beyond a certain trolley position the influence of structural flexibility on positioning accuracy becomes less significant. The natural frequency shows a similarly modest effect.

The main effects on actuator demand follow a similar pattern. Wind speed again emerges as the dominant factor, with both $u_{\max}$ and u_{RMS} increasing strongly with U_{mean}. Payload mass and hoisting length influence actuator demand in the same direction as tracking error. The disturbance force scale similarly shows a comparable influence on actuator demand to that of payload mass and hoisting length, consistent with its effect on positioning accuracy. The structural stiffness, corresponding to trolley position, shows a more pronounced influence on actuator demand than on tracking error, with positions closer to the portal frame resulting in lower maximum and RMS acceleration. This reflects the reduced structural motion at stiffer positions, which reduces the corrective movements required from the drive system. The natural frequency has a negligible effect on actuator demand.

Overall, the parameter sensitivity analysis confirms that wind loading is the governing disturbance in the transverse direction, and that payload mass and hoisting length are the most influential operational parameters. The inter-trolley disturbance force has a comparable effect on positioning accuracy and actuator demand to that of payload mass and hoisting length, indicating that the dynamic interaction between the two main trolleys is a relevant factor in transverse performance. Trolley position along the boom has a modest but consistent beneficial effect on both positioning accuracy and actuator demand when the trolley is closer to the portal frame, while the influence of natural frequency is limited.

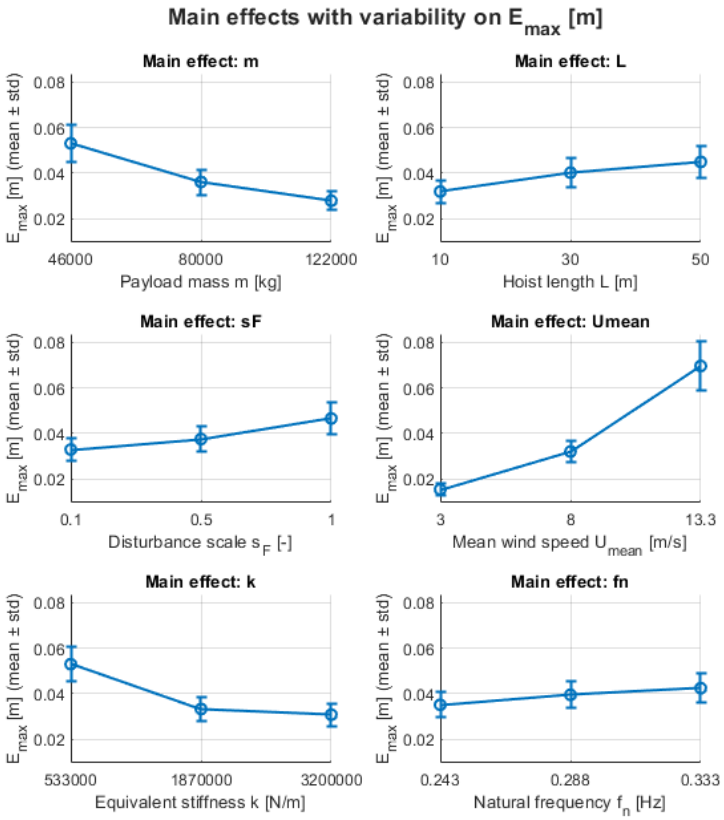

(a) Maximum tracking error $e_{\max}$.

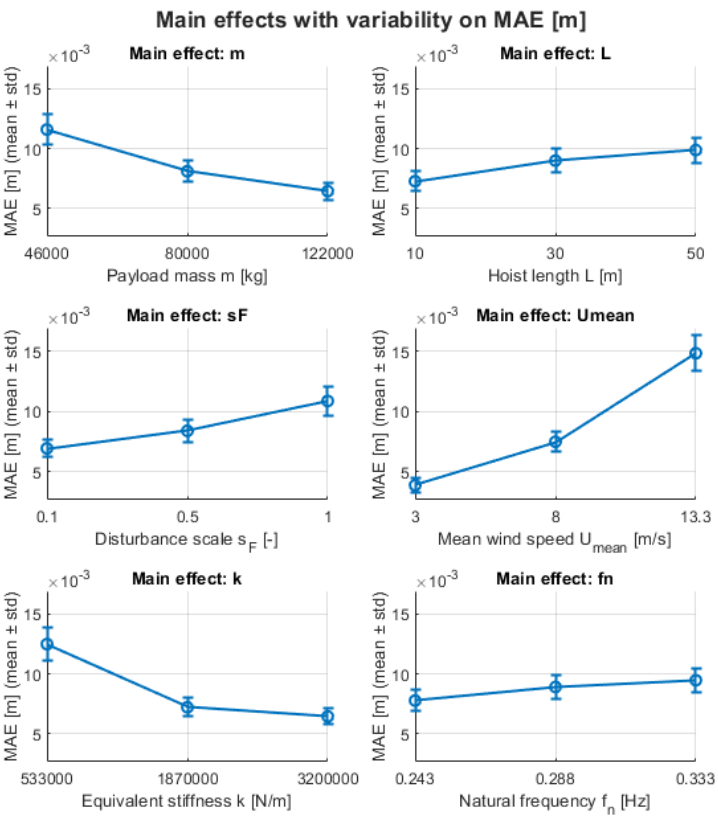

(b) Mean absolute error e_{MAE}.

Figure 60: Main effects of system parameters on positioning accuracy for the Quad Trolley transverse direction.

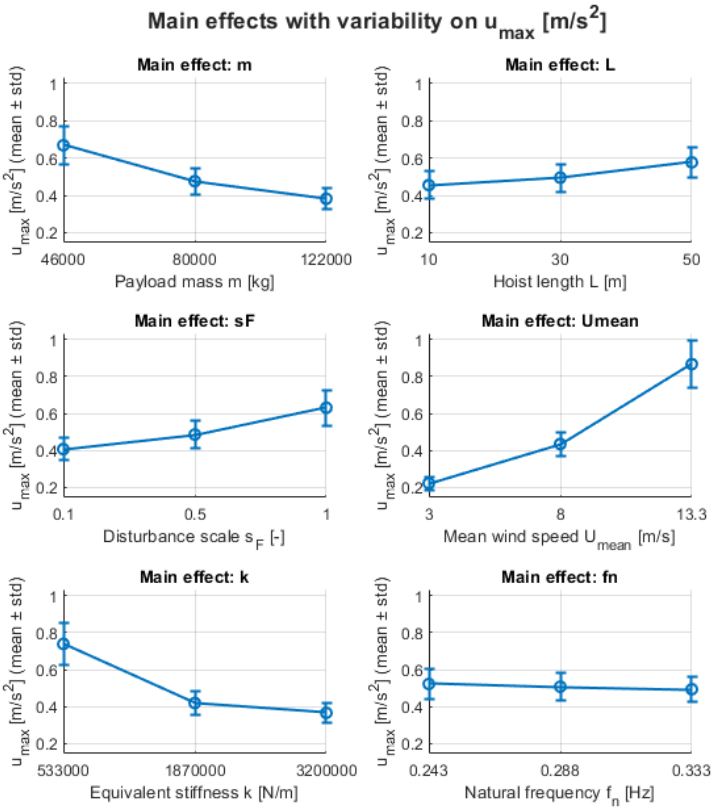

(a) Maximum acceleration $u_{\max}$.

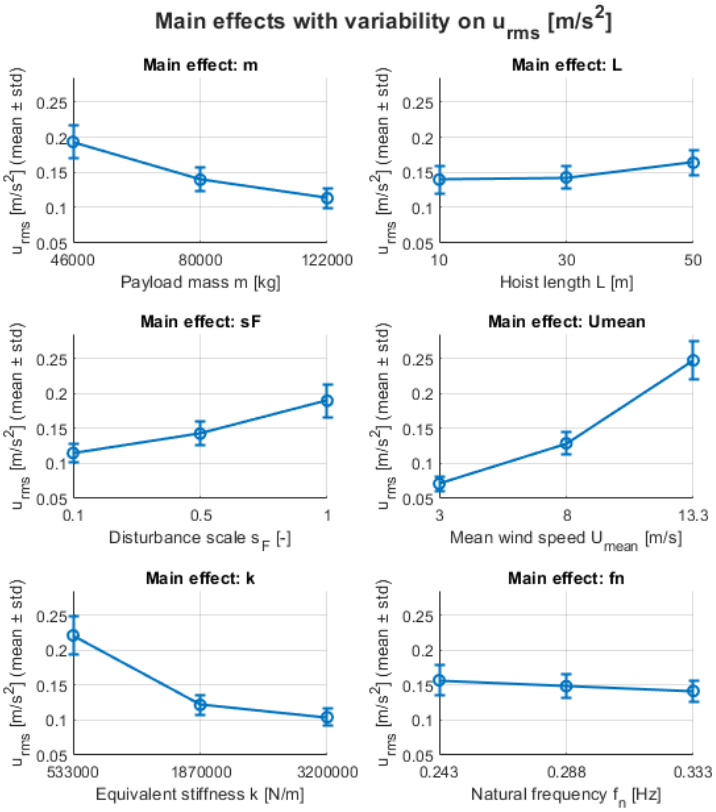

(b) RMS acceleration u_{RMS}.

Figure 61: Main effects of system parameters on actuator demand for the Quad Trolley transverse direction.

7.2.3 Trolley Travel

The trolley travel scenario evaluates the dynamic behaviour of the main trolleys as they travel along the boom between the outreach and landside positions during container handling. This represents the primary motion cycle of the crane and is therefore critical for overall crane performance and cycle time. The dynamic model used for this scenario is described in Section 6.4, and the same performance indicators as for the transverse direction are used. As the actuation concept in this direction is equivalent to that of a conventional STS crane, no separate comparison with the conventional configuration is made.

Trolley Travel – Reference Cases:
The dynamic response in the trolley travel direction is evaluated for the same three severity levels as the transverse direction. Unlike the transverse direction, the structural stiffness and natural frequency do not vary with trolley position in this direction and are therefore kept constant throughout. This results in three reference cases, as summarised in Table 23.

Table 23: Definition of reference cases for the trolley travel direction, representing low, medium, and high control difficulty at a fixed structural configuration.

Case	**Severity**	k [kN/m]	f_n [Hz]	m [t]	L [m]	s_F [-]	U_{mean} [m/s]
RC1	Low	16670	0.542	122	10	0.1	3.0
RC2	Medium	16670	0.542	80	30	0.5	8.0
RC3	High	16670	0.542	46	50	1.0	13.3

The positioning accuracy and actuator demand results for all three reference cases are presented in Figures 62 and 63. Although the structural stiffness and natural frequency in the trolley travel direction are significantly higher than in the transverse direction, reducing the coupling between structural motion and load sway, the overall dynamic performance is worse. This is primarily due to two factors. First, the wind-exposed area of the suspended load is considerably larger in the trolley travel direction, resulting in higher wind-induced disturbance forces on the load. Second, the maximum achievable trolley acceleration in this direction is limited by the wheel-rail friction constraint, which restricts the corrective movements available to the controller. Together, these effects result in larger tracking errors compared to the transverse direction, despite the more favourable structural properties. As with the transverse direction, tracking errors and actuator demand increase with severity level. The time-domain tracking error for the nominal and worst case reference case is shown in Figure 64 and Figure 65 respectively.

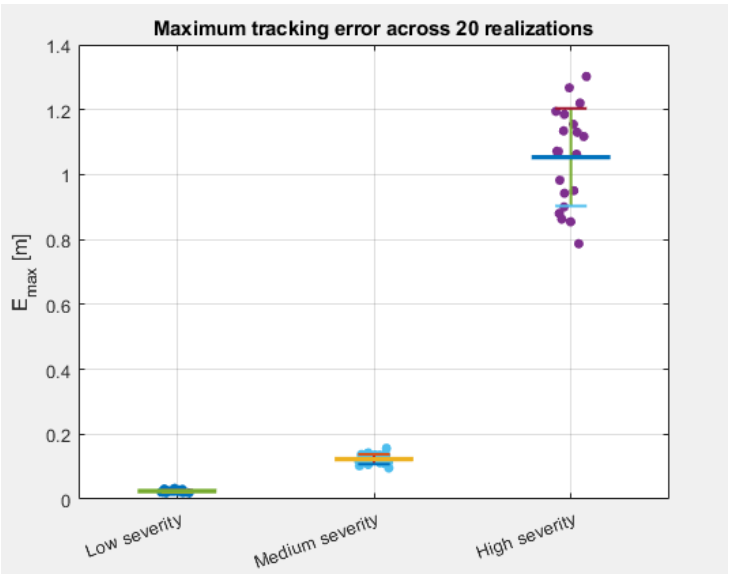

(a) Maximum tracking error.

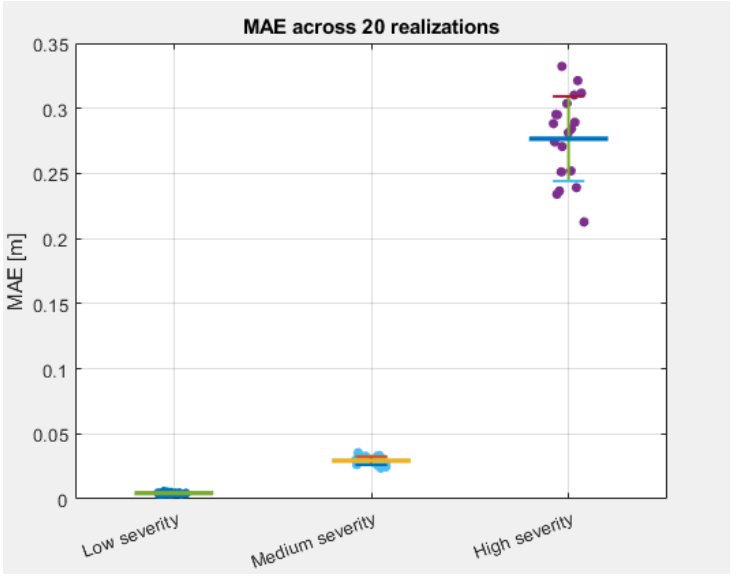

(b) Mean absolute error.

Figure 62: Positioning accuracy (mean ± standard deviation over 20 stochastic realizations) for all three reference cases, trolley travel direction.

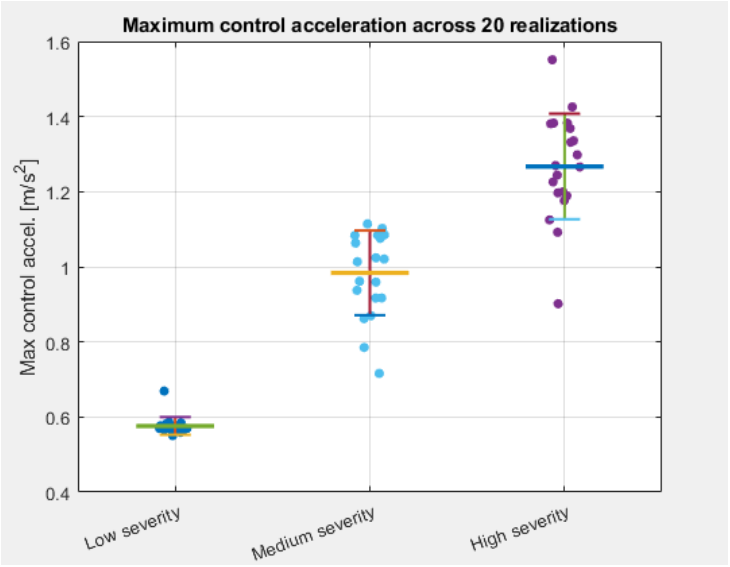

(a) Maximum trolley travel acceleration.

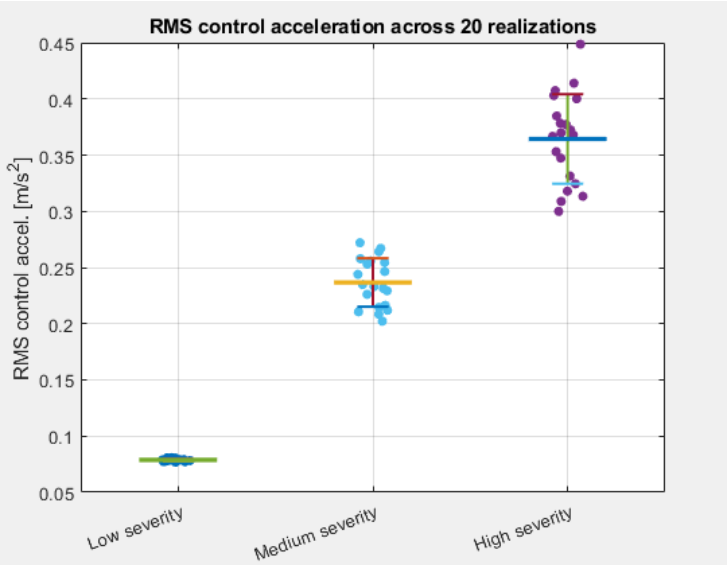

(b) RMS trolley travel acceleration.

Figure 63: Actuator demand (mean ± standard deviation over 20 stochastic realizations) for all three reference cases, trolley travel direction.

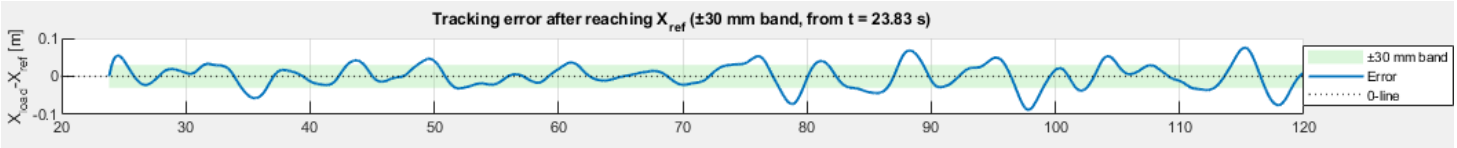

Figure 64: Time-domain tracking error for the nominal reference case in the trolley travel direction (RC2: medium severity), showing the tracking error relative to the 30 mm accuracy threshold.

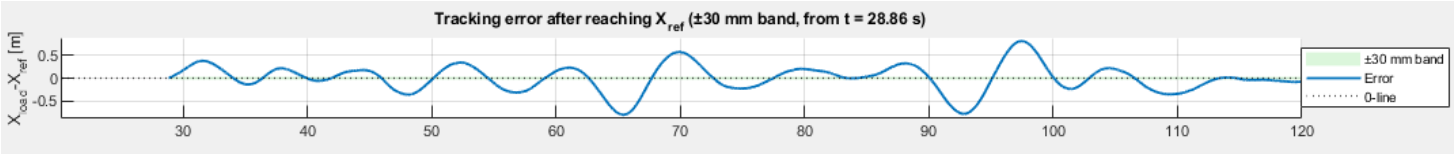

Figure 65: Time-domain tracking error for the worst case reference case in the trolley travel direction (RC3: high severity), showing the tracking error relative to the 30 mm accuracy threshold.

7.2.4 Trolley Travel Parameter Sensitivity

The influence of system parameters on the trolley travel dynamic performance is evaluated using a full factorial Design of Experiments with three levels per parameter, as described in Section 6.7.1. For the trolley travel direction, four parameters are varied: payload mass m, hoisting length L, disturbance force scale s_F, and mean wind speed U_{mean}, resulting in a total of $3^4 = 81$ design points. The equivalent structural stiffness and natural frequency are not varied in this direction, as they remain approximately constant with trolley position. The parameter levels are defined in Table 13. The results are evaluated in terms of the four performance indicators defined in Section 6.6.3: maximum tracking

error $e_{\max}$, mean absolute error e_{MAE}, maximum acceleration $u_{\max}$, and RMS acceleration u_{RMS}.

The main effects on positioning accuracy are presented in Figure 66, and the main effects on actuator demand are presented in Figure 67. The results show a similar hierarchy of parameter influence as observed in the transverse direction. Wind speed is again the dominant factor, with $e_{\max}$ increasing strongly and nonlinearly with U_{mean}, reflecting the large wind-exposed area of the suspended load in the trolley travel direction. Payload mass and hoisting length both have a notable influence on tracking error, with lower payload mass and longer hoisting length resulting in higher tracking errors, consistent with the increased sensitivity to disturbances under these conditions.

The disturbance force scale s_F, which represents the dynamic interaction between the two main trolleys, has a negligible effect on both positioning accuracy and actuator demand across all levels. This contrasts with the transverse direction, where the inter-trolley disturbance has a more notable effect on positioning accuracy. This difference is attributed to the considerably higher structural stiffness in the trolley travel direction, which reduces the structural response to the disturbance force introduced by the second trolley. Since the simultaneous operation of two main trolleys represents the only fundamental difference between the Quad Trolley concept and a conventional STS crane in this direction, the negligible influence of the inter-trolley disturbance indicates that the addition of a second trolley does not compromise dynamic performance in the trolley travel direction.

The main effects on actuator demand follow the same trends as for positioning accuracy. Wind speed is the dominant factor, with $u_{\max}$ increasing strongly with U_{mean}. Both payload mass and hoisting length have a notable influence, while the disturbance force scale has a negligible effect.

Overall, the parameter sensitivity results for the trolley travel direction confirm that wind loading is the governing disturbance and that payload mass and hoisting length are the most influential operational parameters, consistent with the findings for the transverse direction. The negligible influence of the inter-trolley disturbance in the trolley travel direction further supports the dynamic feasibility of the Quad Trolley concept, as it confirms that the addition of a second main trolley does not compromise performance in the primary motion direction of the crane.

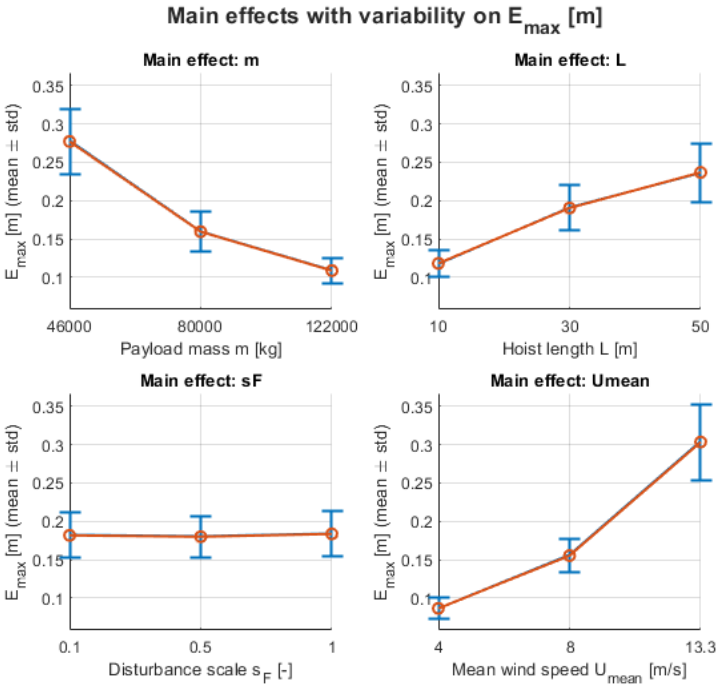

(a) Maximum tracking error $e_{\max}$.

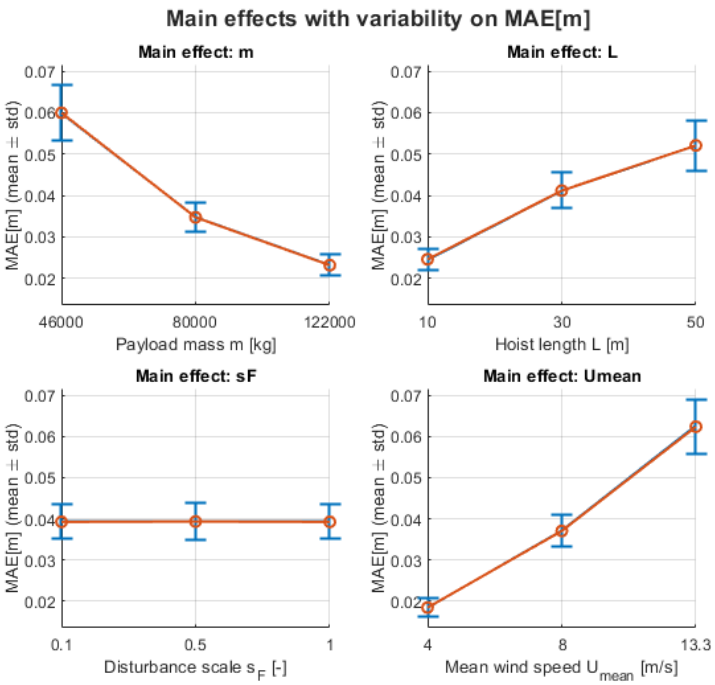

(b) Mean absolute error e_{MAE}.

Figure 66: Main effects of system parameters on positioning accuracy for the trolley travel direction.

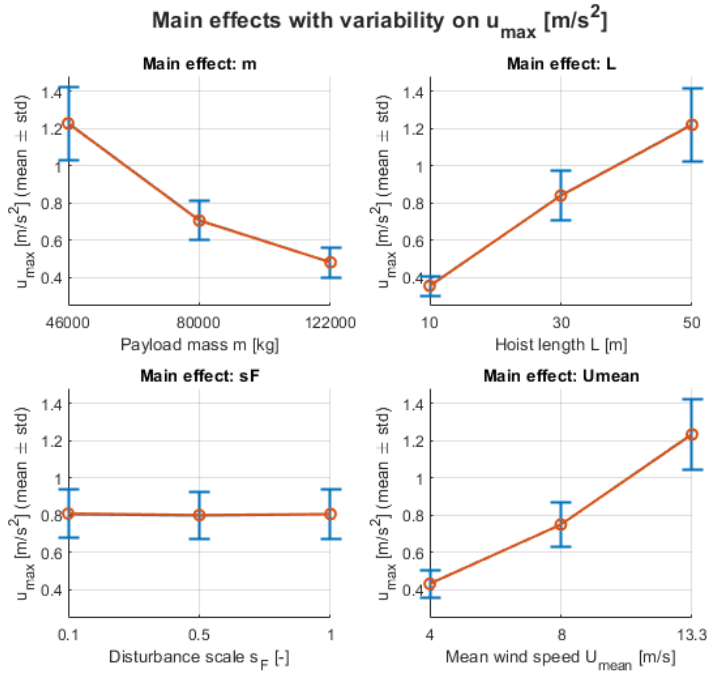

(a) Maximum acceleration $u_{\max}$.

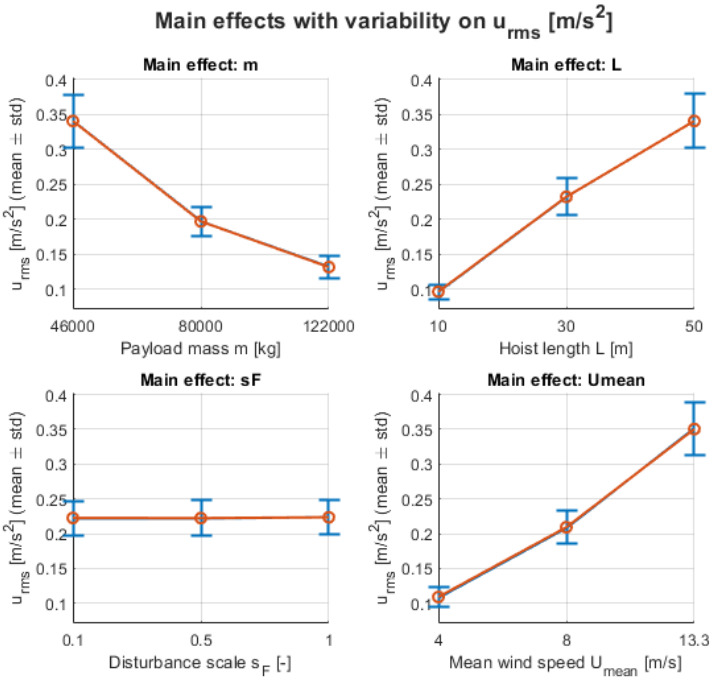

(b) RMS acceleration u_{RMS}.

Figure 67: Main effects of system parameters on actuator demand for the trolley travel direction.

7.2.5 Influence of Structural Stiffness on Trolley Travel Performance

The worst case reference case in the trolley travel direction produces tracking errors that significantly exceed the 30 mm accuracy threshold. The parameter sensitivity analysis has shown that this is not caused by the dynamic interaction between the two main trolleys, as the disturbance force scale has a negligible effect on positioning accuracy. To investigate whether increasing the structural stiffness and natural frequency could bring the performance within the required threshold, a dedicated stiffness sweep is performed for the trolley travel direction.

As noted in Section 7.1.7, the portal sway natural frequency of the Quad Trolley STS crane is $f_n = 0.542$ Hz, and the structural stiffness in the trolley travel direction is $k = 16.670$ MN/m. While this satisfies the minimum of 0.5 Hz specified in ISO 22986, it falls below the minimum of $\geq$0.70 Hz found in industry specifications for conventional STS cranes. This raises the question of whether the degraded trolley travel performance under high-severity conditions is related to these relatively low values, and whether increasing them would result in acceptable positioning accuracy.

To isolate the individual effects of stiffness, modal mass, and natural frequency, three complementary parameter sweeps are performed and presented in Figures 68, 69, and 70:

- A stiffness sweep with fixed modal mass, in which increasing stiffness directly increases the natural frequency.
- A stiffness sweep with fixed natural frequency of 0.542 Hz, in which stiffness and modal mass are varied simultaneously to maintain a constant natural frequency.
- A natural frequency sweep with fixed stiffness of 16.670 MN/m, in which the modal mass is varied to change the natural frequency while stiffness remains constant.

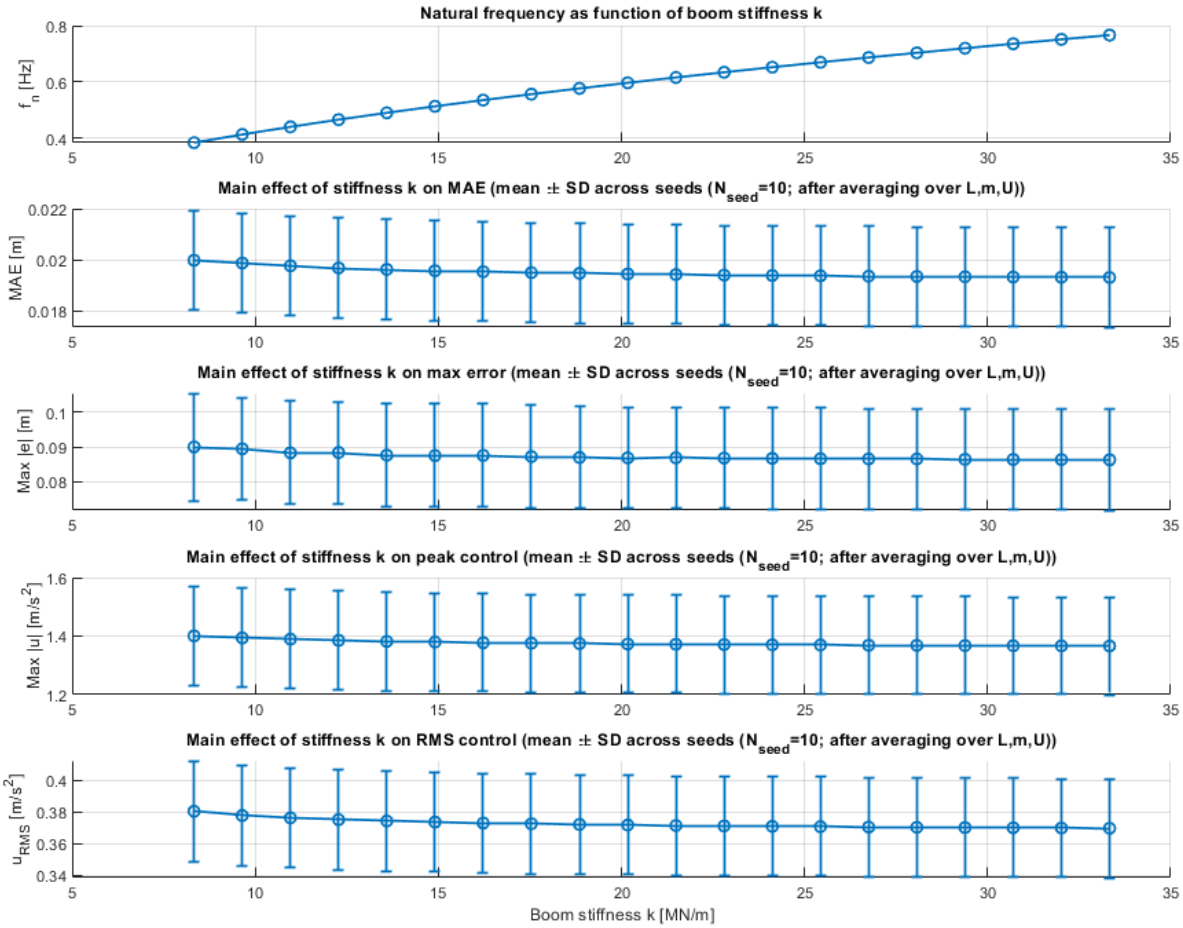

Figure 68: Effect of structural stiffness on trolley travel performance with fixed modal mass. Stiffness is varied from half to twice the baseline design value of $k = 16.670$ MN/m, with the corresponding natural frequency range shown in the top subplot.

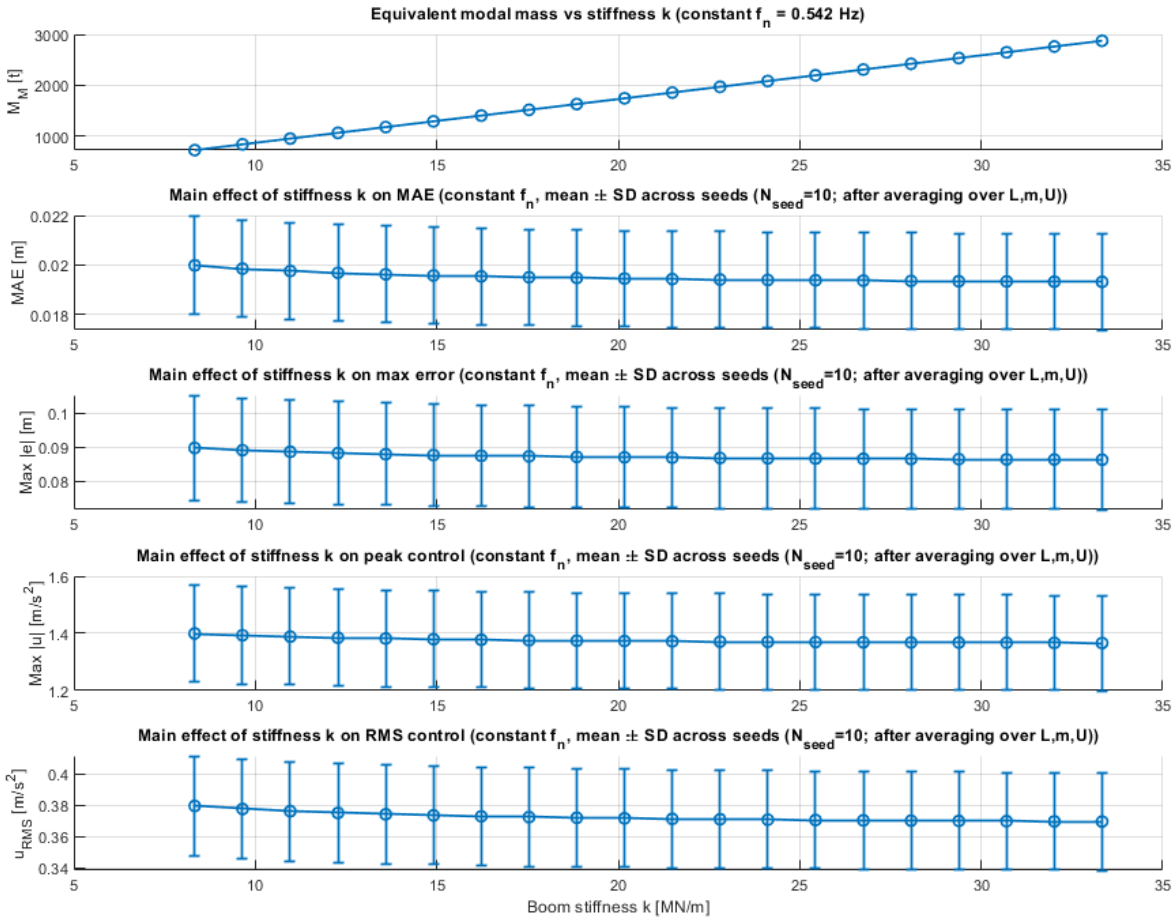

Figure 69: Effect of structural stiffness on trolley travel performance with fixed natural frequency ($f_n = 0.542$ Hz). Modal mass increases proportionally with stiffness as shown in the top subplot.

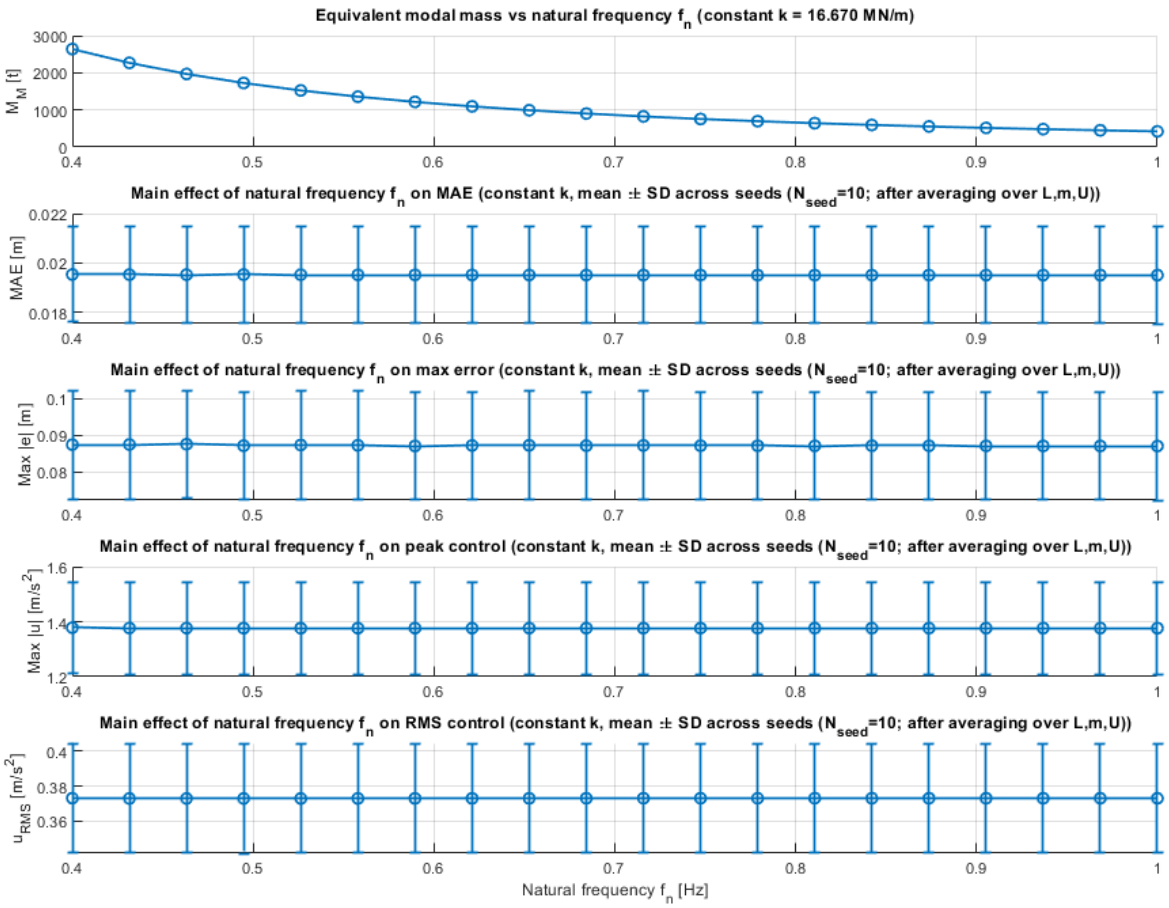

Figure 70: Effect of natural frequency on trolley travel performance with fixed stiffness ($k = 16.670$ MN/m). Modal mass decreases with increasing natural frequency as shown in the top subplot.

The results across all three sweeps point to the same conclusion: structural stiffness and natural frequency have at most a marginal influence on trolley travel dynamic performance.

In Figure 68, stiffness is swept from 8.33 MN/m to 33.33 MN/m, corresponding to half and twice the baseline design value of $k = 16.670$ MN/m respectively. The natural frequency rises correspondingly from approximately 0.38 Hz to 0.77 Hz around the baseline design value of $f_n = 0.542$ Hz, covering the full range from below the ISO 22986 minimum of 0.50 Hz to above the industry specification minimum of 0.70 Hz. A slight improvement in positioning accuracy and actuator demand can be observed with increasing stiffness, but the effect is marginal and well within the variability across stochastic realisations.

Figure 69 isolates the effect of stiffness from that of natural frequency by holding the latter constant at the baseline design value of 0.542 Hz while varying the stiffness and modal mass simultaneously. As with the previous sweep, a slight improvement in positioning accuracy is visible with increasing stiffness, but the effect is marginal. Similarly, Figure 70 isolates the effect of natural frequency by holding stiffness constant at the baseline design value of 16.670 MN/m and varying the modal mass. The natural frequency is swept from 0.4 to 1.0 Hz, covering the full range from below the ISO 22986 minimum to well above the industry specification minimum of 0.70 Hz. All four KPIs remain completely

flat throughout, demonstrating that natural frequency alone has no meaningful effect on trolley travel dynamic performance.

These results unambiguously show that neither structural stiffness nor natural frequency govern the trolley travel dynamic performance. Even doubling the baseline stiffness, which would require significant structural modifications and an associated mass increase, yields only a marginal improvement that is well within the variability across stochastic realisations. Increasing structural stiffness is therefore not a worthwhile design direction for improving trolley travel performance.

The degraded performance under high-severity conditions is instead driven by the combination of high wind-induced disturbance forces and the wheel-rail friction constraint that limits the maximum achievable trolley acceleration. Additionally, the relatively simple LQI control strategy employed in this study contributes to the performance limitation. Extensive research has been conducted on advanced trolley travel control strategies, and more sophisticated controllers would likely improve positioning performance under high-severity conditions. The main takeaway is therefore not that the 30 mm threshold cannot be met, but that the Quad Trolley concept achieves comparable dynamic performance to a conventional STS crane in the trolley travel direction. Neither the addition of a second trolley nor the relatively low structural stiffness and natural frequency introduce any meaningful performance degradation, indicating that the baseline structural design is dynamically adequate for the trolley travel direction.

It should be noted that the assumed trolley acceleration is in line with current engineering practice. Although publicly available data on crane trolley acceleration is limited, available industrial data indicate acceleration times on the order of 5 s [59], corresponding to approximately 0.8 m/s^2 for typical STS trolley travel speeds of 240 m/min. A commonly used engineering rule of thumb assumes acceleration within approximately 3 s, yielding values around 1.33 m/s^2, while experimental and modelling studies report accelerations of approximately 1.2 m/s^2 [60]. The value used in this study therefore lies within the range of typical crane operation and does not represent an unusually restrictive assumption.

7.2.6 Summary of Dynamic Performance

The dynamic assessment demonstrates that the Quad Trolley STS crane concept is dynamically feasible under the control framework applied in this study. The key findings are summarised below.

In the transverse direction, the Quad Trolley configuration achieves substantially improved positioning accuracy compared to a conventional STS crane. The direct trolley transverse drive enables rapid and responsive control, with tracking errors remaining within or close to the 50 mm accuracy threshold across all but the worst case conditions. The conventional STS crane, by contrast, exceeds this threshold across all reference cases, as the indirect gantry-based actuation introduces structural compliance and lag in the force transmission path, and the maximum achievable acceleration is limited by the requirement to accelerate the entire crane structure. This represents a fundamental performance advantage of the Quad Trolley concept that is inherent to the actuation concept rather than the control strategy.

In the trolley travel direction, the Quad Trolley concept achieves comparable dynamic performance to a conventional STS crane. The addition of a second main trolley does

not introduce any meaningful dynamic interaction, and the relatively low structural stiffness and natural frequency in this direction, compared to industry specification limits, have no meaningful effect on positioning accuracy. The worst case tracking errors exceed the 30 mm accuracy threshold, but this is attributable to the combination of high wind-induced disturbance forces, the maximum achievable trolley acceleration, and the relatively simple control strategy employed in this study, rather than to structural or multi-trolley effects. The maximum trolley acceleration in the Quad Trolley concept is governed by the wheel-rail friction constraint of the self-propelled trolleys, but the resulting values are consistent with those reported for modern STS cranes, indicating that the trolley travel performance of the Quad Trolley concept is representative of current crane practice.

Across both motion scenarios, wind loading is identified as the dominant disturbance affecting positioning accuracy and actuator demand. Payload mass and hoisting length are the most influential operational parameters. The inter-trolley disturbance force has a negligible effect in the trolley travel direction, while in the transverse direction its influence is comparable to that of payload mass and hoisting length.

The effect of trolley position along the boom, which determines the effective structural stiffness and natural frequency in the transverse direction, has a modest but consistent beneficial effect on positioning performance. Positions closer to the portal frame, where the structure is stiffer, consistently produce lower tracking errors and lower actuator demand compared to positions at maximum outreach.

It should be noted that the controller used throughout this study is intentionally kept simple and serves primarily as a comparative tool to evaluate dynamic behaviour across configurations and operating conditions. The absolute performance values reported here may therefore differ from those achievable with more advanced control strategies. The main conclusions regarding the relative performance of the configurations and the influence of inter-trolley interaction and structural flexibility are however independent of the specific control strategy and are considered robust findings of this study.

8 Conclusion

This thesis investigated the structural and dynamic feasibility of the Quad Trolley STS crane concept, a novel multi-trolley configuration in which two main trolleys and two secondary trolleys operate simultaneously on a single crane structure. The central research question was:

What structural and dynamic design criteria are required to enable feasible and controllable operation of the Quad Trolley Ship-to-Shore crane concept?

The following sections address each of the supporting sub-questions in turn, before drawing an overall conclusion.

Structural Mass

The Quad Trolley STS crane concept is structurally feasible within the considered design constraints. The structure satisfies both strength and fatigue requirements in accordance with EN 13001 after iterative optimisation of the cross-sectional dimensions, with fatigue governing the final cross-sectional dimensions. The resulting structural mass of approximately 1161 mt shows only a limited increase of 53 mt compared to a conventional STS crane analysed using the same methodology, despite the significantly higher loading introduced by the simultaneous operation of multiple trolleys. This limited increase is explained by the difference in fatigue loading between the two configurations: the higher stress ranges of the Quad Trolley configuration are partially offset by the lower number of cycles per trolley, resulting in a moderate overall increase in structural demand rather than a proportional scaling with the number of trolleys.

Feasibility Within the Conventional 27 m Width Constraint

The results confirm that the Quad Trolley concept is feasible within the conventional 27 m width constraint. A wider 39 m configuration would move the tipping lines further apart and thereby improve stability margins, but the stability considerations at 27 m can be resolved through other means. Under operational conditions, uplift occurs at the landside legs with a maximum force of approximately 180 kN, which can be resolved through the addition of ballast or an operational positioning constraint on the main trolleys. Under storm conditions, tie-downs are required at the waterside legs to resist an uplift force of approximately 2350 kN, with the option to lower the boom angle providing an additional means of reducing uplift demand if foundation capacity is limited. Both operational and storm stability can therefore be ensured without fundamental changes to the structural concept. Nevertheless, stability is identified as a critical design consideration for the Quad Trolley concept at this width and should remain a key focus in further development of the design. Quay loading remains within the range reported for existing STS crane infrastructure, further confirming compatibility with modern port facilities, subject to site-specific verification.

Dynamic Feasibility

The Quad Trolley STS crane concept is dynamically feasible under the control framework applied in this study. In the transverse direction, the direct trolley transverse drive

enables rapid and responsive control, achieving tracking errors within or close to the 50 mm accuracy threshold across all reference cases. This represents a fundamental performance advantage over a conventional STS crane, where the indirect gantry-based actuation introduces structural compliance and lag in the force transmission path, and the maximum achievable acceleration is limited by the requirement to accelerate the entire crane structure. This advantage is inherent to the actuation concept and cannot be replicated through control improvements alone.

In the trolley travel direction, the Quad Trolley concept achieves comparable dynamic performance to a conventional STS crane. The addition of a second main trolley does not introduce any meaningful dynamic interaction, and the relatively low structural stiffness and natural frequency have no meaningful effect on positioning accuracy. The worst case tracking errors exceed the 30 mm accuracy threshold, but this is attributable to the combination of high wind-induced disturbance forces, the maximum achievable trolley acceleration, and the relatively simple control strategy employed in this study, rather than to structural or multi-trolley effects. The maximum trolley acceleration is governed by the wheel-rail friction constraint of the self-propelled trolleys, but the resulting values are consistent with those reported for modern STS cranes, indicating that the trolley travel performance is representative of current crane practice.

Across both motion scenarios, wind loading is the dominant disturbance affecting positioning accuracy and actuator demand, while payload mass and hoisting length are the most influential operational parameters. The inter-trolley disturbance force has a negligible effect in the trolley travel direction, while in the transverse direction its influence is comparable to that of payload mass and hoisting length but does not compromise the overall dynamic feasibility of the concept.

Necessity of Supplemental Mechanical Damping

The results of this study do not indicate a necessity for supplemental mechanical damping to maintain dynamic feasibility of the Quad Trolley concept. In the transverse direction, the direct trolley actuation provides sufficient control authority to maintain acceptable positioning accuracy without additional damping. In the trolley travel direction, the performance limitations are governed by wind loading and actuation constraints rather than by insufficient structural damping.

Structural Flexibility and Controllability

The relationship between structural flexibility and controllability differs between the two motion directions. In the transverse direction, trolley position along the boom determines the effective structural stiffness and natural frequency, with positions closer to the portal frame being considerably stiffer than positions at maximum outreach. This variation has a modest but consistent effect on positioning performance, with stiffer positions consistently producing lower tracking errors and lower actuator demand. This suggests that increasing the overall structural stiffness of the crane would further improve transverse positioning performance, although the results also show that the direct trolley actuation concept maintains acceptable performance even at the most flexible outreach position, meaning that additional stiffening is not required for dynamic feasibility. In the trolley travel direction, structural stiffness and natural frequency have no meaningful effect on

positioning accuracy, even though the portal sway frequency of 0.542 Hz falls below the minimum of $\geq$0.70 Hz found in industry specifications for conventional STS cranes. Even doubling the baseline stiffness yields at most a marginal improvement that does not justify the associated structural modifications and mass increase. The structural properties of the baseline design therefore do not compromise dynamic feasibility in either direction, which is a key finding with respect to structural design freedom.

Structural Optimisation

The dynamic analysis was intended in part to identify whether additional structural stiffness beyond the code-compliant baseline would be required for dynamic feasibility, and if so, where it could most effectively be implemented. The structural design of the Quad Trolley concept is governed by fatigue requirements in accordance with EN 13001, with the final dimensions representing the minimum plate thicknesses required for code compliance. Further structural optimisation beyond this baseline is therefore not possible without compromising code compliance. At the same time, the dynamic analysis shows that the resulting structural stiffness and natural frequencies are dynamically adequate in both directions, meaning that such optimisation is also not required. The code-compliant baseline design therefore represents both the structural minimum and a dynamically sufficient configuration, meaning that further structural optimisation is neither possible nor required.

Overall Conclusion

Drawing together the findings above, the Quad Trolley STS crane concept is both structurally and dynamically feasible within the considered design constraints. In answer to the central research question, the key design criteria required for feasible and controllable operation are: compliance with EN 13001 strength and fatigue requirements, which are both necessary and sufficient for dynamic feasibility; and stability provisions to prevent uplift under both operational and storm conditions. No additional stiffness requirements, supplemental damping, or widening of the crane beyond the conventional 27 m envelope are required. The direct transverse actuation on the main trolleys is identified as the key enabler of the concept's dynamic performance advantage over conventional gantry-based actuation.

Together, these results demonstrate that the Quad Trolley STS crane concept represents a structurally sound and dynamically viable design direction for high-performance container handling, with the potential to significantly increase terminal throughput through the combination of multi-trolley operation and direct transverse actuation.

9 Recommendations and Future Work

The findings of this thesis confirm the structural and dynamic feasibility of the Quad Trolley STS crane concept within the considered design constraints. Based on these findings, the following directions for future research and development are recommended.

9.1 Trolley System Design

The present study treats the trolley systems as lumped masses with specified lifting configurations, without detailed design of the trolley structure, drive mechanisms, or rope routing. A basic feasibility analysis of the rope reeving arrangement indicates that the required routing is achievable with the addition of extra sheaves, but a detailed design of the full trolley and reeving system has not been carried out and is recommended as a priority for further development.

In this study, a semi-rope trolley configuration is adopted for the main trolleys, in which the trolley drive is mounted on the trolley while hoisting is performed centrally from the machine room. This configuration was selected as a compromise between trolley mass and rope reeving complexity. Following detailed design of the reeving system, this configuration may prove to be the most suitable solution. However, depending on the outcome, two alternative directions could also be explored.

If the reeving complexity is deemed possible and acceptable, a full rope-towed trolley configuration could also be considered, in which both the drive and hoisting functions are performed via ropes from the machine room. This would further reduce the trolley mass operating on the cantilevered boom, improving operational stability. In addition, the absence of a wheel-driven trolley would remove the wheel-rail friction constraint on trolley acceleration, potentially enabling higher accelerations and improved dynamic performance in the trolley travel direction. However, these benefits would come at the expense of an even more complex reeving system.

Conversely, if the required rope routing is not favoured from a complexity, maintenance and reliability perspective, a full machine trolley configuration with hoisting winches mounted directly on the trolley should be considered. This would eliminate the need for centralised reeving entirely, but would result in substantially heavier trolleys, adversely affecting operational stability, fatigue loading, and quay loading. These effects should be assessed and the structural design adjusted accordingly.

In addition to the trolley configuration, a detailed design of the transverse drive mechanism on the main trolleys is recommended. The transverse drive is the most novel mechanical feature of the Quad Trolley concept and the key enabler of its transverse positioning performance advantage. The dynamic analysis shows that under high-severity conditions, the required relative sheave block displacement reaches up to approximately 2 m, which governs the required actuator stroke and confirms that the adopted ± 2 m travel range and corresponding 10 m boom girder spacing are appropriate. A detailed design should address the actuator technology (hydraulic or electric) and the force capacity required to achieve the assumed 2.0 m/s^2 acceleration with the 5 mt sheave block assembly.

9.2 Structural Model Refinement

The structural verification confirms that the Quad Trolley concept is feasible at the global level based on a beam-element finite element model. While this level of detail is sufficient for the feasibility assessment conducted in this study, a more detailed model using plate elements is recommended as a next step toward realisation. This would enable fatigue assessment at the weld level, a more accurate evaluation of local stress distributions, and a more precise determination of the structural mass.

9.3 Wind Loading Assessment

The wind loads in this study are based on standard calculations in accordance with EN 13001, with a 20% reduction applied to account for shielding effects not adequately captured by the standard. Scale model wind tunnel testing or computational fluid dynamics analysis of the crane geometry would provide actual drag coefficients for the specific structural configuration. Given that stability is identified as a critical design consideration, more accurate wind loading may result in improved stability margins and potentially reduce or eliminate the need for ballast and reduce the required capacity of the tie-down and anchoring systems.

9.4 Stability Provisions

The stability assessment identifies the need for tie-downs at the waterside legs to resist storm uplift forces of approximately 2350 kN. While tie-downs are well-established practice for large STS cranes, the feasibility of accommodating these forces depends on the capacity of the specific quay structure and foundation at the intended installation site. A site-specific assessment of the tie-down anchoring capacity and its integration with the quay infrastructure is therefore required. Similarly, the operational stability measures identified in this study, including ballast and operational positioning constraints, should be developed into concrete engineering solutions with specified capacities and integration details.

9.5 Dynamic Model Extension

The dynamic models in this study are formulated as linear time-invariant systems that treat the transverse and trolley travel directions independently. In practice, however, the trolley simultaneously travels along the boom, moves transversely, and hoists the load, resulting in coupled motions that may interact through the flexible crane structure. For example, hoisting changes the pendulum length during the motion, which directly affects the load natural frequency and sway behaviour. Similarly, trolley travel shifts the effective structural stiffness and mass distribution along the boom, altering the dynamic properties of the system during operation. These effects are not captured by the current models, in which each direction is evaluated in isolation at fixed parameter values.

For further development, a coupled multi-directional model that includes simultaneous transverse, trolley travel, and hoisting motions would enable the assessment of these cross-directional interactions during realistic handling cycles. Incorporating time-varying dynamics would allow the analysis to capture the continuously changing system properties during operation, providing a more representative evaluation of the dynamic performance

across the full container handling cycle.

9.6 Control Development

The LQR/LQI control framework used in this study is intentionally kept simple and serves primarily as a comparative tool. For further development toward implementation, a full advanced control strategy should be designed and evaluated. This should account for the time-varying nature of the system, in which parameters such as hoisting length, payload mass, and trolley position change continuously during a handling cycle. A gain-scheduled or adaptive controller that adjusts its parameters based on measurable operating conditions would be advised to maintain performance across the full operational envelope.

9.7 Throughput and Economic Assessment

The Quad Trolley concept is motivated by the potential for substantially higher container handling productivity. A quantitative cycle time analysis that accounts for the operational workflow, the coordination between main and secondary trolleys, and the interaction with quayside transport equipment would allow this productivity advantage to be quantified and compared against alternative approaches for increasing terminal throughput. An accompanying economic assessment, covering additional manufacturing cost, operational cost implications, and expected return on investment, would support informed decision-making on the further development of the concept.

Together, these research directions provide a structured pathway from conceptual validation toward detailed engineering and eventual industrial implementation of the Quad Trolley STS crane.

References

[1] L. C. C. Ltd., "Technical Description," Tech. Rep. [Online]. Available: https://www-assets.liebherr.com/media/bu-media/lhbu-mcc/downloads-and-brochures/brochures/lcc/liebherr-sts-cranes-technical-description.pdf

[2] Acreos, "Ship-To-Shore gantry crane simulator (STS) - Acreos," 12 2023. [Online]. Available: https://acreos.eu/en/port/gantry-crane-simulator-sts/

[3] S. H. B.V., "STINIS SPLIT-HEADBLOCK," Tech. Rep. [Online]. Available: https://www.stinis.com/wp-content/uploads/2023/08/SSH_Product_Flyer_QR.pdf

[4] Bromma, "Ship-to-shore spreaders," 2024, accessed: 2025-06-27. [Online]. Available: https://bromma.com/wp-content/uploads/2024/01/Bromma_STS_revision_2024.pdf

[5] "Our cranes cabins – PORTRUCKS." [Online]. Available: https://portrucks.com/our-cranes-cabins/

[6] C. World, "MERFORD Ergonomic Cabin: Gantry Crane Operator at work (Timelapse)," 3 2016. [Online]. Available: https://www.youtube.com/watch?v=S8O0Jczs7Do

[7] Kalmar Industries, "Crane design: Summary of ship-to-shore container cranes," *Internal Presentation Report*, November 2008, a Partek Company. Includes design aspects, spreader technology, and modular crane development. [Online]. Available: https://www.kalmarglobal.com

[8] "Buffers," 12 2024. [Online]. Available: https://bemorail.com/railtechnology/rail-buffers/

[9] "Buffers Bumpers — Conductix Wampfler Global." [Online]. Available: http://www.conductix.com/en/product-groups/buffers-bumpers-0

[10] The American Society of Mechanical Engineers, "The paceco container crane," https://www.asme.org/about-asme/engineering-history/landmarks/85-paceco-container-crane, May 1983, retrieved May 31, 2022.

[11] "How to unload a container megaship," 10 2021. [Online]. Available: https://www.konecranes.com/index.php/discover/how-to-unload-container-megaship

[12] "STS Boom Extension." [Online]. Available: https://www.konecranes.com/port-equipment-services/port-services/port-crane-modernizations/sts-boom-extension

[13] L. A. Parra, E. A. Tannuri, D. o. M. E. Escola Politécnica, University of São Paulo, and I. A. M. Programa de Educação Continuada em Engenharia PECE/USP, "DEFINITION AND NUMERICAL SIMULATION OF AN AUTOMATED SYSTEM FOR CONTAINER CRANE POSITIONING," Tech. Rep., 2012. [Online]. Available: https://www.abcm.org.br/symposium-series/SSM_Vol5/Section_II_Control_Systems/02002.pdf

[14] *Cranes — General design — Part 2: Load actions*, European Committee for Stan-

dardization (CEN) Std. EN 13 001-2:2021, 2021, available via NEN or national standardization bodies.

[15] "STS CRANES – PACECO CORP." [Online]. Available: https://pacecocorp.com/sts-cranes/

[16] Loganx, "Ship to Shore Crane," 9 2022. [Online]. Available: https://gruasyaparejos.com/en/port-crane/ship-to-shore-crane/

[17] "Ship to Shore Container Cranes - Liebherr." [Online]. Available: https://www.liebherr.com/en-us/maritime-cranes/products/port-equipment/ship-to-shore-container-cranes-4433170

[18] Konecranes, "Konecranes Ship-to-Shore Crane (STS)," Tech. Rep., 2024. [Online]. Available: https://www.konecranes.com/system/files/2024-04/7593_sts_monobox_technical_doc_v1.pdf

[19] R. L. T. P. Ltd, "Model 6100 Tandem Headblock - SingFlex for Container Lifting Cranes," Tech. Rep., 2023. [Online]. Available: https://www.ramspreaders.com/wp-content/uploads/2024/10/RAM-6100-202003_lo.pdf.pagespeed.ce.sPYEHMX-GZ.pdf

[20] Stinis, "Understanding telescopic spreaders." [Online]. Available: https://www.stinis.com/understanding-telescopic-spreaders/

[21] "Components and Automation of Ship-to-Shore Cranes - Yuantai Crane." [Online]. Available: https://www.yuantaicrane.com/news/components-and-automation-of-ship-to-shore-cranes.html

[22] Bromma, "Load Sensing System - Bromma." [Online]. Available: https://bromma.com/products/load-sensing-system/

[23] Stinis, "Ship to shore crane spreaders." [Online]. Available: https://www.stinis.com/container-lifting-equipment/ship-to-shore-crane-spreaders/

[24] R. Spreaders, "SPREADER OPTIONS," Tech. Rep. [Online]. Available: https://www.ramspreaders.com/wp-content/uploads/2024/12/10.-RAM-Options-Spreader.pdf

[25] F. Johanson, "Bringing crane operations down to earth: Remotely controlled STS cranes increase efficiency, improve working environments and boost productivity," Tech. Rep. [Online]. Available: https://search-ext.abb.com/library/Download.aspx?DocumentID=9AAK10103A1165&LanguageCode=en&DocumentPartId=&Action=Launch

[26] T. Notteboom and J.-P. Rodrigue, "Containerisation, Box Logistics and Global Supply Chains: The Integration of Ports and Liner Shipping Networks," *Maritime Economics Logistics*, vol. 10, no. 1-2, pp. 152–174, 3 2008. [Online]. Available: https://doi.org/10.1057/palgrave.mel.9100196

[27] N. Zrnić, S. Bošnjak, and V. Papuga, "Automation of ship-to-shore container cranes: A review of state-of-the-art," https://www.researchgate.net/publication/228936324_Automation_of_ship-to-shore_container_cranes_A_review_of_state-of-the-art, 2008, accessed July 2, 2025.

[28] Konecranes, "Konecranes STS: For the fastest ship turnaround time." [Online]. Available: https://www.konecranes.com/sites/default/files/2021-07/STS_crane_typical_technical_spec.pdf

[29] SANY and S. M. M. Company, "SANY Industrial Park, Gaolan Port Economic and Development Zone, Zhuhai, Guangdong, China," Tech. Rep., 2022. [Online]. Available: https://sanyglobal-img.sany.com.cn/product/picture_album/20220919/SANY_STS_Brochure2022_084536.pdf

[30] M. A. Jordan and L. C. Inc., "Quay crane productivity," Tech. Rep., 2002. [Online]. Available: https://www.liftech.net/wp-content/uploads/2002/11/Quay-Crane-Productivity-Paper.pdf

[31] J. Achterkamp and S. P. Solutions, "The effect of mega-ships," Tech. Rep. [Online]. Available: https://wpassets.porttechnology.org/wp-content/uploads/2019/05/25182729/JOOST-PTIONLINE-5.pdf

[32] "STS Crane Automation." [Online]. Available: https://new.abb.com/ports/solutions-for-marine-terminals/our-offerings/container-terminal-automation/sts-crane-automation

[33] J.-P. Rodrigue, T. Notteboom, and A. Pallis, "Chapter 6.6 – Container Terminal Automation — Port Economics, Management and Policy," 7 2025. [Online]. Available: https://porteconomicsmanagement.org/pemp/contents/part6/terminal-automation/

[34] M. G. Reports, "Ship-to-Shore (STS) Container Cranes Market Size, Share Trends, 2033." [Online]. Available: https://www.marketgrowthreports.com/market-reports/ship-to-shore-sts-container-cranes-market-109713

[35] VDL Automated Vehicles. (2023) Port of rotterdam. VDL Automated Vehicles. Accessed: 2026-03-13. [Online]. Available: https://www.vdlautomatedvehicles.com/en/cases/port-of-rotterdam

[36] Stinis Holland B.V., "Stinis split-headblock brochure," https://www.stinis.com, n.d., product brochure. Safe working load 150 t, tare weight 10 t, split headblock enabling tandem and multi-container lifting.

[37] Confidential, "Technical drawings of twin-lift spreader," not publicly available.

[38] Confidential, "Headblock technical drawing," not publicly available.

[39] B. C. T. Ltd., "Technical Specification for Two Quayside Container Cranes (QC)," Tech. Rep., 11 2023. [Online]. Available: https://cdnweb.bct.gdynia.pl/s3fs-public/inline-files/SIWZ%20STS%20EU%2032_2024%20Za%C5%82acznik%205%20Technical%20Specification%20STS%20KPO%202_17.07.2024_.pdf

[40] P. Romanowicz, "Numerical assessment of fatigue load capacity of cylindrical crane wheel using multiaxial high-cycle fatigue criteria," *Archive of Applied Mechanics*, vol. 87, no. 10, pp. 1707–1726, 2017. [Online]. Available: https://doi.org/10.1007/s00419-017-1281-6

[41] Huisman Equipment B.V., "Personal communication on transverse drive acceleration feasibility," Personal communication, 2026.

[42] "Crane rail low," 9 2025. [Online]. Available: https://bemorail.com/railtechnology/crane-rail-low/

[43] ArcelorMittal, "Crane Rail A100 - ArcelorMittal," 5 2024. [Online]. Available: https://rails.arcelormittal.com/profiles/crane-rails/european-standards/rail-a100/

[44] *Cranes — Bridge and gantry cranes*, CEN Std. EN 15 011, 2025, available via NEN or national standardization bodies.

[45] T. L. A. Rasch, "Wind loading of sts cranes: Investigating improved calculation methods," MSc Thesis, Delft University of Technology, Delft, The Netherlands, 2022.

[46] *Cranes — General design — Part 3-1: Limit states and proof of competence of steel structures*, CEN Std. EN 13 001-3-1, 2025, available via NEN or national standardization bodies.

[47] Nevesbu. (n.d.) Damping coefficients by experiments and the application to transient fe analyses of cable trays. Accessed: 2026-03-27. [Online]. Available: https://www.nevesbu.com/insights/damping-coefficients-by-experiments-and-the-application-to-transient-fe-analyses-of-cable-trays/

[48] The Engineering ToolBox, "Drag coefficient," 2004, accessed: 2026-03-27. [Online]. Available: https://www.engineeringtoolbox.com/drag-coefficient-d_627.html

[49] T. Burton *et al.*, "Introduction to micro-meteorology for wind energy," 2011, accessed: 2026-03-27. [Online]. Available: https://backend.orbit.dtu.dk/ws/files/52392430/Introduction_to_micro_meteorology_for_wind_energy.pdf

[50] Confidential, "Sts crane container procedures drawing," not publicly available.

[51] G. C. T. S.A., "Technical Specification for Quayside Container Cranes," 2014. [Online]. Available: https://www.scribd.com/document/456068299/Container-Crane-2DT2014-Cz%C4%99%C5%9B%C4%87-3-STS-Technical-Specification-pdf

[52] Confidential, "Sts crane specification," not publicly available.

[53] Confidential, "Sts crane rail loads," not publicly available.

[54] B. K. Meisuh, J. Seo, J. Huh, J. Kim, and J.-M. Kim, "Seismic response of a container crane subjected to ground motions," *Applied Ocean Research*, vol. 126, p. 103270, 7 2022. [Online]. Available: https://doi.org/10.1016/j.apor.2022.103270

[55] Q. H. Tran, J. Huh, V. B. Nguyen, C. Kang, J.-H. Ahn, and I.-J. Park, "Sensitivity Analysis for Ship-to-Shore Container Crane Design," *Applied Sciences*, vol. 8, no. 9, p. 1667, 9 2018. [Online]. Available: https://doi.org/10.3390/app8091667

[56] D. Huang, X. Guo, H. Wang, H. Wang, and Y. Peng, "A Finite Element Analysis-based Study on the Reliability of Heightened Quayside Container Cranes," *Journal of Engineering Science and Technology Review*, vol. 14, no. 6, pp. 72–82, 1 2021. [Online]. Available: https://doi.org/10.25103/jestr.146.08

[57] L. Solazzi and N. Zrnić, "Mechanical behavior of ship to shore container crane subjected to different stochastic wind actions." *Journal of Physics Conference Series*, vol. 2647, no. 25, p. 252002, 6 2024. [Online]. Available: https://doi.org/10.1088/1742-6596/2647/25/252002

[58] *Cranes — Stiffness - Bridge and gantry cranes*, ISO Std. ISO 22 986, 2007, available via NEN or national standardization bodies.

[59] ABB, "Crane systems: Meeting the demands of larger vessels with larger and faster cranes," ABB Group, Tech. Rep., n.d., accessed: 2026-04-21. [Online]. Available: https://library.e.abb.com/public/bea8c819fb9e8d96852575ad0047ca5a/ABB+Crane+Systems+Meeting+the+demands+of+larger+vessels.pdf

[60] N. . Zrnić, K. Hoffmann, and S. M. Bošnjak, "Modelling of dynamic interaction between structure and trolley for mega container cranes," *Mathematical and Computer Modelling of Dynamical Systems*, vol. 16, no. 3, pp. 295–311, 2010.

A Scientific Paper

Structural and Dynamic Design Criteria for a Quad Trolley Ship-to-Shore Crane Concept

M. Zoutewelle

Department of Maritime and Transport Technology
Faculty of Mechanical, Maritime and Materials Engineering
Delft University of Technology, Delft, The Netherlands

Supervised by: ir. W. van den Bos (TU Delft), ir. R. Nouwens (Huisman Equipment B.V.)

May 4, 2026

Abstract

This paper presents the structural and dynamic feasibility assessment of a Quad Trolley Ship-to-Shore (STS) crane concept, in which two main trolleys and two secondary trolleys operate simultaneously on a single crane structure. The concept aims to substantially increase container terminal throughput through parallel trolley operation while retaining a largely conventional crane architecture. A beam-element finite element model is developed to assess structural strength, fatigue, stability, quay loading, and modal properties in accordance with EN 13001. The structural properties are subsequently used as input for simplified dynamic models of the trolley-payload system, with which the transverse and trolley travel dynamic performance is evaluated through reference case simulations and a full factorial parameter sensitivity study. Results show that the concept is structurally feasible within the conventional 27 m width constraint, with fatigue governing the final cross-sectional dimensions. In the transverse direction, the direct trolley actuation concept provides a fundamental and substantial improvement in positioning accuracy over conventional gantry-based actuation, with the Quad Trolley configuration consistently achieving tracking errors within or close to the accuracy threshold while the conventional crane exceeds it across all reference cases. In the trolley travel direction, performance is comparable to that of a conventional STS crane, as the second trolley introduces no meaningful dynamic interaction and structural stiffness has no meaningful effect on positioning accuracy. Wind loading is identified as the dominant disturbance in both directions. Together, the results confirm that the Quad Trolley STS crane concept is both structurally and dynamically viable as a high-performance container handling system.

I Introduction

As global maritime trade continues to grow, container terminal productivity has become a key factor in port competitiveness. Ship-to-shore (STS) cranes, as the primary interface between vessels and the quay, have a direct impact on vessel turnaround times and terminal throughput [1]. While conventional single-trolley STS cranes have been progressively scaled up in size and speed, with trolley speeds already reaching 210–240 m/min [2, 3, 4], further productivity gains within this architecture are increasingly constrained by cycle time and structural limitations [5].

The shift toward automated and remotely supervised crane operation has, however, opened new possibilities [6]. As of 2025, approximately 59% of newly installed STS cranes are delivered with semi-automated control systems [7], and with a single operator able to supervise multiple automated handling processes, configurations involving multiple coordinated trolleys have become operationally and economically viable. Building on this, this paper investigates an innovative Quad Trolley STS crane concept, developed in collaboration with Huisman Equipment B.V., which integrates two coordinated main trolleys and two secondary trolleys operating in parallel on a single crane structure, with intermediate twistlock stations enabling decoupled vessel-side and landside operations.

The central research question addressed in this paper is: *What structural and dynamic design criteria are required to enable feasible and controllable operation of the Quad Trolley STS crane concept?*

To address this, the study evaluates structural feasibility within the conventional 27 m width constraint, assesses dynamic performance under representative control, investigates the influence of structural flexibility on controllability, and determines whether supplemental mechanical damping is required.

II Concept Description

The Quad Trolley STS crane concept is based on a largely conventional STS crane structure with a double-girder boom and a 72 m outreach, sized to service the largest ultra-large container vessels currently in operation. Two main trolleys operate along the boom and main girder, capable of tandem, twin-lift, and single container handling, with a maximum Safe Working Load of 82 mt in tandem configuration. Two secondary trolleys operate in the lower part of the structure between the twistlock stations and the quayside transport equipment.

A key distinguishing feature of the concept is the transverse drive mounted directly on each main trolley, enabling controlled transverse displacement of approximately ±2 m without moving the entire crane structure. This eliminates the need for gantry travel

for small transverse positioning corrections and enables rapid, independently actuated transverse motion. The concept operates within a buffer-to-buffer width of 27 m, consistent with conventional STS crane infrastructure and terminal layout requirements. Key operational parameters are summarised in Table A.1.

Table A.1: Key operational parameters of the Quad Trolley STS crane concept.

Parameter	Value
Outreach	72 m
Buffer-to-buffer width	27 m
Main trolley travel speed	240 m/min
Main trolley travel acceleration	1.2 m/s^2
Transverse drive acceleration	2.0 m/s^2
Main trolley mass	30 mt
Main trolley transverse mass	5 mt
Secondary trolley mass	100 mt
Max. SWL (tandem)	82 mt
Max. SWL (single/twin)	70 mt

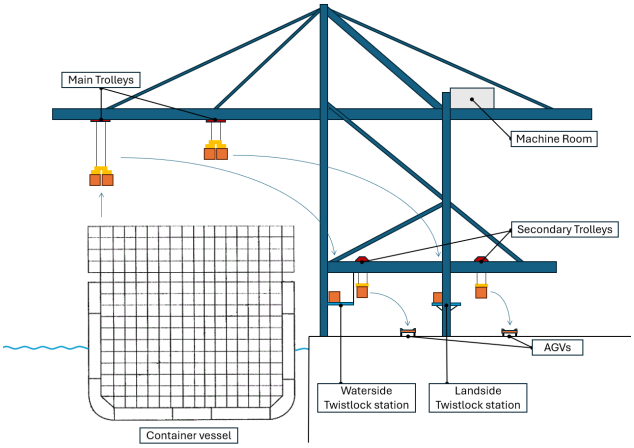

Figure A.1: Schematic overview of the Quad Trolley STS crane concept, showing the two main trolleys, two secondary trolleys, and intermediate twistlock stations.

III Methodology

The study adopts a sequential coupled modelling approach. A beam-element finite element (FE) model is developed in ANSYS and verified using SDC Verifier in accordance with EN 13001 [8], providing global structural stiffness, mass distribution, and modal properties. An equivalent conventional single-trolley STS crane with identical global geometry is modelled using the same FE approach and verification procedure, providing a consistent structural reference. The structural properties extracted from the FE model are subsequently used as input for simplified dynamic models of the trolley-payload system, implemented in MATLAB.

Two dynamic models are developed. The transverse model describes the transverse motion of the main trolley sheave block relative to the boom, capturing the coupled dynamics of the flexible boom and the suspended load pendulum. For the conventional STS comparison, a compliant-drive model is used in which the gantry drive actuates the crane base at the bogie level, transmitting motion through the flexible structure to the suspension point. The trolley travel model describes the motion of the trolley along the boom, accounting for structural compliance and pendulum dynamics. All models are linearised and expressed in state-space form. An LQI controller is designed for each configuration. LQI is selected as a systematic and consistent state-feedback framework that enables explicit weighting of positioning accuracy and actuator demand, with integral action ensuring zero steady-state tracking error under constant disturbances such as wind loading. This makes it well suited as a comparative tool for evaluating dynamic behaviour across configurations rather than as an optimised industrial control solution.

Dynamic performance is evaluated through reference case simulations covering representative combinations of payload mass, hoisting length, wind speed, and structural stiffness. Wind disturbances are modelled using a turbulence model based on the superposition of a slowly varying gust component and a stochastic turbulence component, consistent with common atmospheric turbulence modelling assumptions [9]. The 50 mm transverse accuracy threshold and the 30 mm trolley travel threshold correspond to the positioning tolerances required for accurate container landing, where the twistlocks of the incoming container must align with the corner castings of the container below [10]. A full factorial Design of Experiments (DOE) with three levels per parameter is used to systematically identify the dominant factors affecting positioning accuracy and actuator demand. Performance is assessed using four KPIs: maximum tracking error $e_{\max}$, mean absolute error e_{MAE}, maximum acceleration $u_{\max}$, and RMS acceleration u_{RMS}.

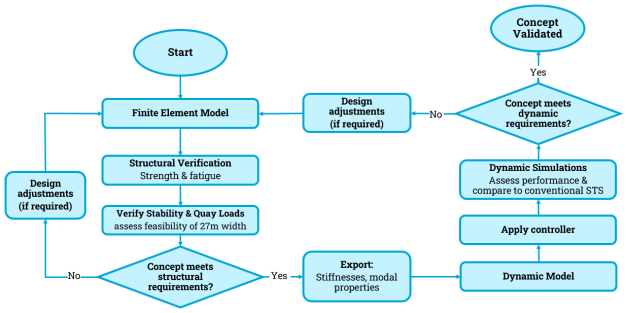

Figure A.2: Overview of the sequential coupled modelling approach linking the FE model to the simplified dynamic models.

IV Structural Results

IV.A Structural Verification

The structural verification confirms that the Quad Trolley STS crane concept satisfies both strength and fatigue requirements under all considered load combinations in accordance with EN 13001 [8]. Fatigue governs the final structural design, with utilisation approaching unity across a large portion of the structure. Strength utilisation peaks under operational loading

with wind at approximately 0.94, as shown in Fig. A.3, while the storm condition produces a different load distribution dominated by the portal frame and lower structure. The primary steel structural mass is approximately 1161 mt, representing only a 53 mt increase compared to the equivalent conventional single-trolley STS crane. This limited increase reflects the partial offsetting of higher stress ranges by the lower number of cycles per trolley in the multi-trolley configuration.

The fatigue utilisation is presented in Fig. A.4, showing that utilisation approaches unity across a large portion of the structure. The final structural dimensions are therefore determined by fatigue rather than peak strength, with cross-sectional properties and plate thicknesses iteratively adjusted until fatigue utilisation remained just below unity throughout.

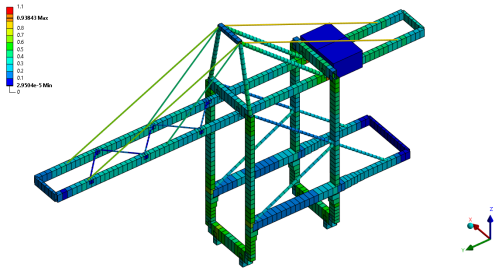

Figure A.3: Utilisation factors for Load Combination B3 (operational with wind), showing the maximum value per element over all load cases. Peak utilisation of approximately 0.94 occurs at the main girder support.

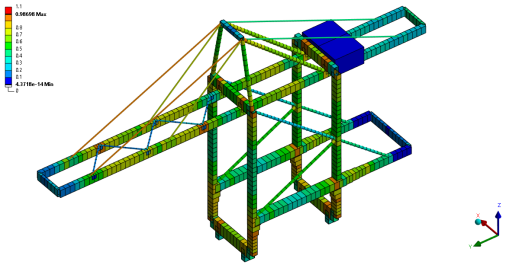

Figure A.4: Fatigue utilisation factors per element, based on the applied load spectrum and 2×10^6 load cycles per main trolley. Utilisation approaches unity across a large portion of the structure, confirming that fatigue governs the final structural design.

A complete mass overview is provided in Table A.2. The total crane mass including all trolleys is approximately 2333 mt, compared to 2021 mt for the conventional crane. The increase is primarily attributable to the additional trolley systems, second twistlock station, and larger machine room requirements.

Table A.2: Mass comparison between the Quad Trolley and conventional STS crane.

Component	Conv.	Quad
Structural mass (incl. 1.25 factor)	1108 mt	1161 mt
Machine room	150 mt	230 mt
Bogies (×4)	312 mt	312 mt
Twistlock stations	50 mt	100 mt
Access, ropes, etc.	149 mt	149 mt
Trolley rails & support	106 mt	106 mt
Total (excl. trolleys)	**1881 mt**	**2058 mt**
Main trolleys	30 mt	60 mt
Secondary trolleys	100 mt	200 mt
Catenary trolleys	10 mt	15 mt
Total (incl. trolleys)	**2021 mt**	**2333 mt**

IV.B Stability

Global stability is evaluated for both operational and storm conditions in accordance with EN 13001 [11]. A zero-uplift criterion is adopted, requiring all bogie reaction forces to remain non-negative under all considered load cases. Under operational loading, uplift of approximately 180 kN occurs at a single landside leg, localised by the direction of wind and transverse acceleration. The restoring moment of the opposite leg is sufficient to prevent overturning in practice, but the zero-uplift criterion is not satisfied. Two solutions are viable: the addition of approximately 20 mt of ballast per landside leg, or an operational positioning constraint increasing the minimum trolley spacing from 10 m to 18 m at maximum outreach. Both can be implemented without fundamental changes to the structural concept, confirming feasibility within the 27 m width constraint.

Under storm conditions with the boom at 80°, uplift at a single waterside leg reaches approximately 2350 kN, exceeding the restoring moment and indicating genuine overturning risk. The application of tie-downs at the waterside bogies is required, which is a well-established practice for large STS cranes. The boom angle offers an additional means of reducing uplift demand if foundation capacity is limited.

IV.C Quay Loading

Line loads are derived from the bogie reaction forces obtained from the finite element model for both configurations. Under operational conditions, the Quad Trolley crane produces line loads of 1010–1030 kN/m, compared to approximately 775 kN/m for the conventional crane, reflecting the significantly higher trolley-induced loading of the former. Under storm conditions the difference is smaller, with 980–1060 kN/m versus 930–970 kN/m, as both configurations share the same structural geometry and wind-exposed area. Comparing these results against reference values reported in technical specifications for existing large STS crane infrastructure, the Quad Trolley line loads fall within the reported range of 785–1400 kN/m [12, 13, 14, 15],

though at the upper end, indicating that the concept does not impose exceptional demands on the quay structure and would generally be compatible with modern port infrastructure, subject to site-specific verification.

IV.D Modal Analysis

The primary vibration modes and natural frequencies are summarised in Table A.3 and compared against literature values for large STS cranes [16, 17, 18, 19]. Modes 1 and 2 vary with trolley position, as the trolley mass distribution influences the transverse structural dynamics. Mode 3 is independent of trolley position. The portal sway frequency of 0.542 Hz satisfies the ISO 22986 [20] minimum of ≥0.50 Hz but falls below the ≥0.70 Hz minimum found in industry specifications for conventional STS cranes. The dynamic implications of this are investigated in the stiffness sweep presented in Section V.D.

Table A.3: Natural frequencies of the primary vibration modes compared to literature and industry specification limits.

Source	Mode 1 [Hz]	Mode 2 [Hz]	Mode 3 [Hz]
This work	0.24–0.27	0.31–0.33	0.54
Meisuh [16]	0.25	0.33	0.60
Tran [17]	0.26	0.47	0.74
Huang [18]	0.26	0.42	–
Solazzi [19]	0.60	0.83	–
ISO 22986 [20]	–	–	≥0.50
Industry spec.	≥0.25	≥0.25	≥0.70

Mode 1: boom sway, Mode 2: frame torsion, Mode 3: portal sway.

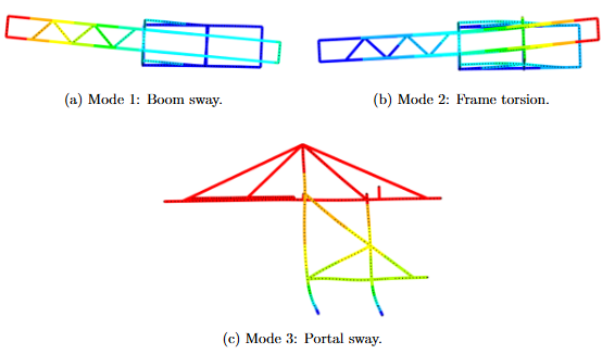

(a) Mode 1: Boom sway. (b) Mode 2: Frame torsion. (c) Mode 3: Portal sway.

Figure A.5: Primary global vibration modes obtained from the FE model.

V Dynamic Results

V.A Transverse Motion

The dynamic performance is evaluated for a set of reference cases covering representative operating conditions. Three levels of control difficulty are defined – low, medium, and high severity – constructed by simultaneously varying payload mass, hoisting length, disturbance magnitude, and wind speed. Each severity level is evaluated at two characteristic trolley positions along the boom: maximum outreach, with an effective structural stiffness of $k = 533$ kN/m, and above the waterside twistlock station, with $k = 3200$ kN/m. This results in six reference cases covering the full range of operating conditions and structural stiffness encountered during normal crane operation.

Results show that the Quad Trolley configuration achieves tracking errors within or close to the 50 mm accuracy threshold across all but the worst case conditions, with only the high-severity outreach case producing occasional peaks exceeding the threshold. By contrast, the conventional STS crane exceeds the threshold across all reference cases, including low-severity conditions, as shown in Fig. A.6.

The fundamental cause of this difference lies in the actuation concept. The direct trolley transverse drive applies corrective movements at the suspension point itself, enabling rapid and precise disturbance rejection. The conventional gantry drive must accelerate the entire crane structure, introducing structural compliance and lag in the force transmission path, while its maximum achievable acceleration is significantly lower due to the requirement to move the entire crane mass. Together, these effects fundamentally limit the achievable positioning accuracy of conventional gantry-based transverse actuation.

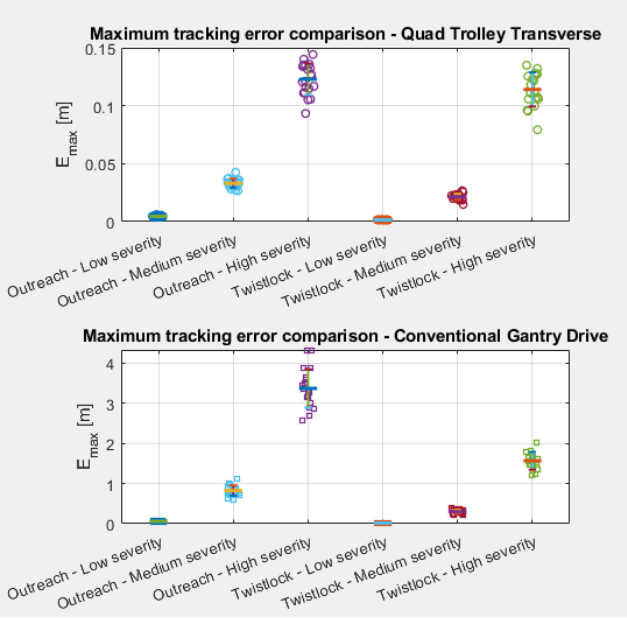

Figure A.6: Maximum transverse tracking error for all reference cases, comparing the Quad Trolley concept with conventional gantry-based actuation.

V.B Transverse Parameter Sensitivity

The DOE reveals a clear hierarchy of parameter influence. Wind speed is the dominant factor, with tracking error and actuator demand increasing strongly and nonlinearly with U_{mean}. Payload mass and hoisting length have a notable secondary influence. The distur-

bance force scale s_F, representing the inter-trolley interaction, shows a comparable effect on both positioning accuracy and actuator demand to that of payload mass and hoisting length, indicating that the dynamic interaction between the two main trolleys has a non-negligible influence on transverse performance. This is consistent with the physical expectation that the disturbance force from the second trolley directly excites the flexible boom in the transverse direction. Trolley position has a modest but consistent effect, with positions closer to the portal frame, where the structure is stiffer, producing lower tracking errors and lower actuator demand, as shown in Fig. A.7.

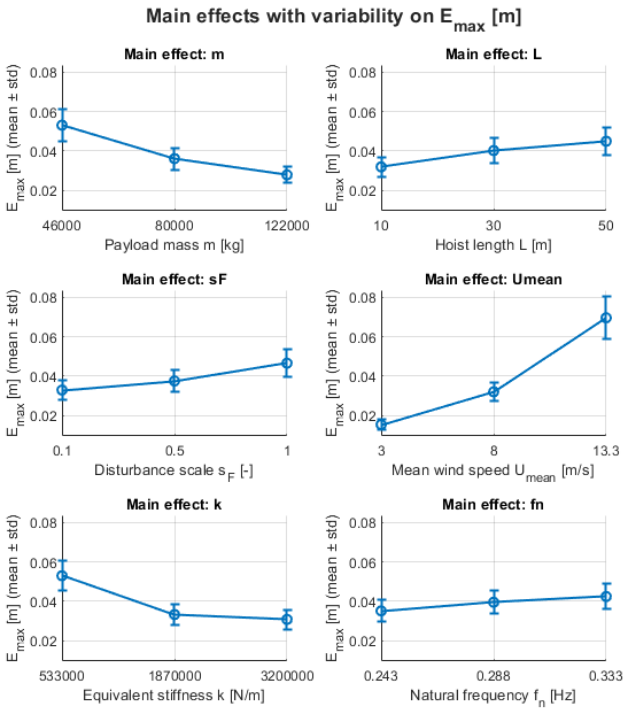

Figure A.7: Main effects of system parameters on maximum transverse tracking error. Wind speed dominates, while trolley position (represented by equivalent stiffness k) and inter-trolley disturbance (s_F) both show notable secondary effects.

V.C Trolley Travel

In the trolley travel direction, the same three severity levels are evaluated at a single fixed structural configuration, as the structural stiffness and natural frequency do not vary meaningfully with trolley position in this direction. The Quad Trolley concept achieves comparable performance to a conventional STS crane. The worst case tracking errors exceed the 30 mm accuracy threshold, but this is attributable to the combination of high wind-induced disturbance forces and the wheel-rail friction constraint limiting the maximum achievable trolley acceleration [13, 21], rather than to structural or multi-trolley effects. The inter-trolley disturbance has a negligible effect in this direction, confirming that the simultaneous operation of two main trolleys, which represents the only fundamental difference from a conventional STS crane in this direction, does not compromise dynamic performance. The relatively simple LQI controller is identified as a contributing factor to the performance limitation under high-severity conditions. The main effects on maximum tracking error are shown in Fig. A.8.

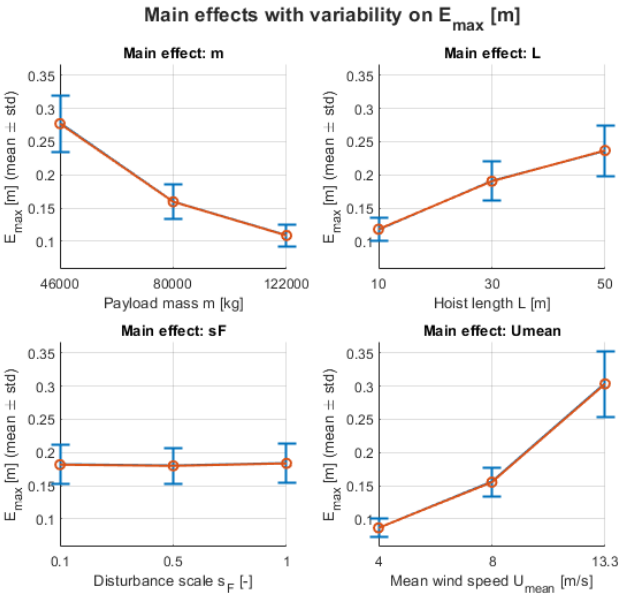

Figure A.8: Main effects of system parameters on maximum trolley travel tracking error. Wind speed dominates, while the inter-trolley disturbance (s_F) has a negligible effect, confirming that the second trolley does not compromise trolley travel performance.

V.D Structural Stiffness Sweep

As noted in the modal analysis, the portal sway frequency of 0.542 Hz falls below the industry specification minimum of $\geq$0.70 Hz. To investigate whether this contributes to the degraded trolley travel performance under high-severity conditions, three complementary parameter sweeps are performed to isolate the individual effects of stiffness and natural frequency: a stiffness sweep with fixed modal mass (Fig. A.9), a stiffness sweep with fixed natural frequency (Fig. A.10), and a natural frequency sweep with fixed stiffness (Fig. A.11). In the fixed modal mass sweep, stiffness is varied from 8.33 MN/m to 33.33 MN/m around the baseline design value of $k = 16.670$ MN/m, corresponding to natural frequencies of approximately 0.38–0.77 Hz, covering the full range from below the ISO 22986 minimum to above the industry specification minimum.

The results across all three sweeps are consistent: structural stiffness and natural frequency have at most a marginal influence on trolley travel dynamic performance. A slight improvement can be observed with increasing stiffness, but the effect is small relative to the variability across stochastic realisations and unlikely to justify the structural modifications required to achieve it. The degraded performance under high-severity conditions is therefore not a structural problem, but is instead driven by the combination of high wind-induced disturbance forces, the wheel-rail friction constraint, and the limitations of the simple LQI control strategy. This confirms that the baseline structural design is dynamically adequate for the trolley travel direction,

and that no additional stiffness requirements need to be imposed beyond the dimensions already required for compliance with the strength and fatigue criteria of EN 13001 [8].

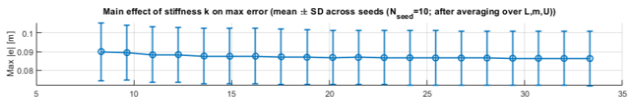

Figure A.9: Effect of structural stiffness on maximum tracking error $e_{\max}$ with fixed modal mass. The natural frequency increases with stiffness as shown in the top panel. The response remains essentially constant across the full range from half to twice the baseline design value of $k = 16.670$ MN/m. Results for all four KPIs show the same trend.

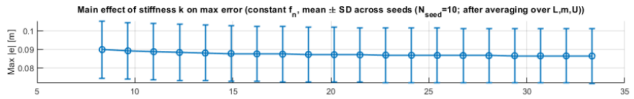

Figure A.10: Effect of structural stiffness on maximum tracking error $e_{\max}$ with fixed natural frequency ($f_n = 0.542$ Hz). All other KPIs show the same response.

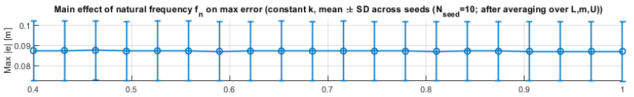

Figure A.11: Effect of natural frequency on maximum tracking error $e_{\max}$ with fixed stiffness ($k = 16.670$ MN/m). The natural frequency is swept from 0.4 to 1.0 Hz, covering the full range from below the ISO 22986 minimum to above the industry specification minimum. All four KPIs remain completely flat throughout.

V.E Summary of Dynamic Performance

The dynamic assessment demonstrates that the Quad Trolley STS crane concept is dynamically feasible under the applied control framework. In the transverse direction, the direct trolley drive provides a fundamental and substantial improvement in positioning accuracy compared to the conventional crane, an advantage inherent to the actuation concept that cannot be replicated through control improvements alone. In the trolley travel direction, the concept performs comparable with that of a conventional STS crane, with neither the second trolley nor the relatively low structural stiffness and natural frequency introducing any meaningful performance degradation. Wind loading governs the dynamic response in both directions, while the inter-trolley disturbance is negligible in the trolley travel direction but has a non-negligible influence in the transverse direction, comparable in magnitude to payload mass and hoisting length. The controller employed is intentionally simple and serves as a comparative tool; the absolute performance values may therefore differ from those achievable with more advanced control strategies, while the relative findings are considered robust and independent of the specific control strategy.

VI Conclusion

This paper investigated the structural and dynamic feasibility of the Quad Trolley STS crane concept, addressing the design criteria required for feasible and controllable operation.

Structural mass: The concept satisfies EN 13001 strength and fatigue requirements, with fatigue governing the final cross-sectional dimensions. The structural mass increase of only 53 mt compared to a conventional STS crane confirms that the multi-trolley loading does not disproportionately increase structural demand.

Feasibility within the 27 m width constraint: The concept is feasible within the conventional 27 m width constraint. Stability is identified as a critical design consideration at this width, but can be resolved through ballast or positioning constraints under operational conditions and tie-downs under storm conditions, without fundamental changes to the structural concept. Quay loading remains within the range reported for existing STS crane infrastructure.

Dynamic feasibility: In the transverse direction, the direct trolley actuation provides a fundamental performance advantage over conventional gantry-based actuation, consistently achieving tracking errors within or close to the 50 mm threshold while the conventional crane exceeds it across all reference cases. This advantage is inherent to the actuation concept. In the trolley travel direction, performance is comparable to that of a conventional STS crane, as the second trolley introduces no meaningful dynamic interaction and structural stiffness has no meaningful effect on positioning accuracy.

Structural flexibility and controllability: In the transverse direction, stiffer trolley positions consistently produce lower tracking errors, but acceptable performance is maintained even at maximum outreach. In the trolley travel direction, even doubling the baseline stiffness yields only marginal improvement. The code-compliant baseline design is therefore both structurally minimal and dynamically sufficient, and no additional stiffness requirements or supplemental damping need to be imposed.

Overall: The key design criteria are compliance with EN 13001 strength and fatigue requirements, stability provisions at the 27 m width, and the adoption of direct transverse actuation as the key enabler of the concept's performance advantage. Together, these results demonstrate that the Quad Trolley STS crane concept represents a structurally sound and dynamically viable direction for high-performance container handling.

Acknowledgements

This research was carried out in partial fulfilment of the requirements for the degree of Master of Science in Mechanical Engineering at the *Delft University of Technology (TU Delft)*, and in collaboration with Huisman Equipment B.V. The author gratefully acknowledges the support and guidance of ir. W. van den Bos

(TU Delft), ir. R. Nouwens, and ing. M. van Wingerden (Huisman Equipment B.V.).

References

[1] J. Achterkamp and S. P. Solutions, "The effect of mega-ships," Tech. Rep. [Online]. Available: https://wpassets.porttechnology.org/wp-content/uploads/2019/05/25182729/JOOST-PTIONLINE-5.pdf

[2] L. C. C. Ltd., "Technical Description," Tech. Rep. [Online]. Available: https://www-assets.liebherr.com/media/bu-media/lhbu-mcc/downloads-and-brochures/brochures/lcc/liebherr-sts-cranes-technical-description.pdf

[3] Konecranes, "Konecranes Ship-to-Shore Crane (STS)," Tech. Rep., 2024. [Online]. Available: https://www.konecranes.com/system/files/2024-04/7593_sts_monobox_technical_doc_v1.pdf

[4] SANY and S. M. M. Company, "SANY Industrial Park, Gaolan Port Economic and Development Zone, Zhuhai, Guangdong, China," Tech. Rep., 2022. [Online]. Available: https://sanyglobal-img.sany.com.cn/product/picture_album/20220919/SANY_STS_Brochure2022_084536.pdf

[5] M. A. Jordan and L. C. Inc., "Quay crane productivity," Tech. Rep., 2002. [Online]. Available: https://www.liftech.net/wp-content/uploads/2002/11/Quay-Crane-Productivity-Paper.pdf

[6] J.-P. Rodrigue, T. Notteboom, and A. Pallis, "Chapter 6.6 – Container Terminal Automation — Port Economics, Management and Policy," 7 2025. [Online]. Available: https://porteconomicsmanagement.org/pemp/contents/part6/terminal-automation/

[7] M. G. Reports, "Ship-to-Shore (STS) Container Cranes Market Size, Share Trends, 2033." [Online]. Available: https://www.marketgrowthreports.com/market-reports/ship-to-shore-sts-container-cranes-market-109713

[8] *Cranes — General design — Part 3-1: Limit states and proof of competence of steel structures*, CEN Std. EN 13 001-3-1, 2025, available via NEN or national standardization bodies.

[9] T. Burton *et al.*, "Introduction to micro-meteorology for wind energy," 2011, accessed: 2026-03-27. [Online]. Available: https://backend.orbit.dtu.dk/ws/files/52392430/Introduction_to_micro_meteorology_for_wind_energy.pdf

[10] Confidential, "Sts crane container procedures drawing," not publicly available.

[11] *Cranes — General design — Part 2: Load actions*, European Committee for Standardization (CEN) Std. EN 13 001-2:2021, 2021, available via NEN or national standardization bodies.

[12] Confidential, "Sts crane specification," not publicly available.

[13] B. C. T. Ltd., "Technical Specification for Two Quayside Container Cranes (QC)," Tech. Rep., 11 2023. [Online]. Available: https://cdnweb.bct.gdynia.pl/s3fs-public/inline-files/SIWZ%20STS%20EU%2032_2024%20Za%C5%82acznik%205%20Technical%20Specification%20STS%20KPO%202_17.07.2024_.pdf

[14] G. C. T. S.A., "Technical Specification for Quayside Container Cranes," 2014. [Online]. Available: https://www.scribd.com/document/456068299/Container-Crane-2DT2014-Cz%C4%99%C5%9B%C4%87-3-STS-Technical-Specification-pdf

[15] Confidential, "Sts crane rail loads," not publicly available.

[16] B. K. Meisuh, J. Seo, J. Huh, J. Kim, and J.-M. Kim, "Seismic response of a container crane subjected to ground motions," *Applied Ocean Research*, vol. 126, p. 103270, 7 2022. [Online]. Available: https://doi.org/10.1016/j.apor.2022.103270

[17] Q. H. Tran, J. Huh, V. B. Nguyen, C. Kang, J.-H. Ahn, and I.-J. Park, "Sensitivity Analysis for Ship-to-Shore Container Crane Design," *Applied Sciences*, vol. 8, no. 9, p. 1667, 9 2018. [Online]. Available: https://doi.org/10.3390/app8091667

[18] D. Huang, X. Guo, H. Wang, H. Wang, and Y. Peng, "A Finite Element Analysis-based Study on the Reliability of Heightened Quayside Container Cranes," *Journal of Engineering Science and Technology Review*, vol. 14, no. 6, pp. 72–82, 1 2021. [Online]. Available: https://doi.org/10.25103/jestr.146.08

[19] L. Solazzi and N. Zrnić, "Mechanical behavior of ship to shore container crane subjected to different stochastic wind actions." *Journal of Physics Conference Series*, vol. 2647, no. 25, p. 252002, 6 2024. [Online]. Available: https://doi.org/10.1088/1742-6596/2647/25/252002

[20] *Cranes — Stiffness - Bridge and gantry cranes*, ISO Std. ISO 22 986, 2007, available via NEN or national standardization bodies.

[21] P. Romanowicz, "Numerical assessment of fatigue load capacity of cylindrical crane wheel using multiaxial high-cycle fatigue criteria," *Archive of Applied Mechanics*, vol. 87, no. 10, pp. 1707–1726, 2017. [Online]. Available: https://doi.org/10.1007/s00419-017-1281-6

B Load definitions

B.1 Main Trolley Hoist load

The hoist load represents the vertical load transferred to the crane structure by the lifted mass together with the trolley mass. In accordance with EN 15011, this load is multiplied by a dynamic factor to account for acceleration and deceleration effects during hoisting operations.

For the present case, the dynamic factor

$$\phi_5 = 1.10$$

is adopted, corresponding to *lowering with stepless speed control*, as defined in EN 15011.

The hoist load is calculated as:

$$F_{\text{hoist}} = g\left(\phi_5 M_{\text{load}} + M_{\text{trolley}}\right) \tag{112}$$

where:

- $g = 9.81$ m/s^2 is the gravitational acceleration,
- $\phi_5 = 1.10$ is the dynamic factor for hoisting,
- $M_{\text{load}} = 122$ t is the lifted mass (payload + headblock + spreaders),
- $M_{\text{trolley}} = 30$ t is the mass of the main trolley.

The lifted mass of 122 t corresponds to the governing tandem lifting configuration of the main trolley, consisting of a 10 t headblock, 30 t of spreaders, and a maximum payload of 82 t.

Substituting the values:

$$F_{\text{hoist}} = 9.81\left(1.10 \cdot 122 + 30\right) = 1610.8 \text{ kN} \tag{113}$$

Thus, the resulting design hoist load is:

$$F_{\text{hoist}} = 1610.8 \text{ kN} \tag{114}$$

B.2 Main Trolley acceleration load

The horizontal inertial load due to trolley travel acceleration is determined in accordance with EN 15011 as the load induced by acceleration of the trolley drive. This load acts in the trolley travel direction and represents the force required to accelerate both the trolley mass and the freely suspended lifted load.

The load is calculated as:

$$F_{\text{trolley}} = a_{\text{trolley}}\left(\phi_2 M_{\text{trolley}} + \phi_3 M_{\text{load}}\right) \tag{115}$$

where:

- $a_{\text{trolley}} = 1.2$ m/s^2 is the trolley acceleration,
- $\phi_2 = 1.2$ is the factor for the trolley mass for stepless speed control,
- $\phi_3 = 2.0$ is the factor for the freely suspended load,
- $M_{\text{trolley}} = 30$ t is the mass of the main trolley,
- $M_{\text{load}} = 122$ t is the lifted mass.

Substituting the values:

$$F_{\text{trolley}} = 1.2\,(1.2 \cdot 30 + 2.0 \cdot 122) = 336 \text{ kN} \tag{116}$$

Thus, the resulting horizontal inertial load due to trolley acceleration is:

$$F_{\text{trolley}} = 336 \text{ kN} \tag{117}$$

B.3 Main trolley transverse acceleration load

The horizontal inertial load due to transverse (sideways) acceleration of the main trolley is determined based on the EN 15011 formulation for acceleration-induced loads. This load acts perpendicular to the boom and represents the force required to accelerate both the transverse trolley mass and the freely suspended lifted load.

In the proposed concept, the suspended load is actively stabilised by the control system. As a result, the load motion is significantly reduced compared to the trolley motion, and the load does not follow the full actuator acceleration.

The load is therefore calculated as:

$$F_{\text{trans}} = a_{\text{trans,trolley}} \cdot \phi_2 M_{\text{trolley,trans}} + a_{\text{trans,load}} \cdot \phi_3 M_{\text{load}} \tag{118}$$

where:

- $a_{\text{trans,trolley}} = 2.0$ m/s^2 is the transverse trolley acceleration,
- $a_{\text{trans,load}} = 0.25$ m/s^2 is the transverse acceleration of the suspended load,
- $\phi_2 = 1.2$ is the factor for rigidly connected masses,
- $\phi_3 = 2.0$ is the factor for the freely suspended load,
- $M_{\text{trolley,trans}} = 5$ t is the transverse moving mass,
- $M_{\text{load}} = 122$ t is the lifted mass.

The value of $a_{\text{trans,load}}$ is obtained from the dynamic simulations and corresponds to the maximum absolute load acceleration observed across all reference cases, providing a conservative estimate of the operational demand.

Substituting the values:

$$F_{\text{trans}} = 2.0 \cdot 1.2 \cdot 5 + 0.25 \cdot 2.0 \cdot 122 = 73 \text{ kN} \tag{119}$$

Thus, the resulting transverse inertial load is:

$$F_{\text{trans}} = 73 \text{ kN} \tag{120}$$

B.4 Secondary trolley hoist load

The hoist load represents the vertical load transferred to the crane structure by the lifted mass together with the secondary trolley mass. In accordance with EN 15011, this load is multiplied by a dynamic factor to account for acceleration and deceleration effects during hoisting operations.

For the present case, the dynamic factor

$$\phi_5 = 1.10$$

is adopted, corresponding to *lowering with stepless speed control*, as defined in EN 15011.

The hoist load is calculated as:

$$F_{\text{hoist,sec}} = g\left(\phi_5 M_{\text{load}} + M_{\text{trolley,sec}}\right) \tag{121}$$

where:

- $g = 9.81$ m/s^2 is the gravitational acceleration,
- $\phi_5 = 1.10$ is the dynamic factor for hoisting,
- $M_{\text{load}} = 90$ t is the lifted mass,
- $M_{\text{trolley,sec}} = 100$ t is the mass of the secondary trolley.

Substituting the values:

$$F_{\text{hoist,sec}} = 9.81\left(1.10 \cdot 90 + 100\right) = 1952.2 \text{ kN} \tag{122}$$

Thus, the resulting design hoist load is:

$$F_{\text{hoist,sec}} = 1952.2 \text{ kN} \tag{123}$$

B.5 Secondary trolley acceleration load

The horizontal inertial load due to acceleration of the secondary trolley is determined in accordance with EN 15011 as the load induced by the trolley drive. This load acts in the direction of trolley motion and represents the force required to accelerate both the trolley mass and the freely suspended lifted load.

The load is calculated as:

$$F_{\text{trolley,sec}} = a_{\text{trolley,sec}}\left(\phi_2 M_{\text{trolley,sec}} + \phi_3 M_{\text{load}}\right) \tag{124}$$

where:

- $a_{\text{trolley,sec}} = 0.8$ m/s^2 is the secondary trolley acceleration,
- $\phi_2 = 1.2$ is the factor for rigidly connected masses,
- $\phi_3 = 2.0$ is the factor for the freely suspended load,
- $M_{\text{trolley,sec}} = 100$ t is the mass of the secondary trolley,

- $M_{\text{load}} = 90$ t is the lifted mass.

Substituting the values:

$$F_{\text{trolley,sec}} = 0.8\,(1.2 \cdot 100 + 2.0 \cdot 90) = 240 \text{ kN} \tag{125}$$

Thus, the resulting horizontal inertial load is:

$$F_{\text{trolley,sec}} = 240 \text{ kN} \tag{126}$$

B.6 Gantry acceleration load

The inertial load due to gantry acceleration is determined as a global body acceleration applied to the crane structure. In accordance with EN 15011, a dynamic factor is included to account for acceleration effects.

The gantry acceleration is defined as:

$$a_{\text{gantry}} = \phi_2 \cdot a = 1.2 \cdot 0.25 = 0.30 \text{ m/s}^2 \tag{127}$$

This acceleration is applied in the finite element model as a body acceleration acting on the entire structure.

During gantry acceleration, the trolleys are assumed to be empty and stationary, as operational gantry motion is not considered in combination with lifting operations. The applied inertial load is therefore governed solely by the structural mass distribution.

Thus, the governing load is represented by:

$$F_{\text{gantry}} = m_{\text{total}} \cdot a_{\text{gantry}} \tag{128}$$

B.7 Hoisting force on boom (main trolleys)

The hoisting force represents the vertical force transmitted to the boom through the hoist ropes at the boom tip. In the Quad Trolley configuration, two main trolleys operate simultaneously, resulting in two independent hoisting systems acting on the structure.

The hoisting force per trolley is given by:

$$F_{\text{hoist,1}} = g \cdot \phi_5 \cdot M_{\text{load}} \tag{129}$$

The total hoisting force acting on the boom is therefore:

$$F_{\text{hoist,tot}} = 2 \cdot g \cdot \phi_5 \cdot M_{\text{load}} \tag{130}$$

where:

- $g = 9.81$ m/s^2 is the gravitational acceleration,
- $\phi_5 = 1.10$ is the dynamic factor for hoisting,
- $M_{\text{load}} = 122$ t is the lifted mass per main trolley.

Substituting the values:

$$F_{\text{hoist,tot}} = 2 \cdot 9.81 \cdot 1.10 \cdot 122 = 2633 \text{ kN} \tag{131}$$

Thus, the resulting hoisting force acting on the boom is:

$$F_{\text{hoist,tot}} = 2633 \text{ kN} \tag{132}$$

B.8 Trolley buffer force

The buffer force represents the impact load generated when the trolley reaches the end stop and is decelerated by the buffer system. In accordance with EN 13001-2, this load is determined from the kinetic energy of the moving mass and multiplied by a dynamic factor to account for buffer characteristics.

The buffer force is calculated as:

$$F_{\text{buffer}} = \phi_7 \cdot \frac{m_{\text{tot}}\, v^2}{2\, s} \tag{133}$$

where:

- $\phi_7 = 1.6$ is the dynamic factor for hydraulic buffers ($\varepsilon = 1.0$),
- $m_{\text{tot}} = M_{\text{trolley}} + M_{\text{load}} = 30 + 122$ t is the total moving mass,
- $v = 4.0$ m/s is the trolley velocity,
- $s = 1.0$ m is the buffer stroke.

Substituting the values:

$$F_{\text{buffer}} = 1.6 \cdot \frac{(122 + 30) \cdot 4.0^2}{2 \cdot 1} = 1946 \text{ kN} \tag{134}$$

Thus, the resulting buffer force is:

$$F_{\text{buffer}} = 1946 \text{ kN} \tag{135}$$

B.9 Secondary trolley buffer force

The buffer force represents the impact load generated when the secondary trolley reaches the end stop and is decelerated by the buffer system. In accordance with EN 13001-2, this load is determined from the kinetic energy of the moving mass and multiplied by a dynamic factor to account for buffer characteristics.

The buffer force is calculated as:

$$F_{\text{buffer,sec}} = \phi_7 \cdot \frac{m_{\text{tot}}\, v^2}{2\, s} \tag{136}$$

where:

- $\phi_7 = 1.6$ is the dynamic factor for hydraulic buffers ($\varepsilon = 1.0$),

- $m_{\text{tot}} = M_{\text{trolley,sec}} + M_{\text{load}} = 100 + 90$ t is the total moving mass,
- $v = 3.0$ m/s is the secondary trolley velocity,
- $s = 1.0$ m is the buffer stroke.

Substituting the values:

$$F_{\text{buffer,sec}} = 1.6 \cdot \frac{(100 + 90) \cdot 3.0^2}{2 \cdot 1} = 1368 \text{ kN} \tag{137}$$

Thus, the resulting buffer force is:

$$F_{\text{buffer,sec}} = 1368 \text{ kN} \tag{138}$$

B.10 Gantry buffer acceleration

The gantry buffer load represents the impact load generated when the crane reaches the end stop and is decelerated by the buffer system. In accordance with EN 13001-2, this load is determined from the kinetic energy of the moving mass and multiplied by a dynamic factor to account for buffer characteristics.

For application in the finite element model, the buffer load is expressed as an equivalent body acceleration:

$$a_{\text{gantry,buffer}} = \phi_7 \cdot \frac{v^2}{2s} \tag{139}$$

where:

- $\phi_7 = 1.6$ is the dynamic factor for hydraulic buffers ($\varepsilon = 1.0$),
- $v = 0.75$ m/s is the gantry travel velocity,
- $s = 1.0$ m is the buffer stroke.

Substituting the values:

$$a_{\text{gantry,buffer}} = 1.6 \cdot \frac{0.75^2}{2 \cdot 1} = 0.45 \text{ m/s}^2 \tag{140}$$

Thus, the resulting buffer-induced deceleration is:

$$a_{\text{gantry,buffer}} = 0.45 \text{ m/s}^2 \tag{141}$$

C Transverse model derivation

This appendix presents the full derivation of the transverse dynamic model of the Quad Trolley STS crane using Lagrange's equations. The trolley motion is treated as a prescribed input, while the structural deformation and load sway are described by generalized coordinates.

Generalized Coordinates

The transverse dynamics are described using the generalized coordinates

$$(q_1, q_2) = (x_b, \theta),$$

where $x_b(t)$ is the transverse displacement of the boom and $\theta(t)$ is the sway angle of the suspended load.

The trolley motion $x_t(t)$ represents the transverse displacement of the trolley relative to the boom and is treated as a prescribed input.

Kinematics

Boom displacement:

$$x_b = x_b(t), \qquad \dot{x}_b = \dot{x}_b(t). \tag{142}$$

Prescribed trolley motion:

$$x_t = x_t(t), \qquad \dot{x}_t = \dot{x}_t(t), \qquad \ddot{x}_t = \ddot{x}_t(t). \tag{143}$$

Absolute position of the trolley suspension point:

$$x_s = x_b + x_t. \tag{144}$$

Load position:

$$x_L = x_b + x_t + L\sin\theta, \tag{145}$$
$$z_L = L - L\cos\theta. \tag{146}$$

Load velocities:

$$\dot{x}_L = \dot{x}_b + \dot{x}_t + L\cos\theta\,\dot{\theta}, \tag{147}$$
$$\dot{z}_L = L\sin\theta\,\dot{\theta}. \tag{148}$$

Squared velocity of the load:

$$v_L^2 = (\dot{x}_b + \dot{x}_t)^2 + 2L\cos\theta\,\dot{\theta}(\dot{x}_b + \dot{x}_t) + L^2\dot{\theta}^2. \tag{149}$$

Kinetic Energy

Boom:

$$T_b = \frac{1}{2} m_c \dot{x}_b^2. \tag{150}$$

Trolley:

$$T_t = \frac{1}{2} m_t (\dot{x}_b + \dot{x}_t)^2. \tag{151}$$

Load:

$$T_L = \frac{1}{2} m_L \left[(\dot{x}_b + \dot{x}_t)^2 + 2L \cos\theta \, \dot{\theta} (\dot{x}_b + \dot{x}_t) + L^2 \dot{\theta}^2 \right]. \tag{152}$$

Total kinetic energy:

$$\begin{aligned} T = {} & \frac{1}{2}(m_c + m_t + m_L)\dot{x}_b^2 + \frac{1}{2}(m_t + m_L)\dot{x}_t^2 \\ & + (m_t + m_L)\dot{x}_b \dot{x}_t \\ & + m_L L \cos\theta \, \dot{\theta}(\dot{x}_b + \dot{x}_t) + \frac{1}{2} m_L L^2 \dot{\theta}^2. \end{aligned} \tag{153}$$

Potential Energy and Dissipation

Spring:

$$V_{\text{spring}} = \frac{1}{2} k_c x_b^2. \tag{154}$$

Gravity:

$$V_g = m_L g L (1 - \cos\theta). \tag{155}$$

Total potential energy:

$$V = \frac{1}{2} k_c x_b^2 + m_L g L (1 - \cos\theta). \tag{156}$$

Dissipation:

$$D = \frac{1}{2} c_c \, \dot{x}_b^2 + \frac{1}{2} c_\theta \dot{\theta}^2. \tag{157}$$

Lagrangian

$$\mathcal{L} = T - V. \tag{158}$$

Generalized Forces

$$Q_{x_b} = F_{\text{dist}} + F_{\text{wind},b} + F_{\text{wind},l} \tag{159}$$

$$Q_\theta = F_{\text{wind},l} L \cos\theta \tag{160}$$

Equations of Motion (Nonlinear)

Applying Lagrange's equations yields:

$$\begin{aligned}(m_c + m_t + m_L)\ddot{x}_b + (m_t + m_L)\ddot{x}_t \\ + m_L L\left(-\sin\theta\,\dot{\theta}^2 + \cos\theta\,\ddot{\theta}\right) + c_c\,\dot{x}_b + k_c x_b \\ = F_{\text{dist}} + F_{\text{wind},b} + F_{\text{wind},l}\end{aligned} \tag{161}$$

$$m_L L^2\ddot{\theta} + c_\theta\dot{\theta} + m_L g L\sin\theta + m_L L\cos\theta(\ddot{x}_b + \ddot{x}_t) = F_{\text{wind},l} L\cos\theta \tag{162}$$

Linearization

For small sway angles:

$$\sin\theta \approx \theta, \qquad \cos\theta \approx 1$$

The equations become:

$$\begin{aligned}(m_c + m_t + m_L)\ddot{x}_b + (m_t + m_L)\ddot{x}_t + m_L L\,\ddot{\theta} \\ + c_c\,\dot{x}_b + k_c x_b = F_{\text{dist}} + F_{\text{wind},b} + F_{\text{wind},l}\end{aligned} \tag{163}$$

$$m_L L^2\ddot{\theta} + c_\theta\dot{\theta} + m_L g L\,\theta + m_L L(\ddot{x}_b + \ddot{x}_t) = F_{\text{wind},l} L \tag{164}$$

Explicit Acceleration Form

From the linearized pendulum equation:

$$\ddot{\theta} = -\frac{c_\theta}{m_L L^2}\,\dot{\theta} - \frac{g}{L}\,\theta - \frac{1}{L}\left(\ddot{x}_b + \ddot{x}_t\right) + \frac{F_{\text{wind},l}}{m_L L} \tag{165}$$

Substituting into the boom equation and solving for $\ddot{x}_b$ yields:

$$\begin{aligned}\ddot{x}_b = -\frac{k_c}{m_c + m_t}\,x_b - \frac{c_c}{m_c + m_t}\,\dot{x}_b + \frac{g\,m_L}{m_c + m_t}\,\theta \\ + \frac{c_\theta}{L(m_c + m_t)}\,\dot{\theta} + \frac{1}{m_c + m_t}\left(F_{\text{dist}} + F_{\text{wind},b} + F_{\text{wind},l}\right) - \frac{m_t}{m_c + m_t}\,\ddot{x}_t\end{aligned} \tag{166}$$

Substituting back into (165) gives:

$$
\begin{aligned}
\ddot{\theta} = & \frac{k_c}{L(m_c+m_t)}\, x_b + \frac{c_c}{L(m_c+m_t)}\, \dot{x}_b \\
& - \frac{g}{L}\left(1 + \frac{m_L}{m_c+m_t}\right)\theta \\
& - \frac{c_\theta}{L^2}\left(\frac{1}{m_L} + \frac{1}{m_c+m_t}\right)\dot{\theta} - \frac{1}{L(m_c+m_t)}\Big(F_{\text{dist}} + F_{\text{wind},b}\Big) \\
& + \left(\frac{1}{m_L L} - \frac{1}{L(m_c+m_t)}\right) F_{\text{wind},l} - \frac{m_c}{L(m_c+m_t)}\, \ddot{x}_t
\end{aligned} \tag{167}
$$

State-Space Representation

The system is expressed in first-order state-space form by defining the state vector:

$$
\mathbf{x} = \begin{bmatrix} x_b \\ \dot{x}_b \\ \theta \\ \dot{\theta} \end{bmatrix} \tag{168}
$$

and the input vector:

$$
\mathbf{u} = \begin{bmatrix} F_{\text{dist}} \\ \ddot{x}_t \\ F_{\text{wind},b} \\ F_{\text{wind},l} \end{bmatrix} \tag{169}
$$

The system dynamics can then be written as:

$$
\dot{\mathbf{x}} = A\mathbf{x} + B\mathbf{u} \tag{170}
$$

with system matrix A:

$$
A = \begin{bmatrix}
0 & 1 & 0 & 0 \\
-\dfrac{k_c}{m_c+m_t} & -\dfrac{c_c}{m_c+m_t} & \dfrac{g\, m_L}{m_c+m_t} & \dfrac{c_\theta}{L(m_c+m_t)} \\
0 & 0 & 0 & 1 \\
\dfrac{k_c}{L(m_c+m_t)} & \dfrac{c_c}{L(m_c+m_t)} & -\dfrac{g}{L}\left(1+\dfrac{m_L}{m_c+m_t}\right) & -\dfrac{c_\theta}{L^2}\left(\dfrac{1}{m_L}+\dfrac{1}{m_c+m_t}\right)
\end{bmatrix} \tag{171}
$$

and input matrix B:

$$B = \begin{bmatrix} 0 & 0 & 0 & 0 \\ \frac{1}{m_c + m_t} & -\frac{m_t}{m_c + m_t} & \frac{1}{m_c + m_t} & \frac{1}{m_c + m_t} \\ 0 & 0 & 0 & 0 \\ -\frac{1}{L(m_c + m_t)} & -\frac{m_c}{L(m_c + m_t)} & -\frac{1}{L(m_c + m_t)} & \left(\frac{1}{m_L L} - \frac{1}{L(m_c + m_t)}\right) \end{bmatrix} \tag{172}$$

D Conventional Transverse Dynamic Model derivation

This appendix presents the full derivation of the conventional STS crane dynamic model in the transverse direction using Lagrange's equations. In this model the trolley is fixed to the boom in the transverse direction, while the gantry drive imposes a lateral motion on the drive-side coordinate through a compliant element.

Model Description

The transverse dynamics are modelled using a compliant gantry-drive formulation. The bogie drive system imposes a commanded lateral motion on a drive-side coordinate $x_D(t)$, which is transmitted to the boom–trolley–suspension point coordinate $x_t(t)$ through an equivalent spring–damper element. This explicitly captures the structural flexibility between the gantry drive and the suspension point.

In this work the gantry actuation is modelled at the motion-control level. The drive coordinate $x_D(t)$ is assumed to be directly commanded by a fast inner servo, such that its lateral acceleration can be prescribed:

$$u(t) = \ddot{x}_D(t).$$

Motor torque/force generation and drive-side inertia are not modelled explicitly. The analysis therefore focuses on the transmitted compliance force and the resulting structural and sway response, rather than actuator sizing.

Generalized Coordinates

The generalized coordinates are chosen as

$$(q_1, q_2, q_3) = (x_D,\, x_t,\, \theta),$$

where

- $x_D(t)$ is the commanded transverse displacement of the drive-side reference point,
- $x_t(t)$ is the transverse displacement of the boom–trolley–suspension point,
- $\theta(t)$ is the sway angle of the suspended load.

The trolley is assumed to be fixed to the boom in the transverse direction.

The absolute horizontal load position is

$$x_{\text{load}} = x_t + L \sin\theta. \tag{173}$$

Kinematics

The load center-of-mass coordinates are

$$x_L = x_t + L\sin\theta, \tag{174}$$
$$z_L = L - L\cos\theta. \tag{175}$$

Velocities:

$$\dot{x}_L = \dot{x}_t + L\cos\theta\,\dot{\theta}, \tag{176}$$
$$\dot{z}_L = L\sin\theta\,\dot{\theta}. \tag{177}$$

Squared speed:

$$v_L^2 = \dot{x}_t^2 + 2L\cos\theta\,\dot{x}_t\dot{\theta} + L^2\dot{\theta}^2. \tag{178}$$

Kinetic Energy

Boom–trolley equivalent inertia:

$$T_t = \frac{1}{2}M_B\dot{x}_t^2. \tag{179}$$

Load:

$$T_L = \frac{1}{2}m_L\left(\dot{x}_t^2 + 2L\cos\theta\,\dot{x}_t\dot{\theta} + L^2\dot{\theta}^2\right). \tag{180}$$

Total kinetic energy:

$$T = \frac{1}{2}(M_B + m_L)\dot{x}_t^2 + m_L L\cos\theta\,\dot{x}_t\dot{\theta} + \frac{1}{2}m_L L^2\dot{\theta}^2. \tag{181}$$

Remark: prescribed drive motion. The drive coordinate $x_D(t)$ is treated as a prescribed motion input and is not assigned kinetic energy. This is consistent with modeling the gantry drive at the motion-control level, where $x_D(t)$ acts as an imposed base motion transmitted through the compliant element.

Potential Energy and Dissipation

Compliant coupling between drive and structure:

$$V_c = \frac{1}{2}k_c(x_D - x_t)^2. \tag{182}$$

Gravitational potential of the load:

$$V_g = m_L g L(1 - \cos\theta). \tag{183}$$

Total potential energy:

$$V = V_c + V_g. \tag{184}$$

Rayleigh dissipation:

$$D = \frac{1}{2} c_c (\dot{x}_D - \dot{x}_t)^2 + \frac{1}{2} c_\theta \dot{\theta}^2. \tag{185}$$

Lagrangian

The Lagrangian is

$$\mathcal{L} = T - V. \tag{186}$$

Generalized Forces

Wind is modelled as external horizontal forces:

- $F_{\text{wind},b}(t)$ acting on the boom/trolley/suspension assembly in the transverse direction,
- $F_{\text{wind},l}(t)$ acting on the load in the transverse direction.

The virtual work contributions are

$$\delta W_t = \left(F_{\text{wind},b} + F_{\text{wind},l}\right) \delta x_t, \tag{187}$$

$$\delta W_\theta = F_{\text{wind},l}\, L \cos\theta\, \delta\theta, \tag{188}$$

so that

$$Q_{x_t} = F_{\text{wind},b} + F_{\text{wind},l}, \qquad Q_\theta = F_{\text{wind},l} L \cos\theta. \tag{189}$$

No generalized force is introduced for x_D because the drive coordinate is prescribed by the motion input $u(t) = \ddot{x}_D(t)$.

Equations of Motion (Nonlinear)

Applying Lagrange's equations with dissipation yields

Boom–trolley motion

$$(M_B + m_L)\ddot{x}_t + m_L L \cos\theta\, \ddot{\theta} - m_L L \sin\theta\, \dot{\theta}^2 = c_c(\dot{x}_D - \dot{x}_t) + k_c(x_D - x_t) + F_{\text{wind},b} + F_{\text{wind},l}. \tag{190}$$

Pendulum motion

$$m_L L^2 \ddot{\theta} + c_\theta \dot{\theta} + m_L g L \sin\theta + m_L L \cos\theta \, \ddot{x}_t = F_{\text{wind},l} L \cos\theta. \tag{191}$$

The drive-side coordinate is imposed through the motion input:

$$\ddot{x}_D = u(t), \tag{192}$$

and, if needed for simulation, x_D and $\dot{x}_D$ follow by integration.

Equations (190)–(192) describe the nonlinear compliant-drive transverse dynamics with a fixed trolley and motion-level gantry actuation.

Small-Angle Linearization

For small sway angles, $\sin\theta \approx \theta$ and $\cos\theta \approx 1$, and the nonlinear term $\sin\theta\,\dot{\theta}^2$ is neglected. The equations reduce to

$$(M_B + m_L)\ddot{x}_t + m_L L \ddot{\theta} = c_c(\dot{x}_D - \dot{x}_t) + k_c(x_D - x_t) + F_{\text{wind},b} + F_{\text{wind},l}, \tag{193}$$

$$m_L L^2 \ddot{\theta} + c_\theta \dot{\theta} + m_L g L\,\theta + m_L L \ddot{x}_t = F_{\text{wind},l} L, \tag{194}$$

$$\ddot{x}_D = u. \tag{195}$$

Explicit Acceleration Form

From (194):

$$\ddot{\theta} = -\frac{c_\theta}{m_L L^2}\dot{\theta} - \frac{g}{L}\theta - \frac{1}{L}\ddot{x}_t + \frac{F_{\text{wind},l}}{m_L L}. \tag{196}$$

Substituting (196) into (193) yields

$$\ddot{x}_t = \frac{c_c}{M_B}(\dot{x}_D - \dot{x}_t) + \frac{k_c}{M_B}(x_D - x_t) + \frac{g m_L}{M_B}\theta + \frac{c_\theta}{L M_B}\dot{\theta} + \frac{1}{M_B}\Big(F_{\text{wind},b} + F_{\text{wind},l}\Big). \tag{197}$$

Using (197) in (196) gives

$$\begin{aligned}\ddot{\theta} = &-\frac{c_c}{L M_B}(\dot{x}_D - \dot{x}_t) - \frac{k_c}{L M_B}(x_D - x_t) - \frac{g}{L}\left(1 + \frac{m_L}{M_B}\right)\theta \\ &- \frac{c_\theta}{L^2}\left(\frac{1}{m_L} + \frac{1}{M_B}\right)\dot{\theta} - \frac{1}{L M_B}F_{\text{wind},b} + \left(\frac{1}{m_L L} - \frac{1}{L M_B}\right)F_{\text{wind},l}.\end{aligned} \tag{198}$$

Equations (195), (197), and (198) make explicit how the imposed drive motion $x_D(t)$ is transmitted through the compliant element to excite structural motion and sway.

State-Space Representation

Define the state vector

$$\mathbf{x} = \begin{bmatrix} x_D & \dot{x}_D & x_t & \dot{x}_t & \theta & \dot{\theta} \end{bmatrix}^\top,$$

the control input $u = \ddot{x}_D$, and the disturbance vector

$$\mathbf{d} = \begin{bmatrix} F_{\text{wind},b} \\ F_{\text{wind},l} \end{bmatrix}.$$

The linearized dynamics can be written as

$$\dot{\mathbf{x}} = A\mathbf{x} + B_u u + B_d \mathbf{d}. \tag{199}$$

The system matrices are

$$A = \begin{bmatrix} 0 & 1 & 0 & 0 & 0 & 0 \\ 0 & 0 & 0 & 0 & 0 & 0 \\ 0 & 0 & 0 & 1 & 0 & 0 \\ \frac{k_c}{M_B} & \frac{c_c}{M_B} & -\frac{k_c}{M_B} & -\frac{c_c}{M_B} & \frac{g m_L}{M_B} & \frac{c_\theta}{L M_B} \\ 0 & 0 & 0 & 0 & 0 & 1 \\ -\frac{k_c}{L M_B} & -\frac{c_c}{L M_B} & \frac{k_c}{L M_B} & \frac{c_c}{L M_B} & -\frac{g}{L}\left(1 + \frac{m_L}{M_B}\right) & -\frac{c_\theta}{L^2}\left(\frac{1}{m_L} + \frac{1}{M_B}\right) \end{bmatrix}, \qquad B_u = \begin{bmatrix} 0 \\ 1 \\ 0 \\ 0 \\ 0 \\ 0 \end{bmatrix},$$

$$B_d = \begin{bmatrix} 0 & 0 \\ 0 & 0 \\ 0 & 0 \\ \frac{1}{M_B} & \frac{1}{M_B} \\ 0 & 0 \\ 0 & \left(\frac{1}{m_L L} - \frac{1}{L M_B}\right) \end{bmatrix}.$$

E Trolley travel model derivation

This appendix presents the full derivation of the trolley travel dynamic model using Lagrange's equations. The trolley motion along the boom is treated as a prescribed input, while the structural deformation of the boom and the sway motion of the suspended load are described by generalized coordinates.

Model Description

The trolley travel dynamics are modelled using a single generalized boom coordinate $x_b(t)$, representing the dominant structural displacement in the trolley travel direction, and the sway angle $\theta(t)$ of the suspended load.

The boom is represented by an equivalent modal mass m_c, stiffness k_c and damping c_c. The trolley of mass m_t moves along the boom, and the payload of mass m_L is suspended on a rigid, massless rope of length L. Gravity acts in the negative z-direction.

The generalized coordinates are

$$(q_1, q_2) = (x_b, \theta),$$

while the trolley motion $x_t(t)$ is a known function of time and acts as an input.

Kinematics

Boom displacement (relative to the ground):

$$x_b = x_b(t), \qquad \dot{x}_b = \dot{x}_b(t). \tag{200}$$

Prescribed trolley motion along the boom:

$$x_t = x_t(t), \qquad \dot{x}_t = \dot{x}_t(t), \qquad \ddot{x}_t = \ddot{x}_t(t). \tag{201}$$

The absolute horizontal position of the trolley suspension point is

$$x_s = x_b + x_t. \tag{202}$$

The load center-of-mass coordinates are

$$x_L = x_b + x_t + L\sin\theta, \tag{203}$$
$$z_L = L - L\cos\theta. \tag{204}$$

Absolute velocities:

$$\dot{x}_L = \dot{x}_b + \dot{x}_t + L\cos\theta\,\dot{\theta}, \tag{205}$$
$$\dot{z}_L = L\sin\theta\,\dot{\theta}. \tag{206}$$

Squared speed of the load:

$$v_L^2 = \Big(\dot{x}_b + \dot{x}_t\Big)^2 + 2L\cos\theta\,\dot{\theta}\Big(\dot{x}_b + \dot{x}_t\Big) + L^2\dot{\theta}^2. \tag{207}$$

Kinetic Energy

Boom:

$$T_b = \frac{1}{2} m_c \dot{x}_b^2. \tag{208}$$

Trolley (absolute velocity $\dot{x}_b + \dot{x}_t$):

$$T_t = \frac{1}{2} m_t \Big(\dot{x}_b + \dot{x}_t\Big)^2. \tag{209}$$

Load:

$$T_L = \frac{1}{2} m_L \left[(\dot{x}_b + \dot{x}_t)^2 + 2L\cos\theta\,\dot{\theta}(\dot{x}_b + \dot{x}_t) + L^2\dot{\theta}^2\right]. \tag{210}$$

Total kinetic energy:

$$\begin{aligned} T = {} & \frac{1}{2}(m_c + m_t + m_L)\dot{x}_b^2 + \frac{1}{2}(m_t + m_L)\dot{x}_t^2 \\ & + (m_t + m_L)\dot{x}_b\dot{x}_t \\ & + m_L L\cos\theta\,\dot{\theta}(\dot{x}_b + \dot{x}_t) + \frac{1}{2} m_L L^2 \dot{\theta}^2. \end{aligned} \tag{211}$$

Note that the trolley mass m_t appears explicitly in the kinetic energy, so its inertia influences the boom and sway dynamics, even though $x_t(t)$ is not a generalized coordinate.

Potential Energy and Dissipation

Boom spring:

$$V_{\text{spring}} = \frac{1}{2} k_c x_b^2. \tag{212}$$

Gravitational potential of the load:

$$V_g = m_L g L(1 - \cos\theta). \tag{213}$$

Total potential energy:

$$V = \frac{1}{2} k_c x_b^2 + m_L g L(1 - \cos\theta). \tag{214}$$

Rayleigh dissipation (boom + pendulum damping):

$$D = \frac{1}{2} c_c\, \dot{x}_b^2 + \frac{1}{2} c_\theta \dot{\theta}^2. \tag{215}$$

Lagrangian

The Lagrangian is

$$\mathcal{L} = T - V. \tag{216}$$

Fully expanded, dropping the input-only term $\frac{1}{2}(m_t + m_L)\dot{x}_t^2$, which does not affect the equations since $x_t(t)$ is prescribed:

$$\begin{aligned}\mathcal{L} = &\frac{1}{2}(m_c + m_t + m_L)\dot{x}_b^2 + (m_t + m_L)\dot{x}_b\dot{x}_t \\ &+ m_L L\cos\theta\,\dot{\theta}(\dot{x}_b + \dot{x}_t) + \frac{1}{2}m_L L^2\dot{\theta}^2 \\ &- \frac{1}{2}k_c x_b^2 - m_L g L(1-\cos\theta).\end{aligned} \tag{217}$$

The generalized coordinates are $(q_1, q_2) = (x_b, \theta)$, while $x_t(t)$ enters the Lagrangian as a known time-dependent input.

Generalized Forces (including wind)

A disturbance force $F_{\text{dist}}(t)$ acts on the boom in the horizontal direction. In addition, wind is included as an external horizontal disturbance.

Let

- $F_{\text{wind},b}(t)$ be the resultant wind force acting on the boom/trolley assembly in the trolley travel direction,
- $F_{\text{wind},l}(t)$ be the resultant wind force acting on the suspended load in the same direction.

The trolley drive force is internal to the actuator and is not modelled explicitly; instead, its effect on the structure is captured through the prescribed trolley motion $x_t(t)$.

The virtual work of boom/trolley wind and disturbance is

$$\delta W_b = \left(F_{\text{dist}} + F_{\text{wind},b}\right)\delta x_b.$$

Wind on the load does virtual work

$$\delta W_l = F_{\text{wind},l}\,\delta x_L = F_{\text{wind},l}\left(\delta x_b + L\cos\theta\,\delta\theta\right),$$

since $x_t(t)$ is prescribed (no variation).

Hence the generalized forces are

$$Q_{x_b} = F_{\text{dist}} + F_{\text{wind},b} + F_{\text{wind},l}, \qquad Q_\theta = F_{\text{wind},l}\,L\cos\theta. \tag{218}$$

Equations of Motion (Nonlinear)

The Lagrange equations with dissipation:

$$\frac{d}{dt}\frac{\partial\mathcal{L}}{\partial\dot{q}_i} - \frac{\partial\mathcal{L}}{\partial q_i} + \frac{\partial D}{\partial\dot{q}_i} = Q_i, \qquad (q_1, q_2) = (x_b, \theta), \tag{219}$$

lead to the following nonlinear equations.

Boom motion x_b: From (217),

$$\frac{\partial \mathcal{L}}{\partial \dot{x}_b} = (m_c + m_t + m_L)\dot{x}_b + (m_t + m_L)\dot{x}_t + m_L L \cos\theta\, \dot{\theta}, \tag{220}$$

$$\frac{d}{dt}\frac{\partial \mathcal{L}}{\partial \dot{x}_b} = (m_c + m_t + m_L)\ddot{x}_b + (m_t + m_L)\ddot{x}_t + m_L L \left(-\sin\theta\, \dot{\theta}^2 + \cos\theta\, \ddot{\theta}\right), \tag{221}$$

$$\frac{\partial \mathcal{L}}{\partial x_b} = -k_c x_b, \qquad \frac{\partial D}{\partial \dot{x}_b} = c_c\, \dot{x}_b. \tag{222}$$

Thus

$$\begin{aligned}(m_c + m_t + m_L)\ddot{x}_b + (m_t + m_L)\ddot{x}_t \\ + m_L L \left(-\sin\theta\, \dot{\theta}^2 + \cos\theta\, \ddot{\theta}\right) \\ + c_c\, \dot{x}_b + k_c x_b = F_{\text{dist}} + F_{\text{wind},b} + F_{\text{wind},l}.\end{aligned} \tag{223}$$

Pendulum angle θ:

$$\frac{\partial \mathcal{L}}{\partial \dot{\theta}} = m_L L \cos\theta(\dot{x}_b + \dot{x}_t) + m_L L^2 \dot{\theta}, \tag{224}$$

$$\frac{d}{dt}\frac{\partial \mathcal{L}}{\partial \dot{\theta}} = m_L L\Big[-\sin\theta\, \dot{\theta}(\dot{x}_b + \dot{x}_t) + \cos\theta(\ddot{x}_b + \ddot{x}_t)\Big] + m_L L^2 \ddot{\theta}, \tag{225}$$

$$\frac{\partial \mathcal{L}}{\partial \theta} = -m_L L \sin\theta(\dot{x}_b + \dot{x}_t)\dot{\theta} + m_L g L \sin\theta, \tag{226}$$

$$\frac{\partial D}{\partial \dot{\theta}} = c_\theta \dot{\theta}. \tag{227}$$

Hence

$$m_L L^2 \ddot{\theta} + c_\theta \dot{\theta} + m_L g L \sin\theta + m_L L \cos\theta\, (\ddot{x}_b + \ddot{x}_t) = F_{\text{wind},l}\, L \cos\theta. \tag{228}$$

Equations (223)–(228) describe the full nonlinear boom–trolley–load dynamics with prescribed trolley motion $x_t(t)$ including wind.

Small-Angle Approximation

Since the system is controlled and anti-sway control is applied, the sway angles are assumed to remain relatively small. For these small sway angles, $\sin\theta \approx \theta$, $\cos\theta \approx 1$, and the nonlinear term $\sin\theta\, \dot{\theta}^2$ is neglected. The equations (223)–(228) then linearize to

$$\begin{aligned}(m_c + m_t + m_L)\ddot{x}_b + (m_t + m_L)\ddot{x}_t + m_L L\, \ddot{\theta} \\ + c_c\, \dot{x}_b + k_c x_b = F_{\text{dist}} + F_{\text{wind},b} + F_{\text{wind},l},\end{aligned} \tag{229}$$

$$m_L L^2 \ddot{\theta} + c_\theta \dot{\theta} + m_L g L\, \theta + m_L L(\ddot{x}_b + \ddot{x}_t) = F_{\text{wind},l}\, L. \tag{230}$$

Here $\ddot{x}_t(t)$ is the prescribed trolley acceleration along the boom, and $F_{\text{dist}}(t)$, $F_{\text{wind},b}(t)$, $F_{\text{wind},l}(t)$ are external horizontal disturbance forces.

Explicit Acceleration Form

From (230):

$$\ddot{\theta} = -\frac{c_\theta}{m_L L^2}\,\dot{\theta} - \frac{g}{L}\,\theta - \frac{1}{L}\Big(\ddot{x}_b + \ddot{x}_t\Big) + \frac{F_{\text{wind},l}}{m_L L}. \tag{231}$$

Substituting (231) into (229) and solving for $\ddot{x}_b$ yields

$$\begin{aligned}
&(m_c + m_t + m_L)\ddot{x}_b + (m_t + m_L)\ddot{x}_t + m_L L\,\ddot{\theta} + c_c\,\dot{x}_b + k_c x_b = F_{\text{dist}} + F_{\text{wind},b} + F_{\text{wind},l},\\
\Rightarrow\quad &(m_c + m_t + m_L)\ddot{x}_b + (m_t + m_L)\ddot{x}_t + m_L L\left[-\frac{c_\theta}{m_L L^2}\dot{\theta} - \frac{g}{L}\theta - \frac{1}{L}(\ddot{x}_b + \ddot{x}_t) + \frac{F_{\text{wind},l}}{m_L L}\right]\\
&\qquad + c_c\,\dot{x}_b + k_c x_b = F_{\text{dist}} + F_{\text{wind},b} + F_{\text{wind},l},\\
\Rightarrow\quad &(m_c + m_t)\ddot{x}_b + m_t\,\ddot{x}_t + c_c\,\dot{x}_b + k_c x_b - m_L g\,\theta - \frac{c_\theta}{L}\dot{\theta} = F_{\text{dist}} + F_{\text{wind},b}.
\end{aligned} \tag{232}$$

Therefore,

$$\begin{aligned}
\ddot{x}_b = &-\frac{k_c}{m_c + m_t}\,x_b - \frac{c_c}{m_c + m_t}\,\dot{x}_b + \frac{g\,m_L}{m_c + m_t}\,\theta + \frac{c_\theta}{L(m_c + m_t)}\,\dot{\theta}\\
&+ \frac{1}{m_c + m_t}\Big(F_{\text{dist}} + F_{\text{wind},b}\Big) - \frac{m_t}{m_c + m_t}\,\ddot{x}_t.
\end{aligned} \tag{233}$$

Substituting (233) back into (231) gives

$$\begin{aligned}
\ddot{\theta} = &-\frac{c_\theta}{m_L L^2}\,\dot{\theta} - \frac{g}{L}\,\theta - \frac{1}{L}\left(-\frac{k_c}{m_c + m_t}\,x_b - \frac{c_c}{m_c + m_t}\,\dot{x}_b + \frac{g\,m_L}{m_c + m_t}\,\theta + \frac{c_\theta}{L(m_c + m_t)}\,\dot{\theta}\right)\\
&- \frac{1}{L}\left(\frac{1}{m_c + m_t}(F_{\text{dist}} + F_{\text{wind},b}) - \frac{m_t}{m_c + m_t}\ddot{x}_t\right) - \frac{1}{L}\ddot{x}_t + \frac{F_{\text{wind},l}}{m_L L},\\
\Rightarrow\quad \ddot{\theta} = &\frac{k_c}{L(m_c + m_t)}\,x_b + \frac{c_c}{L(m_c + m_t)}\,\dot{x}_b - \frac{g}{L}\left(1 + \frac{m_L}{m_c + m_t}\right)\theta\\
&- \frac{c_\theta}{L^2}\left(\frac{1}{m_L} + \frac{1}{m_c + m_t}\right)\dot{\theta} - \frac{1}{L(m_c + m_t)}\Big(F_{\text{dist}} + F_{\text{wind},b}\Big) + \frac{F_{\text{wind},l}}{m_L L}\\
&- \frac{m_c}{L(m_c + m_t)}\,\ddot{x}_t.
\end{aligned} \tag{234}$$

Equations (233)–(234) show explicitly how the trolley mass m_t, prescribed trolley acceleration $\ddot{x}_t(t)$, disturbance force $F_{\text{dist}}(t)$ and wind forces $F_{\text{wind},b}(t)$ and $F_{\text{wind},l}(t)$ influence the structural and sway accelerations.

State-Space Representation

We define the state vector and input vector as

$$\mathbf{x} = \begin{bmatrix} x_b \\ \dot{x}_b \\ \theta \\ \dot{\theta} \end{bmatrix}, \qquad \mathbf{u} = \begin{bmatrix} F_{\text{dist}} \\ \ddot{x}_t \\ F_{\text{wind},b} \\ F_{\text{wind},l} \end{bmatrix}. \tag{235}$$

Using (233)–(234), the linearized dynamics can be written in first-order form

$$\dot{\mathbf{x}} = A\mathbf{x} + B\mathbf{u}, \tag{236}$$

with

$$A = \begin{bmatrix} 0 & 1 & 0 & 0 \\ -\dfrac{k_c}{m_c + m_t} & -\dfrac{c_c}{m_c + m_t} & \dfrac{g\, m_L}{m_c + m_t} & \dfrac{c_\theta}{L(m_c + m_t)} \\ 0 & 0 & 0 & 1 \\ \dfrac{k_c}{L(m_c + m_t)} & \dfrac{c_c}{L(m_c + m_t)} & -\dfrac{g}{L}\Big(1 + \dfrac{m_L}{m_c + m_t}\Big) & -\dfrac{c_\theta}{L^2}\Big(\dfrac{1}{m_L} + \dfrac{1}{m_c + m_t}\Big) \end{bmatrix}, \tag{237}$$

$$B = \begin{bmatrix} 0 & 0 & 0 & 0 \\ \dfrac{1}{m_c + m_t} & -\dfrac{m_t}{m_c + m_t} & \dfrac{1}{m_c + m_t} & 0 \\ 0 & 0 & 0 & 0 \\ -\dfrac{1}{L(m_c + m_t)} & -\dfrac{m_c}{L(m_c + m_t)} & -\dfrac{1}{L(m_c + m_t)} & \dfrac{1}{m_L L} \end{bmatrix}. \tag{238}$$

F Structural Cross sections

Properties

This paragraph contains properties information.

Properties Summary

Title	Elements	Material	Mass [kg]
1..Diagonal Brace Sec. Backreach (2 bodies)	30	30..Steel ST52	17947.56
2..Diagonal Brace Upper (2 bodies)	46	30..Steel ST52	27460.74
3..Crossgirder (6 bodies)	16	30..Steel ST52	48118.39
4..Crossgirder Backreach 1 (2 bodies)	4	30..Steel ST52	6582.73
5..Crossgirder Backreach 2 (2 bodies)	4	30..Steel ST52	6150.23
6..Crossgirder Backreach 3 (2 bodies)	4	30..Steel ST52	5589.08
7..Crossgirder Backreach 4 (4 bodies)	20	30..Steel ST52	35390.01
8..Crossgirder End	12	30..Steel ST52	17574.19
9..WS Legs Taper 3 (2 bodies)	2	30..Steel ST52	3713.05
10..WS Legs Taper 2 (2 bodies)	2	30..Steel ST52	3713.05
11..WS Legs Taper 1 (2 bodies)	2	30..Steel ST52	3713.05
12..WS Legs Lower (4 bodies)	12	30..Steel ST52	25743.09
13..LS Legs Middle Joint (4 bodies)	8	30..Steel ST52	14852.20
14..LS Legs Middle (4 bodies)	32	30..Steel ST52	53375.09
15..LS Legs Lower (4 bodies)	12	30..Steel ST52	21255.05
16..LS Legs Taper 3 (2 bodies)	2	30..Steel ST52	3713.05
17..LS Legs Taper 2 (2 bodies)	2	30..Steel ST52	3713.05
18..LS Legs Taper 1 (2 bodies)	2	30..Steel ST52	3713.05
19..LS Legs Upper (2 bodies)	4	30..Steel ST52	7969.32
20..LS Portal Beam Middle	6	30..Steel ST52	16836.29
21..LS Portal Beam Outer (2 bodies)	6	30..Steel ST52	16104.27
22..WS Portal Beam Middle	6	30..Steel ST52	14884.09
23..Boom Backtreach 2 (4 bodies)	36	30..Steel ST52	62657.72
24..Backstay (2 bodies)	2	30..Steel ST52	22482.90
25..Boom Backtreach 1 (2 bodies)	8	30..Steel ST52	12531.54
26..Boom Bridge (2 bodies)	36	30..Steel ST52	69731.55
27..Boom Connect LS (2 bodies)	4	30..Steel ST52	4439.17
28..Boom Connect WS (2 bodies)	4	30..Steel ST52	4439.17
29..Boom Outreach 1 (8 bodies)	34	30..Steel ST52	76791.84
30..Boom Outreach 2 (10 bodies)	36	30..Steel ST52	72356.59
31..Boom Outreach 3 (4 bodies)	10	30..Steel ST52	18565.25
32..WS Legs Upper (2 bodies)	4	30..Steel ST52	7969.32
33..WS Legs Middle (2 bodies)	38	30..Steel ST52	68227.29
34..Boom Outreach End	6	30..Steel ST52	8982.36
35..Boom Stiffener (5 bodies)	44	30..Steel ST52	12229.70
36..Boom Stiffener Connector (6 bodies)	6	30..Steel ST52	6146.55
37..Forestay 1 (2 bodies)	2	30..Steel ST52	19750.00
38..Forestay 2 (2 bodies)	2	30..Steel ST52	32562.68
39..Pylon Legs (2 bodies)	28	30..Steel ST52	37839.75

40..Pylon Head	6	30..Steel ST52	6725.49
41..Pylon Diagonal Brace (2 bodies)	48	30..Steel ST52	42494.98
42..Machine House (2 bodies)	2	26..Machine House	230000.64
43..WS Legs Taper Lower 3 (2 bodies)	2	30..Steel ST52	6452.70
44..Diagonal Brace Lower (2 bodies)	40	30..Steel ST52	24156.22
45..WS Portal Beam Outer (2 bodies)	6	30..Steel ST52	14236.96
46..Boom Backtreach End	6	30..Steel ST52	8982.36
47..WS Legs Taper Lower 2 (2 bodies)	2	30..Steel ST52	5863.95
48..WS Legs Taper Lower 1 (2 bodies)	2	30..Steel ST52	5275.20
49..LS Legs Taper Lower 1 (2 bodies)	2	30..Steel ST52	5859.24
50..LS Legs Taper Lower 2 (2 bodies)	2	30..Steel ST52	6565.74
51..LS Legs Taper Lower 3 (2 bodies)	2	30..Steel ST52	7272.24
52..Bogies (4 bodies)	12	32..Bogies	312000.00
53..WS Sill Beam Outer (2 bodies)	4	30..Steel ST52	12343.97
54..WS Sill Beam Middle	8	30..Steel ST52	23263.63
55..LS Sill Beam Outer (2 bodies)	4	30..Steel ST52	12950.15
56..LS Sill Beam Middle	8	30..Steel ST52	24406.04
57..Crossgirder Middle (2 bodies)	24	30..Steel ST52	58498.20
Summed Over Properties	714		1703161.73
Full Model	714		1703161.73

1..Diagonal Brace Sec. Backreach (2 bodies)

Property	Value	Property Shape
Type / Elements	Beam / 30	
Material	30..Steel ST52	
Mass [kg]	17947.56	
Area, [m^2]	0.03	
I1, [m^4]	3.810e-03	
I2, [m^4]	3.810e-03	
I12, [m^4]	0	
Torsion Constant, [m^4]	0.01	
Y Shear Area, [m^2]	0	
Z Shear Area, [m^2]	0	
Nonstructural Mass, [kg]	0	
Perimeter, [m]	0	
Warping Constant, [m^6]	0	
Y Neutral Axis Offset A, [m]	1.00	
Z Neutral Axis Offset A, [m]	0	
r [m]	0.50	
t [m]	0.01	

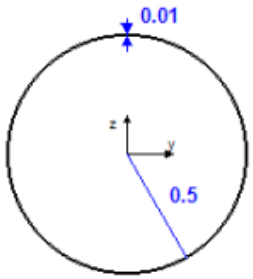

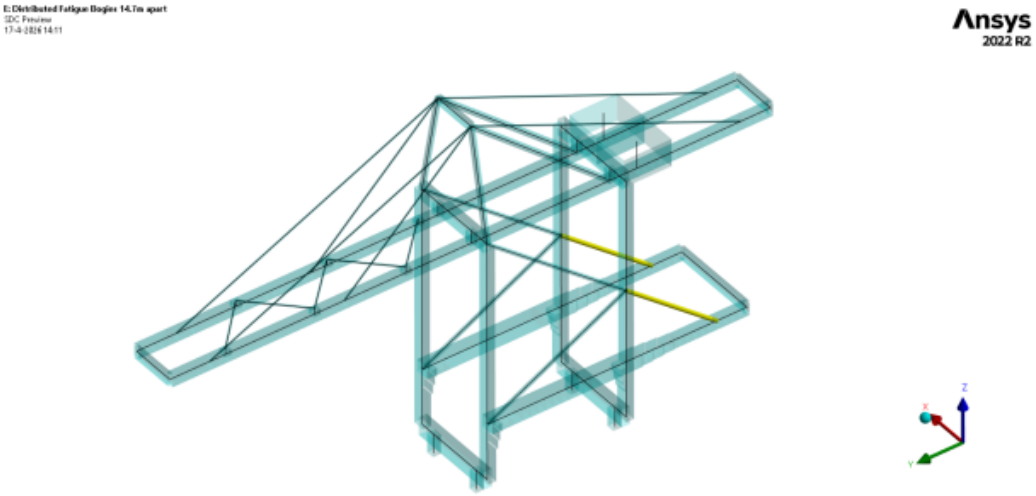

2..Diagonal Brace Upper (2 bodies)

Property	Value
Type / Elements	Beam / 46
Material	30..Steel ST52
Mass [kg]	27460.74
Area, [m^2]	0.03
I1, [m^4]	3.810e-03
I2, [m^4]	3.810e-03
I12, [m^4]	0
Torsion Constant, [m^4]	0.01
Y Shear Area, [m^2]	0
Z Shear Area, [m^2]	0
Nonstructural Mass, [kg]	0
Perimeter, [m]	0
Warping Constant, [m^6]	0
Y Neutral Axis Offset A, [m]	0
Z Neutral Axis Offset A, [m]	0
r [m]	0.50
t [m]	0.01

Property Shape

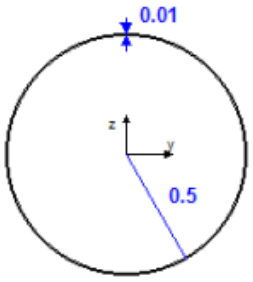

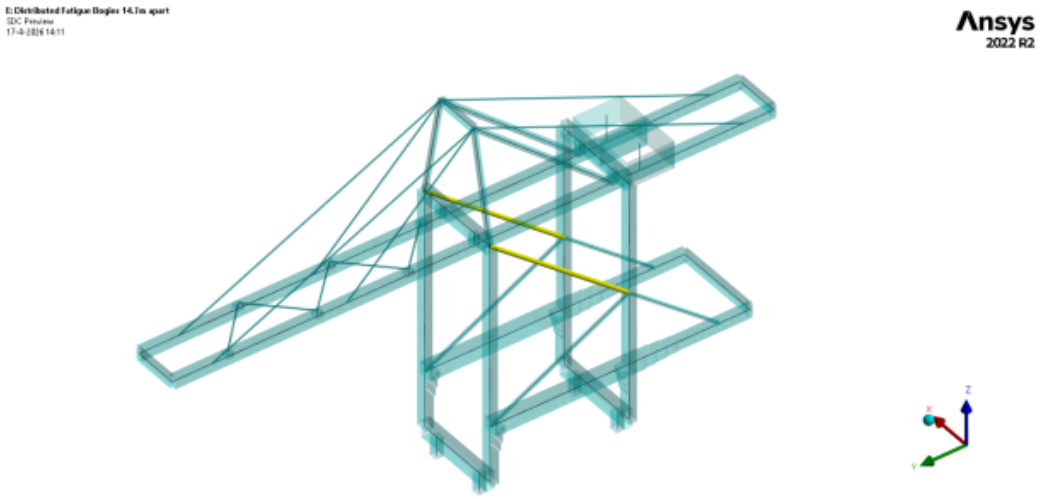

3..Crossgirder (6 bodies)

Property	Value
Type / Elements	Beam / 16
Material	30..Steel ST52
Mass [kg]	48118.39
Area, [m^2]	0.16
I1, [m^4]	0.28
I2, [m^4]	0.29
I12, [m^4]	0
Torsion Constant, [m^4]	0.41
Y Shear Area, [m^2]	1.50
Z Shear Area, [m^2]	1.75
Nonstructural Mass, [kg]	0
Perimeter, [m]	0
Warping Constant, [m^6]	0.01
Y Neutral Axis Offset A, [m]	1.50
Z Neutral Axis Offset A, [m]	2.13
w [m]	3.00
h [m]	3.50
t1 [m]	0.01
t2 [m]	0.01
t3 [m]	0.02
t4 [m]	0.02

Property Shape

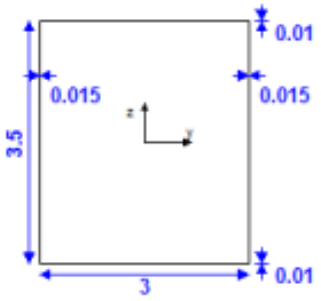

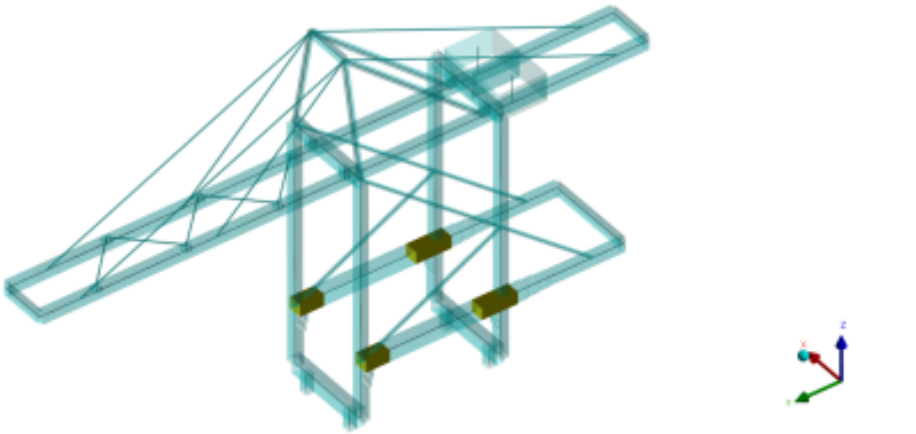

4..Crossgirder Backreach 1 (2 bodies)

Property	Value
Type / Elements	Beam / 4
Material	30..Steel ST52
Mass [kg]	6582.73
Area, [m^2]	0.12
I1, [m^4]	0.18
I2, [m^4]	0.18
I12, [m^4]	0
Torsion Constant, [m^4]	0.27
Y Shear Area, [m^2]	1.50
Z Shear Area, [m^2]	1.50
Nonstructural Mass, [kg]	0
Perimeter, [m]	0
Warping Constant, [m^6]	2.793e-06
Y Neutral Axis Offset A, [m]	1.50
Z Neutral Axis Offset A, [m]	2.13
w [m]	3.00
h [m]	3.00
t1 [m]	0.01
t2 [m]	0.01
t3 [m]	0.01
t4 [m]	0.01

Property Shape

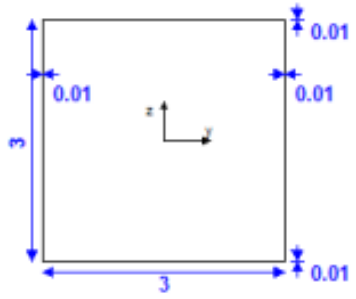

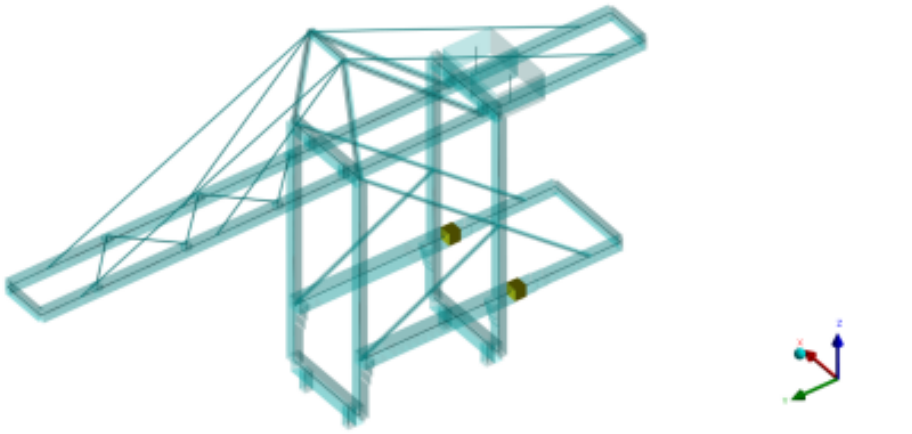

5..Crossgirder Backreach 2 (2 bodies)

Property	Value	Property Shape
Type / Elements	Beam / 4	
Material	30..Steel ST52	
Mass [kg]	6150.23	
Area, [m^2]	0.11	
I1, [m^4]	0.16	
I2, [m^4]	0.12	
I12, [m^4]	0	
Torsion Constant, [m^4]	0.20	
Y Shear Area, [m^2]	1.50	
Z Shear Area, [m^2]	1.25	
Nonstructural Mass, [kg]	0	
Perimeter, [m]	0	
Warping Constant, [m^6]	1.071e-03	
Y Neutral Axis Offset A, [m]	1.50	
Z Neutral Axis Offset A, [m]	2.13	
w [m]	3.00	
h [m]	2.50	
t1 [m]	0.01	
t2 [m]	0.01	
t3 [m]	0.01	
t4 [m]	0.01	

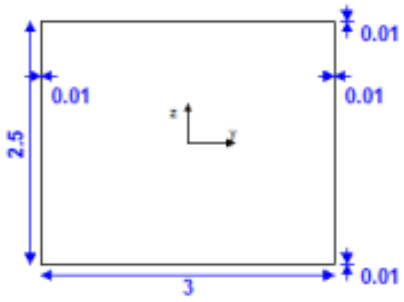

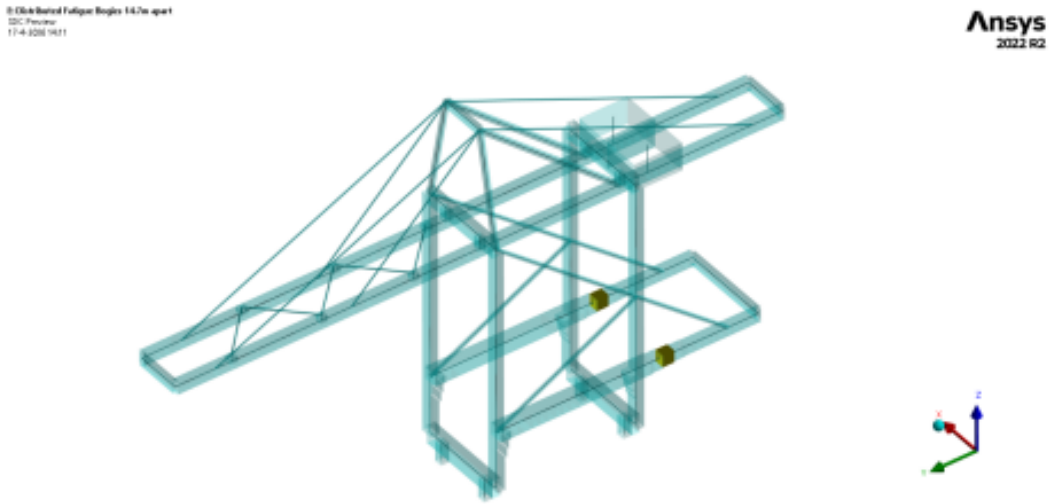

6..Crossgirder Backreach 3 (2 bodies)

Property	Value
Type / Elements	Beam / 4
Material	30..Steel ST52
Mass [kg]	5589.08
Area, [m^2]	0.10
I1, [m^4]	0.13
I2, [m^4]	0.07
I12, [m^4]	0
Torsion Constant, [m^4]	0.14
Y Shear Area, [m^2]	1.50
Z Shear Area, [m^2]	1.00
Nonstructural Mass, [kg]	0
Perimeter, [m]	0
Warping Constant, [m^6]	3.010e-03
Y Neutral Axis Offset A, [m]	1.50
Z Neutral Axis Offset A, [m]	2.13
w [m]	3.00
h [m]	2.00
t1 [m]	0.01
t2 [m]	0.01
t3 [m]	0.01
t4 [m]	0.01

Property Shape

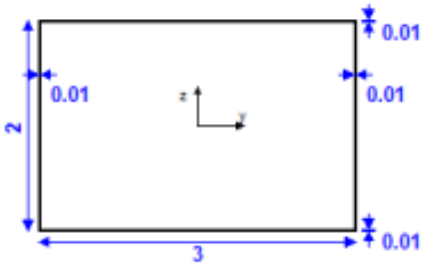

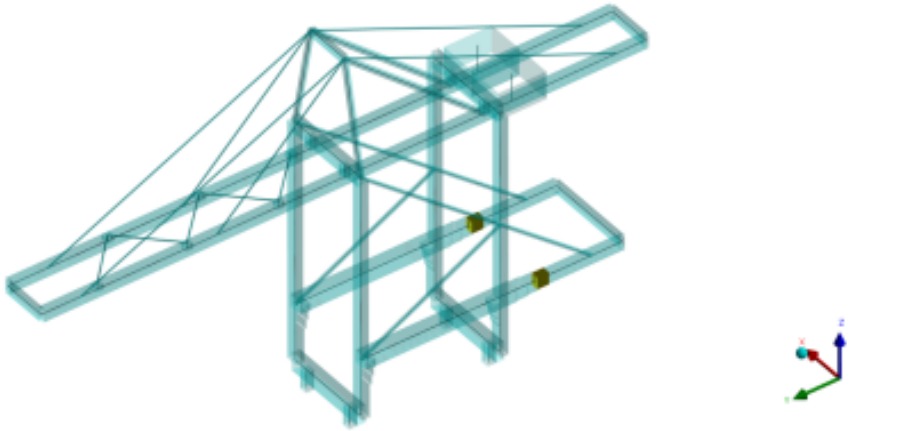

7..Crossgirder Backreach 4 (4 bodies)

Property	Value	Property Shape
Type / Elements	Beam / 20	
Material	30..Steel ST52	
Mass [kg]	35390.01	
Area, [m^2]	0.09	
I1, [m^4]	0.12	
I2, [m^4]	0.05	
I12, [m^4]	0	
Torsion Constant, [m^4]	0.11	
Y Shear Area, [m^2]	1.50	
Z Shear Area, [m^2]	0.87	
Nonstructural Mass, [kg]	0	
Perimeter, [m]	0	
Warping Constant, [m^6]	3.787e-03	
Y Neutral Axis Offset A, [m]	1.50	
Z Neutral Axis Offset A, [m]	2.13	
w [m]	3.00	
h [m]	1.75	
t1 [m]	0.01	
t2 [m]	0.01	
t3 [m]	0.01	
t4 [m]	0.01	

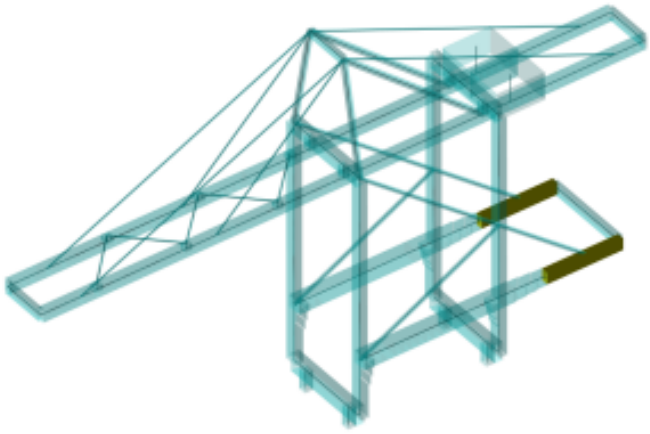

8..Crossgirder End

Property	Value
Type / Elements	Beam / 12
Material	30..Steel ST52
Mass [kg]	17574.19
Area, [m^2]	0.08
I1, [m^4]	0.09
I2, [m^4]	0.02
I12, [m^4]	0
Torsion Constant, [m^4]	0.04
Y Shear Area, [m^2]	1.50
Z Shear Area, [m^2]	0.50
Nonstructural Mass, [kg]	0
Perimeter, [m]	0
Warping Constant, [m^6]	3.739e-03
Y Neutral Axis Offset A, [m]	0
Z Neutral Axis Offset A, [m]	0
w [m]	3.00
h [m]	1.00
t1 [m]	0.01
t2 [m]	0.01
t3 [m]	0.01
t4 [m]	0.01

Property Shape

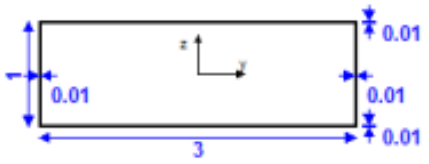

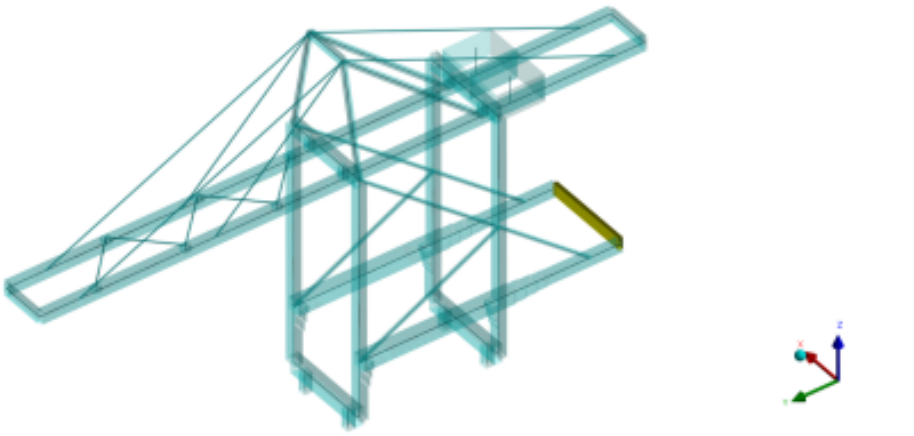

9..WS Legs Taper 3 (2 bodies)

Property	Value	Property Shape
Type / Elements	Beam / 2	
Material	30..Steel ST52	
Mass [kg]	3713.05	
Area, [m^2]	0.09	
I1, [m^4]	0.12	
I2, [m^4]	0.05	
I12, [m^4]	0	
Torsion Constant, [m^4]	0.11	
Y Shear Area, [m^2]	1.50	
Z Shear Area, [m^2]	0.87	
Nonstructural Mass, [kg]	0	
Perimeter, [m]	0	
Warping Constant, [m^6]	3.787e-03	
Y Neutral Axis Offset A, [m]	1.50	
Z Neutral Axis Offset A, [m]	0.88	
w [m]	3.00	
h [m]	1.75	
t1 [m]	0.01	
t2 [m]	0.01	
t3 [m]	0.01	
t4 [m]	0.01	

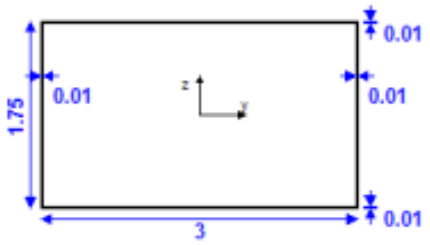

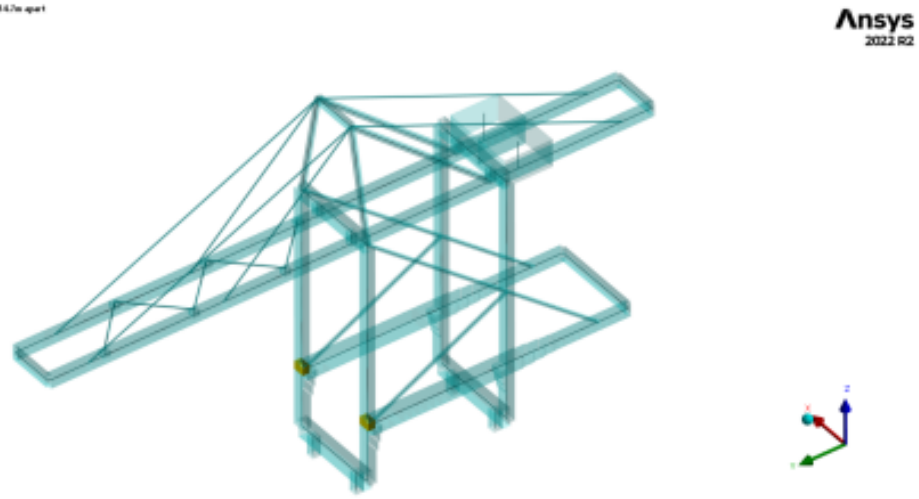

10..WS Legs Taper 2 (2 bodies)

Property	Value
Type / Elements	Beam / 2
Material	30..Steel ST52
Mass [kg]	3713.05
Area, [m^2]	0.09
I1, [m^4]	0.12
I2, [m^4]	0.05
I12, [m^4]	0
Torsion Constant, [m^4]	0.11
Y Shear Area, [m^2]	1.50
Z Shear Area, [m^2]	0.87
Nonstructural Mass, [kg]	0
Perimeter, [m]	0
Warping Constant, [m^6]	3.787e-03
Y Neutral Axis Offset A, [m]	1.50
Z Neutral Axis Offset A, [m]	0.88
w [m]	3.00
h [m]	1.75
t1 [m]	0.01
t2 [m]	0.01
t3 [m]	0.01
t4 [m]	0.01

Property Shape

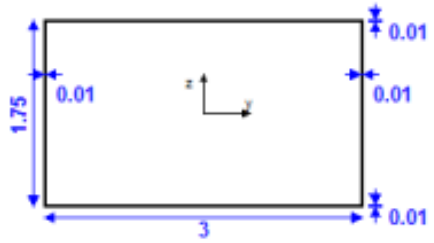

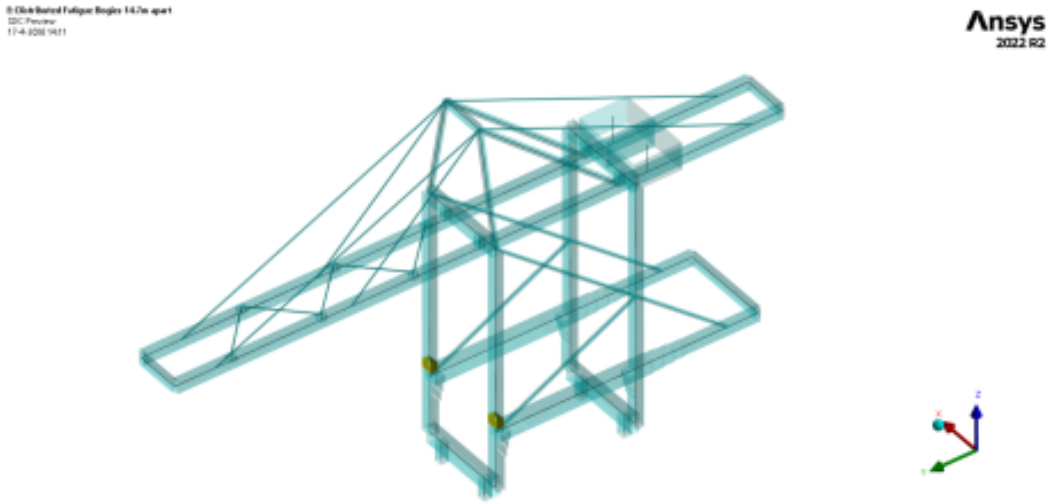

11..WS Legs Taper 1 (2 bodies)

Property	Value
Type / Elements	Beam / 2
Material	30..Steel ST52
Mass [kg]	3713.05
Area, [m^2]	0.09
I1, [m^4]	0.12
I2, [m^4]	0.05
I12, [m^4]	0
Torsion Constant, [m^4]	0.11
Y Shear Area, [m^2]	1.50
Z Shear Area, [m^2]	0.87
Nonstructural Mass, [kg]	0
Perimeter, [m]	0
Warping Constant, [m^6]	3.787e-03
Y Neutral Axis Offset A, [m]	1.50
Z Neutral Axis Offset A, [m]	0.88
w [m]	3.00
h [m]	1.75
t1 [m]	0.01
t2 [m]	0.01
t3 [m]	0.01
t4 [m]	0.01

Property Shape

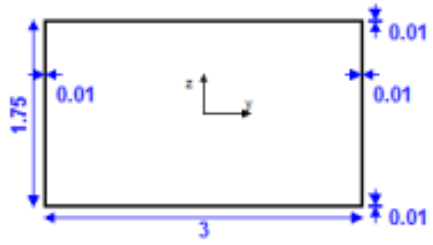

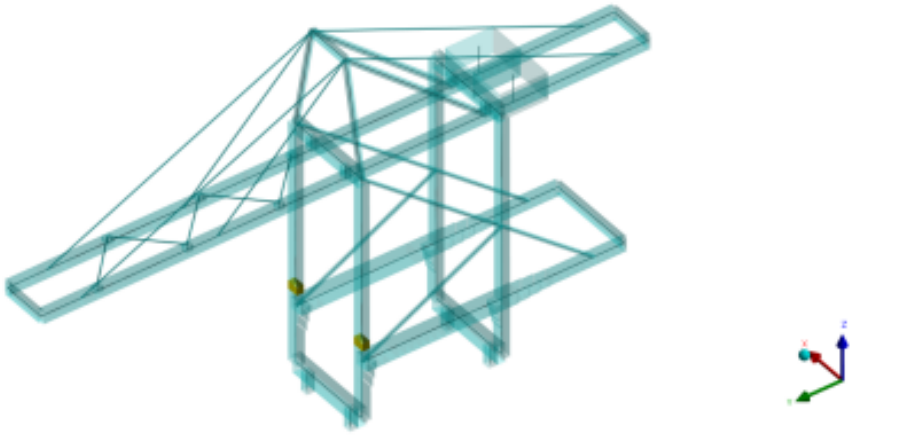

12..WS Legs Lower (4 bodies)

Property	Value
Type / Elements	Beam / 12
Material	30..Steel ST52
Mass [kg]	25743.09
Area, [m^2]	0.16
I1, [m^4]	0.26
I2, [m^4]	0.09
I12, [m^4]	0
Torsion Constant, [m^4]	0.19
Y Shear Area, [m^2]	1.50
Z Shear Area, [m^2]	1.00
Nonstructural Mass, [kg]	0
Perimeter, [m]	0
Warping Constant, [m^6]	0.04
Y Neutral Axis Offset A, [m]	1.50
Z Neutral Axis Offset A, [m]	0.88
w [m]	3.00
h [m]	2.00
t1 [m]	0.01
t2 [m]	0.01
t3 [m]	0.03
t4 [m]	0.03

Property Shape

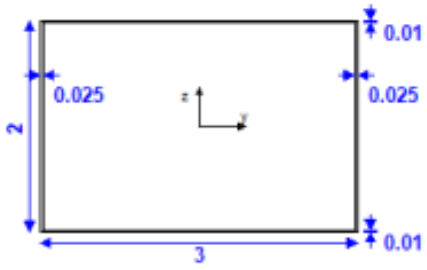

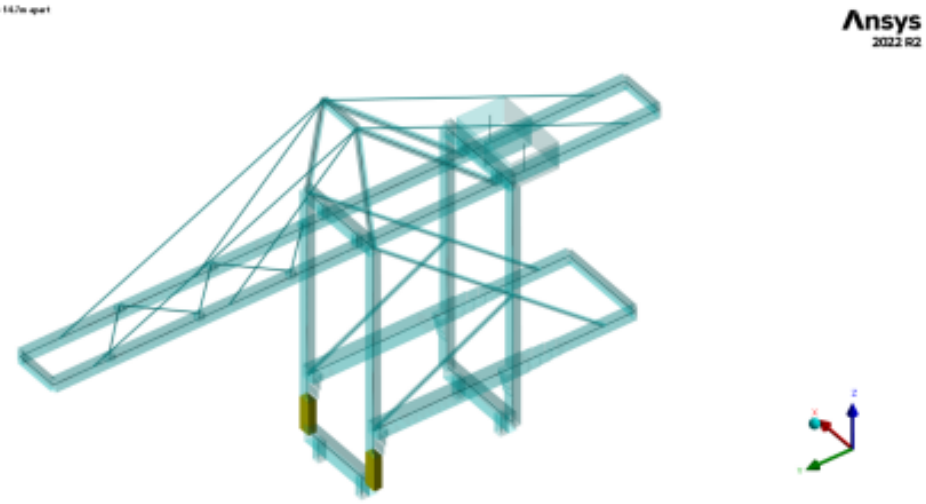

13..LS Legs Middle Joint (4 bodies)

Property	Value
Type / Elements	Beam / 8
Material	30..Steel ST52
Mass [kg]	14852.20
Area, [m^2]	0.09
I1, [m^4]	0.12
I2, [m^4]	0.05
I12, [m^4]	0
Torsion Constant, [m^4]	0.11
Y Shear Area, [m^2]	1.50
Z Shear Area, [m^2]	0.87
Nonstructural Mass, [kg]	0
Perimeter, [m]	0
Warping Constant, [m^6]	3.787e-03
Y Neutral Axis Offset A, [m]	0
Z Neutral Axis Offset A, [m]	0
w [m]	3.00
h [m]	1.75
t1 [m]	0.01
t2 [m]	0.01
t3 [m]	0.01
t4 [m]	0.01

Property Shape

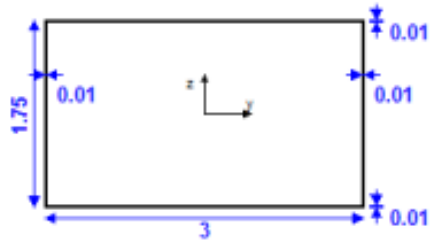

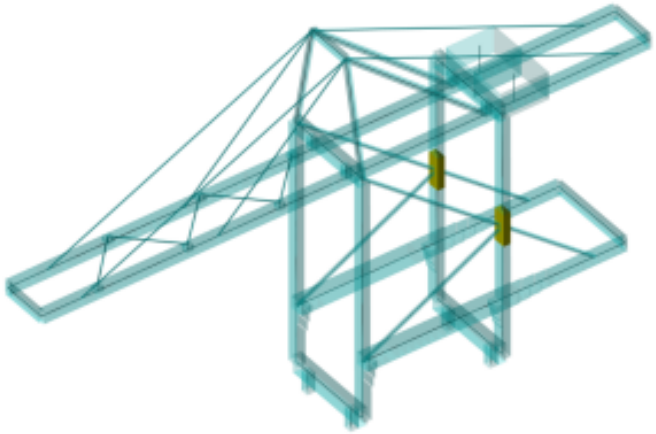

14..LS Legs Middle (4 bodies)

Property	Value
Type / Elements	Beam / 32
Material	30..Steel ST52
Mass [kg]	53375.09
Area, [m^2]	0.09
I1, [m^4]	0.12
I2, [m^4]	0.05
I12, [m^4]	0
Torsion Constant, [m^4]	0.11
Y Shear Area, [m^2]	1.50
Z Shear Area, [m^2]	0.87
Nonstructural Mass, [kg]	0
Perimeter, [m]	0
Warping Constant, [m^6]	3.787e-03
Y Neutral Axis Offset A, [m]	0
Z Neutral Axis Offset A, [m]	0
w [m]	3.00
h [m]	1.75
t1 [m]	0.01
t2 [m]	0.01
t3 [m]	0.01
t4 [m]	0.01

Property Shape

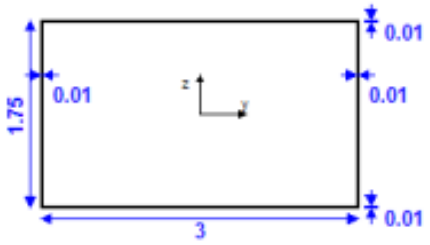

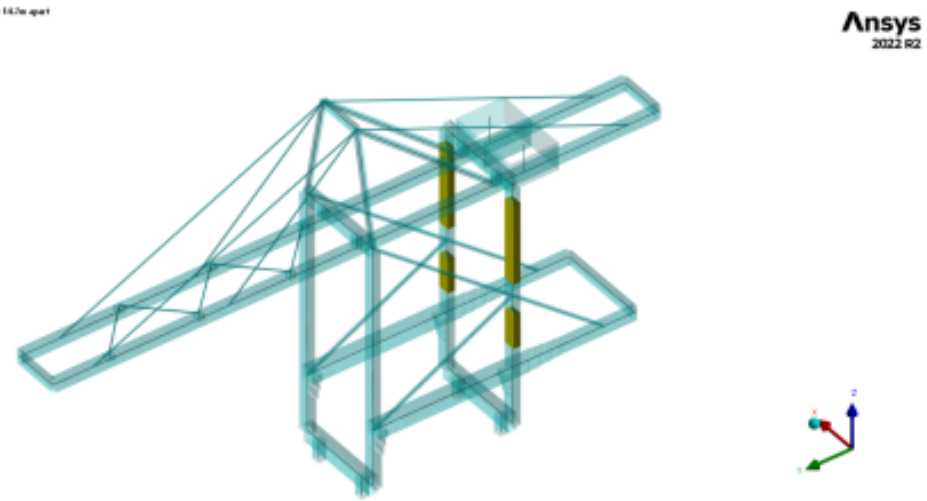

15..LS Legs Lower (4 bodies)

Property	Value	Property Shape
Type / Elements	Beam / 12	
Material	30..Steel ST52	
Mass [kg]	21255.05	
Area, [m^2]	0.13	
I1, [m^4]	0.20	
I2, [m^4]	0.08	
I12, [m^4]	0	
Torsion Constant, [m^4]	0.17	
Y Shear Area, [m^2]	1.50	
Z Shear Area, [m^2]	1.00	
Nonstructural Mass, [kg]	0	
Perimeter, [m]	0	
Warping Constant, [m^6]	0.02	
Y Neutral Axis Offset A, [m]	1.50	
Z Neutral Axis Offset A, [m]	1.13	
w [m]	3.00	
h [m]	2.00	
t1 [m]	0.01	
t2 [m]	0.01	
t3 [m]	0.02	
t4 [m]	0.02	

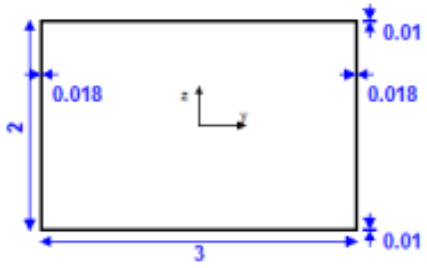

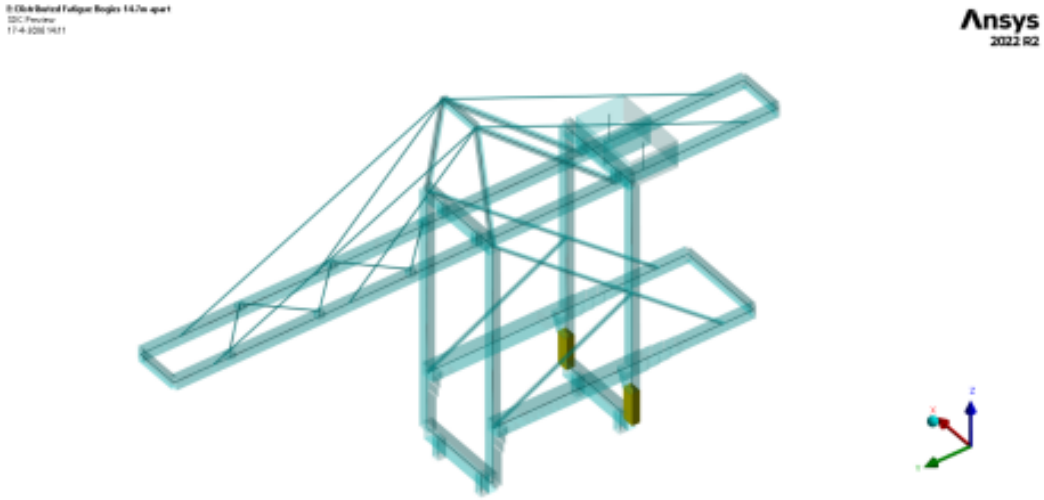

16..LS Legs Taper 3 (2 bodies)

Property	Value
Type / Elements	Beam / 2
Material	30..Steel ST52
Mass [kg]	3713.05
Area, [m^2]	0.09
I1, [m^4]	0.12
I2, [m^4]	0.05
I12, [m^4]	0
Torsion Constant, [m^4]	0.11
Y Shear Area, [m^2]	1.50
Z Shear Area, [m^2]	0.87
Nonstructural Mass, [kg]	0
Perimeter, [m]	0
Warping Constant, [m^6]	3.787e-03
Y Neutral Axis Offset A, [m]	5.00
Z Neutral Axis Offset A, [m]	0
w [m]	3.00
h [m]	1.75
t1 [m]	0.01
t2 [m]	0.01
t3 [m]	0.01
t4 [m]	0.01

Property Shape

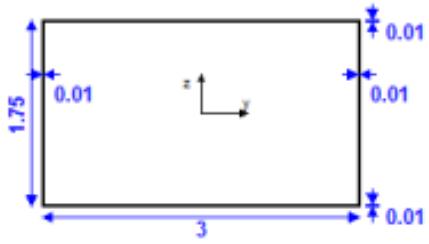

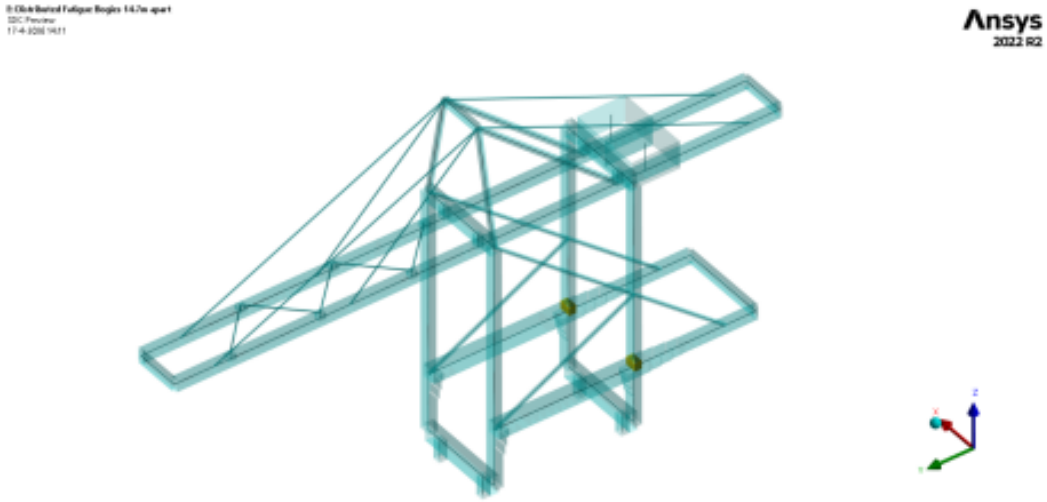

17..LS Legs Taper 2 (2 bodies)

Property	Value
Type / Elements	Beam / 2
Material	30..Steel ST52
Mass [kg]	3713.05
Area, [m^2]	0.09
I1, [m^4]	0.12
I2, [m^4]	0.05
I12, [m^4]	0
Torsion Constant, [m^4]	0.11
Y Shear Area, [m^2]	1.50
Z Shear Area, [m^2]	0.87
Nonstructural Mass, [kg]	0
Perimeter, [m]	0
Warping Constant, [m^6]	3.787e-03
Y Neutral Axis Offset A, [m]	0
Z Neutral Axis Offset A, [m]	0
w [m]	3.00
h [m]	1.75
t1 [m]	0.01
t2 [m]	0.01
t3 [m]	0.01
t4 [m]	0.01

Property Shape

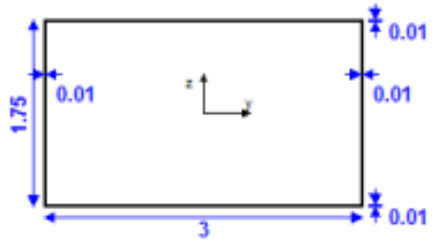

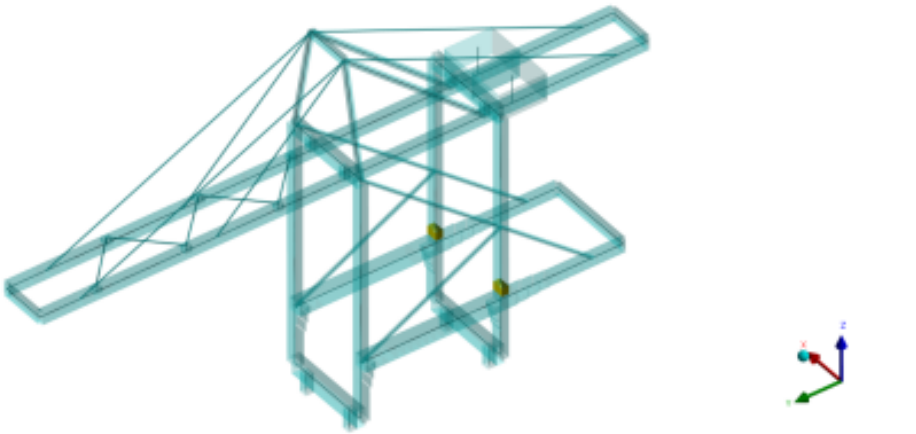

18..LS Legs Taper 1 (2 bodies)

Property	Value
Type / Elements	Beam / 2
Material	30..Steel ST52
Mass [kg]	3713.05
Area, [m^2]	0.09
I1, [m^4]	0.12
I2, [m^4]	0.05
I12, [m^4]	0
Torsion Constant, [m^4]	0.11
Y Shear Area, [m^2]	1.50
Z Shear Area, [m^2]	0.87
Nonstructural Mass, [kg]	0
Perimeter, [m]	0
Warping Constant, [m^6]	3.787e-03
Y Neutral Axis Offset A, [m]	0
Z Neutral Axis Offset A, [m]	0
w [m]	3.00
h [m]	1.75
t1 [m]	0.01
t2 [m]	0.01
t3 [m]	0.01
t4 [m]	0.01

Property Shape

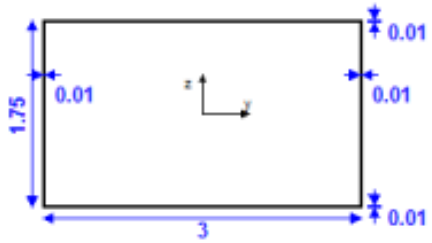

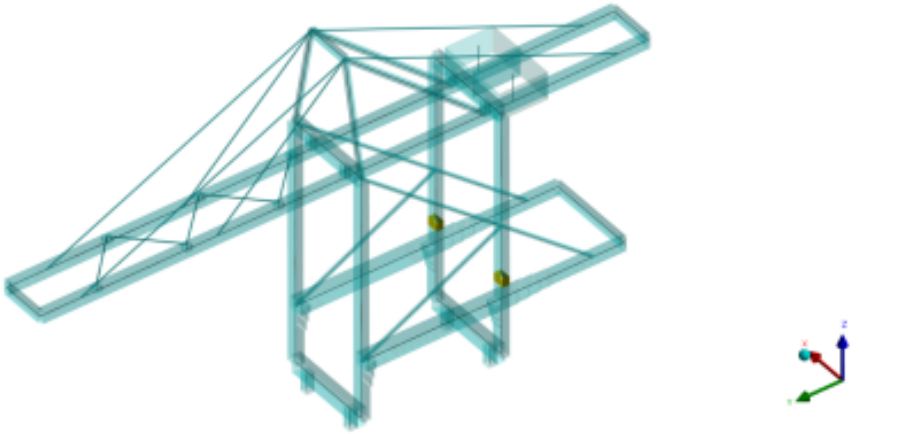

19..LS Legs Upper (2 bodies)

Property	Value	Property Shape
Type / Elements	Beam / 4	
Material	30..Steel ST52	
Mass [kg]	7969.32	
Area, [m^2]	0.10	
I1, [m^4]	0.14	
I2, [m^4]	0.06	
I12, [m^4]	0	
Torsion Constant, [m^4]	0.12	
Y Shear Area, [m^2]	1.50	
Z Shear Area, [m^2]	0.87	
Nonstructural Mass, [kg]	0	
Perimeter, [m]	0	
Warping Constant, [m^6]	0.01	
Y Neutral Axis Offset A, [m]	1.50	
Z Neutral Axis Offset A, [m]	0.88	
w [m]	3.00	
h [m]	1.75	
t1 [m]	0.01	
t2 [m]	0.01	
t3 [m]	0.01	
t4 [m]	0.01	

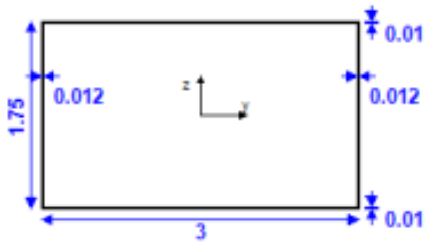

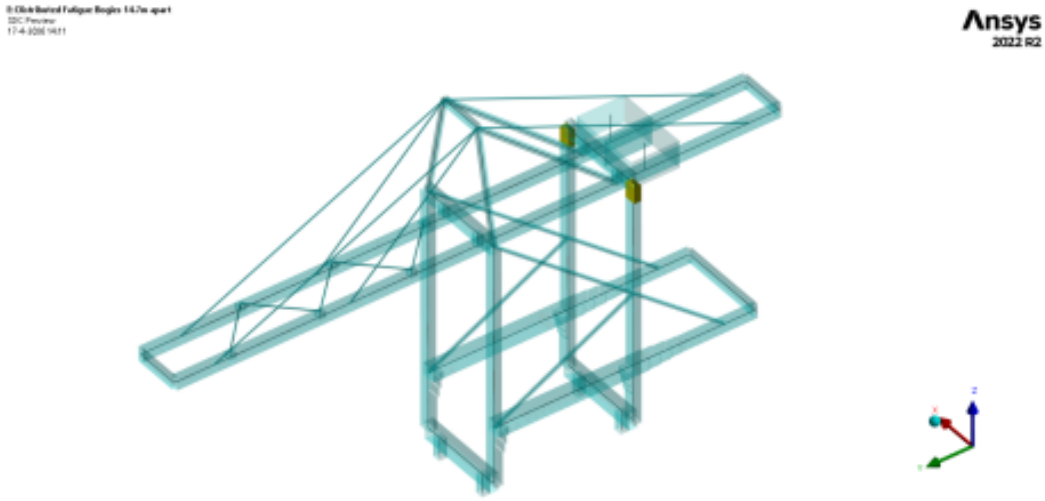

20..LS Portal Beam Middle

Property	Value	Property Shape
Type / Elements	Beam / 6	
Material	30..Steel ST52	
Mass [kg]	16836.29	
Area, [m^2]	0.15	
I1, [m^4]	0.38	
I2, [m^4]	0.08	
I12, [m^4]	0	
Torsion Constant, [m^4]	0.20	
Y Shear Area, [m^2]	2.00	
Z Shear Area, [m^2]	0.88	
Nonstructural Mass, [kg]	0	
Perimeter, [m]	0	
Warping Constant, [m^6]	0.06	
Y Neutral Axis Offset A, [m]	2.25	
Z Neutral Axis Offset A, [m]	0.88	
w [m]	4.00	
h [m]	1.75	
t1 [m]	0.01	
t2 [m]	0.01	
t3 [m]	0.02	
t4 [m]	0.02	

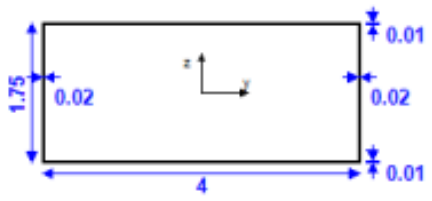

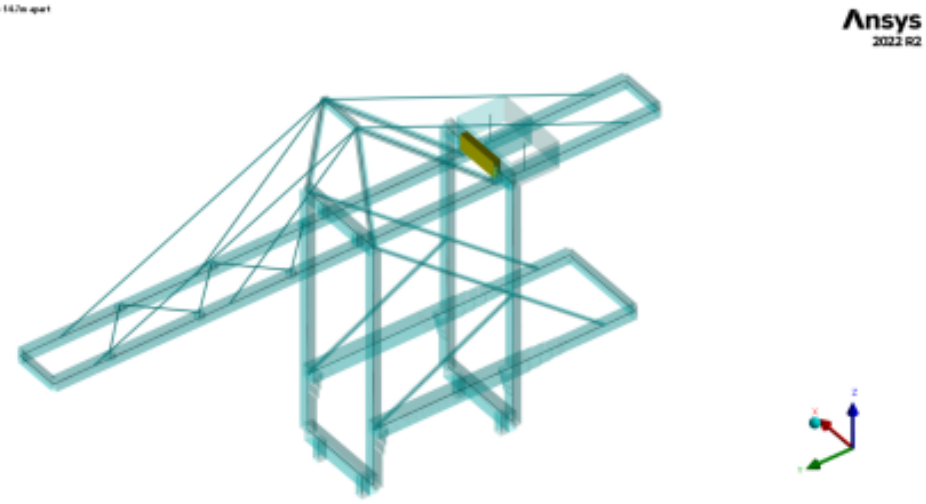

21..LS Portal Beam Outer (2 bodies)

Property	Value
Type / Elements	Beam / 6
Material	30..Steel ST52
Mass [kg]	16104.27
Area, [m^2]	0.15
I1, [m^4]	0.38
I2, [m^4]	0.08
I12, [m^4]	0
Torsion Constant, [m^4]	0.20
Y Shear Area, [m^2]	2.00
Z Shear Area, [m^2]	0.88
Nonstructural Mass, [kg]	0
Perimeter, [m]	0
Warping Constant, [m^6]	0.06
Y Neutral Axis Offset A, [m]	2.25
Z Neutral Axis Offset A, [m]	0.88
w [m]	4.00
h [m]	1.75
t1 [m]	0.01
t2 [m]	0.01
t3 [m]	0.02
t4 [m]	0.02

Property Shape

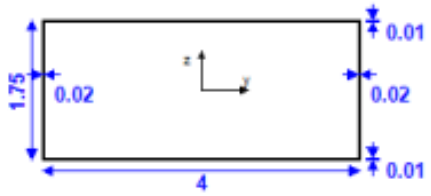

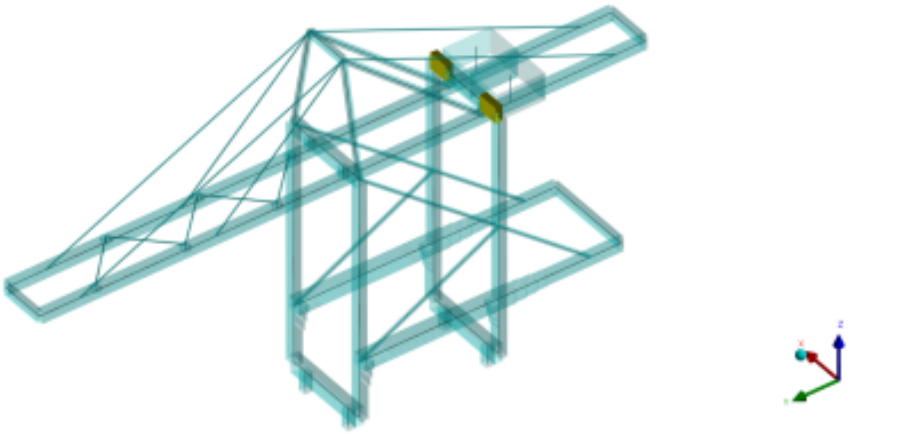

22..WS Portal Beam Middle

Property	Value	Property Shape
Type / Elements	Beam / 6	
Material	30..Steel ST52	
Mass [kg]	14884.09	
Area, [m^2]	0.13	
I1, [m^4]	0.31	
I2, [m^4]	0.07	
I12, [m^4]	0	
Torsion Constant, [m^4]	0.19	
Y Shear Area, [m^2]	2.00	
Z Shear Area, [m^2]	0.87	
Nonstructural Mass, [kg]	0	
Perimeter, [m]	0	
Warping Constant, [m^6]	0.04	
Y Neutral Axis Offset A, [m]	0	
Z Neutral Axis Offset A, [m]	0	
w [m]	4.00	
h [m]	1.75	
t1 [m]	0.01	
t2 [m]	0.01	
t3 [m]	0.02	
t4 [m]	0.02	

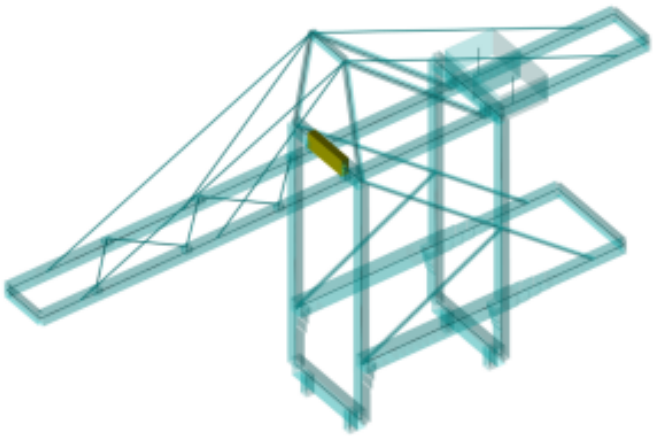

23..Boom Backtreach 2 (4 bodies)

Property	Value
Type / Elements	Beam / 36
Material	30..Steel ST52
Mass [kg]	62657.72
Area, [m^2]	0.09
I1, [m^4]	0.12
I2, [m^4]	0.05
I12, [m^4]	0
Torsion Constant, [m^4]	0.11
Y Shear Area, [m^2]	1.50
Z Shear Area, [m^2]	0.87
Nonstructural Mass, [kg]	0
Perimeter, [m]	0
Warping Constant, [m^6]	3.787e-03
Y Neutral Axis Offset A, [m]	0
Z Neutral Axis Offset A, [m]	0
w [m]	3.00
h [m]	1.75
t1 [m]	0.01
t2 [m]	0.01
t3 [m]	0.01
t4 [m]	0.01

Property Shape

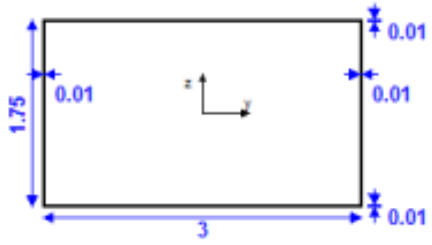

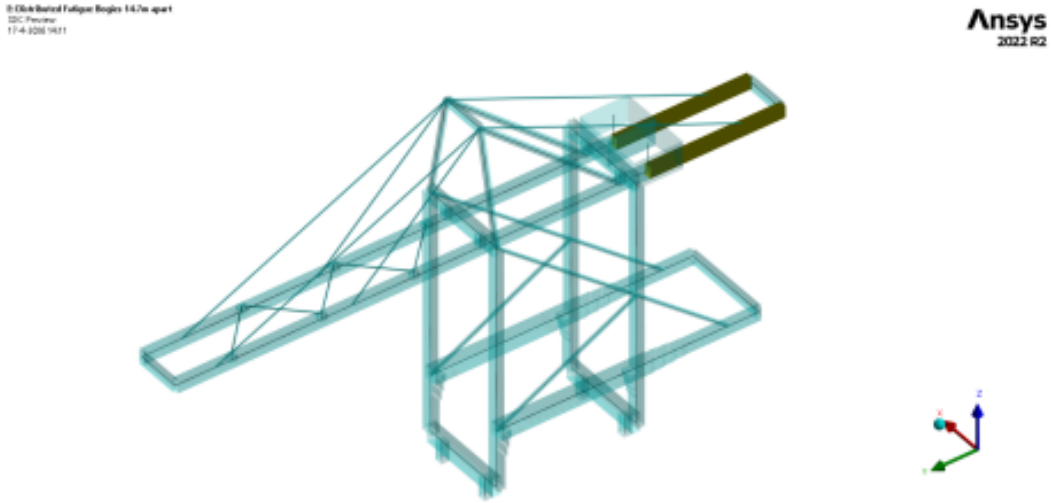

24..Backstay (2 bodies)

Property	Value
Type / Elements	Beam / 2
Material	30..Steel ST52
Mass [kg]	22482.90
Area, [m^2]	0.02
I1, [m^4]	4.621e-04
I2, [m^4]	4.621e-04
I12, [m^4]	0
Torsion Constant, [m^4]	9.243e-04
Y Shear Area, [m^2]	0
Z Shear Area, [m^2]	0
Nonstructural Mass, [kg]	0
Perimeter, [m]	0
Warping Constant, [m^6]	0
Y Neutral Axis Offset A, [m]	0
Z Neutral Axis Offset A, [m]	0
r [m]	0.25
t [m]	0.01

Property Shape

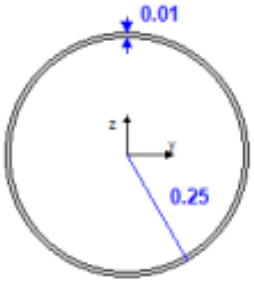

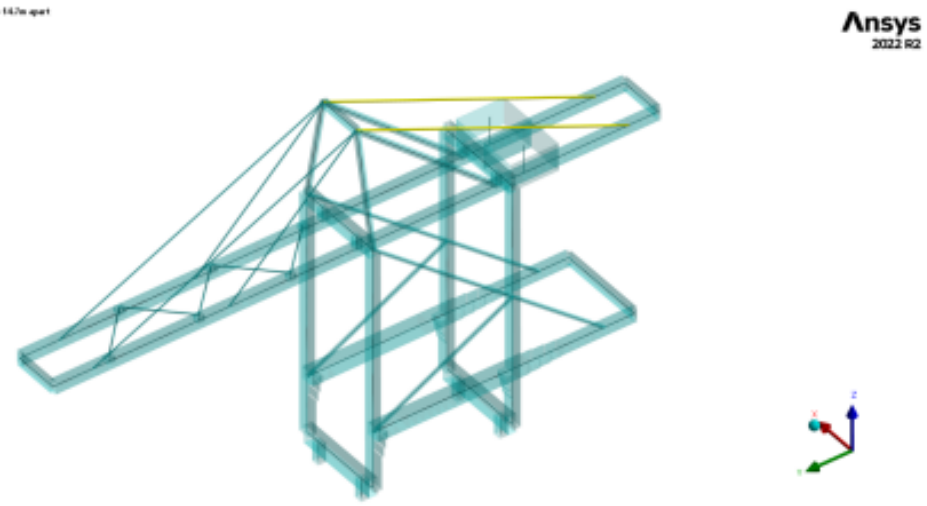

25..Boom Backtreach 1 (2 bodies)

Property	Value
Type / Elements	Beam / 8
Material	30..Steel ST52
Mass [kg]	12531.54
Area, [m^2]	0.09
I1, [m^4]	0.12
I2, [m^4]	0.05
I12, [m^4]	0
Torsion Constant, [m^4]	0.11
Y Shear Area, [m^2]	1.50
Z Shear Area, [m^2]	0.87
Nonstructural Mass, [kg]	0
Perimeter, [m]	0
Warping Constant, [m^6]	3.787e-03
Y Neutral Axis Offset A, [m]	0
Z Neutral Axis Offset A, [m]	0
w [m]	3.00
h [m]	1.75
t1 [m]	0.01
t2 [m]	0.01
t3 [m]	0.01
t4 [m]	0.01

Property Shape

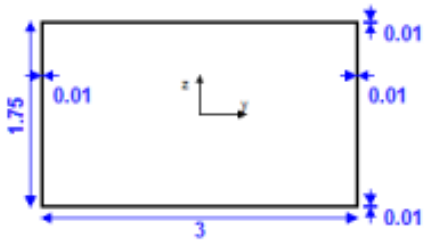

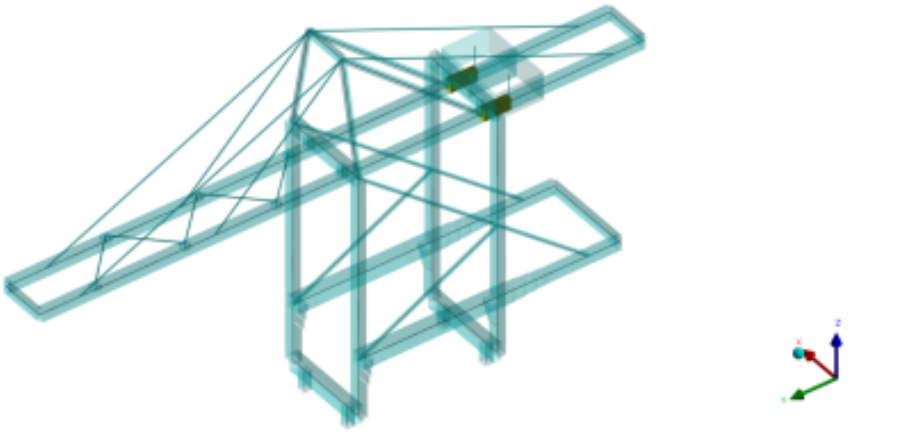

26..Boom Bridge (2 bodies)

Property	Value
Type / Elements	Beam / 36
Material	30..Steel ST52
Mass [kg]	69731.55
Area, [m^2]	0.10
I1, [m^4]	0.14
I2, [m^4]	0.06
I12, [m^4]	0
Torsion Constant, [m^4]	0.12
Y Shear Area, [m^2]	1.50
Z Shear Area, [m^2]	0.87
Nonstructural Mass, [kg]	0
Perimeter, [m]	0
Warping Constant, [m^6]	0.01
Y Neutral Axis Offset A, [m]	0
Z Neutral Axis Offset A, [m]	0
w [m]	3.00
h [m]	1.75
t1 [m]	0.01
t2 [m]	0.01
t3 [m]	0.01
t4 [m]	0.01

Property Shape

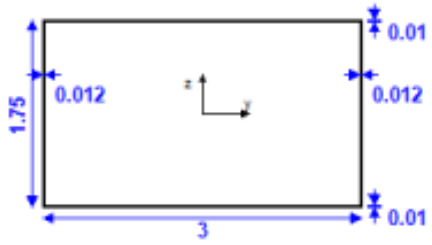

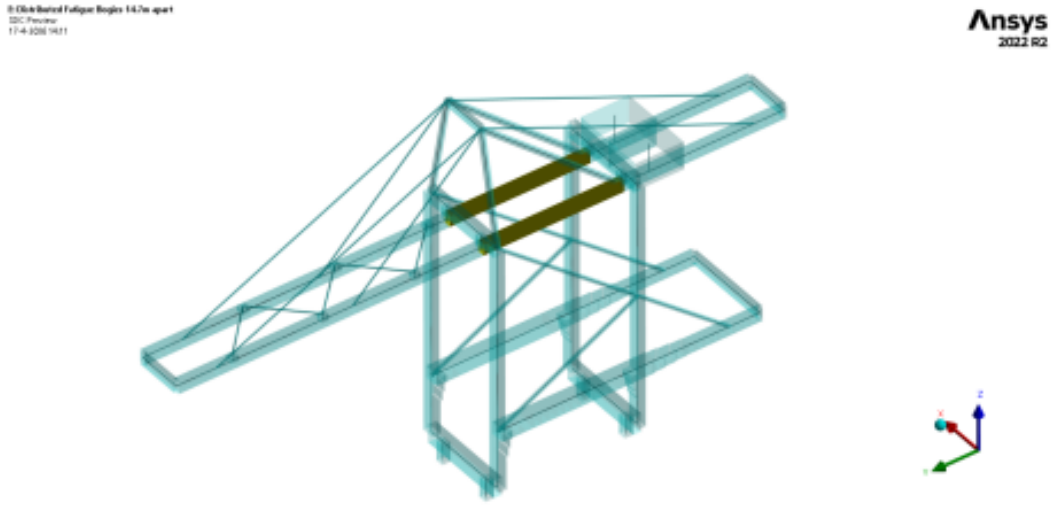

27..Boom Connect LS (2 bodies)

Property	Value
Type / Elements	Beam / 4
Material	30..Steel ST52
Mass [kg]	4439.17
Area, [m^2]	0.07
I1, [m^4]	0.04
I2, [m^4]	0.04
I12, [m^4]	0
Torsion Constant, [m^4]	0.05
Y Shear Area, [m^2]	0.88
Z Shear Area, [m^2]	0.88
Nonstructural Mass, [kg]	0
Perimeter, [m]	0
Warping Constant, [m^6]	5.278e-07
Y Neutral Axis Offset A, [m]	0
Z Neutral Axis Offset A, [m]	0
w [m]	1.75
h [m]	1.75
t1 [m]	0.01
t2 [m]	0.01
t3 [m]	0.01
t4 [m]	0.01

Property Shape

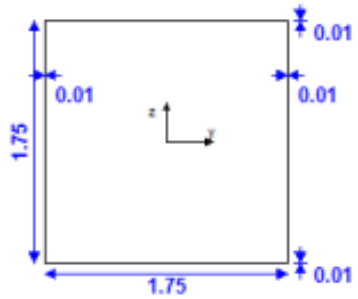

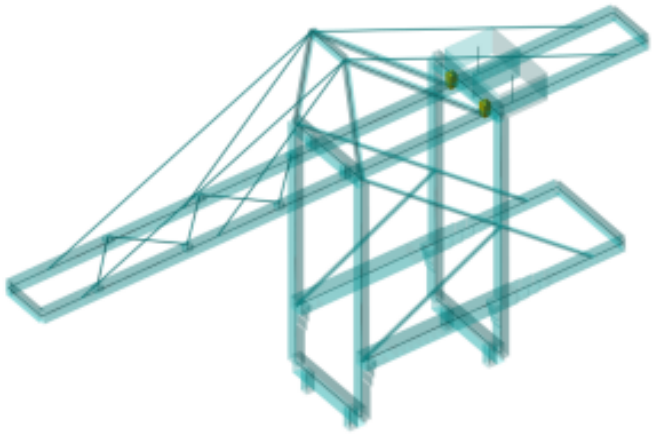

28..Boom Connect WS (2 bodies)

Property	Value
Type / Elements	Beam / 4
Material	30..Steel ST52
Mass [kg]	4439.17
Area, [m^2]	0.07
I1, [m^4]	0.04
I2, [m^4]	0.04
I12, [m^4]	0
Torsion Constant, [m^4]	0.05
Y Shear Area, [m^2]	0.88
Z Shear Area, [m^2]	0.88
Nonstructural Mass, [kg]	0
Perimeter, [m]	0
Warping Constant, [m^6]	5.278e-07
Y Neutral Axis Offset A, [m]	0
Z Neutral Axis Offset A, [m]	0
w [m]	1.75
h [m]	1.75
t1 [m]	0.01
t2 [m]	0.01
t3 [m]	0.01
t4 [m]	0.01

Property Shape

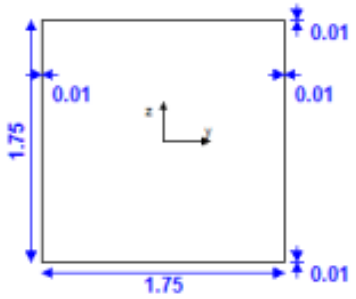

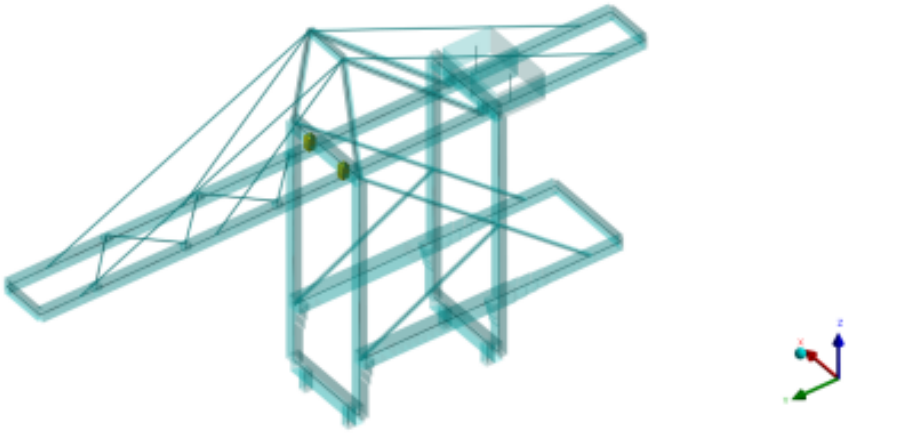

29..Boom Outreach 1 (8 bodies)

Property	Value	Property Shape
Type / Elements	Beam / 34	
Material	30..Steel ST52	
Mass [kg]	76791.84	
Area, [m^2]	0.12	
I1, [m^4]	0.18	
I2, [m^4]	0.06	
I12, [m^4]	0	
Torsion Constant, [m^4]	0.14	
Y Shear Area, [m^2]	1.50	
Z Shear Area, [m^2]	0.88	
Nonstructural Mass, [kg]	0	
Perimeter, [m]	0	
Warping Constant, [m^6]	0.02	
Y Neutral Axis Offset A, [m]	0	
Z Neutral Axis Offset A, [m]	0	
w [m]	3.00	
h [m]	1.75	
t1 [m]	0.01	
t2 [m]	0.01	
t3 [m]	0.02	
t4 [m]	0.02	

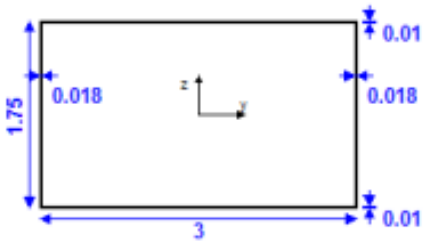

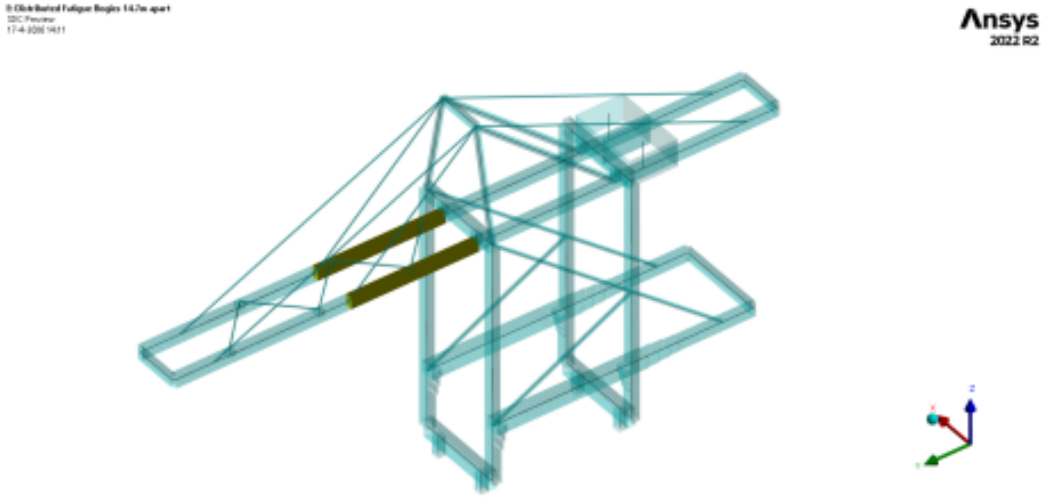

30..Boom Outreach 2 (10 bodies)

Property	Value
Type / Elements	Beam / 36
Material	30..Steel ST52
Mass [kg]	72356.59
Area, [m^2]	0.11
I1, [m^4]	0.15
I2, [m^4]	0.06
I12, [m^4]	0
Torsion Constant, [m^4]	0.13
Y Shear Area, [m^2]	1.50
Z Shear Area, [m^2]	0.88
Nonstructural Mass, [kg]	0
Perimeter, [m]	0
Warping Constant, [m^6]	0.01
Y Neutral Axis Offset A, [m]	0
Z Neutral Axis Offset A, [m]	0
w [m]	3.00
h [m]	1.75
t1 [m]	0.01
t2 [m]	0.01
t3 [m]	0.01
t4 [m]	0.01

Property Shape

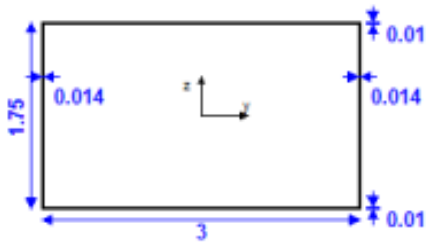

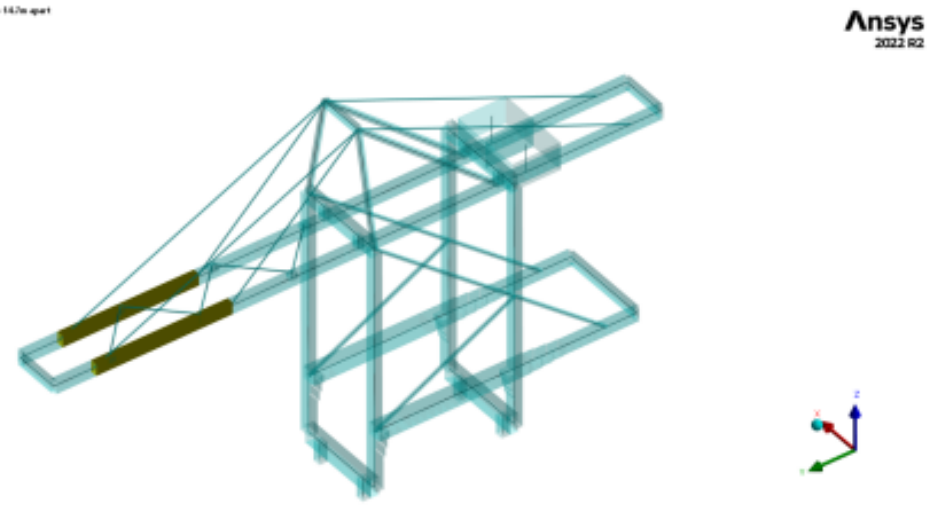

31..Boom Outreach 3 (4 bodies)

Property	Value
Type / Elements	Beam / 10
Material	30..Steel ST52
Mass [kg]	18565.25
Area, [m^2]	0.09
I1, [m^4]	0.12
I2, [m^4]	0.05
I12, [m^4]	0
Torsion Constant, [m^4]	0.11
Y Shear Area, [m^2]	1.50
Z Shear Area, [m^2]	0.87
Nonstructural Mass, [kg]	0
Perimeter, [m]	0
Warping Constant, [m^6]	3.787e-03
Y Neutral Axis Offset A, [m]	0
Z Neutral Axis Offset A, [m]	0
w [m]	3.00
h [m]	1.75
t1 [m]	0.01
t2 [m]	0.01
t3 [m]	0.01
t4 [m]	0.01

Property Shape

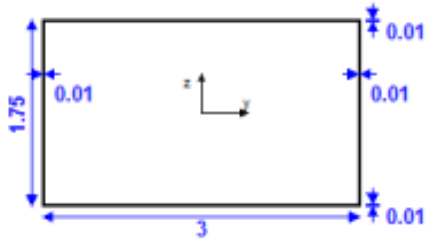

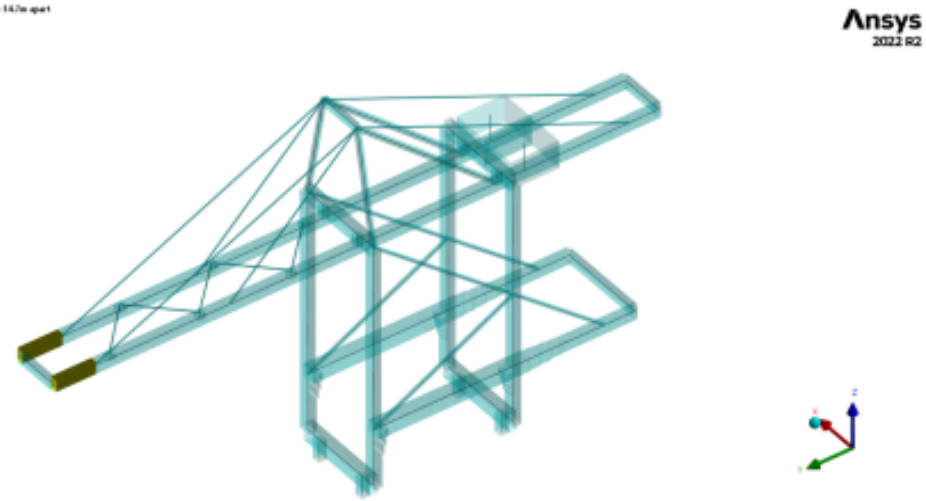

32..WS Legs Upper (2 bodies)

Property	Value
Type / Elements	Beam / 4
Material	30..Steel ST52
Mass [kg]	7969.32
Area, [m^2]	0.10
I1, [m^4]	0.14
I2, [m^4]	0.06
I12, [m^4]	0
Torsion Constant, [m^4]	0.12
Y Shear Area, [m^2]	1.50
Z Shear Area, [m^2]	0.87
Nonstructural Mass, [kg]	0
Perimeter, [m]	0
Warping Constant, [m^6]	0.01
Y Neutral Axis Offset A, [m]	0
Z Neutral Axis Offset A, [m]	0
w [m]	3.00
h [m]	1.75
t1 [m]	0.01
t2 [m]	0.01
t3 [m]	0.01
t4 [m]	0.01

Property Shape

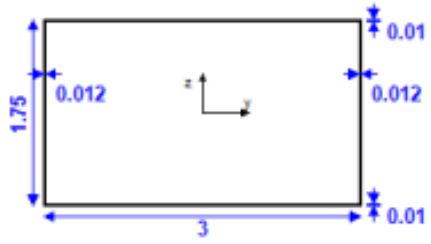

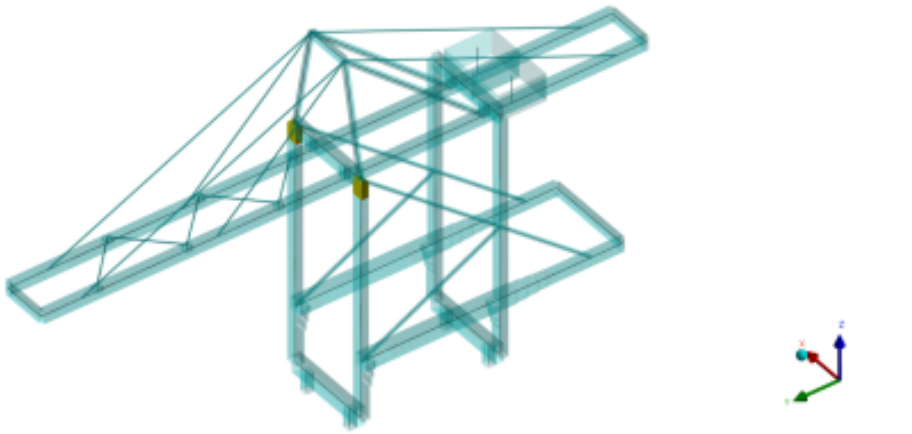

33..WS Legs Middle (2 bodies)

Property	Value
Type / Elements	Beam / 38
Material	30..Steel ST52
Mass [kg]	68227.29
Area, [m^2]	0.09
I1, [m^4]	0.12
I2, [m^4]	0.05
I12, [m^4]	0
Torsion Constant, [m^4]	0.11
Y Shear Area, [m^2]	1.50
Z Shear Area, [m^2]	0.87
Nonstructural Mass, [kg]	0
Perimeter, [m]	0
Warping Constant, [m^6]	3.787e-03
Y Neutral Axis Offset A, [m]	0
Z Neutral Axis Offset A, [m]	0
w [m]	3.00
h [m]	1.75
t1 [m]	0.01
t2 [m]	0.01
t3 [m]	0.01
t4 [m]	0.01

Property Shape

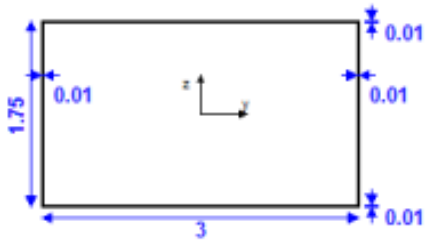

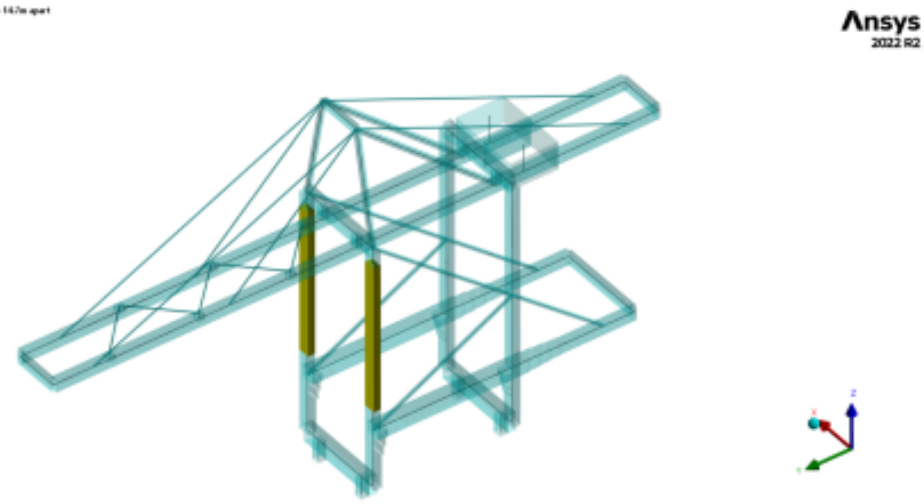

34..Boom Outreach End

Property	Value	Property Shape
Type / Elements	Beam / 6	
Material	30..Steel ST52	
Mass [kg]	8982.36	
Area, [m^2]	0.08	
I1, [m^4]	0.09	
I2, [m^4]	0.02	
I12, [m^4]	0	
Torsion Constant, [m^4]	0.04	
Y Shear Area, [m^2]	1.50	
Z Shear Area, [m^2]	0.50	
Nonstructural Mass, [kg]	0	
Perimeter, [m]	0	
Warping Constant, [m^6]	3.739e-03	
Y Neutral Axis Offset A, [m]	0	
Z Neutral Axis Offset A, [m]	0	
w [m]	3.00	
h [m]	1.00	
t1 [m]	0.01	
t2 [m]	0.01	
t3 [m]	0.01	
t4 [m]	0.01	

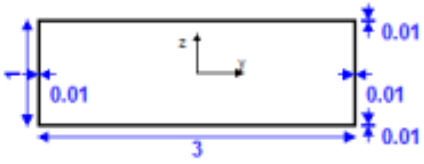

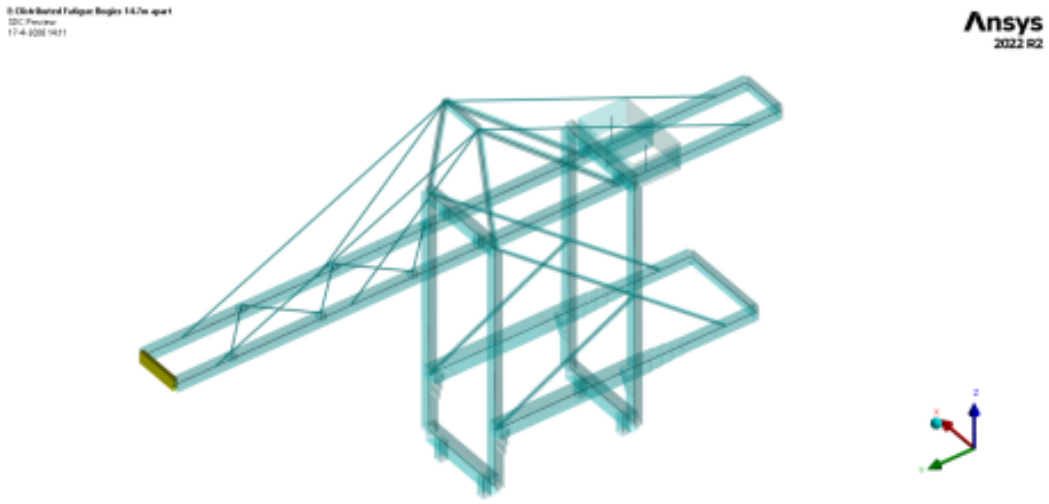

35..Boom Stiffener (5 bodies)

Property	Value	Property Shape
Type / Elements	Beam / 44	
Material	30..Steel ST52	
Mass [kg]	12229.70	
Area, [m^2]	0.02	
I1, [m^4]	4.621e-04	
I2, [m^4]	4.621e-04	
I12, [m^4]	0	
Torsion Constant, [m^4]	9.243e-04	
Y Shear Area, [m^2]	0	
Z Shear Area, [m^2]	0	
Nonstructural Mass, [kg]	0	
Perimeter, [m]	0	
Warping Constant, [m^6]	0	
Y Neutral Axis Offset A, [m]	0	
Z Neutral Axis Offset A, [m]	0	
r [m]	0.25	
t [m]	0.01	

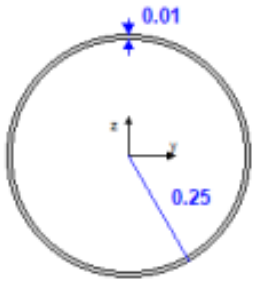

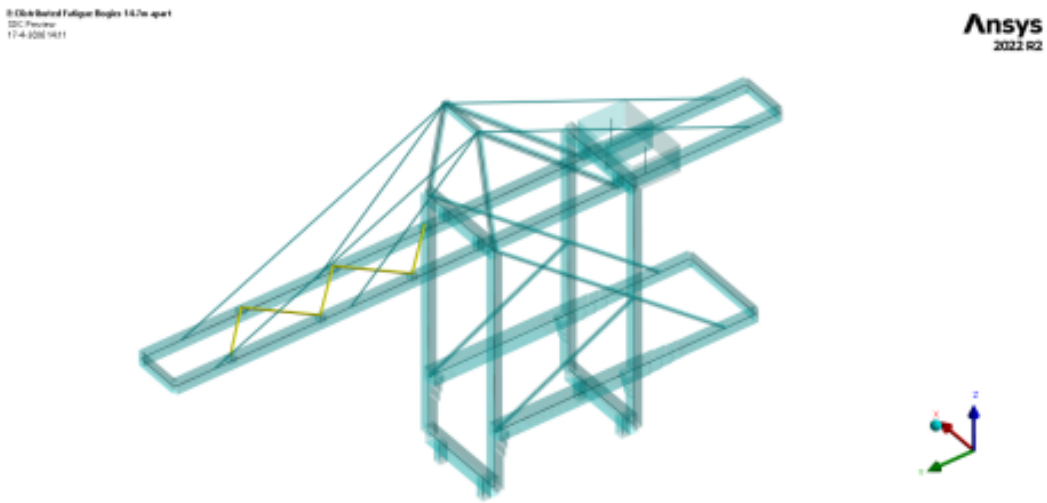

36..Boom Stiffener Connector (6 bodies)

Property	Value
Type / Elements	Beam / 6
Material	30..Steel ST52
Mass [kg]	6146.55
Area, [m^2]	0.07
I1, [m^4]	0.04
I2, [m^4]	0.04
I12, [m^4]	0
Torsion Constant, [m^4]	0.05
Y Shear Area, [m^2]	0.88
Z Shear Area, [m^2]	0.88
Nonstructural Mass, [kg]	0
Perimeter, [m]	0
Warping Constant, [m^6]	5.278e-07
Y Neutral Axis Offset A, [m]	0
Z Neutral Axis Offset A, [m]	0
w [m]	1.75
h [m]	1.75
t1 [m]	0.01
t2 [m]	0.01
t3 [m]	0.01
t4 [m]	0.01

Property Shape

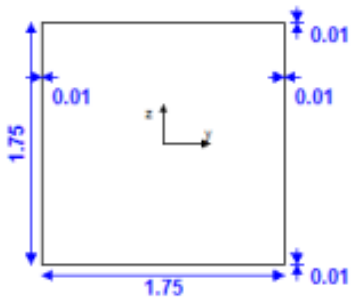

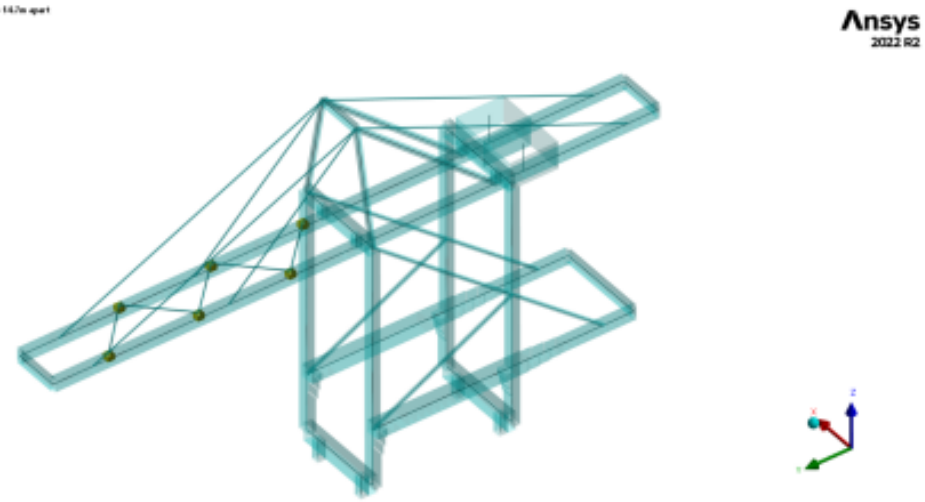

37..Forestay 1 (2 bodies)

Property	Value
Type / Elements	Beam / 2
Material	30..Steel ST52
Mass [kg]	19750.00
Area, [m^2]	0.02
I1, [m^4]	6.726e-04
I2, [m^4]	6.726e-04
I12, [m^4]	0
Torsion Constant, [m^4]	1.345e-03
Y Shear Area, [m^2]	0
Z Shear Area, [m^2]	0
Nonstructural Mass, [kg]	0
Perimeter, [m]	0
Warping Constant, [m^6]	0
Y Neutral Axis Offset A, [m]	0
Z Neutral Axis Offset A, [m]	0
r [m]	0.25
t [m]	0.02

Property Shape

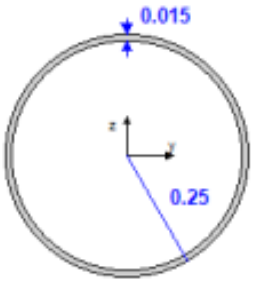

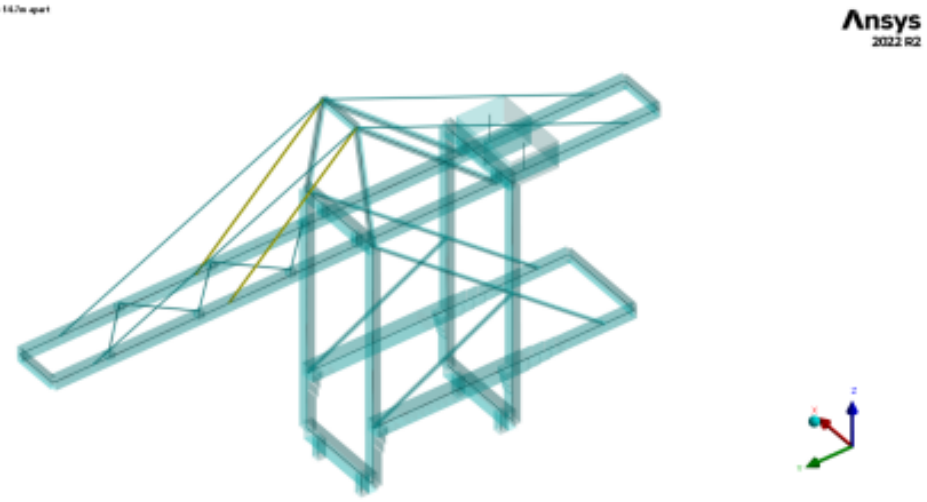

38..Forestay 2 (2 bodies)

Property	Value	Property Shape
Type / Elements	Beam / 2	
Material	30..Steel ST52	
Mass [kg]	32562.68	
Area, [m^2]	0.02	
I1, [m^4]	6.726e-04	
I2, [m^4]	6.726e-04	
I12, [m^4]	0	
Torsion Constant, [m^4]	1.345e-03	
Y Shear Area, [m^2]	0	
Z Shear Area, [m^2]	0	
Nonstructural Mass, [kg]	0	
Perimeter, [m]	0	
Warping Constant, [m^6]	0	
Y Neutral Axis Offset A, [m]	0	
Z Neutral Axis Offset A, [m]	0	
r [m]	0.25	
t [m]	0.02	

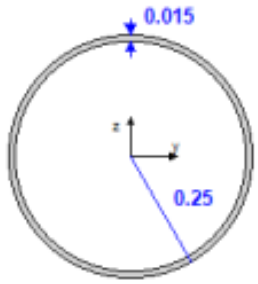

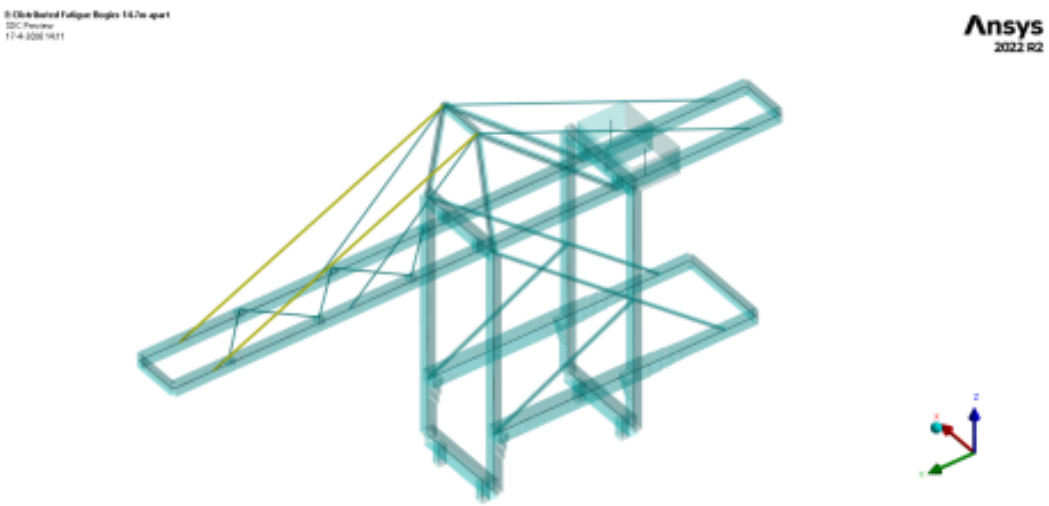

39..Pylon Legs (2 bodies)

Property	Value
Type / Elements	Beam / 28
Material	30..Steel ST52
Mass [kg]	37839.75
Area, [m^2]	0.07
I1, [m^4]	0.02
I2, [m^4]	0.02
I12, [m^4]	0
Torsion Constant, [m^4]	0.04
Y Shear Area, [m^2]	0
Z Shear Area, [m^2]	0
Nonstructural Mass, [kg]	0
Perimeter, [m]	0
Warping Constant, [m^6]	0
Y Neutral Axis Offset A, [m]	0
Z Neutral Axis Offset A, [m]	0
r [m]	0.75
t [m]	0.02

Property Shape

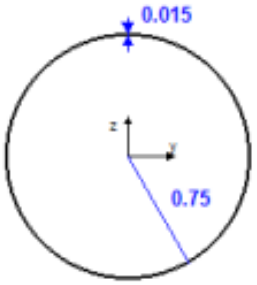

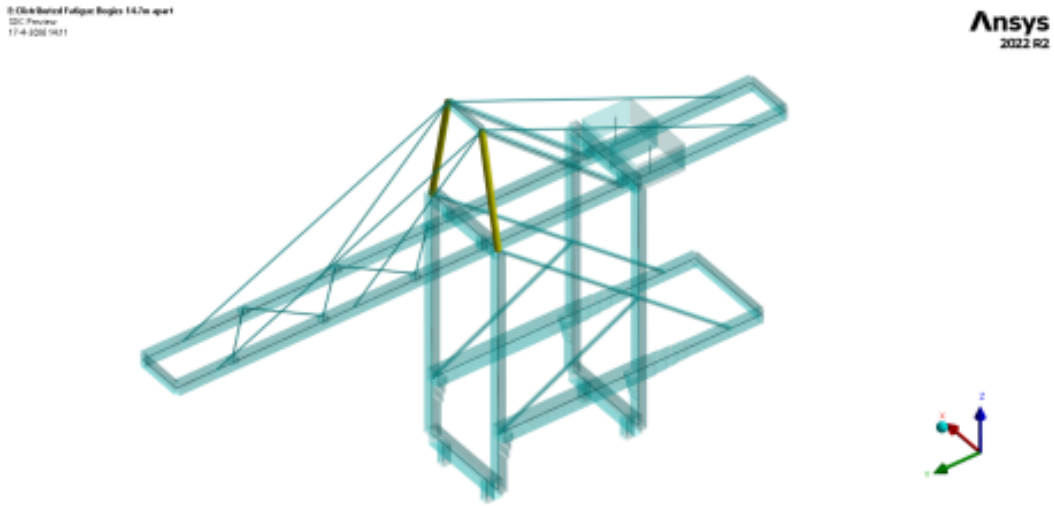

40..Pylon Head

Property	Value
Type / Elements	Beam / 6
Material	30..Steel ST52
Mass [kg]	6725.49
Area, [m^2]	0.06
I1, [m^4]	0.02
I2, [m^4]	0.02
I12, [m^4]	0
Torsion Constant, [m^4]	0.03
Y Shear Area, [m^2]	0.75
Z Shear Area, [m^2]	0.75
Nonstructural Mass, [kg]	0
Perimeter, [m]	0
Warping Constant, [m^6]	3.261e-07
Y Neutral Axis Offset A, [m]	0
Z Neutral Axis Offset A, [m]	0
w [m]	1.50
h [m]	1.50
t1 [m]	0.01
t2 [m]	0.01
t3 [m]	0.01
t4 [m]	0.01

Property Shape

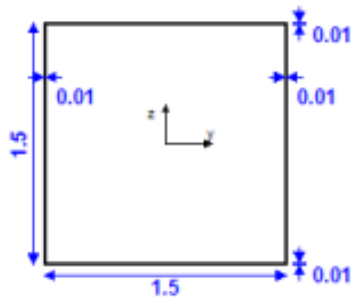

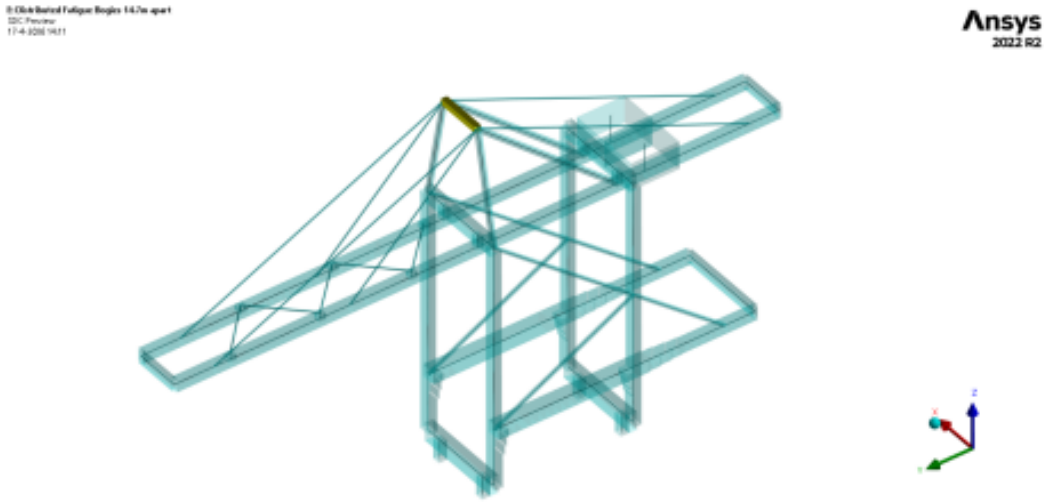

41..Pylon Diagonal Brace (2 bodies)

Property	Value
Type / Elements	Beam / 48
Material	30..Steel ST52
Mass [kg]	42494.98
Area, [m^2]	0.05
I1, [m^4]	0.01
I2, [m^4]	0.01
I12, [m^4]	0
Torsion Constant, [m^4]	0.03
Y Shear Area, [m^2]	0
Z Shear Area, [m^2]	0
Nonstructural Mass, [kg]	0
Perimeter, [m]	0
Warping Constant, [m^6]	0
Y Neutral Axis Offset A, [m]	0
Z Neutral Axis Offset A, [m]	0
r [m]	0.75
t [m]	0.01

Property Shape

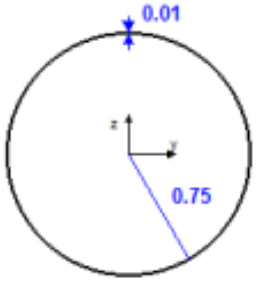

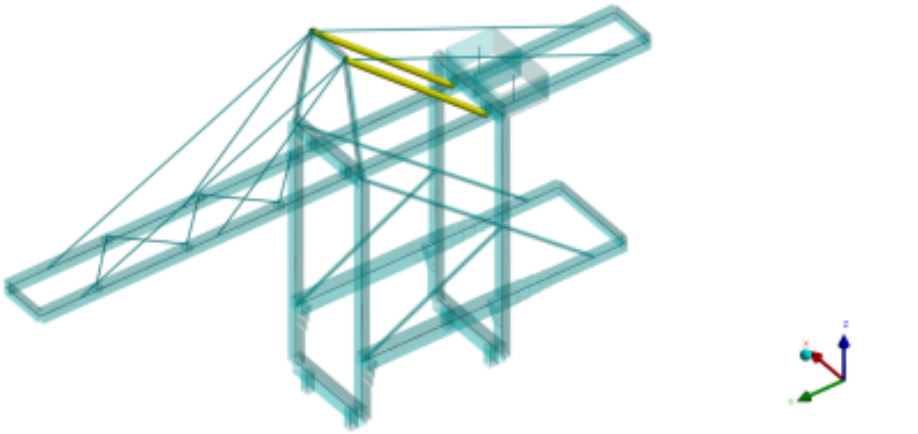

42..Machine House (2 bodies)

Property	Value	Property Shape
Type / Elements	Beam / 2	
Material	26..Machine House	
Mass [kg]	230000.64	
Area, [m^2]	112.25	
I1, [m^4]	1346.98	
I2, [m^4]	818.45	
I12, [m^4]	0	
Torsion Constant, [m^4]	1747.58	
Y Shear Area, [m^2]	0	
Z Shear Area, [m^2]	0	
Nonstructural Mass, [kg]	0	
Perimeter, [m]	0	
Warping Constant, [m^6]	693.91	
Y Neutral Axis Offset A, [m]	-0.13	
Z Neutral Axis Offset A, [m]	1.07	
h [m]	9.35	
w [m]	12.00	

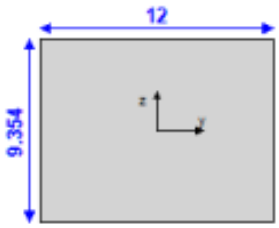

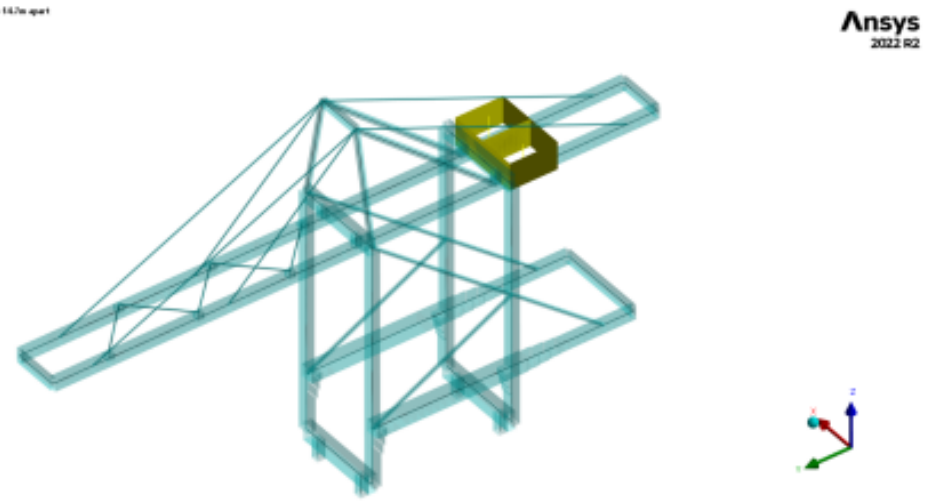

43..WS Legs Taper Lower 3 (2 bodies)

Property	Value
Type / Elements	Beam / 2
Material	30..Steel ST52
Mass [kg]	6452.70
Area, [m^2]	0.16
I1, [m^4]	0.28
I2, [m^4]	0.29
I12, [m^4]	0
Torsion Constant, [m^4]	0.41
Y Shear Area, [m^2]	1.50
Z Shear Area, [m^2]	1.75
Nonstructural Mass, [kg]	0
Perimeter, [m]	0
Warping Constant, [m^6]	0.01
Y Neutral Axis Offset A, [m]	1.50
Z Neutral Axis Offset A, [m]	0.88
w [m]	3.00
h [m]	3.50
t1 [m]	0.01
t2 [m]	0.01
t3 [m]	0.02
t4 [m]	0.02

Property Shape

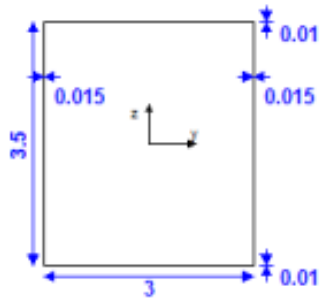

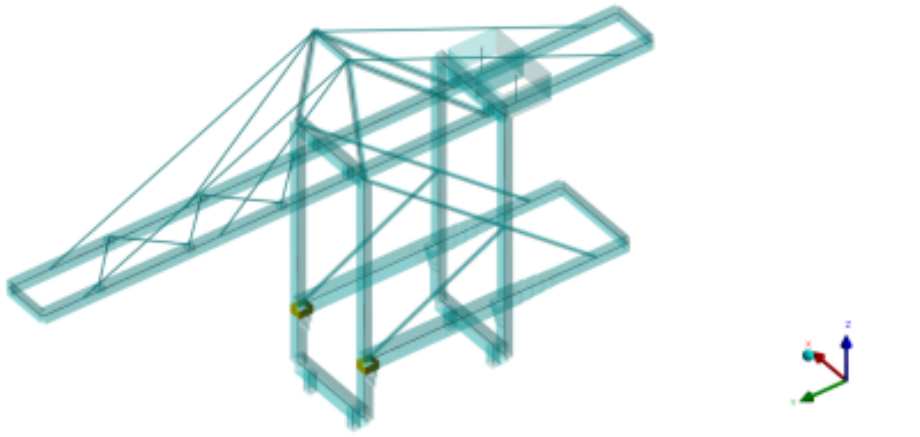

44..Diagonal Brace Lower (2 bodies)

Property	Value	Property Shape
Type / Elements	Beam / 40	
Material	30..Steel ST52	
Mass [kg]	24156.22	
Area, [m^2]	0.03	
I1, [m^4]	3.810e-03	
I2, [m^4]	3.810e-03	
I12, [m^4]	0	
Torsion Constant, [m^4]	0.01	
Y Shear Area, [m^2]	0	
Z Shear Area, [m^2]	0	
Nonstructural Mass, [kg]	0	
Perimeter, [m]	0	
Warping Constant, [m^6]	0	
Y Neutral Axis Offset A, [m]	0	
Z Neutral Axis Offset A, [m]	0	
r [m]	0.50	
t [m]	0.01	

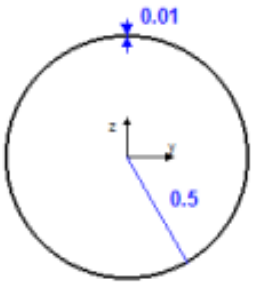

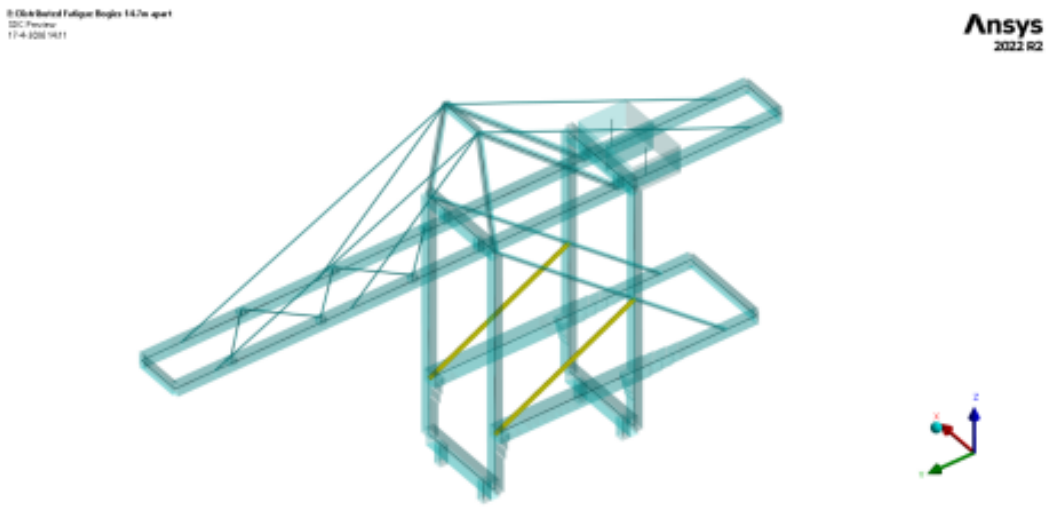

45..WS Portal Beam Outer (2 bodies)

Property	Value	Property Shape
Type / Elements	Beam / 6	
Material	30..Steel ST52	
Mass [kg]	14236.96	
Area, [m^2]	0.13	
I1, [m^4]	0.31	
I2, [m^4]	0.07	
I12, [m^4]	0	
Torsion Constant, [m^4]	0.19	
Y Shear Area, [m^2]	2.00	
Z Shear Area, [m^2]	0.87	
Nonstructural Mass, [kg]	0	
Perimeter, [m]	0	
Warping Constant, [m^6]	0.04	
Y Neutral Axis Offset A, [m]	0	
Z Neutral Axis Offset A, [m]	0	
w [m]	4.00	
h [m]	1.75	
t1 [m]	0.01	
t2 [m]	0.01	
t3 [m]	0.02	
t4 [m]	0.02	

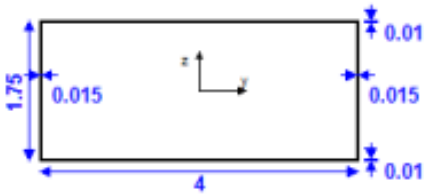

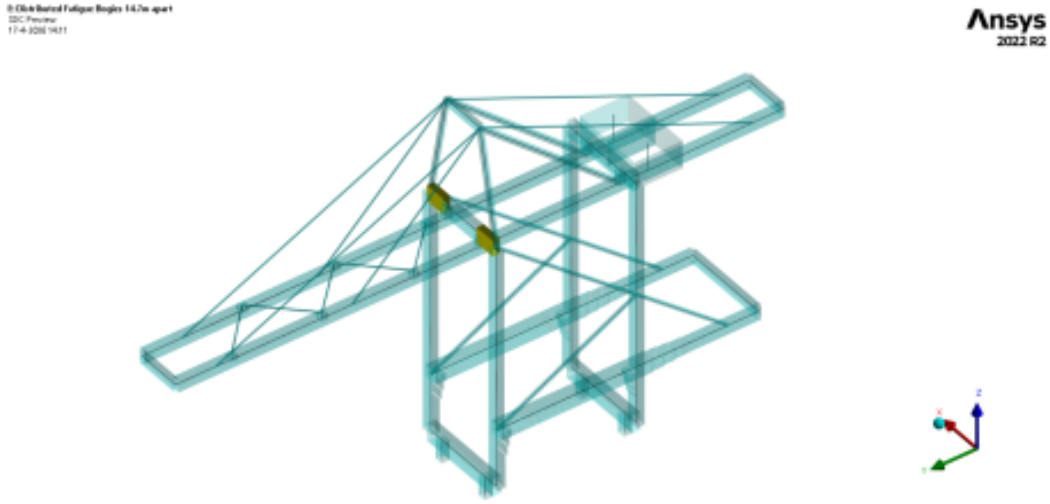

46..Boom Backtreach End

Property	Value	Property Shape
Type / Elements	Beam / 6	
Material	30..Steel ST52	
Mass [kg]	8982.36	
Area, [m^2]	0.08	
I1, [m^4]	0.09	
I2, [m^4]	0.02	
I12, [m^4]	0	
Torsion Constant, [m^4]	0.04	
Y Shear Area, [m^2]	1.50	
Z Shear Area, [m^2]	0.50	
Nonstructural Mass, [kg]	0	
Perimeter, [m]	0	
Warping Constant, [m^6]	3.739e-03	
Y Neutral Axis Offset A, [m]	0	
Z Neutral Axis Offset A, [m]	0	
w [m]	3.00	
h [m]	1.00	
t1 [m]	0.01	
t2 [m]	0.01	
t3 [m]	0.01	
t4 [m]	0.01	

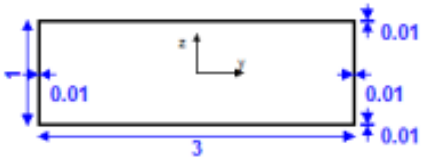

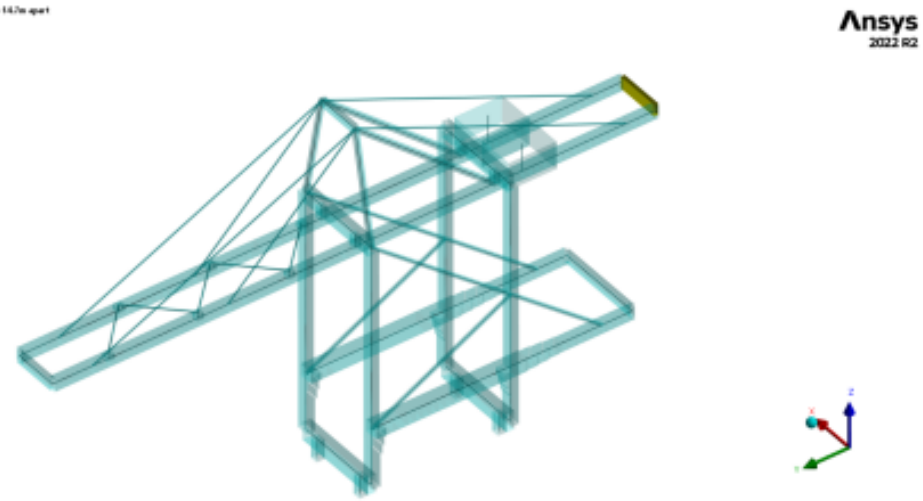

47..WS Legs Taper Lower 2 (2 bodies)

Property	Value	Property Shape
Type / Elements	Beam / 2	
Material	30..Steel ST52	
Mass [kg]	5863.95	
Area, [m^2]	0.15	
I1, [m^4]	0.24	
I2, [m^4]	0.20	
I12, [m^4]	0	
Torsion Constant, [m^4]	0.32	
Y Shear Area, [m^2]	1.50	
Z Shear Area, [m^2]	1.50	
Nonstructural Mass, [kg]	0	
Perimeter, [m]	0	
Warping Constant, [m^6]	0.01	
Y Neutral Axis Offset A, [m]	1.50	
Z Neutral Axis Offset A, [m]	0.88	
w [m]	3.00	
h [m]	3.00	
t1 [m]	0.01	
t2 [m]	0.01	
t3 [m]	0.02	
t4 [m]	0.02	

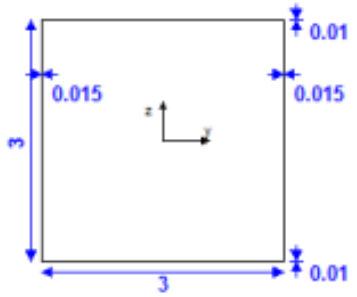

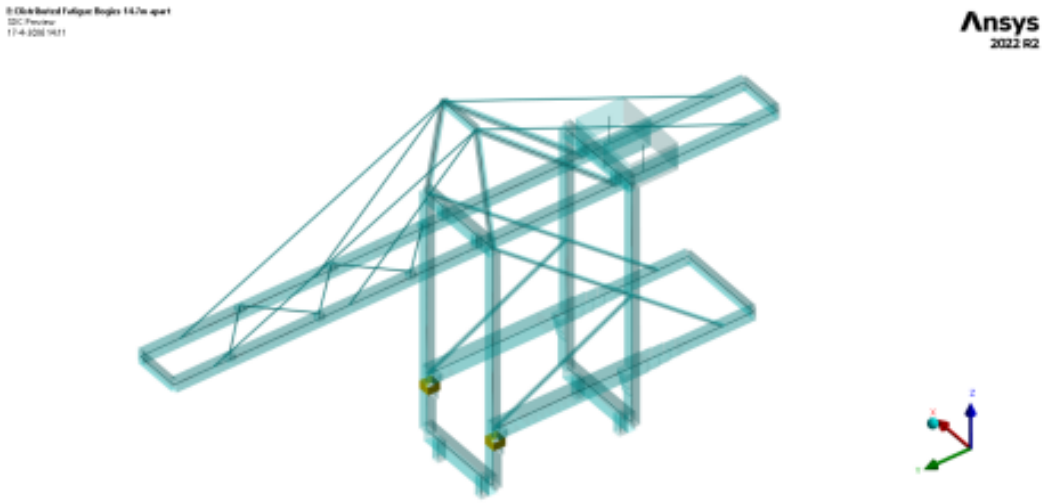

48..WS Legs Taper Lower 1 (2 bodies)

Property	Value
Type / Elements	Beam / 2
Material	30..Steel ST52
Mass [kg]	5275.20
Area, [m^2]	0.13
I1, [m^4]	0.21
I2, [m^4]	0.13
I12, [m^4]	0
Torsion Constant, [m^4]	0.24
Y Shear Area, [m^2]	1.50
Z Shear Area, [m^2]	1.25
Nonstructural Mass, [kg]	0
Perimeter, [m]	0
Warping Constant, [m^6]	0.01
Y Neutral Axis Offset A, [m]	1.50
Z Neutral Axis Offset A, [m]	0.88
w [m]	3.00
h [m]	2.50
t1 [m]	0.01
t2 [m]	0.01
t3 [m]	0.02
t4 [m]	0.02

Property Shape

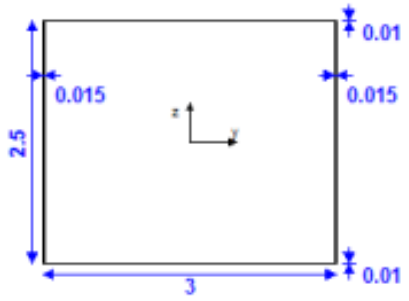

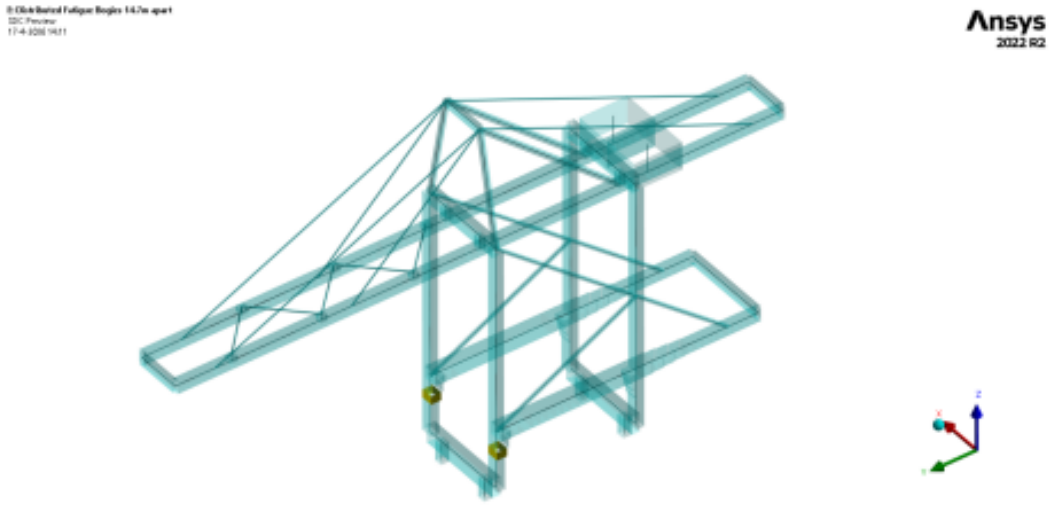

49..LS Legs Taper Lower 1 (2 bodies)

Property	Value
Type / Elements	Beam / 2
Material	30..Steel ST52
Mass [kg]	5859.24
Area, [m^2]	0.15
I1, [m^4]	0.24
I2, [m^4]	0.14
I12, [m^4]	0
Torsion Constant, [m^4]	0.25
Y Shear Area, [m^2]	1.50
Z Shear Area, [m^2]	1.25
Nonstructural Mass, [kg]	0
Perimeter, [m]	0
Warping Constant, [m^6]	0.02
Y Neutral Axis Offset A, [m]	1.50
Z Neutral Axis Offset A, [m]	1.63
w [m]	3.00
h [m]	2.50
t1 [m]	0.01
t2 [m]	0.01
t3 [m]	0.02
t4 [m]	0.02

Property Shape

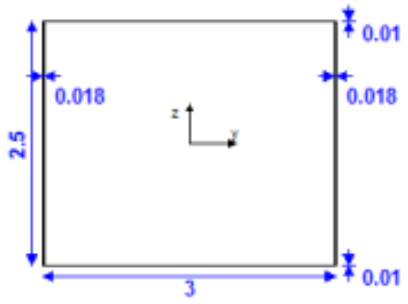

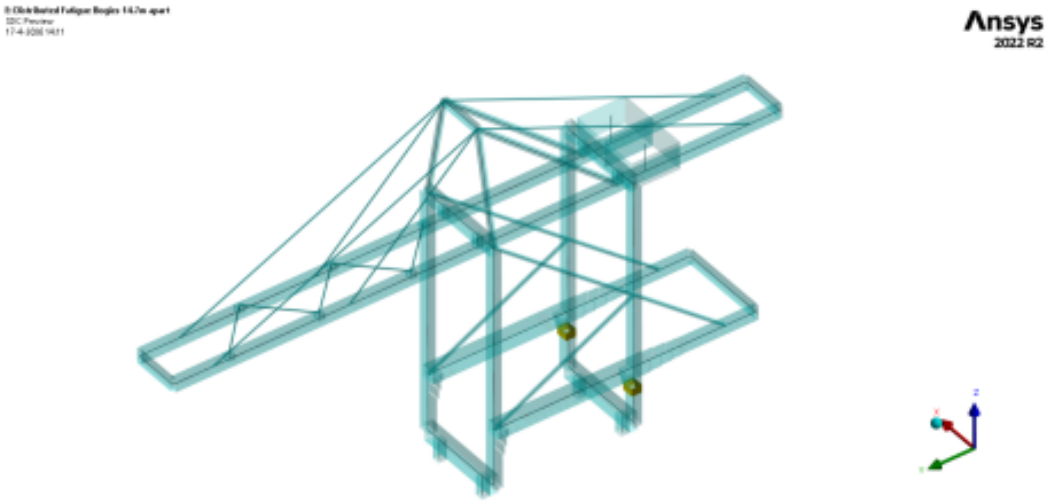

50..LS Legs Taper Lower 2 (2 bodies)

Property	Value
Type / Elements	Beam / 2
Material	30..Steel ST52
Mass [kg]	6565.74
Area, [m^2]	0.17
I1, [m^4]	0.28
I2, [m^4]	0.21
I12, [m^4]	0
Torsion Constant, [m^4]	0.34
Y Shear Area, [m^2]	1.50
Z Shear Area, [m^2]	1.50
Nonstructural Mass, [kg]	0
Perimeter, [m]	0
Warping Constant, [m^6]	0.02
Y Neutral Axis Offset A, [m]	1.50
Z Neutral Axis Offset A, [m]	2.13
w [m]	3.00
h [m]	3.00
t1 [m]	0.01
t2 [m]	0.01
t3 [m]	0.02
t4 [m]	0.02

Property Shape

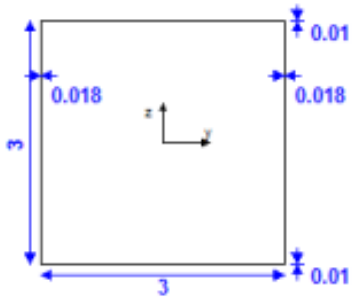

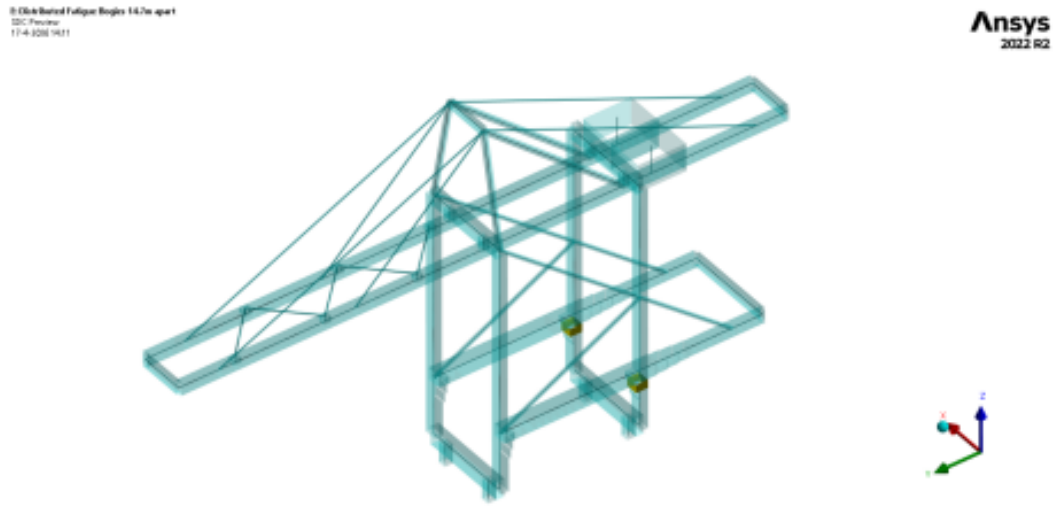

51..LS Legs Taper Lower 3 (2 bodies)

Property	Value
Type / Elements	Beam / 2
Material	30..Steel ST52
Mass [kg]	7272.24
Area, [m^2]	0.19
I1, [m^4]	0.32
I2, [m^4]	0.31
I12, [m^4]	0
Torsion Constant, [m^4]	0.44
Y Shear Area, [m^2]	1.50
Z Shear Area, [m^2]	1.75
Nonstructural Mass, [kg]	0
Perimeter, [m]	0
Warping Constant, [m^6]	0.02
Y Neutral Axis Offset A, [m]	1.50
Z Neutral Axis Offset A, [m]	2.63
w [m]	3.00
h [m]	3.50
t1 [m]	0.01
t2 [m]	0.01
t3 [m]	0.02
t4 [m]	0.02

Property Shape

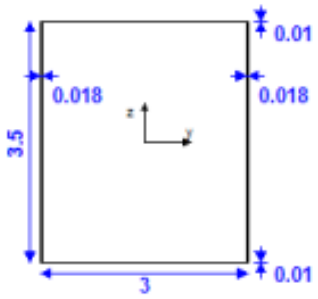

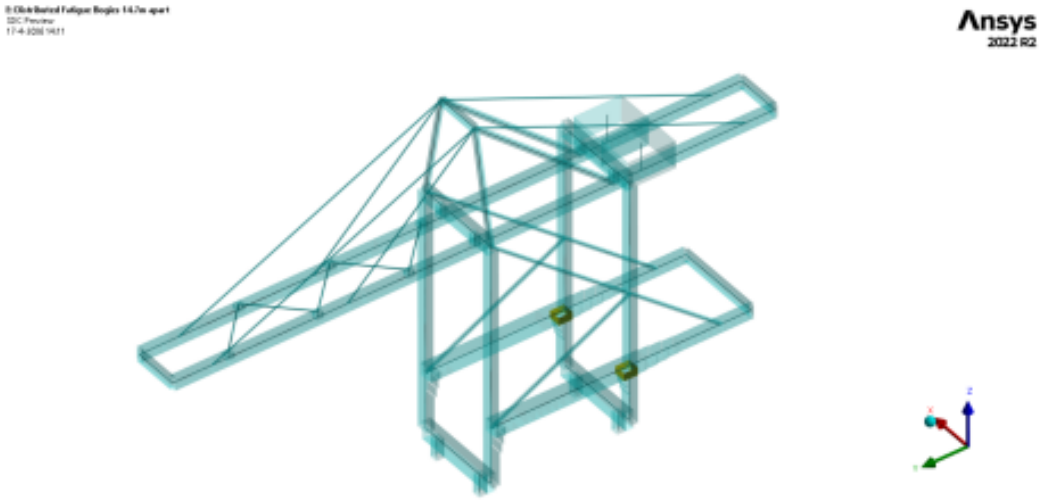

52..Bogies (4 bodies)

Property	Value
Type / Elements	Beam / 12
Material	32..Bogies
Mass [kg]	312000.00
Area, [m^2]	0.16
I1, [m^4]	0.10
I2, [m^4]	0.10
I12, [m^4]	0
Torsion Constant, [m^4]	0.16
Y Shear Area, [m^2]	1.00
Z Shear Area, [m^2]	1.00
Nonstructural Mass, [kg]	0
Perimeter, [m]	0
Warping Constant, [m^6]	5.792e-06
Y Neutral Axis Offset A, [m]	1.00
Z Neutral Axis Offset A, [m]	0.88
w [m]	2.00
h [m]	2.00
t1 [m]	0.02
t2 [m]	0.02
t3 [m]	0.02
t4 [m]	0.02

Property Shape

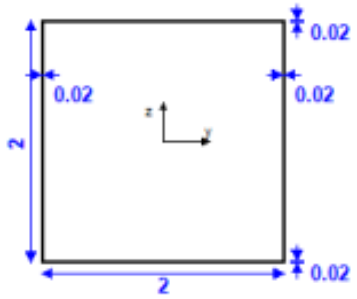

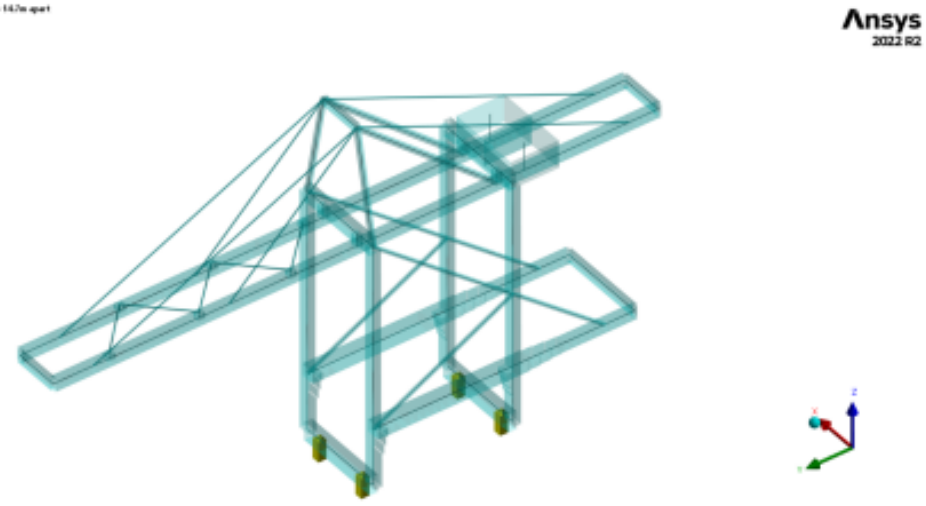

53..WS Sill Beam Outer (2 bodies)

Property	Value
Type / Elements	Beam / 4
Material	30..Steel ST52
Mass [kg]	12343.97
Area, [m^2]	0.16
I1, [m^4]	0.51
I2, [m^4]	0.11
I12, [m^4]	0
Torsion Constant, [m^4]	0.29
Y Shear Area, [m^2]	2.25
Z Shear Area, [m^2]	1.00
Nonstructural Mass, [kg]	0
Perimeter, [m]	0
Warping Constant, [m^6]	0.10
Y Neutral Axis Offset A, [m]	2.25
Z Neutral Axis Offset A, [m]	1.13
w [m]	4.50
h [m]	2.00
t1 [m]	0.01
t2 [m]	0.01
t3 [m]	0.02
t4 [m]	0.02

Property Shape

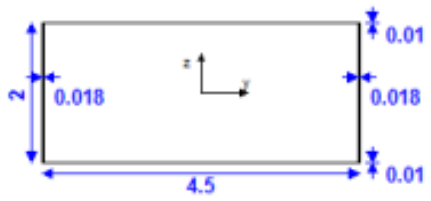

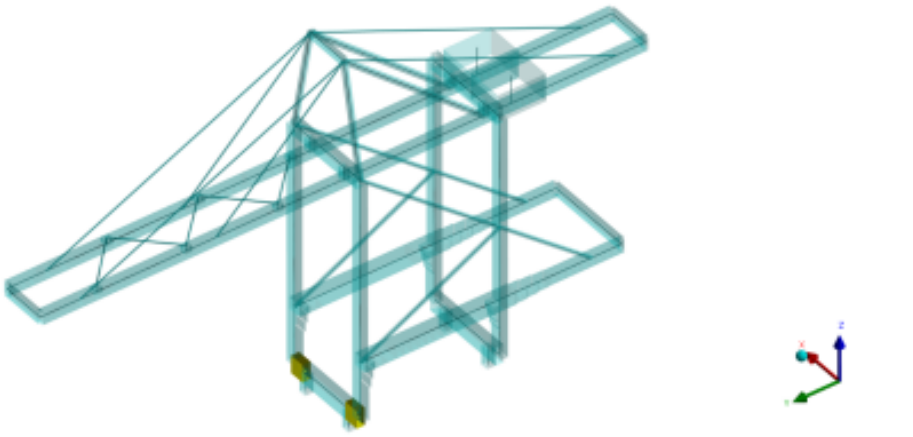

54..WS Sill Beam Middle

Property	Value	Property Shape
Type / Elements	Beam / 8	
Material	30..Steel ST52	
Mass [kg]	23263.63	
Area, [m^2]	0.16	
I1, [m^4]	0.51	
I2, [m^4]	0.11	
I12, [m^4]	0	
Torsion Constant, [m^4]	0.29	
Y Shear Area, [m^2]	2.25	
Z Shear Area, [m^2]	1.00	
Nonstructural Mass, [kg]	0	
Perimeter, [m]	0	
Warping Constant, [m^6]	0.10	
Y Neutral Axis Offset A, [m]	2.25	
Z Neutral Axis Offset A, [m]	0.88	
w [m]	4.50	
h [m]	2.00	
t1 [m]	0.01	
t2 [m]	0.01	
t3 [m]	0.02	
t4 [m]	0.02	

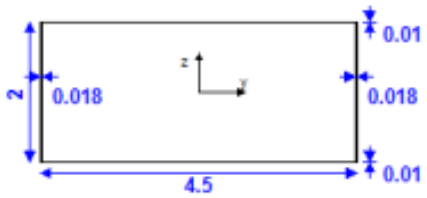

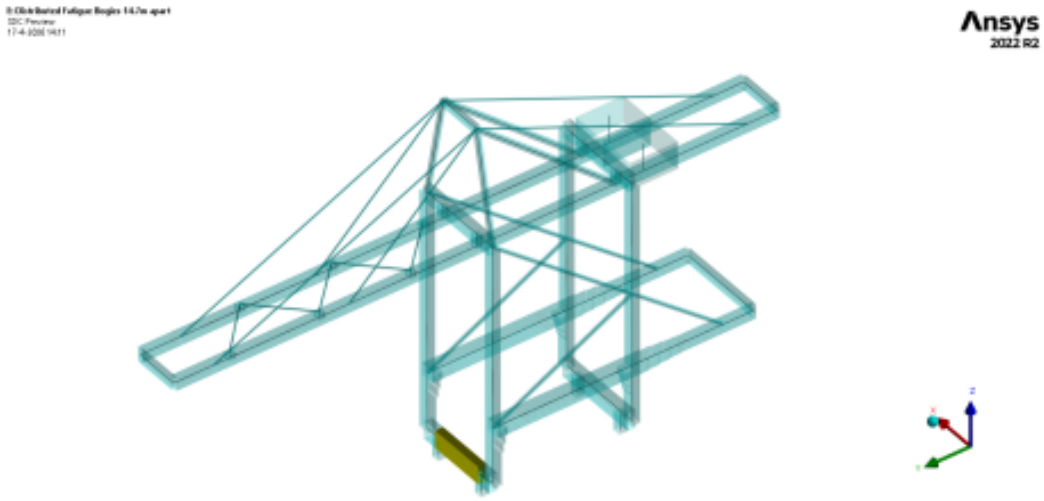

55..LS Sill Beam Outer (2 bodies)

Property	Value
Type / Elements	Beam / 4
Material	30..Steel ST52
Mass [kg]	12950.15
Area, [m^2]	0.17
I1, [m^4]	0.55
I2, [m^4]	0.11
I12, [m^4]	0
Torsion Constant, [m^4]	0.29
Y Shear Area, [m^2]	2.25
Z Shear Area, [m^2]	1.00
Nonstructural Mass, [kg]	0
Perimeter, [m]	0
Warping Constant, [m^6]	0.11
Y Neutral Axis Offset A, [m]	2.25
Z Neutral Axis Offset A, [m]	1.13
w [m]	4.50
h [m]	2.00
t1 [m]	0.01
t2 [m]	0.01
t3 [m]	0.02
t4 [m]	0.02

Property Shape

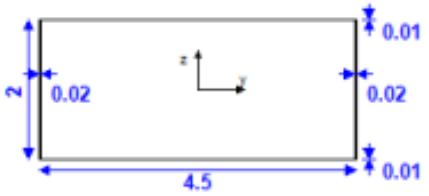

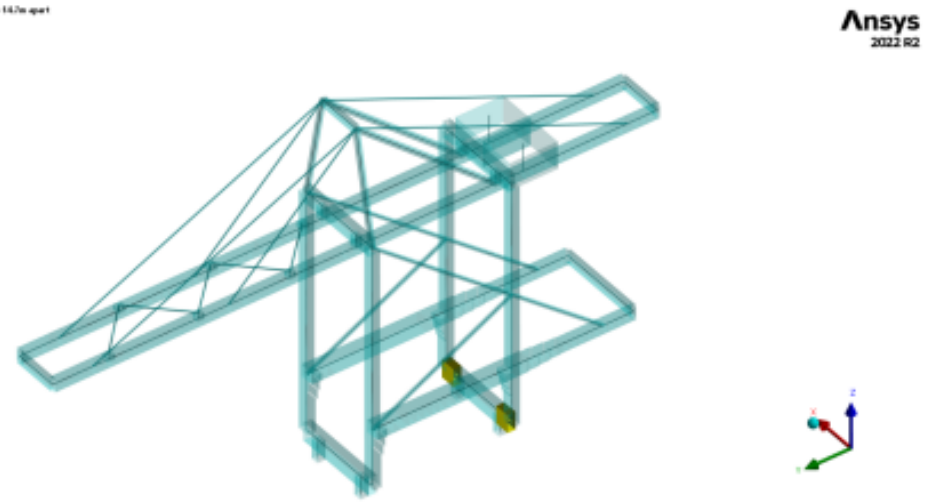

56..LS Sill Beam Middle

Property	Value
Type / Elements	Beam / 8
Material	30..Steel ST52
Mass [kg]	24406.04
Area, [m^2]	0.17
I1, [m^4]	0.55
I2, [m^4]	0.11
I12, [m^4]	0
Torsion Constant, [m^4]	0.29
Y Shear Area, [m^2]	2.25
Z Shear Area, [m^2]	1.00
Nonstructural Mass, [kg]	0
Perimeter, [m]	0
Warping Constant, [m^6]	0.11
Y Neutral Axis Offset A, [m]	2.25
Z Neutral Axis Offset A, [m]	1.13
w [m]	4.50
h [m]	2.00
t1 [m]	0.01
t2 [m]	0.01
t3 [m]	0.02
t4 [m]	0.02

Property Shape

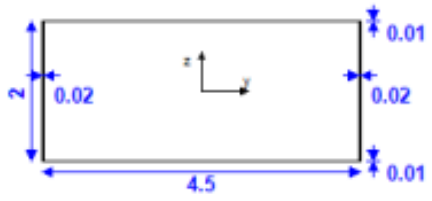

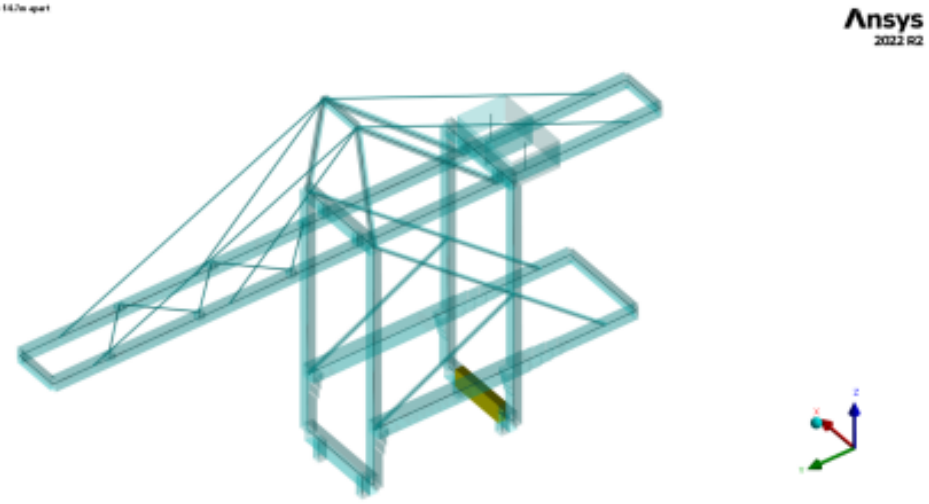

57..Crossgirder Middle (2 bodies)

Property	Value
Type / Elements	Beam / 24
Material	30..Steel ST52
Mass [kg]	58498.20
Area, [m^2]	0.13
I1, [m^4]	0.25
I2, [m^4]	0.20
I12, [m^4]	0
Torsion Constant, [m^4]	0.34
Y Shear Area, [m^2]	1.75
Z Shear Area, [m^2]	1.50
Nonstructural Mass, [kg]	0
Perimeter, [m]	0
Warping Constant, [m^6]	1.775e-03
Y Neutral Axis Offset A, [m]	0
Z Neutral Axis Offset A, [m]	0
w [m]	3.50
h [m]	3.00
t1 [m]	0.01
t2 [m]	0.01
t3 [m]	0.01
t4 [m]	0.01

Property Shape

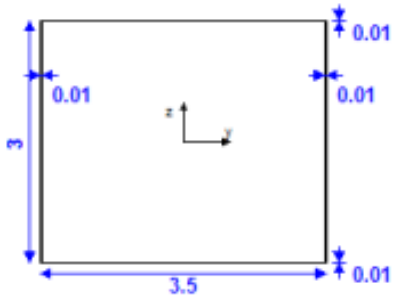

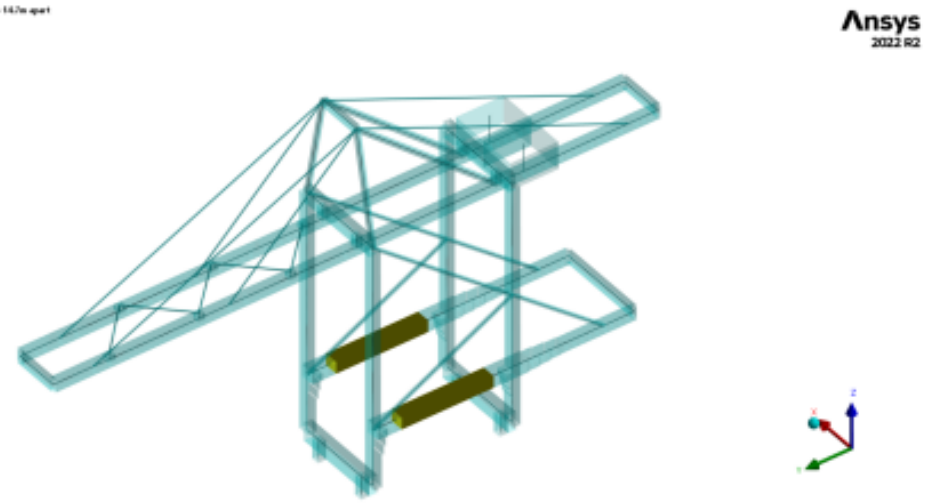

G FEM - Bogie Reaction Forces

This appendix presents the bogie reaction forces for the governing stability and corner load cases.

Operational Stability – Critical Load Cases

Entity ID	Fx [N]	Fy [N]	Fz [N]
822			
LS1..Stability LC B3.325	0.00e+3	199.82e+3	9139.61e+3
LS2..Stability LC B3.341	0.00e+3	-211.30e+3	-122.89e+3
LS3..Stability LC B3.686	0.00e+3	276.75e+3	12490.72e+3
LS4..Stability LC B3.707	0.00e+3	253.32e+3	3483.21e+3
461			
LS1..Stability LC B3.325	-503.36e+3	233.25e+3	12225.45e+3
LS2..Stability LC B3.341	-341.08e+3	323.71e+3	3424.26e+3
LS3..Stability LC B3.686	538.59e+3	157.70e+3	8876.66e+3
LS4..Stability LC B3.707	281.10e+3	-139.67e+3	-179.52e+3
81			
LS1..Stability LC B3.325	0.00e+3	-13.06e+3	1975.90e+3
LS2..Stability LC B3.341	0.00e+3	-439.07e+3	10301.68e+3
LS3..Stability LC B3.686	0.00e+3	16.98e+3	4482.30e+3
LS4..Stability LC B3.707	0.00e+3	-61.06e+3	12447.02e+3
815			
LS1..Stability LC B3.325	-416.09e+3	-24.03e+3	4536.63e+3
LS2..Stability LC B3.341	-537.88e+3	10.72e+3	12295.03e+3
LS3..Stability LC B3.686	380.86e+3	-54.18e+3	2027.91e+3
LS4..Stability LC B3.707	597.85e+3	-367.29e+3	10147.37e+3

Figure 12: Bogie reaction forces for the governing operational stability load case. Node 81: waterside left, Node 815: waterside right, Node 822: landside left, Node 461: landside right.

Storm Stability – Boom at 80°

1527			
LS5..Stability C2.1	-1629.79e+03	-181.17e+03	-2304.38e+03
LS6..Stability C2.2	1638.62e+03	-94.16e+03	12376.45e+03
LS7..Stability C2.3	-7.02e+03	-673.43e+03	6995.85e+03
LS8..Stability C2.4	15.85e+03	398.10e+03	3076.22e+03
1520			
LS5..Stability C2.1	-1807.22e+03	-49.99e+03	198.33e+03
LS6..Stability C2.2	1798.39e+03	304.30e+03	13236.76e+03
LS7..Stability C2.3	6.22e+03	-475.91e+03	4845.26e+03
LS8..Stability C2.4	-15.05e+03	730.22e+03	8589.84e+03
1513			
LS5..Stability C2.1	0.00e+03	315.00e+03	13069.31e+03
LS6..Stability C2.2	0.00e+03	-41.43e+03	32.64e+03
LS7..Stability C2.3	0.00e+03	-491.58e+03	4638.64e+03
LS8..Stability C2.4	0.00e+03	765.16e+03	8463.31e+03
1534			
LS5..Stability C2.1	0.00e+03	-84.41e+03	12329.75e+03
LS6..Stability C2.2	0.00e+03	-168.15e+03	-2346.42e+03
LS7..Stability C2.3	0.00e+03	-687.15e+03	7001.99e+03
LS8..Stability C2.4	0.00e+03	434.59e+03	2981.34e+03

Figure 13: Bogie reaction forces for the stability storm load case (boom at 80°). Node 1527: waterside left, Node 1534: waterside right, Node 1520: landside left, Node 1513: landside right.

Storm Stability – Boom at 60°

Entity ID	Fx [N]	Fy [N]	Fz [N]
539			
LS5..Stability C2.1	0.00e+03	505.16e+03	13583.71e+03
LS6..Stability C2.2	0.00e+03	-227.33e+03	114.05e+03
LS7..Stability C2.3	0.00e+03	505.16e+03	13583.71e+03
LS8..Stability C2.4	0.00e+03	-227.33e+03	114.05e+03
111			
LS5..Stability C2.1	-1667.07e+03	-236.56e+03	279.40e+03
LS6..Stability C2.2	1658.22e+03	494.96e+03	13754.64e+03
LS7..Stability C2.3	-1667.07e+03	-236.56e+03	279.40e+03
LS8..Stability C2.4	1658.22e+03	494.96e+03	13754.64e+03
527			
LS5..Stability C2.1	0.00e+03	85.81e+03	11844.29e+03
LS6..Stability C2.2	0.00e+03	-342.58e+03	-1976.68e+03
LS7..Stability C2.3	0.00e+03	85.81e+03	11844.29e+03
LS8..Stability C2.4	0.00e+03	-342.58e+03	-1976.68e+03
520			
LS5..Stability C2.1	-1774.53e+03	-356.03e+03	-1933.89e+03
LS6..Stability C2.2	1783.38e+03	76.56e+03	11887.09e+03
LS7..Stability C2.3	-1774.53e+03	-356.03e+03	-1933.89e+03
LS8..Stability C2.4	1783.38e+03	76.56e+03	11887.09e+03

Figure 14: Bogie reaction forces for the stability storm load case (boom at 60°). Node 520: waterside left, Node 527: waterside right, Node 111: landside left, Node 539: landside right.

Storm Stability – Boom at 45°

Entity ID	Fx [N]	Fy [N]	Fz [N]
1499			
LS5..Stability C2.1	-1872.89e+03	-382.22e+03	-1637.28e+03
LS6..Stability C2.2	1883.18e+03	278.82e+03	11373.41e+03
LS7..Stability C2.3	-6.43e+03	-516.88e+03	6426.62e+03
LS8..Stability C2.4	16.73e+03	413.48e+03	3309.51e+03
1492			
LS5..Stability C2.1	-1580.68e+03	-447.42e+03	266.10e+03
LS6..Stability C2.2	1570.39e+03	526.32e+03	14032.14e+03
LS7..Stability C2.3	3.58e+03	-488.61e+03	5696.04e+03
LS8..Stability C2.4	-13.87e+03	567.51e+03	8602.20e+03
1485			
LS5..Stability C2.1	0.00e+03	538.61e+03	13860.74e+03
LS6..Stability C2.2	0.00e+03	-435.39e+03	102.68e+03
LS7..Stability C2.3	0.00e+03	-492.46e+03	5509.27e+03
LS8..Stability C2.4	0.00e+03	595.68e+03	8454.15e+03
1506			
LS5..Stability C2.1	0.00e+03	288.77e+03	11331.61e+03
LS6..Stability C2.2	0.00e+03	-367.49e+03	-1682.54e+03
LS7..Stability C2.3	0.00e+03	-520.99e+03	6436.35e+03
LS8..Stability C2.4	0.00e+03	442.27e+03	3212.72e+03

Figure 15: Bogie reaction forces for the stability storm load case (boom at 45°). Node 1499: waterside left, Node 1506: waterside right, Node 1492: landside left, Node 1485: landside right.

Operational Corner loading – Critical Load Cases

Entity ID	Fx [N]	Fy [N]	Fz [N]
81			
LS5..Corner Load LC B3.1	0.00e+3	-582.23e+3	10309.38e+3
LS6..Corner Load LC B3.305	0.00e+3	-183.91e+3	2452.16e+3
LS7..Corner Load LC B3.372	0.00e+3	-84.40e+3	12135.46e+3
LS8..Corner Load LC B3.686	0.00e+3	7.38e+3	4261.21e+3
815			
LS5..Corner Load LC B3.1	-602.02e+3	-24.59e+3	12122.26e+3
LS7..Corner Load LC B3.372	565.53e+3	-522.41e+3	10294.18e+3
LS8..Corner Load LC B3.686	304.62e+3	50.90e+3	1830.03e+3
822			
LS5..Corner Load LC B3.1	0.00e+3	-315.29e+3	444.92e+3
LS7..Corner Load LC B3.372	0.00e+3	275.73e+3	4040.82e+3
LS8..Corner Load LC B3.686	0.00e+3	255.39e+3	12197.93e+3
461			
LS5..Corner Load LC B3.1	-300.67e+3	341.58e+3	4125.95e+3
LS6..Corner Load LC B3.305	-566.48e+3	-92.05e+3	11273.13e+3
LS7..Corner Load LC B3.372	121.15e+3	-248.38e+3	532.04e+3
LS8..Corner Load LC B3.686	598.06e+3	266.87e+3	8713.34e+3

Figure 16: Bogie reaction forces for the governing operational corner load case. Node 81: waterside left, Node 815: waterside right, Node 822: landside left, Node 461: landside right.

Storm Corner loading – Critical Load Cases

1527			
LS9..Corner Load C2.1	-1481.23e+03	-177.21e+03	-1637.07e+03
LS10..Corner Load C2.2	1490.06e+03	-98.12e+03	11709.14e+03
LS11..Corner Load C2.3	-5.99e+03	-624.72e+03	6817.68e+03
LS12..Corner Load C2.4	14.81e+03	349.39e+03	3254.39e+03
1520			
LS9..Corner Load C2.1	-1643.33e+03	-33.88e+03	790.99e+03
LS10..Corner Load C2.2	1634.50e+03	288.19e+03	12644.10e+03
LS11..Corner Load C2.3	5.25e+03	-421.09e+03	5015.46e+03
LS12..Corner Load C2.4	-14.08e+03	675.40e+03	8419.63e+03
1513			
LS9..Corner Load C2.1	0.00e+03	298.80e+03	12476.74e+03
LS10..Corner Load C2.2	0.00e+03	-25.22e+03	625.21e+03
LS11..Corner Load C2.3	0.00e+03	-434.45e+03	4812.49e+03
LS12..Corner Load C2.4	0.00e+03	708.03e+03	8289.46e+03
1534			
LS9..Corner Load C2.1	0.00e+03	-88.22e+03	11662.65e+03
LS10..Corner Load C2.2	0.00e+03	-164.34e+03	-1679.32e+03
LS11..Corner Load C2.3	0.00e+03	-636.16e+03	6819.23e+03
LS12..Corner Load C2.4	0.00e+03	383.60e+03	3164.10e+03

Figure 17: Bogie reaction forces for the governing corner loading storm load case (boom at 80°). Node 1527: waterside left, Node 1534: waterside right, Node 1520: landside left, Node 1513: landside right.